CRANFIELD UNIVERSITY

MARKO PRATNEKAR

THE DESIGN OF BEYOND LEO MISSION SCENARIO FOR A BIOLOGICAL PAYLOAD WITH A CUBESAT

SCHOOL OF AEROSPACE, TRANSPORT AND MANUFACTURING
Astronautics and Space Engineering

MRes
Academic Year: 2016 - 2019

Supervisor: Prof. David Cullen
Associate Supervisor: Dr. Jennifer Kingston
June 2019

CRANFIELD UNIVERSITY

SCHOOL OF AEROSPACE, TRANSPORT AND MANUFACTURING
Astronautics and Space Engineering

MRes

Academic Year 2016 - 2019

MARKO PRATNEKAR

The Design of Beyond LEO Mission Scenario for a Biological Payload with a CubeSat

Supervisor: Prof. David Cullen
Associate Supervisor: Dr. Jennifer Kingston
June 2019

ABSTRACT

CubeSat technology has been well established in the area of space engineering for almost two decades. Because of standardisation of components and procedures, development and launch costs of space missions are greatly reduced and space based experiments become more affordable for the broader community. Up to now, all CubeSat missions except for one have been launched in Low Earth Orbit. With recent developments and new launch opportunities, sending CubeSat missions with various on board experiments beyond Low Earth Orbit into interplanetary space becomes possible.

Major space agencies have ambitious plans to send human space missions to Mars and other bodies in the Solar System. Traveling beyond Earth's orbit, living cells in the human body will be exposed to harmful effects of space radiation. Therefore, before such interplanetary mission takes place, detailed study of effects of space radiation on human like mammalian cells should be conducted. An interplanetary mission based on the CubeSat platform would be the most affordable way of conducting such experiment.

The main aim of the reported research work is to investigate if adequate space radiation protection and strict thermal environment requirement can be achieved and maintained for biological payload with higher forms of living cells, within a CubeSat spacecraft platform during interplanetary flight. This thesis is divided into a theoretical part – the literature review and methodological part – numerical simulations which are for space radiation performed by NASA developed software OLTARIS and for thermal analysis of the spacecraft and installed components with ESATAN –TMS modelling software.

From the performed research work it can be concluded that adequate radiation protection can be implemented within the CubeSat payload compartment, so as not to exceed the acute dose limit set even during long duration interplanetary space flight, while at the same time leaving enough payload volume for the installation of the experimental biological payload and experimental instrumentation within the extra installed radiation protection.

In maintaining the thermal environment inside the payload bay with biological material as well as in maintaining the survival temperature of some electronic components, careful heat management and active thermal control – additional electrical heating is required. There was no requirement for active cooling in the realistic mission scenarios considered.

Keywords:

space radiation, thermal environment, interplanetary space flight, mammalian cells, OLTARIS, ESATAN - TMS, spacecraft

ACKNOWLEDGEMENTS

I am deeply grateful for the advice and mentoring of Professor David Cullen; without his guidance this thesis would not have been possible. Special thanks also goes to my associate supervisor Dr. Jennifer Kingston for her many suggestions and helpful revisions.

My sincere thanks also to ITP Engines UK Ltd and their support personnel for providing me with the licence for the ESATAN – TMS thermal modelling software free of charge and tirelessly answering my project questions. I would also like to express my gratitude to Dr. Chris Sandridge for enabling the use of the OLTARIS space radiation modelling software.

Gratitude also goes to Dr. Bogdan Blagojevič and Dr. Martin Rott who recognized my passion for space technology and helped me along the way.

Finally, I would like to thank to my parents, who have given me love and support throughout the years and helped me to follow my dreams.

Sofia, you were born during the heights of this thesis work and filled my life with endless joy and motivation.

TABLE OF CONTENTS

LIST OF FIGURES

LIST OF TABLES

LIST OF DIAGRAMS

LIST OF EQUATIONS

LIST OF ABBREVIATIONS

ACS	Acute Radiation Syndrome
ADCS	Attitude Determination and Control System
AU	Astronomical Unit
BFO	Blood Forming Organs
C&DH	Command and Data Handling
CME	Coronal Mass Ejection
CNS	Central Nervous System
DNA	Deoxyribonucleic Acid
ESA	European Space Agency
GCR	Galactic Cosmic Radiation
GMM	Geometric Mathematical Model
HF	Heat Flux
HZTRN	High charge (Z) and energy transport
ICRP	International Commission for Radiation Protection
ICS	Inertial Coordinate System
ISS	International Space Station
JAXA	Japanese Space Agency
LEO	Low Earth Orbit
LET	Linear Energy Transfer
MiPS	Micro Propulsion System
MLI	Multi Layer Insulation
MCS	Model Coordinate System
NEIL	Non Ionizing Energy Loss
NOAA	National Oceanic and Atmospheric Administration
OLTARIS	On Line Tool for The Assessment of Radiation in Space
PCB	Printed Circuit Board
R_E	Earth radius
REF	Radiation Exchange Factor
SAA	South Atlantic Anomaly
SEU	Single Event Upset
SPE	Solar Particle Event
SPENVIS	Space environment information system

TLE	Two Line Element
TMD	Thermal Model Data
TMM	Thermal Mathematical Model
TMS	Thermal Modelling suite
TPEC	Tissue Equivalent Proportional Counter
TVC	Thermal Vacuum Chamber
VF	View Factor

1.INTRODUCTION

1.1 Motivation

Recently intentions have been revealed by major space agencies around the world, including new space power China, for serious plans to be made to send manned missions back to the Moon and even further into the Solar system, to the neighbouring planet of Mars.

Up to now, with exception of ten Apollo missions (from Apollo 8 to Apollo 17) no man has left the protective orbit of Earth to fly a space mission in Interplanetary space. Therefore, a lot of open questions exist, especially regarding the effects of harmful space radiation on living cells and the human body, during long period interplanetary space flights. This questions will need to be investigated in details before such a mission could take place.

Space missions present big scientific, technological, organizational and financial challenges which can easily be to extensive for a single institution, organization or even for a single nation. With the implementation of CubeSat technology and their opportunities for secondary payload launching, space based experiments and technology demonstrators become more accessible for only a fraction of a cost. Furthermore, with the introduction of bigger 6U CubeSats modules even more sophisticated instrumentation and complex experimental set-ups can be sent into Earth's orbit or beyond into interplanetary space. CubeSat platforms are therefore ideal for Biological payload experiments. Many Bio CubeSat missions have already been successfully launched in Low Earth Orbit around the Earth. NASA is also planning the first Interplanetary BioCubeSat mission named BioSentinel, which will fly in the near future as a secondary payload of the Space Launch System and is going to study the effects of space radiation on simple yeast cells. In the presented research work, BioSentinel is used as it has a similar platform and payload as an example mission.

The aim of the present research work is to advance the status and to propose conceptual design of an Interplanetary space mission within CubeSat standards, which could be able to carry advanced living forms, similar to human

cells – C.elegans worms, which are discussed in more detail later in this work (Subchapter 5.2.2.7). The major difference between BioSentinel biological payload and mission payloads proposed for the BAMMSat concept (Subchapter 2.3.3), as well as for the mission design studied in this thesis, is that during the BioSentinel mission, lower forms of living organisms – yeast cells, will be investigated. Therefore, not such strict requirements arise regarding space radiation protection, thermal control and general payload environmental conditions. On the other hand, advanced forms of living organisms, such as mammalian cells, present much more adequate experiment samples for studying effects of space environment on human cells during long duration interplanetary flights. For both, the BAMMSat concept and mission design studied in this research work, higher forms of living organisms are proposed to fly as biological payload. Such advanced biological material requires much stricter radiation protection and needs to maintain sophisticated environmental control throughout the duration of the mission experiment.

Therefore, the first important task is to provide adequate space radiation protection. During the experiment it is important that payload biological material is not fatally damaged in a short period, but at the same time certain exposure of the biology sample to space radiation is anticipated and needed for study purposes. Because of this, convenient radiation protection of biological payload, to maintain radiation within set limits is very important.

The second important parameter for survival of human like biology cells is maintaining a suitable temperature environment throughout the duration of the mission. Not just the payload, but also batteries and sensible electronic components have certain temperature limits for normal operation and survival.

It can be seen, that designing adequate radiation protection and being able to maintain a strict temperature environment inside the satellite, and especially in the payload compartment where ~~is~~ the biological material is, are the most important requirements which are needed to be fulfilled for successful Interplanetary Bio CubeSat mission with human similar - mammalian cells.

The first part of the thesis consists of a review of the literature on the subject, from where major aims and objectives of the thesis are derived. After the initial part there are two core research chapters investigating the radiation environment during long period deep space CubeSat mission and secondly, the spacecraft bus design and component selection to maintain adequate thermal environment and investigating the temperature response of the designed CubeSat with thermal modelling software. The final chapter concludes the work with a discussion of results and the outlining of possible further work.

2. SCIENTIFIC BACKGROUND AND LITERATURE REVIEW

2.1 Introduction

The present chapter is an overview of knowledge and solutions which have already been discussed and published in the scientific community in the general area of CubeSat technology. This field of space technology is relatively new with special technological and operational requirements which need to be fulfilled for such mission.

A special section of CubeSat missions with Biological payload experiments will be further studied and overviewed. Some such missions have already flown and many more are still in the design and development phase. Up to now all BioCubeSat missions have flown in Earth's orbit, interplanetary missions are still in the designing phase and are scheduled for the near future. BioSentinel is the first such mission.

Cranfield University, in collaboration with other educational and scientific institutions, is developing the BioCubeSat mission platform known as BAMMSat, which is presented and overviewed.

2.2 CubeSat Technology

The CubeSat project began in 1999 as a collaborative effort between California State University (Cal Poly) and Stanford University Space System Development Laboratory (SSDL). The purpose of the project was to provide a standard for design of pico (0.1 – 1 kg) and nano (1 – 10 kg) satellites to reduce costs, development time, increase accessibility to space and sustain frequent launches also for small actors such as universities and research institutions [1]. With CubeSat platforms they are able to try new ideas, concepts, processes, techniques and and to push the boundaries of development forward.

The physical standard that resulted is based on a 10 x 10 x 10 cm cube, that has a volume of one litre and a mass of 1.33 kg or less. This dimension standard is referred as one unit "1U" CubeSat and is scalable in 1U increments

[2]. Design specifications and requirements are described and discussed in detail in the CubeSat Design Specification publication [1], [5].

As developers have continued to push the limits of CubeSats, there has been an increasing demand for larger satellite standard. So by combining basic units 2U, 3U and 6U satellites are formed. With this configuration there is usually one unit dedicated to the bus and the other(s) to the payload. With 3U there is usually 1U bus and 2U payload, while for 6U, 2U are used for bus and 4U for payload [3].

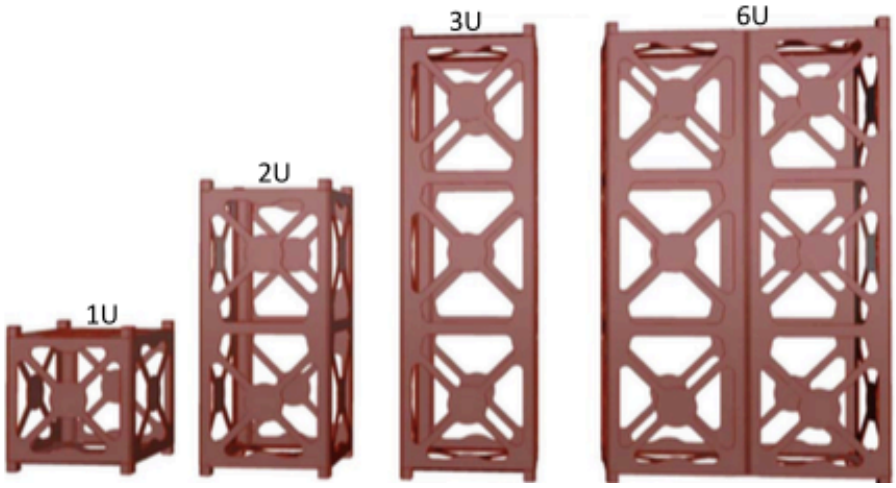

Figure 2-1: Framework of 1, 2, 3 and 6U CubeSats [6]

A key factor to the CubeSat approach is the use of a standardized deployment system which from a launch provider's perspective appears identical from mission to mission in terms of interface and functionality [4]. The most widely used deployment system is the Poly - Picosatellite Orbital Deployer (P-POD). The P-POD system has been used to deploy over 90% of all CubeSat launched to date, and 100% of all CubeSats launched since 2007 [2]. P-POD is able to deploy up to 3U CubeSats.

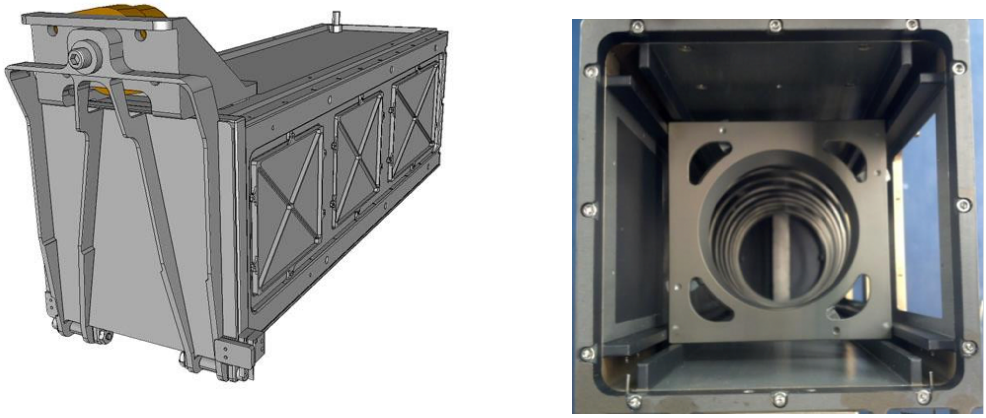

Figure 2-2: Poly Picosatellite Orbital Deployer (P-POD) and cross section [1]

Dispensers for 6U CubeSats are still under development by multiple companies and are similar to P-POD system [5].

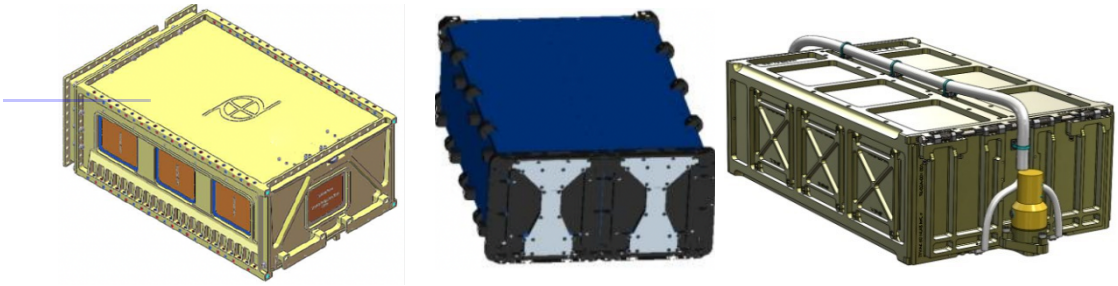

Figure 2-3: Dispensers for 6U CubeSats designed by Planetary Systems Corporation (left) ISIS (canter) and Tyvak (right) [5]

A large proportion of all CubeSat launched to date have been in the 1U to 3U range. The first 6U examples have been launched just recently – in 2017 (NASA designed MarCO and ASTERIA). Plans for even bigger 12U and 27U are in development but currently there are no deployers with flight heritage for such big units [6].

The utility of CubeSats as scientific research and technology validation platform is increasingly recognized and is successfully used in several different science and technology mission platforms. To date, CubeSat missions have focused on following applications:

- Technology demonstrator

- Earth remote sensing
- Biology and Astrobiology
- Astronomy
- Atmospheric Science
- Ecology
- Space weather
- Materials processing

Numerous CubeSat missions have produced interesting and important scientific results. Further some CubeSat missions with Biology payloads are investigated.

2.3 Bio CubeSat

With Biology and Astrobiology experiments there are conducted studies about origin, evolution, distribution and effects of space environment on life in the universe. CubeSats enable exposure of micro-organisms, as well as organic compounds - particularly those considered potential building blocks of biology, or biomarkers - to astrobiologically important aspects of the space environment, including microgravity, vacuum and solar ultraviolet and ionizing radiation. These studies are a key to understanding how such compounds and organisms survive in, or are modified by, the space environment. These studies are of ~~a~~ great importance for present and future human presence in the space environment. It is already known that exposure to the space environment has many negative effects on mammalian organisms like: altered fluid distribution, immune stress, decrease of bone density, muscle atrophy, cell damage by space radiation and many others. CubeSats are well suited to study of fundamental space biology using well - grown organism such as: E. coli, S. cerevisiae, C. elegans and others. Such studies help elucidate effects relevant to long duration human space travel, planned for the future.

Similar studies have already been carried out on the International Space Station (ISS) with post-flight ground analysis. But the CubeSat platform has many advantages, because experiments can be placed in higher orbits, where the radiation dose is significantly higher than on ISS and they can be spatially

oriented to receive much longer daily Solar UV exposure. CubeSat biological experiments can also stay in orbit for many months and with in-situ measurement technology, the dynamics of space - induced changes can be continuously monitored, rather than being limited to simple before-and-after flight comparisons [3].

With new knowledge and the introduction of bigger 6U and above CubeSat modules, there are arising possibilities for beyond Low Earth Orbit (LEO) missions which will be able to investigate the effects on biological material in harsh deep space environment, which will be explored by human missions in decades to come.

2.3.1 Low Earth Orbit Bio CubeSat Missions

Up to now, all CubeSat missions with biological payload were placed in Low Earth Orbit. Described are some most influential missions.

- **GeneSat 1 (2006)**

GeneSat CubeSat mission was launched as a secondary payload onboard a Minotaur-1 launch vehicle in 2006. A result of collaboration between NASA Ames, industry partners and university institutions. The satellite consisted of a satellite bus confined to 1U while the payload was contained in a 2U structure – a configuration that is typical for 3U CubeSat system. GeneSat's mission objective was to develop a miniature life support system that could fit into a triple CubeSat structure and could deliver nutrients and ~~and~~ perform analysis for genetic changes in biological samples, in this case E. Coli. A pressurized sealed vessel and an integrated analytical fluids card assembly, which included media pump, valves, microchannels, filters, membranes and wells to maintain biological viability of the microorganisms, comprised in the payload compartment.

A dedicated blue LED – excited fluorescent detection optical system probes gene expression levels by quantifying levels of light emitted by green fluorescent protein (GFP) which has been fused to a bacterial gene associated

with metabolism. Concurrent light scattering measurements were made in order to normalize the fluorescence results to culture population as it grows. Results were transmitted to Earth at S-band [7]. An environmental system was required to maintain a specific temperature within 0.5 °C during the experimental phase, which was nominally planned for 96 h. The system monitored internal and external temperature as well as radiation environment.

GeneSat-1 was NASA's first CubeSat mission and the first biological experiment conducted with a CubeSat platform [2].

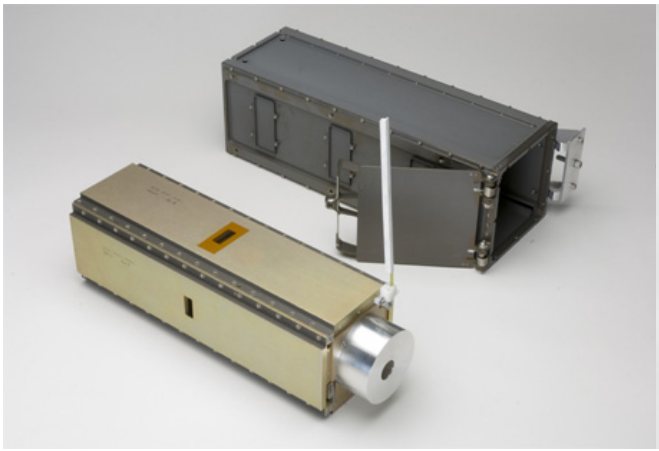

Figure 2-4: GeneSat-1 triple-cube nanosatellite (left) next to the P-POD (right) (NASA/ARC)

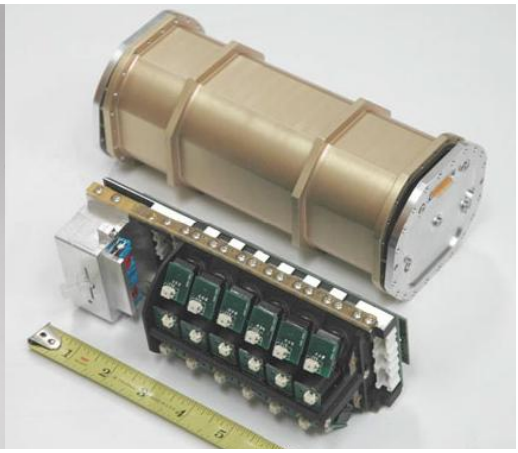

Figure 2-5: The pressurized payload volume and optical bench of GeneSat-1 (NASA/ARC)

- **PharmaSat (2009)**

Similarly to GeneSat – 1 its successor, PharmaSat CubeSat experiment platform was launched with Minotaur - 1 rocket on May 2009, as a secondary payload. The biological payload compartment comprised 2U, containing bio/fluidic, optical, thermal, sensor and payload electronics subsystems, while 1U was used for spacecraft bus.

The PharmaSat experiment supported microbial growth within 48 microfluidic wells with dosed microbes. In single wells there were different concentrations of pharmaceutical agents where microbial growth and metabolic activity was monitored using a dedicated 3 - color optical absorbance system. The main objective of the mission was to assess the efficacy of antifungal drugs in a microgravity environment. The onboard experiment lasted for 96 hours.

Astronauts in space have already experienced bacterial infections. Effective treatment of bacterial infections has required therapy customized for the space environment, as evidence has accumulated that microbes respond differently to antimicrobials in the space environment. The PharmaSat experiment was focused on directly documenting alterations in antimicrobial resistance in the space environment using well defined microbial system – the yeast, S. cerevisiae. The optical system in payload compartment tracks organism growth in two ways: optical density changes due to light scattering by the yeast cells, which is directly proportional to cell number and colour change of a viability dye, almar blue, which is deliberately added to the growth medium [8].

There was strict payload ambient thermal control, provided with system microcontroller, maintaining temperature stability within fluidic cards of < 0.3 °C at 27 °C which is optimal growth temperature of yeast.

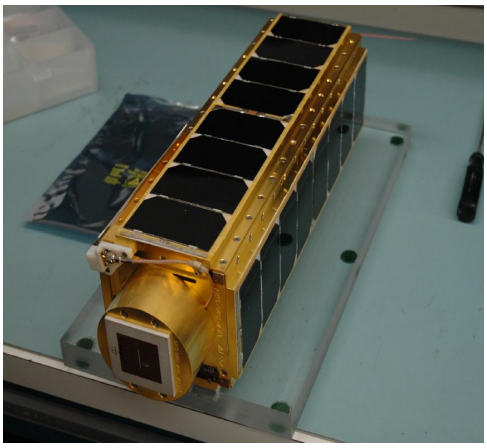

Figure 2-6: PharmaSat 3U CubeSat (NASA)

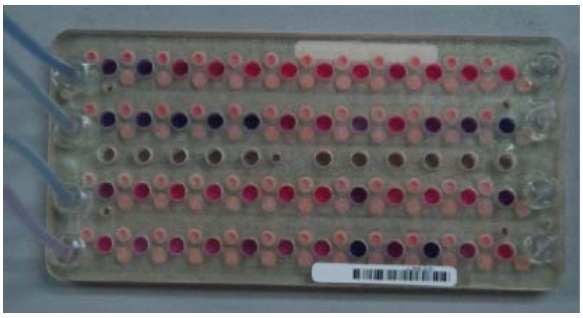

Figure 2-7: PharmaSat thermally controlled wellplate for biology sample (NASA)

- **SESLO/ SEVO experiment on O/OREOS (2010)**

After the success of GeneSat and PharmaSat, NASA launched the O/ OREOS *(Organism / Organic Exposure to Orbital Stress)*, 3U CubeSat mission in 2010 onboard a Minotaur IV launch rocket. It was NASA's first CubeSat mission to demonstrate the capability to have two distinct completely independent science experiments on an autonomous satellite. The first experiment was designed to test how microorganisms survive and adapt to the stress of space and was named **SESLO** for ***S****pace Environment* ***S****urvivability of* ***L****iving* ***O****rganisms*. The other experiment monitored stability of organic molecules in space and was named **SEVO**, short for **S**pace **E**nvironment **V**iability of **O**rganics.

The satellite was launched in November 2010 650 km into Earth's orbit with a 72 ° inclination. This position provided access to the radiation environment in orbit in relatively weak regions of Earth's protective magnetosphere as it passed close to the north and south magnetic poles. The total dose rate was about 15 times that in the orbit of International Space Station [9].

The SESLO experiment measured the long term survival, germination and growth response, including metabolic activity of Bacillus subtilis spores exposed to the microgravity, ionizing radiation and heavy ion bombardment in its high

inclination orbit. Six microwelles contained wild - type and six more contained radiation sensitive mutant strains of dried B. subtilis spores which were rehydrated with nutrient medium after 14 days in space, to allow the spores to germinate and grow. Similarly, the same distribution of organisms in a different set of microwells was rehydrated with nutrient medium after 97 days in space. The nutrient medium included the redox dye Alamar blue, which changes colour in response to cellular metabolic activity. Using 3 - color LED illumination (470, 525, and 615 nm), the growth and metabolism of the microbe Bacillus subtilis was successfully measured during the mission at 2 weeks, 3 months and 6 months after launch [9], [10].

Three colour transmitted intensity measurements of all microwells were telemetered to Earth within days of each of the 48h growth experiment. Onboard experiment data were evaluated and interpreted in comparison to synchronous laboratory ground control experiment [9].

A second experiment platform on O/OREOS CubeSat platform was named SEVO. The experiment exposed four astrobiologically relevant organic molecules (an amino acid, a quinone, a polycyclic aromatic hydrocarbon and metallo – porphyrin) to solar radiation in Low Earth Orbit (LEO). Each type of molecule was deposited as a thin film and contained in four separate micro environments representative of either Mars (CO_2) atmosphere, H_2O atmosphere, interstellar space, or lunar (mineral) surface. The experiment continuously exposed the organic matter to radiation in the form of solar UV radiation, visible light, trapped-particle and cosmic radiation in over six month of mission duration.

The degradation and/or alteration of each sample on the satellite was monitored in-situ with UV/V spectroscopy. To complement flight data, laboratory controls were designed to exposed to a solar simulator at regular intervals to match the exposure experienced onboard the satellite [11]. The survival rate of these molecules helped to determine whether some of Earth’s biochemistry might have been performed in space and later delivered by meteorites. The experiment obtained data also helped to determine which molecules are good

biomarkers that can signal the existence of past or present life on another world and can be helpful in answering astrobiologically fundamental questions on the origin, evolution and distribution of life.

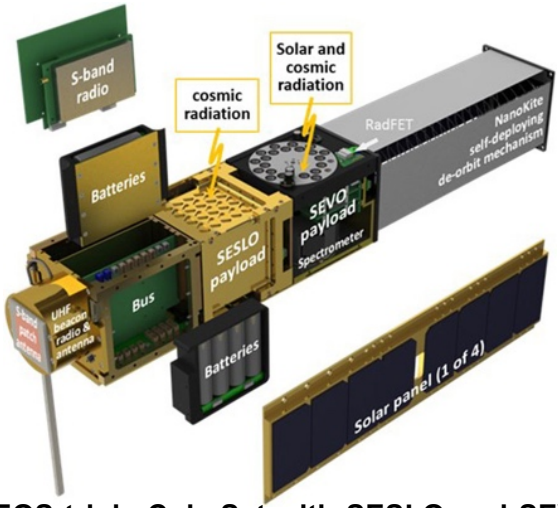

Figure 2-8: O/OREOS triple CubeSat with SESLO and SEVO experiment payload and deorbit mechanism deployed [10]

- **SporeSat (2014)**

In 2014 NASA, together with Purdue University, developed the 3U CubeSat mission on the heritage of previous successfully flown similar experiments with living material. The SporeSat space biology science experiment was investigating the effects of gravity on the reproductive spores of the fern, Ceratopteris richardii. Some plants, including C. richardii, use gravity to determine direction and to guide their roots to grow down into the soil, where they find nutrients for growth. Calcium is important to overall plant growth and development, but it also plays an important role in the process of sensing gravity and signalling the response of downward plant growth.

To better understand the role of the on/off modulation of cellular calcium ion channels in gravity sensing, the SporeSat experiment measured the effects of different artificial gravity levels on calcium concentrations that resulted from the opening and closing of these channels. SporeSat carried three lab-on-a-chip-devices, called Bio CDs, which integrated the sensors that allowed real-time measurements of calcium signalling at each of the variable gravity treatments

planned for the experiment. In the microgravity Earth orbit environment, two of the Bio CDs spun to exert a range of artificial gravitational forces (for example like gravity fields equivalent to Moon and Mars) on the spores during the experiment. A third Bio CD remained stationary as a microgravity control. Each disc shaped BioCD carried up to 32 spore's samples. The gravitational response of the fern spores was monitored by measuring the threshold for activation of their calcium ion channels [12], [13].

This research was also important, since ion channels are critical for the functioning of biological organisms including humans. Ion Channels are key components of the nervous system, as well as cardiac, skeletal and smooth muscle function, transport of nutrients and ions, T - cell activation and pancreatic beta-cell insulin release. Ion channels are therefore often the target of the search for new drugs.

SporeSat was first of its kind – a small science satellite that coupled novel miniaturized technology to novel biological science: a variable-rate centrifuge which allowed testing response of fern ion channels at different ranges from microgravity to hypergravity [13].

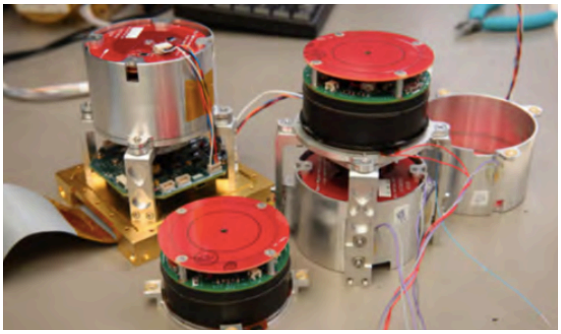

Figure 2-9: Two rotating BioCDs for exerting artificial g - forces and one standby assembly [13]

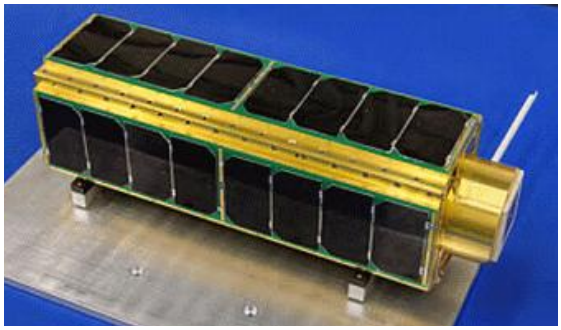

Figure 2-10: SporeSat 3U Spacecraft (NASA)

- **DIDO – 1 and DIDO – 2 (2017)**

DIDO – 1 and DIDO – 2 are 3U CubeSat missions designed by the Israeli/ Swiss company SpacePharma. The DIDO - 1 was planed to fly on multi-satellite mission on a Falcon-9 rocket already in 2016, bust was postponed.

DIDO – 2 was successfully launched in February 2017 on Indian PSLV-C37 launcher which released load of 104 satellites at the same time.

The purpose of the DIDO – 1 and DIDO – 2 projects is to test a miniaturized end to end pharmaceutical laboratory in space, allowing microgravity conditions.

The satellites contain laboratory, that can be remote controlled from the third party from anywhere. The unit can perform experiments on bacterial growth, antibiotics resistance, self-assembly, enzymatic reactions, polymerization, nanoparticle synthesis, particle aggregation dynamics, emulsion stability and crystallization.

DIDO platform is based on a flight proven satellite bus that takes up only half a CubeSat unit, leaving 2.5U available for research equipment and experiment [14].

Figure 2-11: DIDO 3U CubeSat mission with Bio experimental platform (SpacePharma) [14]

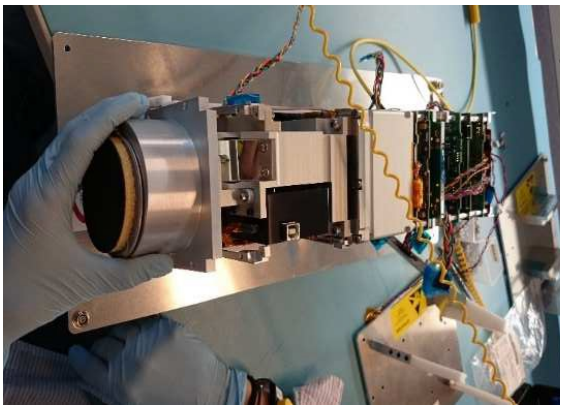

Figure 2-12: DIDO experiment platform [14]

2.3.2 Interplanetary Bio CubeSat Missions

With constant progress and development of CubeSat technology, missions that will fly beyond low earth orbit are becoming reality.

On May 2018 NASA launched a stationary lander called InSight to Mars. Riding along with InSight were two CubeSats called MarCo (Mars Cube One) – the first of this kind of spacecraft to fly a mission into deep space. The technology onboard each will provide NASA with the ability to quickly transmit status information about Insight as it lands on Mars. Success of this mission will demonstrate that technologies for interplanetary missions are feasible and will lead to send many other CubeSat applications for exploring our Solar system [15].

Over the coming decades, further development of distinct technological areas~~,~~ could enable comparatively low-cost Solar System exploration missions with capabilities far beyond those demonstrated in small satellites to date. These technologies are [20], [21]:

1. CubeSat electronics and subsystems extended to operate in the interplanetary environment, focusing on duration of operation and radiation.
2. Flying away from the Sun causes decrease in solar irradiation, requires more efficient solar panels and energy storage units, with the purpose ~~to~~ of covering high electrical energy demands.
3. Progress of optical telecommunications to enable very small, low power uplink/ downlink over interplanetary distances.
4. Solar sail and other alternative ways of propulsion to enable high Δv manoeuvring using little or no propellant.
5. Navigation of the Interplanetary Superhighway to enable multiple destinations over reasonable mission duration using achievable Δv.
6. Small, highly capable instrumentation enabling acquisition of high-quality scientific and exploration data.

7. Onboard storage and processing of raw instrument data and navigation information to enable maximum utility of uplink and downlink telecom capacity and minimal operations stuffing.

The interplanetary CubeSat will be built on existing Earth orbiting CubeSat architecture. The target interplanetary spacecraft volume is 6U, where 2U or 4U are usually reserved for scientific payload - depends on the propulsion system, the rest is spacecraft bus.

Many Interplanetary CubeSat missions from diverse scientific areas such as: technical demonstrators, small solar system body science, heliophysics and terrestrial applications, planetary science, astrophysics and also biology, life science experiments and astrobiology could be proposed.

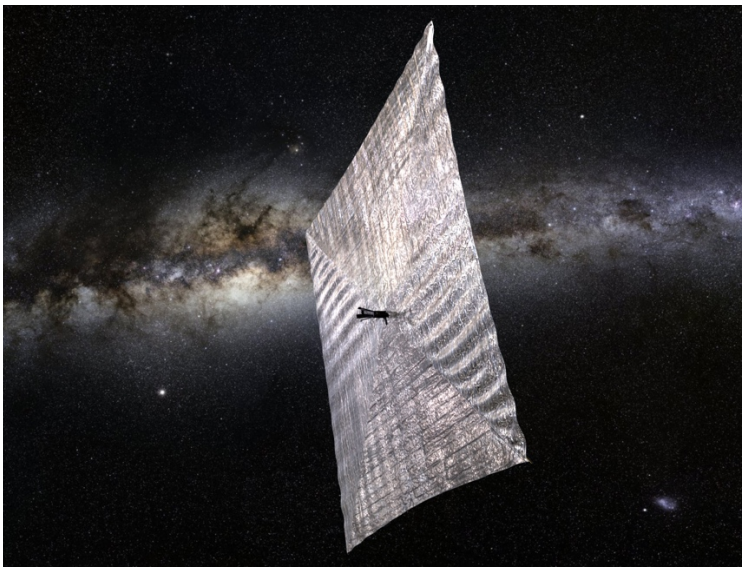

Figure 2-13: Artistic interpretation of CubeSat with deployable Solar Sail as a mean of deep space propulsion (NASA)

NASA is from its announcement in 2013, developing an ambitious 6U CubeSat mission named BioSentinel, with the purpose of studying effects of space on living organism outside the Earth's orbit. Since Fobos – Grunt, the Russian interplanetary space mission with LIFE (Living Interplanetary Flight Experiment) onboard, which was designed to test if selected organisms can survive many years in the deep space environment, failed to leave Earth's orbit and was destroyed shortly after launch in 2012, BioSentinel and more recently Chinese

Chang'e 4 will be the first space missions to carry biology related experiments beyond LEO, since Apollo mission in 1960s and 1970s.

In January 2019, the Chinese lunar exploration mission Chang'e 4 made its first soft landing on the far side of the Moon. The Biosphere experiment included six types of organisms: cottonseeds, potatoes, Arabidopsis thaliana, rapeseeds, as well as fruit fly eggs and yeast. The aim of the experiment was to develop a life support system for long duration missions in space stations or space habitats for eventual space farming. As reported, cottonseeds ~~had~~ sprouted during the stay on the Moon's surface [43].

- **BioSentinel**

BioSentinel is a 6U CubeSat mission that is planned to fly aboard NASAs Space Launch System (SLS) as a secondary payload in the near future. For the first time in more than forty years, direct experimental data from biological study beyond low earth orbit (LEO) will be obtained during the 12 to 18 - month mission where spacecraft will be deployed into heliocentric orbit between 0.92 and 0.98 AU. Its main objective is to measure the damage and repair of DNA in a biological organism and compare that to information from onboard physical radiation sensors. This data will be available for validation and extrapolation to humans, to mitigate risk to astronauts during future long-term space exploration missions beyond Earth's orbit. This will be achieved by studying the impact of the deep space radiation environment on genetically modified yeast cells. Monucellular eukaryotic organism Saccharomyces Cerevisiae (yeast) will be used to report DNA double strand break events that result from ambient space radiation. Yeast was selected due to its similarity to cells in higher organisms and the spaceflight heritage from the past missions. BioSentinel will provide critical information about what impact deep space radiation may have on future manned missions [15].

The yeast cells are dehydrated prior to launch and then are rehydrated and kept alive in deep space using a microfluidic system and heaters. Special environmental conditions (temperatures of 23 °C±1 °C, pressure of 1 atm,

humidity) must be maintained inside the 4U payload compartment throughout the mission life. The reaction of the yeast cells to the deep space radiation environment will be monitored using optical measurements inside the payload container. The yeast will be cultured in multiple independent culture microwells which are built into the well plate. Optical measurements will be performed using 3 colour LEDs shining through the culture wells, similar to those used previously for the O/OREOS mission. Broadband detectors at the bottom will measure the intensity of the light, which will indicate growth and metabolism of the culture [17]. Biological measurements will be compared to data provided by onboard physical sensors and dosimeters to obtain total ionizing radiation dose and particle characterization, and to Earth based experiments using relevant energetic particle types, energies and doses. Additionally, three identical BioSentinel payloads will be developed – one for the International Space Station (ISS), where there is similar microgravity but a comparatively low radiation environment, one for use as a delayed-synchronous ground control at Earth's gravity and also with a low radiation environment, and one as ground payload that will be used in the laboratory for radiation testing. Thus the BioSentinel payload will help calibrate the biological effects of radiation in deep space to analogous measurements conducted on Earth and on the ISS [18].

As can be seen from the Figure 2-14 the spacecraft has been designed to allocate 4U of volume to payload, while the remaining 2U of volume will be occupied by spacecraft bus subsystems including Command and Data Handling, communications, attitude determination and control and power management units.

Beside from performing biological experiment, the BioSentinel mission will ~~be~~ also be a technology demonstrator, showing CubeSat platform deep space capabilities as well as a validation check for the SLS secondary payload interfaces and accommodations [19].

The BioSentinel design and installed components will also serve as a role model for designing and developing our interplanetary CubeSat mission.

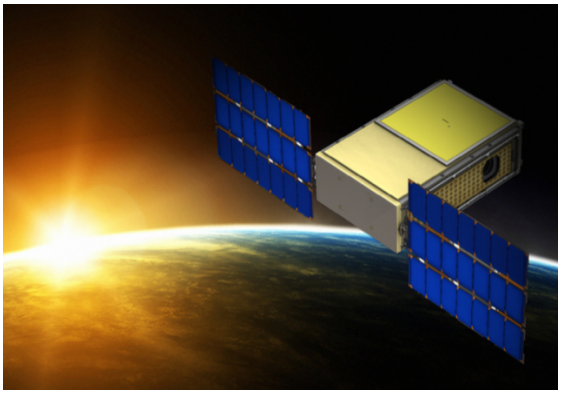

Figure 2-14: Artistic view of 6U BioSentinel CubeSat leaves Earth into a lunar fly-by trajectory and into a heliocentric orbit (NASA)

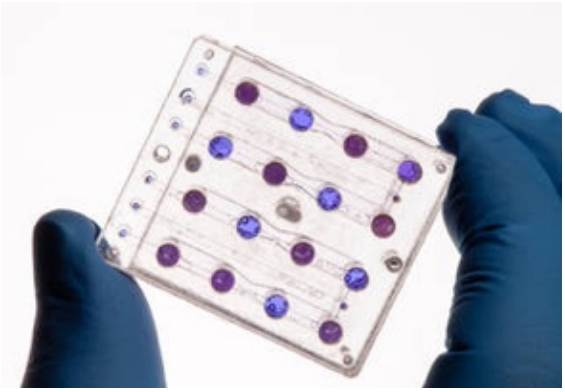

Figure 2-15: BioSentinel microfluidics card with biological samples (NASA)

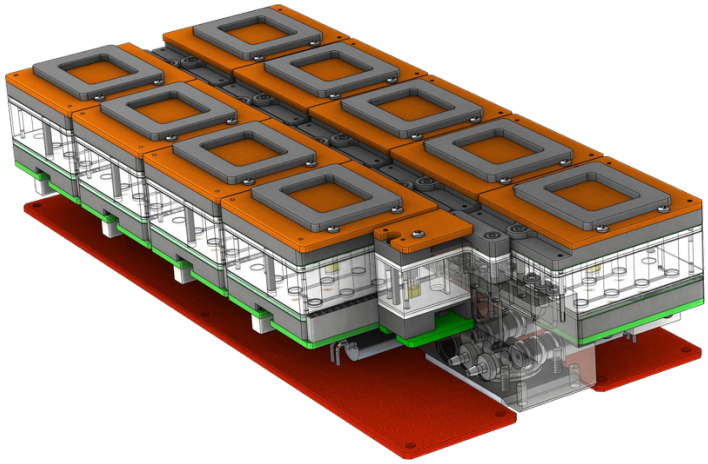

Figure 2-16: Artistic demonstration of the BioSentinel science experiment payload in which are placed colonies of yeast cells [16]

2.3.3 BAMMSat CubeSat Project – Cranfield University

Past successfully flown Bio CubeSat space missions have shown great potential for studies on biology and related materials. Therefore, in addition at Cranfield University, in collaboration with other partners, an initiative begins to investigate the BAMMSat concept – to develop expertise and platform capability to exploit CubeSat opportunities for bioscience, astrobiology, medicine and

material science applications, which share a common 2U hardware platform design. Important requirements of the platform are:

- being able to house multiple samples,
- maintaining / maintenance of samples in a controlled environment,
- taking care of appropriate perturbation and fluidisation of samples,
- being able to properly monitor samples.

The Payload breadboard has already been developed, with the ability to house forty discrete samples and observe these with a miniaturised fluorescence microscope. The goal is to design a platform in size of 2U, being able to fly in space and conduct studies on mammalian cell cultures in a Bio - CubeSat mission.

The idea that arose together with the development of the BAMMSat project is to plan a step forward and to think also about possibilities and design challenges ~~of~~ for beyond LEO, interplanetary Bio - CubeSat missions which would help to provide answers to some fundamental questions within bioscience, astrobiology and astrochemistry [22], [23].

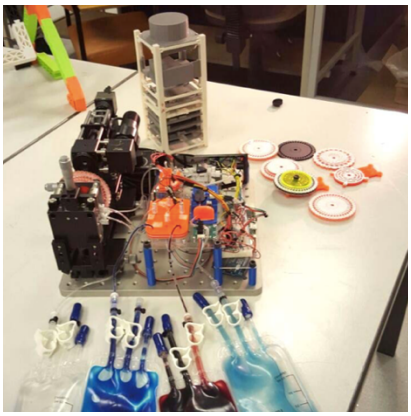

Figure 2-17: BAMMSat integrated fluidic and microscopic breadboard [23]

Mammalian cell cultures which are proposed to fly with the BAMMSat experiment have strict thermal requirements, are difficult to store for long periods of time and are difficult to keep alive once the study has begun. Therefore, planning an interplanetary BAMMSat would require detailed design and study, being able to maintain strict controlled environment conditions

throughout the entire duration of the planned interplanetary mission. Maintaining a controlled temperature environment would be one of the main requirements. One of main aims of this thesis work is to investigate and to advance technical solutions for the providing of strict environmental conditions needed during such missions.

2.4. Conclusion

In Chapter 2 a general review of the literature was presented. In the first part general CubeSat technology and their specific requirements were discussed, which were taken into account during geometry design and component installation presented in Chapter 5. Further special considerations were outlined for CubeSats with biological payload. As seen, quite a few successful CubeSat missions with biology experiments have been launched already. What is common to all of these missions is they were all placed in Low Earth Orbit, performing experiments with lower form of living material (bacteria, yeast cells…). The first interplanetary CubeSat mission with biology payload, BioSentinel is to be launched in near future on board the first Space Launch System flight. BioSentinel will be first biology platform experimenting flown beyond Low Earth Orbit since the Apollo space program.

What is common to all the previously launched and also the planned CubeSat biology payload space missions, including interplanetary BioSentinel, is the usage of lower forms of living material. Therefore, a proper investigation of harmful effects that the space environment, especially space radiation will have on human like cells during long duration missions to the Moon, Mars and other places in Solar system cannot be performed.

With the intention of further developing experimental platforms, being able to accommodate human like mammalian cells experiments among others, BAMMSat was initiated as a common effort between Cranfield University and other partners and research institutions. The BAMMSat platform is to be used for Low Earth Orbit missions as well as for interplanetary flights.

In the subsequent chapters, all literature review acquired knowledge is taken into consideration and further technological solutions are investigated with goal to design CubeSat geometry and perform suitable component selection to provide adequate radiation protection (Chapter 4) and required temperature environment (Chapter 5) to successfully perform experiments with human like mammalian cells during interplanetary CubeSat missions.

3. PROJECT AIMS AND OBJECTIVES

3.1 Project aims

The main research ***aims*** for the work are:

(1) To investigate known technological solutions and future challenges of beyond LEO CubeSat missions.

As investigated through the literature review in Chapter 2, CubeSat technology is already very well established, developed and mature for various space mission applications in Low Earth Orbit. Up to the present (August 2018), 985 nanosatellites have been launched out of which 875 were described as CubeSats of different sizes [29]. Additionally, increased effort is being put into the development of CubeSat platforms which will be able to fly beyond Earth orbits and into interplanetary space. Up to now only one mission – MarCO in mid 2018 has left LEO and travelled to Mars. For successful interplanetary CubeSat missions new applications, technologies and components need to be studied and developed in areas such as communication, propulsion, ADCS as well as new science and mission applications or goals. For the current study the main interest is missions with biological experiments as payloads.

By means of the literature review, previously researched and published work in the area of Interplanetary CubeSats was highlighted. Knowledge of previously investigated technology solutions and future challenges of interplanetary CubeSats represented the base for further research work.

(2) To advance the Interplanetary CubeSats mission design aspect in area of radiation protection and thermal control, with focus on flying biological payload with higher forms of living organisms.

All biological experiments on CubeSat platforms flown in Low Earth Orbit up to date, contained cells or biological material from simpler forms of living organisms. The first interplanetary CubeSat mission with biological payload – BioSentinel will also carry an experiment with simple living form - yeast cells.

Research work will focus on finding technical solutions, mainly in space radiation protection and thermal control requirements for interplanetary CubeSat missions with more demanding mammalian cells onboard. It is the main difference with the proposed BioSentinel mission.

(3) Improving development status of the BAMMSat Bio-CubeSat platform in preparation for beyond LEO missions.

The BAMMSat CubeSat platform (Chapter 2.3.3) is being developed to be able to accommodate various experiments, including bioscience and astrobiology applications, inside of 2U Cubes. Effects of space environment will be investigated on mammalian cells. Use of mammalian cells as experimental material, require much stricter operational and environmental requirements inside payload compartment during duration of experiment, as for example simpler yeast cells. Conducting thesis research, important technological questions regarding component selection and environmental support, which could be also used at designing BAMMSat platform, will be investigated and solved.

3.2 Project objectives

With defined project aims, the main thesis **objectives** can be outlined as:

(1) Literature review.

Within the literature review already presented in Chapter 2, current up to date knowledge and research efforts in the area of CubeSat technology, specially technology for interplanetary flights were investigated. Focus was put on CubeSat platforms with biological experiments onboard. Most important bio CubeSat missions flown to Low Earth Orbit were reviewed, as well as the first interplanetary bio CubeSat mission – BioSentinel, which is planned for the near future. This will be the first life science experiment performed after the Apollo manned space program, flown 50 years ago. Development of the CubeSat platform BAMMSat was also discussed in a subchapter.

In addition to the general literature review in Chapter 2, in research Chapter 4 and Appendix B, general knowledge about different space radiation sources, suitable protection, effects of space radiation on human cells are outlined. Before the methodological part of Chapter 4, space radiation modelling software is selected, introduced and explained.

In Chapter 5, the thermal response of CubeSat geometry with installed components and biological payload compartment with mammalian cells is investigated. Further on, selection of every installed component is theoretically supported and justified. During the thermal modelling process, each individual step is followed and explained in detail. Additionally, in Appendix D thermal environment in space together with different heat transfer models is explained with a review of the literature.

(2) Modelling of the internal radiation environment, inside of the biological payload compartment containing higher forms / a higher form of earth organisms, during the interplanetary CubeSat mission.

(2.1) Selection of the mission scenario for interplanetary CubeSat mission (for example Earth to Mars cruise).
(2.2) Implement radiation modelling.
(2.3) Choose and implement appropriate shielding approach.

(3) Modelling of the ***thermal environment of the interplanetary CubeSat mission suitable for hosting experiments with a higher form of living organisms.***

(3.1) Outline basic design of suitable interplanetary CubeSat spacecraft bus
(3.2) Design realistic thermal model of spacecraft geometry.
(3.3) Implement thermal modelling.
(3.4) Implement modifications to the spacecraft design, with the purpose of optimising thermal control based on a / the thermal model.

3.3 Outline of the project and thesis document

The report in its structure follows the performed thesis project and does not differ from it.

Chapter 1 presents an introduction, focusing on the motivation for the research work conducted. It initially describes the present status of the research field and what the further challenges are which will be investigated in the work. It is briefly explained how the research work is performed during the thesis and what the general aims and objectives are.
Chapter 2 is a literature review, where the concept of CubeSat technology with its special characteristics is outlined. Of special interest were a CubeSat mission with biological experiment payloads which has already flown in the Low Earth Orbit and also a mission planned to fly beyond into interplanetary space. While the research focuses on interplanetary CubeSat missions, this research also aims to contribute to the BAMMSat project which is currently in progress at Cranfield University. It is hoped that the results will contribute to the advancement of the BAMMSat project.

In Chapter 3, the main thesis aims and objectives are developed. On the basis of the previously documented literature review, where up to date discoveries were investigated through the review of scientific papers and other relevant sources. Basic outlines of the project and thesis document are also presented in this section.

Chapter 4 is one of the main research chapters of the thesis work. It consists of a theoretical and methodological part. In the first part, different sources of space radiation and possible protection against it are discussed. The second part of the chapter is the experimental part with performed simulations of the radiation environment for different mission durations, material composition and thicknesses. Results are discussed in the chapters' conclusion. The Results section of the radiation environment chapter presents the initial input for our further work of designing CubeSat model and investigating thermal response.

In Chapter 5 the preliminary geometry design of the interplanetary CubeSat is documented, with the purpose of investigating its thermal response during deep space mission scenarios. Around the payload bay the entire spacecraft bus was developed, with selected components being able to support Interplanetary CubeSat missions. For the designed CubeSat geometry with installed components, thermal analysis at certain locations in the Solar system was performed. Thermal response mainly in the payload compartment with the biological payload was studied and design corrections were suggested. At the end of the section in the conclusion to the chapter the results are presented and evaluated.

Chapter 6 is a presentation of conclusions and a final discussion of performed simulation work, further evaluation of the results and it outlines future short, medium and long term research plans.

3.4. Conclusion

This chapter outlined the main aims and objectives of the project which were performed and investigated during the work. Also the outline of the project and thesis document were discussed for each section.

4 RADIATION ENVIRONMENT IN SPACE

4.1 Introduction

Exposure to space radiation presents one of the main risks for human space exploration in Low Earth Orbit (LEO) and beyond in interplanetary space.

Space radiation is different from radiation we experience on Earth (X - rays, gamma rays and others). It consists primarily of ionizing radiation in the form of high energy charged particles.

Astronauts on long duration missions beyond Earth's magnetosphere will be exposed to radiation levels that will significantly exceed values faced by the crew members in near Earth spacecraft such as International Space Station (ISS).

The aim of the radiation chapter is to overview the knowledge already known about different sources of space radiation and their effect on exposed biological material. Further on two possible construction - shielding materials are introduced, and how their thickness and composition could reduce the amount of space radiation on biological payload on long duration missions.

The first part of the chapter presents a detailed literature review explaining different sources of space radiation, effects of space radiation on exposed biological material and the limits which are set for exposure. Different shielding methods to reduce space radiation are discussed. In the following research sub-chapter, different software tools are introduced which can be used to model radiation in space. Finally, there are performed calculations of the radiation environment inside the CubeSat platform for different materials, their thickness and mission durations based on future planned Mars missions. At the end, results are presented and discussed.

The aim of the radiation environment chapter is to set limits for space radiation exposure of biological material and to investigate which and how thick the material should be in designing the CubeSat platform in order to fulfill mission requirements (Discussed in Chapter 4.3.4.1).

4.2 Review of space radiation relevant to humans in space

4.2.1 Introduction and methodology

This section of the chapter presents the reviewed literature. The aim is to summarize the state of the scientific understanding of different sources of radiation in space, their effects on biological material and possible ways of protecting - shielding against it.

Numerous sources were used to perform the review. The main sources of information presented were reviewed papers, scientific literature, software manuals, tutorials and online available technical documentation including various standards for terrestrial ionizing radiation dose limits.

4.2.2 Source of radiation in space

There are three main natural sources of space radiation (Figure 4-1):

- particles shot into space during solar flares and coronal mass ejections, called **Solar Particle Events (SPE),**
- **Galactic Cosmic Radiation (GCR),**
- **Particle trapped in Earth's magnetic field (van Allen Belts).**

In low Earth orbit, a fourth source, albedo protons and neutrons are sometimes also mentioned. These are secondary particles, produced in interactions between GCR and Earth's atmosphere. Their contribution is small and of low energy and as such not considered as a significant source.

Each of three major sources, make contribution to the primary radiation flux encountered by spacecraft. The relative size, energy and charge distribution of each component are dependent on a large number of parameters including: altitude and inclination of spacecraft's orbit, orientation of the spacecraft relative to the Earth and Sun and the particular phase of the 11 - year solar cycle. Trapped radiation is not found in interplanetary space, but the fluxes of GCR and SPE encountered in interplanetary space are more intense due to lack of Earth's geomagnetic field protection.

Passing through the human body and structure of a spacecraft, primary particles can undergo nuclear interactions, producing wide variety of secondary particles [30].

The space radiation environment in LEO and in interplanetary space

	Galactic cosmic rays	Earth's radiation belts	Solar particle events
Primary composition	98% hadrons { 87% protons; 12% α-particles; 1% heavy ions } 2% leptons (electrons and positrons)	• Electrons <6 MeV • Protons <250 MeV	• Mostly low-energy protons & electrons • Rarely higher-energy protons • Some heavy ions
Effect of solar cycle	• Flux inversely proportional to solar cycle • Solar modulation affects ⩽ 1 GeV/n component	• Solar cycle affects atmospheric scale height and east/west proton anisotropy • Creation of temporary belts during solar max	Frequency and magnitude of SPE proportional to solar cycle • High probability at solar max • Low probability at solar min
Effect of geomagnetic field	Protection in LEO due to cutoff Rigidity, function of geomagnetic latitude	• Raison d'être • South Atlantic Anomaly	Protection in LEO due to cutoff Rigidity, function of geomagnetic latitude
Effect of spacecraft shielding	• Little attenuation through ionization • Projectile and Target Fragmentation by heavy ions • Target fragmentation by protons	• Electrons fully attenuated, some production of Bremsstrahlung • Attenuation of low-energy protons • Target fragmentation by higher-energy protons	• Low-energy protons attenuated • Higher-energy protons and heavy ions can undergo nuclear interactions
Models/predictive capability	Good agreement with measurements • Badhwar/O'Neill • CREME96 (Nymmik)	Electrons: AE-8 (empirical model, old dataset, some refinements) Protons: AP-8 (empirical model, old dataset, some refinements) underpredicts at solar max overpredicts at solar min	Little predictive capability • NOAA Space Environment Center • GOES satellites • Neutron ground monitors
Relative contribution in LEO	• Dominates for high-inclination orbits • ~50% of ISS dose	• Dominates for low-inclination, high-altitude orbits • ~50% of ISS dose	• More severe in higher-inclination orbits • Unknown contribution to ISS Dose
	In LEO, relative contributions from all sources are dependent on orbital parameters (orbital inclination, altitude), spacecraft orientation, solar cycle and temporal variations in the geomagnetic field in a highly complex way.		
Relative contribution in free space	Omnipresent	N/A	Presents potentially large risk, especially during solar maximum
	In free space, relative contributions dependent on solar modulation and spacecraft shielding		

Figure 4-1: Radiation environment in LEO and Interplanetary space [30]

4.2.2.1 Solar Particle Events (SPE)

The Sun is always active with nuclear fusion reaction taking place in its core creating vast amounts of heat, radiation and neutrinos, constantly leaving the surface. But it has been observed that there is a definite periodicity to the level of activity. The complex environment of Sun - Earth space therefore consists of time varying ultraviolet, X - ray, plasma and high particle environments with minimum and maximum phases.

Since the Sun is a gas, its solar magnetic field is convoluted and highly variable, which causes solar events such as sunspots, solar prominences, solar flares and coronal mass ejections. The faster rotation of the Sun's equator causes the magnetic poles of the Sun to swap every eleven years. Before the poles flip, the magnetic fields become warped, causing them to twist in loops outside of the Sun's surface creating solar prominences. When the lines become so tightly twisted, the field lines break, releasing plasma as one of two types of Solar

Particle Events (SPEs) (Figure 4-2), impulsive Solar Flares or Coronal Mass Ejections (CMEs) [32].

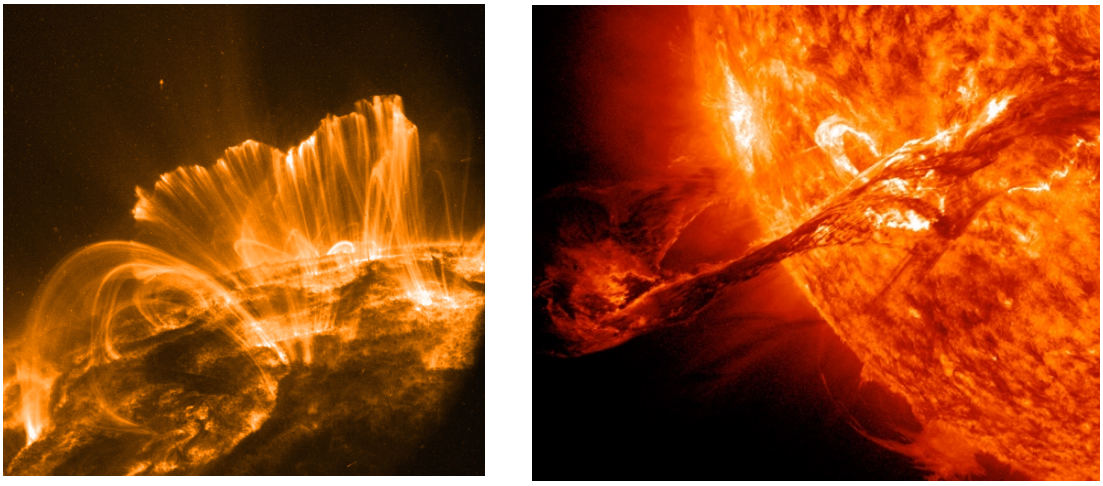

Figure 4-2: Presentation of Solar flares (left) and Coronal mass ejections (right) (NASA)

Solar Particle Events are composed primarily of protons (≈ 92%), helium nuclei (≈ 6%) and smaller part (≈ 2%) of heavy ions and electrons [31].

Events associated with impulsive solar flares are short lived, usually of the order of hours, and are characterized by relative large fluxes of electrons. Total fluence is small, between 10^7 and 10^8 cm^{-2} and these events are restricted to a 30± 45 ° angle in solar longitude.

The second type of SPE associated with large Coronal Mass Ejections is much longer-lived, then the order of days and is characterized by much larger fluxes of protons. Total fluence can exceed 10^9 cm^{-2} and the event can spread over a broad angle in solar longitude extending from 60 ° to as much as 180 °.

Solar particles arrive on Earth in tens of minutes to few hours, depending on their energy. Large events with potentially life-threatening consequences usually occur at the beginning or end of maximum solar activity with a 11 - year cycle. Their build-up can be detected a few minutes before it occurs, since there is an increase of visible lights, X - rays and radiofrequency radiation [30].

The National Oceanic and Atmospheric Administration (NOAA) introduced Space Weather Scales with purpose to describe severity of Solar Radiation Storms in the form of particle flux and energy and their possible effects on people and systems (Figure 4-3) [34].

Solar Radiation Storms			Flux level of ≥ 10 MeV particles (ions)*	Number of events when flux level was met**
S 5	Extreme	Biological: unavoidable high radiation hazard to astronauts on EVA (extra-vehicular activity); passengers and crew in high-flying aircraft at high latitudes may be exposed to radiation risk. *** Satellite operations: satellites may be rendered useless, memory impacts can cause loss of control, may cause serious noise in image data, star-trackers may be unable to locate sources; permanent damage to solar panels possible. Other systems: complete blackout of HF (high frequency) communications possible through the polar regions, and position errors make navigation operations extremely difficult.	10^5	Fewer than 1 per cycle
S 4	Severe	Biological: unavoidable radiation hazard to astronauts on EVA; passengers and crew in high-flying aircraft at high latitudes may be exposed to radiation risk.*** Satellite operations: may experience memory device problems and noise on imaging systems; star-tracker problems may cause orientation problems, and solar panel efficiency can be degraded. Other systems: blackout of HF radio communications through the polar regions and increased navigation errors over several days are likely.	10^4	3 per cycle
S 3	Strong	Biological: radiation hazard avoidance recommended for astronauts on EVA; passengers and crew in high-flying aircraft at high latitudes may be exposed to radiation risk.*** Satellite operations: single-event upsets, noise in imaging systems, and slight reduction of efficiency in solar panel are likely. Other systems: degraded HF radio propagation through the polar regions and navigation position errors likely.	10^3	10 per cycle
S 2	Moderate	Biological: passengers and crew in high-flying aircraft at high latitudes may be exposed to elevated radiation risk.*** Satellite operations: infrequent single-event upsets possible. Other systems: effects on HF propagation through the polar regions, and navigation at polar cap locations possibly affected.	10^2	25 per cycle
S1	Minor	Biological: none. Satellite operations: none. Other systems: minor impacts on HF radio in the polar regions.	10	50 per cycle

* Flux levels are 5 minute averages. Flux in particles·s^{-1}·ster^{-1}·cm^{-2} Based on this measure, but other physical measures are also considered.
** These events can last more than one day.
*** High energy particle (>100 MeV) are a better indicator of radiation risk to passenger and crews. Pregnant women are particularly susceptible.

Figure 4-3: Space Weather Scale for Solar Radiation Storms [34]

4.2.2.2 Galactic Cosmic Radiation (GCR)

Galactic cosmic radiation originates outside the Solar System. Distribution of GCR is believed to be isotropic throughout interstellar space. Energies of GCR particles range from 10 up to 10^{12} MeV and within the solar system GCR spectrum peaks around 1 GeV. The GCR spectrum consists 98% of baryons (protons and heavier ions) and 2% lepton component (electrons, positrons).

The baryon component is composed of 87% protons, 12% helium ions (α particles) and the remaining 1% of heavy ions from Lithium (3) to Uranium (92). Highly energetic particles in the heavy ion component, referred as HZE particles, especially iron nuclei which are relatively abundant compared to the other high Z ions, possess high LET (Linear Energy Transfer – amount of energy that an ionizing particle transfers to the material traversed per unit distance), and are highly penetrating, giving them a large potential for radiobiological damage.

Flux of GCR with energy below about 1 GeV is affected by the Sun's 11 - year

cycle. GCR flux entering the solar system interacts with the solar wind and is partially attenuated. This attenuation is greater during solar maximum when solar wind is most intense [35]. During solar minimum GCR flux is highest because of the reduced effect of solar wind (Figure 4-4). Dependence of GCR flux on solar cycle has important implication for long duration space travel to Mars and the outer solar system [30].

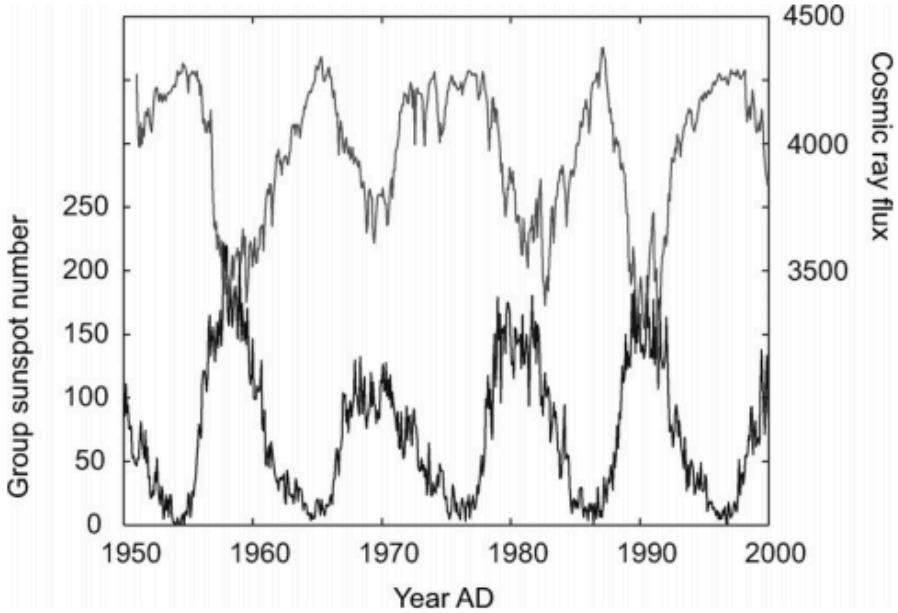

Figure 4-4: Monthly variation of the cosmic ray intensity (count rate) observed by the Climax neutron monitor (upper line) and the group sunspot numbers (lower line) [35]

GCR being composed of charged particles, is also affected by the Earth's magnetic field – charged particles tend to follow the lines of geomagnetic field. Therefore, LEO spacecraft receives its greatest exposure to GCR while near the Earth's poles and a minimum of exposure near the equator.

4.2.2.3 Trapped radiation belt

Radiation belts around Earth were discovered by James van Allen in 1958 during the Explorer 1 satellite mission.

Trapped radiation belts – van Allen belts consists mainly from energetic protons and electrons. These particles are trapped by Earth's geomagnetic field where they follow a complex cyclotron motion around field lines.

Trapped electrons exist in two regions. The first inner zone extends to about 2.4 Earth radii (R_E) and consists mostly of electrons with energy less than 5 MeV. The second, outer zone extends from about 2.8 to 12 R_E and contains electrons with energies up to about 7 MeV (Figure 4-5). The gap between the inner and outer electron belt is referred to as the slot region. Since most of the electron flux is of low energy, it is easily stopped by the shielding provided by the structure of the spacecraft, meaning that trapped electrons present little risk to human health during spaceflight.

Trapped protons occur only in a single region that decreases in intensity as a function of distance from the Earth, starting at 800 km. Trapped protons extend in energy from a few to several hundred MeV and form a broad energy distribution between 150 – 250 MeV and present greater risk of radiation exposure of astronauts inside space vehicles in LEO.

They originate from capturing of solar particles, proton diffusion and from decay of albedo neutrons which are secondary particles from the interaction of GCR with Earths atmosphere.

The majority of the trapped proton belt lie at altitudes above those traversed by the orbit of ISS and other manned flights in LEO. The exception is a region over the coast of Brazil (following the ranges in longitude from – 80 ° to 20 ° and latitude of – 60 ° to 0 °), where the radiation belt reaches down to an altitude of 200 km, caused by the difference in the Earth's rotation axis from its magnetic axis. The region is called the South Atlantic Anomaly (SAA). The SAA impacts astronaut dose LEO space flights. Therefore, for 51.56 ° inclined and 400 km high orbit of the ISS, about half the ionizing radiation dose is from trapped protons in the SAA and half from GCR at higher latitudes [30], [36].

Trapped particles are also modulated by the solar cycle: proton intensity decreases with high solar activity, while electron intensity increase, and opposite is observed with low solar activity [33].

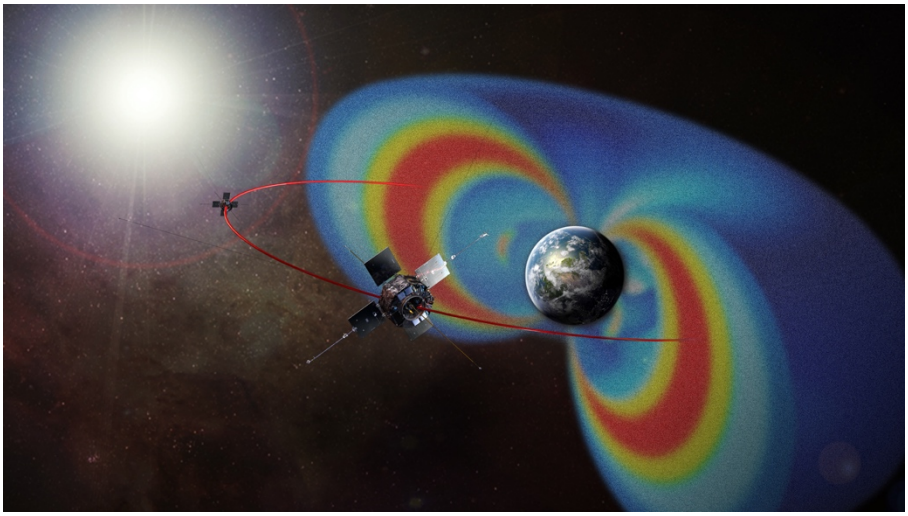

Figure 4-5: Presentation of Earth's space environment with inner and outer radiation belts (NASA)

4.2.2.4 Secondary particles

Most of the energy loss experienced by primary particles as they pass through a spacecraft takes on the form of ionization. Energy of many of these particles entering are sufficiently high and the amount of shielding represented by spacecraft is sufficiently large, that fraction of these primary particles undergoes nuclear interaction with the nuclei from spacecraft material and its contents, producing secondary particles (Figure 4-6).

Depending on the kinetic energy of the primary charged particle, the nuclear interaction can follow in a production of two or more secondary particles.

Secondary particles can be in the form of: protons, neutrons, α - particles and heavy nuclei [30].

Fragmentation occurs in both the projectile, which is usually moving at high speeds, and in the target, which is usually stationary. More energetic secondary radiations are generally produced from the projectile nuclei [37].

The secondary particles produced by target and projectile fragmentation continue to traverse the volume of the spacecraft and may themselves undergo further nuclear reactions.

These products can present a significant fraction of a total mission dose and have an ability to damage critical cellular components when passing through the human body. For an ISS type orbit (51.6 ° inclination, 450 km altitude) estimates of the neutron contribution to astronauts total a dose equivalent range from 30% - 60% [30].

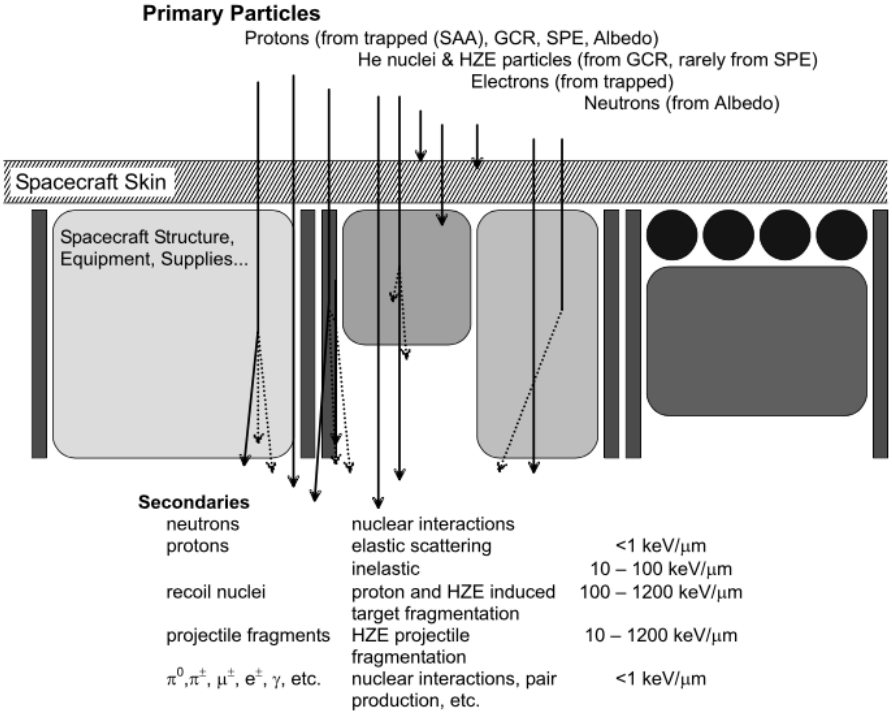

Figure 4-6: The transport of primary radiation through the spacecraft structure and generation of secondary particles [30]

4.2.3 Shielding

As documented, exposure to space radiation has a negative effect on biological material and the human body.

There are two main categories of approaches for shielding humans from radiation in space: passive shielding and active shielding.

4.2.3.1 Passive shielding

Passive forms of space radiation shielding presents placing physical material in between a person and the source of radiation.

The main source of space radiation on long duration interplanetary travel in the future will be presented by galactic cosmic radiation (GCR) and sporadic and intense solar particle events (SPE). With the passive shielding method, shielding is more demanding with high – energy galactic cosmic radiation which is very penetrating.

A thin or moderate thickness of shielding material is generally efficient in reducing the energy of radiation, but as thickness increases, shield effectiveness drops until certain breaking point. This is the result of the production of secondary particles, including neutrons, that are caused by nuclear interactions of the GCR with the shielding material. Secondary particles have generally lower energy, but they can have higher quality factors (W_R) than incident cosmic primary particles. As a result, shielding material must be thick enough to also absorb most of the secondary radiation as well as primaries.

The best shielding materials for space radiation, particularly GCR are dominated by hydrogen. This is because heavy positively charged particles with a lot of energy are stopped primarily by electromagnetic interactions with electrons rather than collisions with nuclei. Liquid hydrogen might be the ideal shielding material from this perspective, but it is difficult to handle and maintain. Among the best practical materials are polyethylene and water [53], [54].

For SPE shielding, the situation is much better (Figure 4-7), the majority of the events can be reduced to low dose levels (<100 mSv) with localized shielding of polyethylene inside a lightly shielded vehicle or habitat [54].

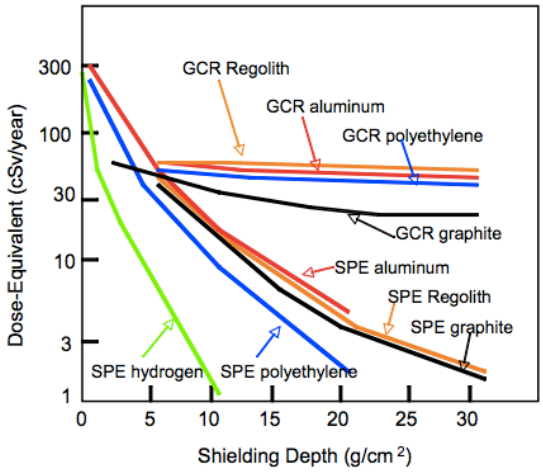

Figure 4-7: Effective dose vs. depth in several materials for GCR at solar minimum and the August 1972 SPE [55]

4.2.3.2 Active shielding

During the 1960' and into 1970', investigations were started related to the feasibility of using active radiation shielding methods, such as afforded by electromagnetic fields, as alternative to passive, bulk material shielding to attenuate space radiations [56]. Active radiation shielding is inspired by the Earth's magnetic field, which serves both to deflect and trap portions of the incoming space radiation. Since the field is still under development, many suggested approaches exist.

4.2.3.2.1 Electrostatic shielding

This approach creates an electric field around an astronaut habitat, with the negative potential facing outwards to slow down negative charged particles and positive closer to the ground to repel positive particles, since radiation comes in both positive and negative charged forms (Figure 4-8).

Engineering challenges considered when designing such a system include the dielectric breakdown strength of the electrostatic material, the maximum voltage

capabilities of the power supply, and the mechanical limits of the support structure in comparison to the internal Coulomb forces generated by the charged components of the shield. There are also unknown major physiological issues associated with humans held inside a large electrostatic field [58].

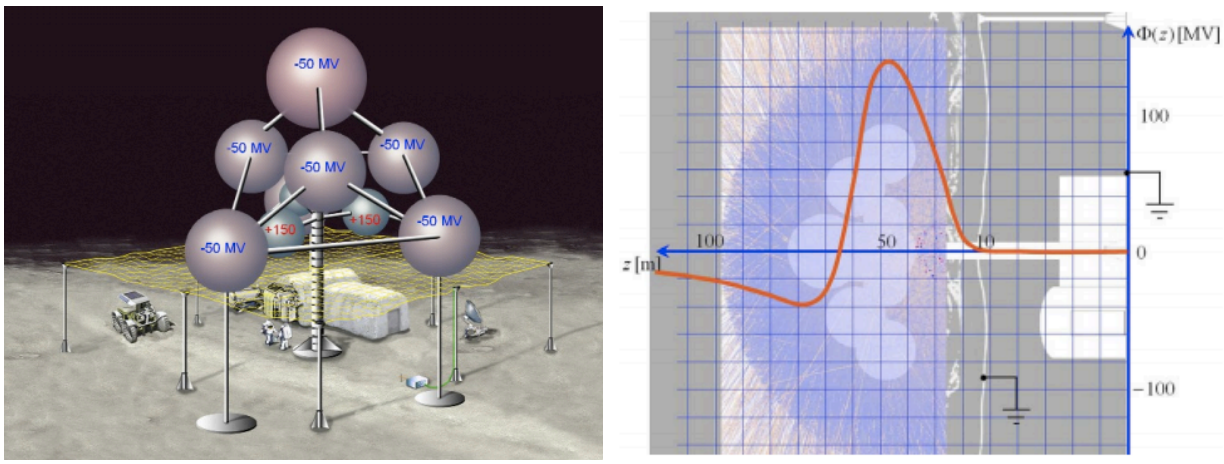

Figure 4-8: Artist's concept of a sphere tree (left), consisting positively charged inner spheres and negatively charged outer spheres. Electric field potential profile (right) along the vertical axis of symmetry (Z - axis) [58]

4.2.3.2.2 Magnetic shielding

Magnetic shielding consists of forming a large magnetic field around the spacecraft, usually through the use of superconducting solenoids (Figure 4-9). Unlike with electric fields, there are known and suspected physiological effects of moving within a strong magnetic field.

In order to use this approach for space radiation shielding, the design must allow for a habitable region without significant magnetic field strength. Usually, this is done by using a torus – shaped design that has a shielded region internal to the torus. These layouts allow for a small region between the solenoids that is free of magnetic fields, while still generating a magnetic field that is comparable to an ideal dipole at large distances. Charged particles are either deflected by the magnetic field, or trapped along the magnetic field lines, well before they approach the internal shield region of the torus. The weak side of magnetic shielding presents the overall mass of the system [57].

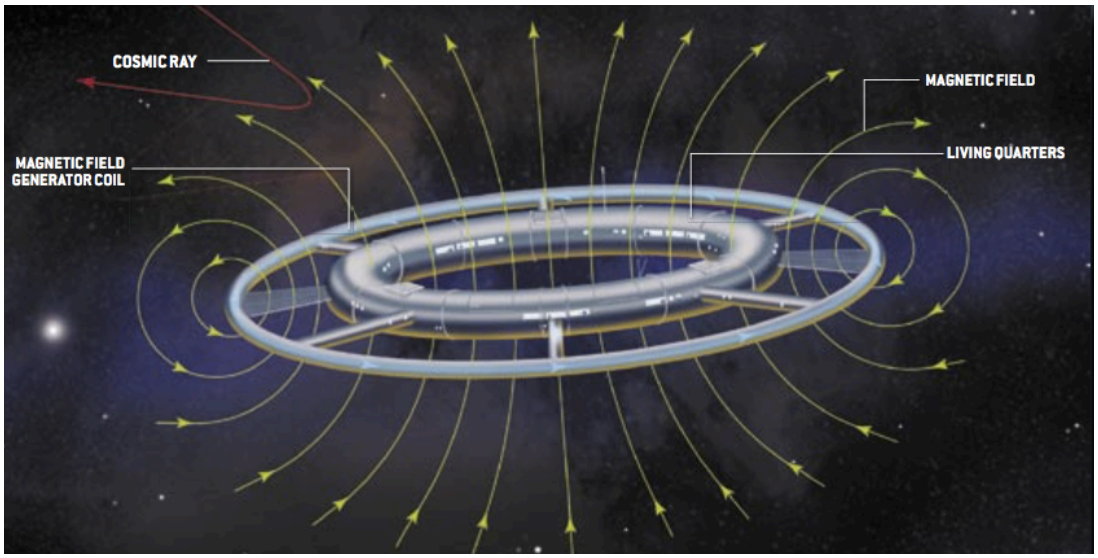

Figure 4-9: Futuristic presentation of Space station with active magnetic shielding [59]

4.2.3.2.3 Plasma shielding

Plasma shields are the most lightweight and least power - consuming of all three presented approaches, which is still technologically immature and in the ongoing research phase.

Fundamentally it consists of a mass of ionizing particles entrapped by electromagnetic fields, swirling around a spacecraft enclosure and serving to deflect charged particles [57].

4.2.4 Conclusion

In Subchapter 4.2 ongoing research state of the art knowledge in area of space radiation was reviewed. As discussed, there are different sources of space radiation which are consequences of different physical phenomena. Some components of radiation are more or less constant with the time location (GCR) while others are limited by location (trapped particles in Earth magnetosphere) and time (Solar particle events). Therefore, understanding the physical mechanism behind the space radiation phenomena is of great importance in designing space missions even more deep space manned mission.

Effect of space radiation on human cells are well known and are needed to be carefully studied. For protecting astronauts from fatal effects of harmful radiation dose limits needed to be set and should not be exceeded. Exceeding dose limits has a fatal effect on living cells and organisms. Therefore, different dose limits were reviewed and further discussed in Appendix B with title Effects of space radiation on biological material.

For long duration interplanetary space missions with humans onboard adequate shielding against space radiation, will be of great importance. In particular passive shielding offers a variety of possibilities with investigating different new materials and their composites, with the intention of determining the optimum ration between shielding characteristics on the one hand and mass and volume values on the other. Both are of fundamental importance, first in keeping living organisms alive throughout the mission and secondly in making missions possible from the perspective of weight and volume budget.

In the next, methodological, subchapter 4.3, knowledge gained in theoretical subchapter 4.2 about the nature of radiation and shielding, will make it possible to select suitable material or composite of materials to protect biological payload, containing human like mammalian cells or organisms, from harmful effects of space radiation during long duration mission in interplanetary space.

4.3 Modelling the radiation environment inside a Bio CubeSat in open space

4.3.1 Introduction and methodology

The aim of the following research subchapter is to model the real radiation environment inside a CubeSat platform in Low Earth Orbit (LEO) environment and in open free space at a distance of 1 Astronomical Unit (1 AU). The results will be broken down into the contributing components (trapped particles, SPE, GCR). Simulations will be performed for the period of solar maximum and solar minimum which effects a strength of GCR. For every mission we also predicted single solar particle event (SPE) eruption.

There are two major online tools available for modelling of space radiation: **SPENVIS (SP**ace **ENV**ironment **I**nformation **S**ystem) developed by the European Space Agency (ESA) and **OLTARIS (O**n-**L**ine **T**ool for the **A**ssessment of **R**adiation **I**n **S**pace) developed by NASA.

For research performed in this thesis, modelling of the radiation environment inside the biological payload compartment of CubeSat was modelled with OLTARIS. Choice of modelling software selection was not made by any clear technical reasons, but was a pragmatic choice by the author, as the user interface during learning phase was much clearer – user friendly, as well was the very efficient and responsive user support from NASA during software installation and later.

4.3.2 SPENVIS

The European Space Agency (ESA) **SP**ace **ENV**ironment **I**nformation **S**ystem (SPENVIS) (Figure 4-10) provides standardized access to models of the hazardous space environment through a user – friendly web interface, available at: http://www.spenvis.oma.be.

SPENVIS is designed to help spacecraft engineers perform rapid analyses of space environmental problems and obtaining reliable results. The platform is based on internationally recognized standard models and methods. It generates spacecraft trajectories using an orbit generator, which allows for creating

multiple segments with mission – based start date and duration. The trajectories may be specific as elliptical, hyperbolic, geostationary, interplanetary, two-line element (TLE) trajectory file or geographical coordinate grid for Earth or other planets.

Apart from radiation and plasma environments, SPENVIS includes meteoroid and debris models, atmospheric models and magnetic field models. The results of a SPENVIS model run are presented in the form of reports and data files.

The radiation sources currently included in SPENVIS are:

- Trapped protons and electrons (implemented through several models: AP-8, AE-8, AFRL models, CRRESPRO and CRRESELE, SAMPEX/PET model, PSB97…)
- Solar energetic protons (JPL-91, ESP total fluence and worst case models and the King model)
- Cosmic rays and solar energetic ions (particle spectra and LET conversion routines based on CREME-86 code)

SPENVIS implements models and tools to estimate various radiation effects such as ionizing doses, solar cell damage equivalent, non-ionizing energy loss (NEIL) for calculating displacement damage effects, single event upset (SEU) rates from cosmic and solar ions and trapped and solar protons. In addition, a geometric tool to calculate shielding distributions for simple spacecraft geometries is available [60].

Figure 4-10: SPENVIS home web platform [61]

4.3.3 OLTARIS

OLTARIS is a web-based program that allows engineers and scientists to assess the effects of space radiation environments on humans and electronics while inside spacecraft, spacecraft, habitats and rovers (Figure 4-12) [62].

There are five basic elements a user must define in order for OLTARIS to perform computation: **(1) radiation environment**, **(2) the geometry of the object** being analysed by program, **(3) the material properties**, **(4) the method of radiation transport** and **(5) the desired response functions (outputs)** that the user wishes to have output to the web interface.

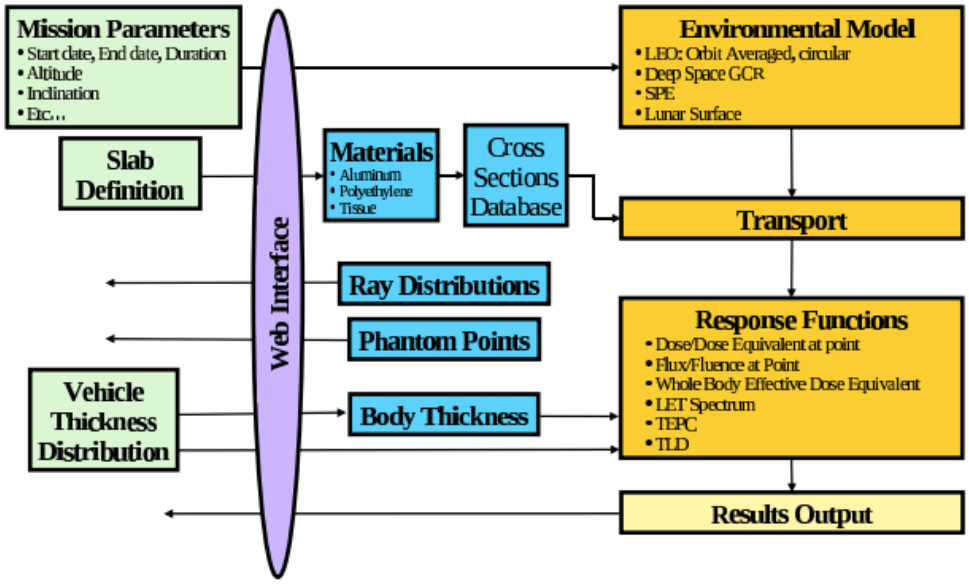

Figure 4-11: Program flow for OLTARIS [63]

Figure 4-11 shows the program and data flow for OLTARIS. The boxes indicate different components or modules of the system. The green boxes indicate the data that the user needs to supply: a slab definition or a thickness distribution of the vehicle, and a mission parameter that will determine how the external radiation environment is computed. The blue boxes indicate data that the user can either download from the web server or data used in the calculations and stored on the execution host. The gold boxes represent the computations which are performed on the execution host and consist of three modules: the environmental model, the particle transport and the response functions. The

environmental model is where the external radiation environment is computed. The output of these environments is a spectral flux or fluence. This flux/ fluence is then used as the boundary condition for transport. The transport module is composed of two paths depending on the type of geometry the user selects, either slab or thickness distribution. Both paths use nuclear transport methods based on HZETRN (High Charge (Z) and Energy TRaNsport) code which was developed by NASA to study the effects of cosmic radiation on astronauts and instrumentation shielded by various materials. The response function model takes the resulting flux/ fluence calculated with the transport module and computes selected responses for each depth of the various materials and the total responses at the end of the slab or at selected location. For thickness distribution an array of response function versus depth curves are computed for the same set of material spatial grids selected for the flux/ fluence transport. The total quantity at a target point is then calculated by integrating over all of the rays. In the case of whole body effective dose equivalent (effective dose) an additional step is performed to combine the vehicle thickness distributions with the body thickness distributions for a large number of target points in a human phantom. The process for calculating the dose equivalent at a single target point is then repeated for each body target point and weighted average of these values is taken. Finally all the results are transferred back to the users account on the website for viewing, plotting or downloading [63].

All simulations presented research work were performed with OLTARIS software. Individual settings and commands will be detailed outlined in next subchapters.

Figure 4-12: OLTARIS web platform [70]

4.3.3.1 Radiation environment

Users can choose from nine pre - defined external radiation environments. Each of these radiation environments are modular combinations of galactic cosmic rays (GCR), solar particle events (SPE), trapped electrons within a geomagnetic field, trapped protons within a geomagnetic field and albedo neutrons. Selection of radiation environments contains:

- **GCR** GCR, Free Space 1 AU
  GCR, Lunar Surface
  GCR, Mars Surface
- **SPE** SPE, Free Space 1 AU
  SPE, Lunar Surface
  SPE, Mars Surface
- **Earth Orbit** Circular Earth Orbit
  User Trajectory
- **Europa** Europa Mission

For research simulations three environments were used: **GCR - Free space 1 AU, SPE - Free space 1 AU and Earth Orbit – Circular Earth Orbit**. The first two present radiation conditions in deep space and with the last one, the radiation environment in the circular low earth orbit (LEO) was modelled.

4.3.3.1.1 GCR environment

The model developed by Badhwar - O'Neill is used as GCR input for OLTARIS. This GCR model is based on fitting the existing balloon and satellite measured energy spectra from 1954 to 1992 and more recent measurements from the Advanced Composition Explorer satellite from 1997 to 2002 with the stationary Fokker-Planck equation. The fit solves the diffusion, convection and energy loss boundary value problem and obtains an estimate of an appropriate diffusion coefficient. These coefficients are seen to fluctuate on a 22 - year period, correlating with the solar minima and maxima. For periods situated in between available data, the correlation of this diffusion coefficient data allows an estimation of the diffusion coefficient for these intermediary times.

The end result of this environment's implementation is a single value of the deceleration parameter, which describes the level of the solar cycle modulation and determines the GCR differential energy spectrum for elements from hydrogen to nickel at any given radial distance from the Sun [63].

GCR environment can be defined in OLTARIS by one of three ways as:

- Historical Solar Min/Max (by choosing one of many historical minimums or solar maximums),
- Enter Date (by entering start and end date for the mission)
- Enter fitting parameter (enter fitting parameter and duration in days) [61].

4.3.3.1.2 SPE environment

Solar Particle Events (SPE) events is a large number of protons accelerated by the Sun's magnetic field. The historical SPE events are in OLTARIS calculated using differential formulas. For SPE environments, time is measured in events, rendering a fluence output. Users can either individually define SPE, or they can be choosen from a list of historical recorded SPE [63]. **For simulations historically recorded SPE from September 1989 were used, with multiplication factor 1.** This event was selected because of its great intensity and other scientific papers already take it as a reference. [47], [64]. It was the intention to gain radiation values for worst case scenarios.

4.3.3.1.3 Earth orbit

For simulating the radiation environment in Earth's Orbit, a circular earth orbit can be selected, or pre – defined by user trajectory data. If the user inputs a custom trajectory, OLTARIS can compute responses averaged over entire trajectory or at each point along the trajectory. For simulations performed during the research, circular Low Earth Orbit (LEO) was simulated (Figure 4-13), with altitude of 600 km and inclination of 0 ° and 30 °.

Inclination was changed because of the presence of South Atlantic Anomaly (area where van Allen belts comes closer to the Earth surface and radiation values are significantly increased), which is much more obvious in higher inclination orbits between 25 ° – 50 °.

Earth orbit radiation environment simulation includes: trapped protons, albedo neutrons and a modulated GCR environment.

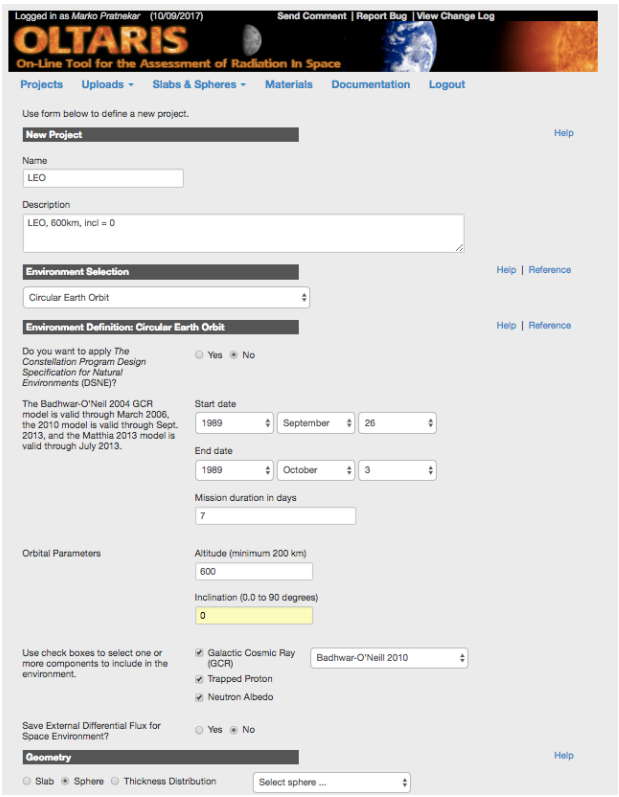

Figure 4-13: Example input for Circular Earth Orbit [70]

4.3.3.2 Geometry

The geometry of an OLTARIS input can be defined in three ways: via a slab or a sphere definition and as a thickness distribution. In examples simulated in research work, only sphere defined geometries were used.

Spheres as well as slabs are defined by any number of materials and any number of layers. The advantage of the sphere geometry is that whole body dose equivalence can be computed. In this case, the flux/ fluence is computed at the center of the sphere and then applied isotropic to the chosen body material of the geometry.

When defining the sphere (Figure 4-14), also material and its thickness needs to be defined (in unit kg/m^2). For research simulations the following were selected:

- Massless sphere (to simulate radiation environment at a given point without any passive radiation protection),
- Aluminium layer sphere (presents simplified CubeSat basic platform),
- Polyethylene layer sphere,
- Aluminium – polyethylene dual layer composit sphere (present CubeSat enhanced protected platform).

The sphere was selected as an approximation to the CubeSat payload compartment geometry, where biological material will be placed. Simulation results could therefore vary slightly from real life situation. As already mentioned the sphere is isotropic geometry while really the geometry of the payload compartment is a box. Nevertheless, the obtained results should not differ in a level to be non-relevant and it is also important all simulations were performed with the same geometry and are therefore comparable among themselves.

All combination of materials were calculated in different thicknesses (details presented in the next subchapter, 4.3.4.1.1).

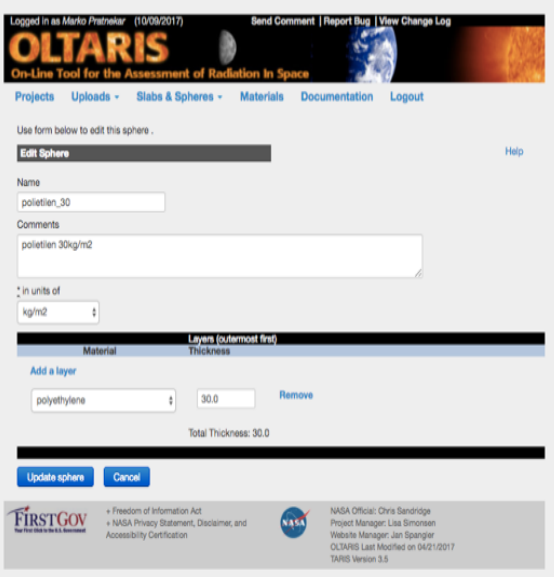

Figure 4-14: Definition of sphere in OLTARIS [70]

4.3.3.3 Material properties

Material properties are an important part of the transport algorithm, presented in next sub-chapter. Materials can be selected from the database available in the program, or by custom definition in terms of elemental mass percentage, molecular mass percentage or by chemical formulation. Material dependent cross sections are used to predict the ways in which neutrons and charged particles will interact. It affects shielding characteristics as well as generation of secondary radiation. List of pre -defined materials available in OLTARIS can be seen on Figure 4-15.

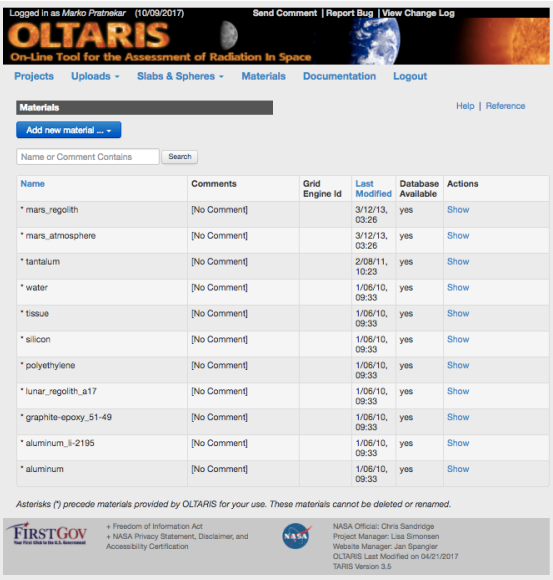

Figure 4-15: List of pre defined materials available in OLTARIS [70]

For the research Aluminium and polyethylene from software pre-defined material database were used.

4.3.3.4 Method of radiation transport

OLTARIS uses HZETRN (High Z and Energy TRaNsport) as the basic particle transport code. It uses a straight – ahead (1 - D) approximation along a ray, that brings in benefit the speed of the calculation, afforded by such approximation. For rays along which particles are propagated through three materials or less, the thickness distribution is calculated by computing flux vs. depth for varying thickness, creating an interpolation table to enable fast calculation along each ray, and afterwards integrating all responses along all rays to determine the total response for the system. This approach ignores certain scattering particles and other minor approximations, which are assumed to be minimal when so few materials are being used.

Thickness distribution with more than three materials, uses ray – by - ray process, in which a full transport with bi - directional neutrons is performed for each ray in the distribution, rather than an interpolation table. In case of slab and spherical geometries, an addition of a coupled bi-directional neutron is included to increase the accuracy of the response, while not substantially decreasing its run time [63].

4.3.3.5 Response function

Once a flux or fluence spectrum as a function of particles and energies is calculated from the Bolzman equation, then that flux has to be modified to represent the response wanted by the user. Currently OLTARIS determines dose, dose equivalent (H_T), thermoluminescence detector (TLD) response, Linear energy transfer (LET), Tissue Equivalent Proportional Counter (TPEC) response, and effective whole-body dose equivalent. For the purpose of our work we calculated dose and dose equivalence on ~~at~~ the inside of the modelled sphere [63].

4.3.4 Simulations

The basic idea of the project is to simulate a specific space radiation environment and to observe its effects on biological material sent into interplanetary space – beyond low earth orbit (LEO) incorporated in a CubeSat platform. As the materials are modelled Aluminium, polyethylene and composition of both with different thickness. All simulations were performed with OLTARIS software. At the end of the chapter results will be presented ~~in~~ and discussed.

4.3.4.1 Overview

4.3.4.1.1 Mission design requirements

To satisfy CubeSat standards, various operational, dimensional, structural and other strict requirements must be fulfilled as already described in the CubeSat design subchapter 2.2.

Following this were basic design guidelines learned from the past (GeneSat, PharmaSat, SESLO/ SEVO, SporeSat, DIDO…) and solutions proposed for future planned (BioSentinel, BAMMSat platform) CubeSat missions. The decision was made for proposing useful payload capacity of **4U**.

On the basis of design limitations, materials and their thickness distribution was chosen for purpose of adequate passive protection against the radiation environment. Aluminium was selected as a primary material, as it presents basic structural material for satellite design. The disadvantage of Aluminium as

a constructing material is, that as an atomic element with high Z number. It generates a reasonable amount of secondary particle radiation. Polyethylene was proposed as an alternative with great hydrogen content and therefore very good shielding characteristics. Secondary particle generation is much lower in polyethylene than in Aluminium.

The simulations were run with various thicknesses independently for **Aluminium (3 mm, 10 mm, 20 mm, 30 mm)** and **polyethylene (10 mm, 20 mm, 30 mm)**, as well as for a combination of both materials together **(3 mm Al – 10 mm poly., 3 mm Al – 20 mm poly., 3 mm Al – 30 mm poly., 6 mm Al – 10 mm poly., 6 mm Al – 20 mm poly., 6 mm Al – 30 mm poly.)**.

The payload compartment with biological material was modelled as a closed geometrical form. As a most suitable geometrical form for space radiation modelling was selected a **sphere** with a single layer (Aluminium or polyethylene with a different thicknesses) or possible multiple concentric layers of polyethylene and Aluminium (polyethylene oriented on the payload side and Aluminium to the open space side) with material thickness discussed above. The advantage of the sphere geometry is that whole body effective dose equivalent can be computed [70]. The radiation flux is calculated at the centre of the sphere where the biological material – payload is placed.

As a reference for natural space radiation, simulation for a **massless sphere** was performed. A way of modelling zero shielding effect as an absence of spacecraft structure and other means of radiation shielding with purpose to calculate space radiation amount received into a volume/ mass of biological material on certain location. In simple it calculates the space radiation biological material would receive freely floating in open space.

4.3.4.1.2 Location and duration of the mission

The proposed mission is designed to study effects of space radiation on biological material as a test platform for long duration human missions in Solar system. The ESA study of human response, limits and needs for a long duration mission to Moon and Mars, called HUMEX (Figure 4-16) [47], was chosen as a reference. Within HUMEX there were also radiation risks, mainly occurring during the interplanetary transfer phase and severely augmented in the case of an eruption of a solar particle event were discussed. In this study two scenarios were proposed: a long - term **1000 days** mission with a 525 day stay on Mars and a short-term mission lasting **500 days** with only 30 days stay on Mars [66] (Figure 4-16). In addition to the HUMEX scenarios, a simulation for **200 days** was also run, which represents a scenario for future long duration Lunar missions.

For the first examples (massless sphere and Al sphere with 3 mm wall) the radiation environment in LEO was also modelled. A **7 day** stay was proposed in a circular orbit with 600 km and inclination of 0 ° (equatorial orbit) and inclination of 30 °, to check for the contribution of South Atlantic Anomaly. Initial calculations and results showed that radiation gained in the LEO in a few days is negligible comparing to radiation exposure during long term interplanetary travel, and that is why it was excluded from further simulations and calculations.

Mission type	Characteristics	Mission phase				Total mission
		Earth–Mars transfer	Stay on Mars	Mars orbit	Mars–Earth transfer	
~1000 days	Duration (days)	225[a]	525	525	204[b]	954
	Crew number	6	4	2	6	6
	EVA number	0	175[c]	0	0	175
~500 days	Duration (days)	179[d]	30	30	248[e]	457
	Crew number	6	4	2	6	6
	EVA number	0	30[f]	0	0	30

[a] Including 7 days in LEO and 14 days in Mars orbit.
[b] Including 14 days in Mars orbit.
[c] Extravehicular activity (EVA), each EVA includes two astronauts for 8 h maximum.
[d] Including 7 days in LEO and 7 days in Mars orbit.
[e] Including 3 days in Mars orbit.
[f] Each EVA includes two astronauts for 8 h maximum, or four astronauts for 4 h.

Figure 4-16: Characteristics of the two Mars missions, selected for the HUMEX study [66]

Different radiation environments are simulated following:

- **Low Earth Orbit (LEO) – Solar MAX/ MIN – material and thickness (mm) – orbit inclination (°)**

Simulations in low Earth Orbit were performed for the period of **Solar Maximum** for a period of **7 days (26.9.1989 – 3.10.1989)** and separately also for the period of **Solar Minimum (15.9.1996 – 22.9.1996)**. Dates were selected on the basis of scientific references for space weather. [64], [67], [68]. 7 days period was selected as a time period spent in Low Earth orbit during preparations for interplanetary transfer to Mars or other Solar system destination.

As a response function was calculated **dose** and **dose equivalence** inside the sphere. Contributed particles are: **galactic cosmic rays (GCR)** and **trapped protons (p^+)** and **neutron albedo (n^0)** of Earth's magnetosphere.

Deep space transfers in 200, 500 and 1000 days were simulated separately for galactic cosmic rays (GCR) and for solar particle event (SPE):

- **Nr. of days – GCR – Solar MIN/ MAX - material and thickness (mm)**
- **Nr. of days – SPE – Solar Min/MAX – material and thickness (mm)**

Both GCR and SPE were simulated as **Free space** at **1 AU**. Simulations on Mars or Moon surfaces were not included, since was intention to get highest values for radiation. Surface time would decrease total values.

For the **GCR** model, the **Solar maximum of 1991** and **Solar minimum from 1997** were chosen. Both values were obtained from the OLTARIS Menu. The GCR is calculated using the Badhwar - O'Neill 2010 model.

For **Solar particle event (SPE)** was used from **September 1989** with multiplication factor 1. The Solar Particle Event at 29 September 1989 began with a large coronal mass ejection on the west limb of the Sun and was one of the strongest in recorded history, producing large intensities of high-energy particles [64]. It was chosen for simulation because of its great intensity. One SPE was calculated for single mission simulation.

4.3.4.1.3 Project radiation dose limit

It was necessary to propose meaningful radiation dose limits for biology payload for the project. The purpose of the planned mission is to expose live material to space radiation and to observe long term molecular damage/ changes within it. With too little radiation affecting biological material, changes will not be substantial enough, and with too much of the radiation, the accepted dose would be fatal for biological material in a very short time.

The goal was to expose a biological payload to a level of radiation above astronaut yearly exposure limiting dose and below the acute dose. Following ~~this~~ these guidelines, for the **lower limit 0.5 Sv** was proposed – as an annual acceptable dose for NASA astronauts in low earth orbit (LEO) [46]. Taking into consideration missions scenarios proposed - 500 and 1000 day mission durations, the limit set at the same value as the annual acceptable dose for astronauts is quite conservative.

For the **upper limit5 Sv** was suggest, where severe symptoms, with 50 – 90% mortality rate occurs from damage to the hematopoietic system, if exposure and radiation sickness not treated properly [51].

In the case that the radiation dose is too low, the thickness of shielding material could be reduced to increase the amount of radiation affecting the biological material.

In the opposite situation, where the radiation dose exceeds the upper set limit, there would be need to reconsider the design of the proposed mission, especially the payload compartment, since the biological experiment might not fit the CubeSat payload platform anymore. Effects of space radiation on biological material and different dose limits are in details discussed in Appendix B.

4.3.4.2 Results of the modelling

Results of the simulation are presented in the form of absorbed dose measured in Grays (Gy) and equivalent dose measured in Sieverts (Sv). Modelled material that the dose is being applied to is biological tissue. The weighting factor used

for calculating equivalent dose is referenced from ICRP60 document [63]. Results of the simulations are presented in Appendix C, with Tables C-1 through C-45.

4.3.4.2.1 Massless sphere

First a massless sphere in Low Earth Orbit (Table C-1) and in free space at 1 AU was modelled, for a different mission duration (Tables C-2, C-3, C-4). This simulation shows the amount of space radiation to which biological payload would be exposed during mission, not being protected by any shielding material.

Discussion:

Simulation was performed for 7 days spent in equatorial (inclination = 0 °) Low Earth Orbit (LEO) at the altitude of 600 km (Diagram 4-1). The massless sphere was simulated, meaning biological material would be exposed directly to the environment.

Highest radiation is shown from trapped protons and albedo neutrons during the period of solar minimum (8.13E+02 mSv) (yellow marker). Contribution from GCR which are also more present during solar minimum is almost negligible. During solar maximum total values are significantly lower than during solar minimum (Table C-1).

With orbital inclination of 30 °, effect of the South Atlantic Anomaly is clearly observable. All values are increased. Mostly notably for trapped protons and albedo neutrons during solar maximum.

Total values are as expected very high mainly on the part of trapped protons and albedo neutrinos, since no shielding material is used. Contribution of GCR radiation component in LEO is minor. In the case of circular equatorial (0 ° inclination) values are very high exceeding the astronaut year limit of 0.5 Sv/y during solar minimum (0.814 Sv) and in the case of more inclined orbit (30 ° inclination) also the acute limit of 5 Sv is almost reached during solar maximum (4.37 Sv) and well exceeded during solar minimum (8.74 Sv) (Diagram 4-1).

Next simulations were performed for open space at a distance of 1 AU, for mission duration of 200, 500 and 1000 days (Diagram 4-2). Contribution of GCR is highly increased (by factor of 2.7) during solar minimum (red marker presents highest value) compared to solar maximum.

Contribution of solar particle events (SPE) is extremely high (violet marker) (Tables C-2, C-3, C-4), because no shielding material is present and would in this case well exceed the acute dose limit. Most of space radiation comes from the SPE component, contribution of GCR part is very small. The Solar particle event (SPE) component is very sensible to any form of shielding material and is significantly reduced with implementation of any material.

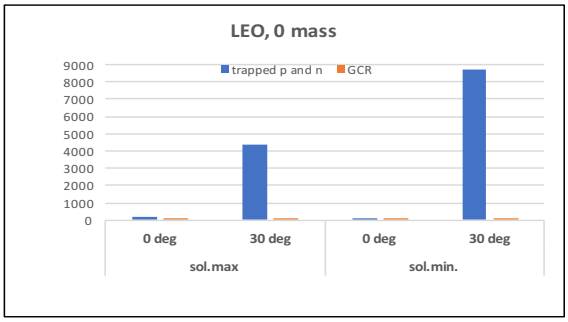

Diagram 4-1: Radiation situation in LEO for massless sphere

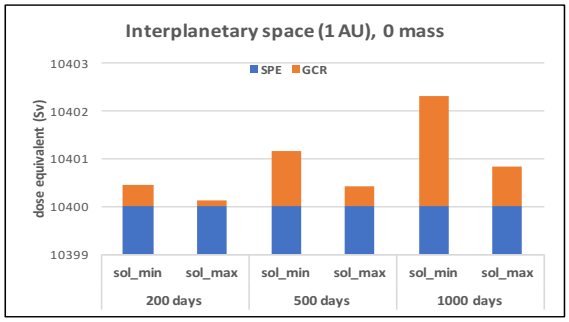

Diagram 4-2:Radiation in interplanetary space (1AU) for massless sphere

4.3.4.2.2 Sphere Aluminium 3 mm (8.1 kg/m^2)

The next set of simulations was performed again firstly in LEO (Table A-5) and the second part in open space (1 AU) (Tables C-6, C-7, C-8) for Aluminium sphere with 3 mm wall thickness and surface density of 8.1 kg/m^2. The effect of the radiation was measured inside the sphere on biological material.

Discussion:

Simulations were performed on the same time scale and in the same location as in the first example. The main difference is that Aluminium sphere with a 3 mm wall thickness was introduced into the simulation set as radiation protection. Aluminium with a 3 mm of wall thickness is considered as basic structure material in CubeSat design.

Value of trapped proton and neutron contribution to radiation drops significantly (factor of 50 – 70) with the presence of shielding. Clearly showing shielding of any kind is a very efficient protection from charged protons and neutron (Table C-1, and Table C-5, yellow marker). Radiation values in LEO falls well below set limits and do not present significant threat for astronaut health anymore (Diagrams 4-3, 4-4).

Comparing to massless sphere, GCR increased in both cases – in LEO as well as in open space. Increase of around 5% compared to no shielding material present is noticed. Increase is a consequence of secondary radiation production in Aluminium walls (Subchapter 4-2-2-4).

GCR alone in open space during all mission scenarios (200, 500, 1000 days) still remains below acute radiation limit (red marker) (Tables C-6, C-7, C-8). Value of SPE also drops significantly with shielding material, from 1.04E+07 mSv to 1.88E+04 mSv (violet marker). Total contribution of GCR part is minor compared to SPE fraction. Acute dose limit is well exceeded in all cases (Diagram 4-6).

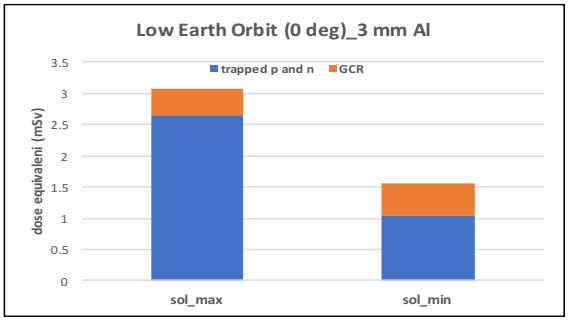

Diagram 4-3: Radiation in Low Earth Orbit (3 mm Al) incl. 0 °

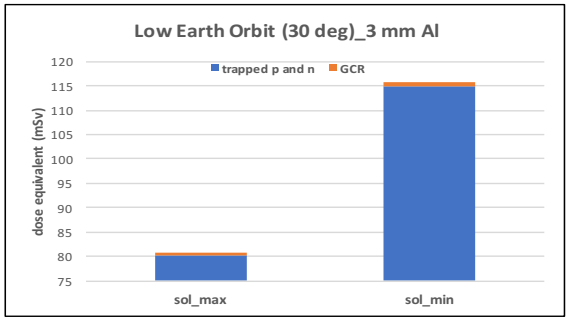

Diagram 4-4: Radiation in Low Earth Orbit (3 mm Al) incl. 30 °

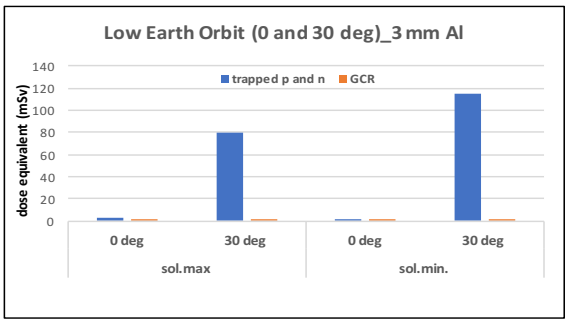

Diagram 4-5: Fractional presentation of radiation components in Low Earth Orbit for 3 mm Al wall thickness, with 0 ° and 30 ° inclination

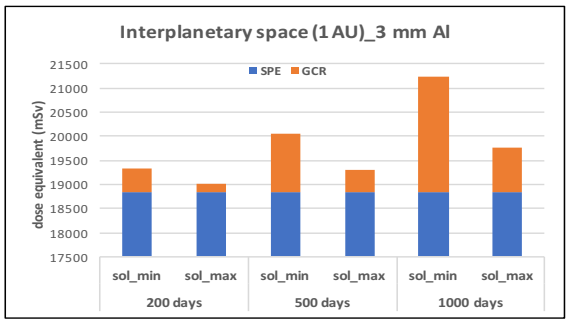

Diagram 4-6: Space radiation at 1 AU for different mission duration (3 mm Al)

4.3.4.2.3 Sphere Aluminium 10 mm (27 kg/m^2)

The following simulations were performed for an Aluminium sphere with 10 mm wall thickness and 27 kg/m^2 surface density. Simulation results are presented in Tables C-9 to C-12.

Discussion:

Next simulation for an Aluminium sphere with a 10 mm thick wall was performed. Values for radiation in Low Earth Orbit drop even further and will be because of their insignificant contribution excluded from further simulations and evaluations (Table C-9).

In the open space scenario, a decrease can be noticed in equivalent dose radiation value, received from the GCR segment, which drops with the implementation of thicker material (Tables C-10, C-11, C-12).

Thicker material also contributes greatly in reducing the effects of SPE. The value is reduced from 1.88E+04 mSv for a 3 mm Aluminium wall to 3.26E+03 mSv at 10 mm of Aluminium (violet marker).

In the long duration scenario, taking into consideration 1000 days in space at solar minimum (bigger contribution of GCR), 2.21E+03 mSv (red marker) of radiation is received from GCR and additional 3.26E+03 mSv from sudden hypothetic solar particle event (violet marker). Total dose in this case would still exceed the acute limit for radiation set at value of 5 Sv. For shorter mission durations (200, 500 days) total values (sum of GCR and SPE) for received radiation dose equivalents are bellow acute limit (Diagram 4-7).

4.3.4.2.4 Sphere Aluminium 20 mm (54 kg/m^2)

Simulations for the Aluminium sphere with a 20 mm wall thickness were performed for deep space mission scenarios. Contribution of space radiation in Low Earth Orbit (LEO) was excluded from further discussion because of its insignificance compared to deep space radiation. Simulation results are presented in Tables C-13 to C-15.

4.3.4.2.5 Sphere Aluminium 30 mm (81 kg/m^2)

An aluminium sphere with a 30 mm wall thickness presents design limit for CubeSat platform. Sole Aluminium material for radiation protection would weigh more than 12 kg and would be from a weight and volume perspective almost unacceptable for CubeSat design. The purpose of this simulation set is more to show effects of thicker metal as radiation protection. Simulation results are presented in Tables C-16 to C-18.

Discussion:

Results for Aluminium spheres with a 20 mm and 30 mm wall thickness are presented. A 30 mm thick wall of Aluminium also presents construction limit for the proposed CubeSat platform (results in Tables C-16, C-17, C-18). Value of equivalent dose decreases further. In the worst case scenario for a 1000 days deep space trip, with 30 mm thick Aluminium and with solar minimum activity, GCR contribution is 1.78E+03 mSv (red marker) and with SPE event of 5.86E+02 mSv. With 20 mm of Aluminium shielding already, part of equivalent dose received from GCR during 1000 day trip with minimum solar activity overtake part from SPE (Diagram 4-8). With thicker material effect of SPE drops significantly. Aluminium is an effective protection against SPE formed radiation. See Diagram 4-11.

Below are graphical presentations (Diagrams 4-7, 4-8 and 4-9) for different components of space radiation (GCR and SPE) in interplanetary space at 1AU for Aluminium spheres with 10 mm, 20 mm and 30 mm of wall thickness. Sole GCR component contribution for different mission durations and different thicknesses of Aluminium material shielding is presented further below in Diagram 4-10. Bigger contribution of GCR component during the solar minimum

can be clearly observed. Solar activity, during solar maximum cycle reduces influence of GCR.

Total contribution of both components SPE and GCR can be checked in Diagram 4-12.

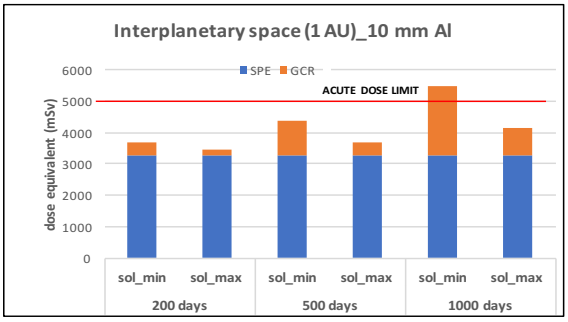

Diagram 4-7: Space radiation at 1 AU for different mission duration (10 mm Al)

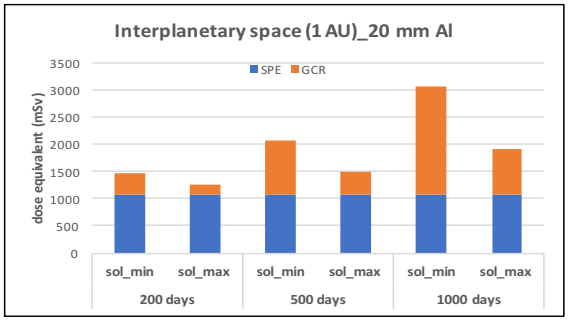

Diagram 4-8: Space radiation at 1 AU for different mission duration (20 mm Al)

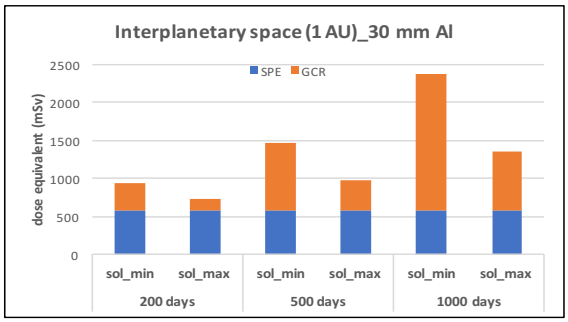

Diagram 4-9: Space radiation at 1 AU for different mission duration (30 mm Al)

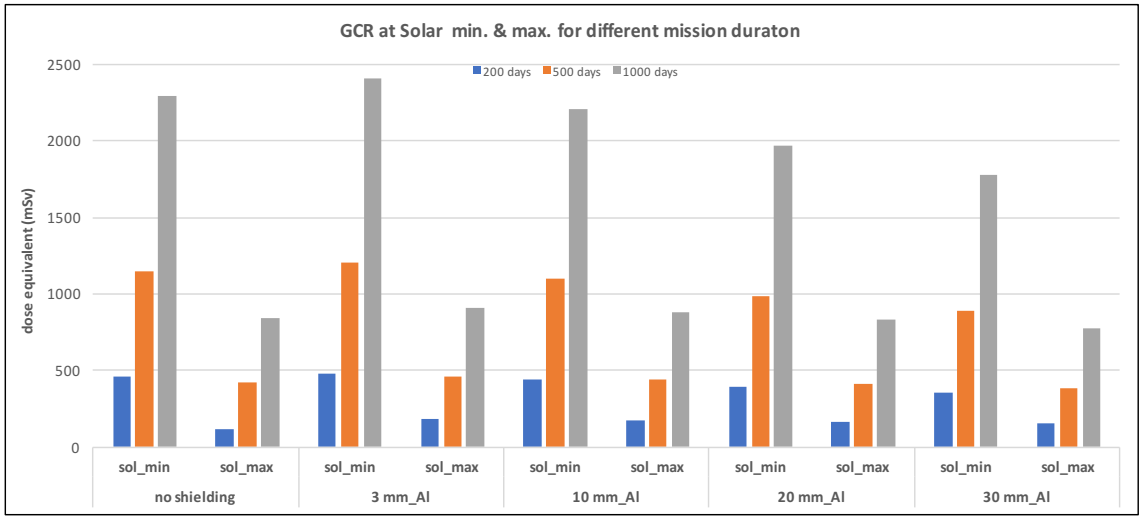

Diagram 4-10: Radiation dose equivalents caused by GCR, for various mission durations for Al sphere with different wall thicknesses

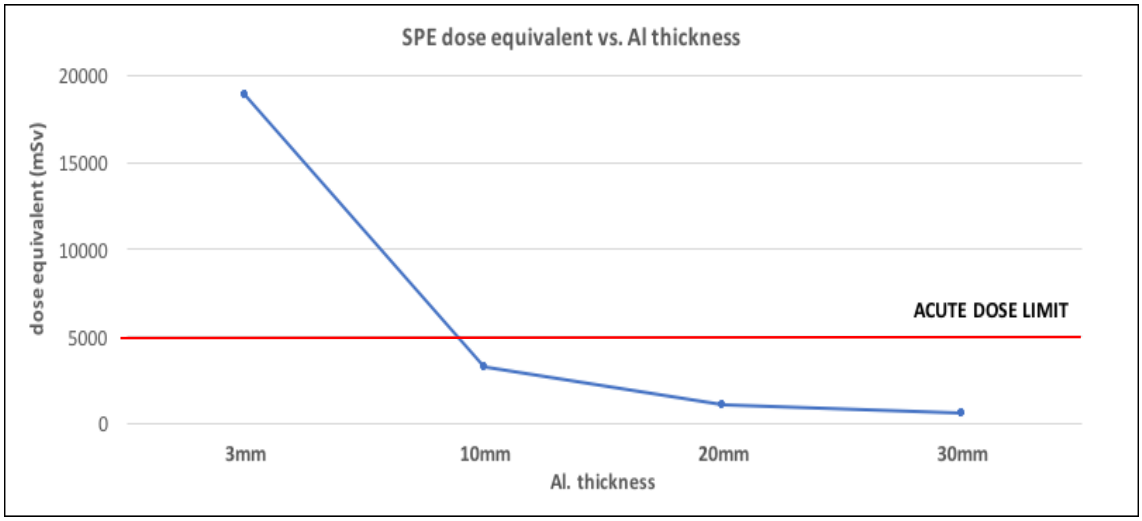

Diagram 4-11: SPE dose equivalent values for different Al shielding thickness

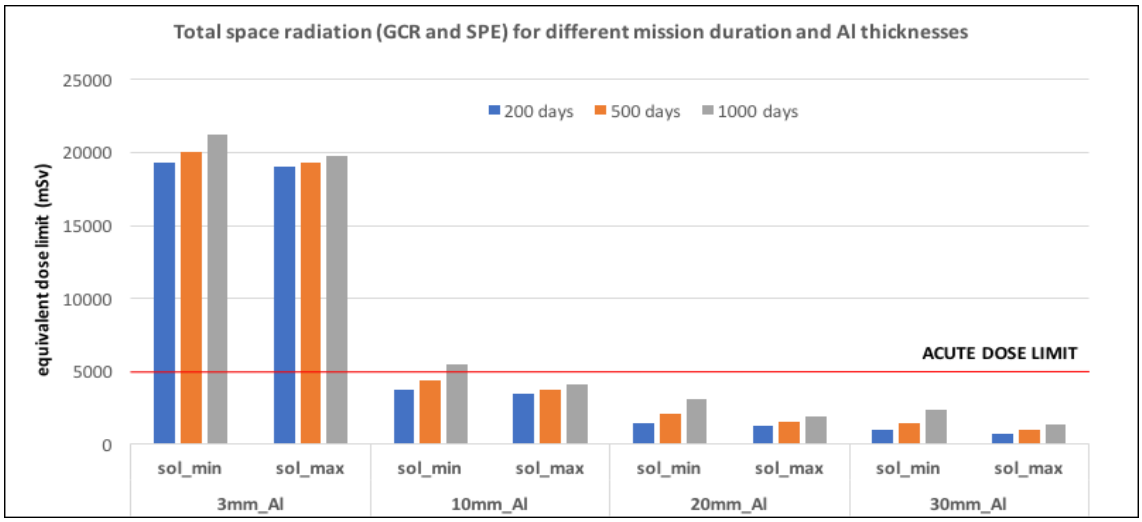

Diagram 4-12: Space radiation (both GCR and SPE components) dose equivalent values for various mission duration for Al sphere with different wall thicknesses

4.3.4.2.6 Sphere polyethylene 10 mm, (9 kg/m^2)

Hydrogen rich materials present one of the best space radiation protection solutions (Figure 4-7), stopping heavy charged particles with a lot of energy by electromagnetic interactions with electrons rather than collision with nuclei. Liquid hydrogen would be an ideal shielding material from this perspective, but it is difficult to handle and maintain. Therefore, one of the most practical materials is hydrogen rich polyethylene. Another benefit polyethylene has is that it is lighter than Aluminium.

In the next set of simulations polyethylene spheres with different thicknesses were modelled as space radiation protection material. Simulation results are presented in Tables C-19 to C-21.

As already explained before, Low Earth Orbit (LEO) data will be excluded from modelling, because of low contribution to overall value of space radiation.

4.3.4.2.7 Sphere polyethylene 20 mm (18 kg/m^2)

Simulations made for 20 mm thick polyethylene sphere for different deep space missions at 1 AU. Simulation results are presented in Tables C-22 to C-24.

4.3.4.2.8 Sphere polyethylene 30 mm (27 kg/m^2)

Presented are results for the polyethylene sphere with 30 mm wall thickness. Simulation results are presented in Tables C-25 to C-27.

Discussion:

A further set of simulations was performed with polyethylene. Polyethylene is considered as a good material for space radiation protection because of its high content of hydrogen molecules, as well as being much lighter (density ≈ 900 kg/m^3) compared to Aluminium (density ≈ 2700 kg/m^3).

Comparing polyethylene with Aluminium of the same thickness, very similar radiation protection characteristics can be noticed, for the GCR component. (Diagrams 4-10, 4-16). Generation of secondary particle radiation is also not observed when using polyethylene. What is more noticeable is the increase in the SPE related radiation (violet marker) component when same thickness of shielding material is used, Aluminium or polyethylene (Diagrams 4-17, 4-18). At the same surface density (kg/m^2) polyethylene provides better radiation protection, but what represents a problem in space engineering and especially in CubeSat design, where volume constraints are important, is need for greater thickness of the shielding material, consequently losing precious space for payload.

For interplanetary missions (Diagrams 4-13, 4-14, 4-15), values of received acute dose equivalent of radiation are exceeded in every case, except for 30mm of polyethylene protection. With this thickness of polyethylene protection, during the longest duration 1000 days mission, with low solar activity (solar minimum) the SPE component drops below the GCR part (Table C-27, difference between violet and red marker). Red and violet markers present maximum values for the SPE and the GCR parts.

As shown in diagram 4-19, where total values for the sum of GCR and SPE is presented, with 20 mm of polyethylene during a 1000 day mission and low solar activity, acute dose limit is just exceeded. With 20 mm of Aluminium, values are way below acute dose limit (Diagram 4-12).

Using 30 mm of polyethylene, equivalent doses remain below acute limit, but such a thickness of a shielding material already presents geometrical limit for

designing of payload compartment and would not be practical to be used in CubeSat design.

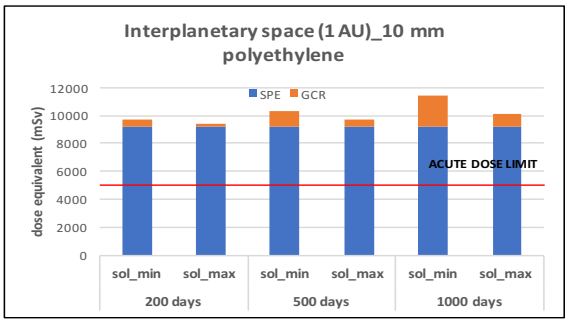

Diagram 4-13: Space radiation at 1 AU for different mission duration (10 mm poly.)

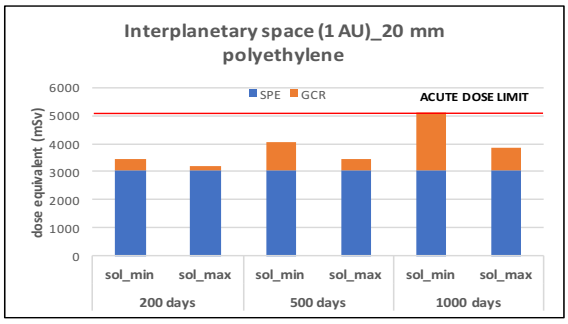

Diagram 4-14: Space radiation at 1 AU for different mission duration (20 mm poly.)

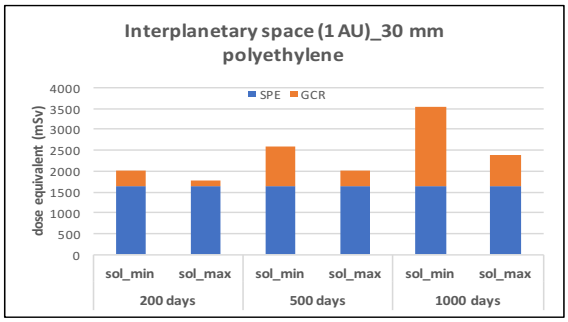

Diagram 4-15: Space radiation at 1 AU for different mission duration (30 mm poly.)

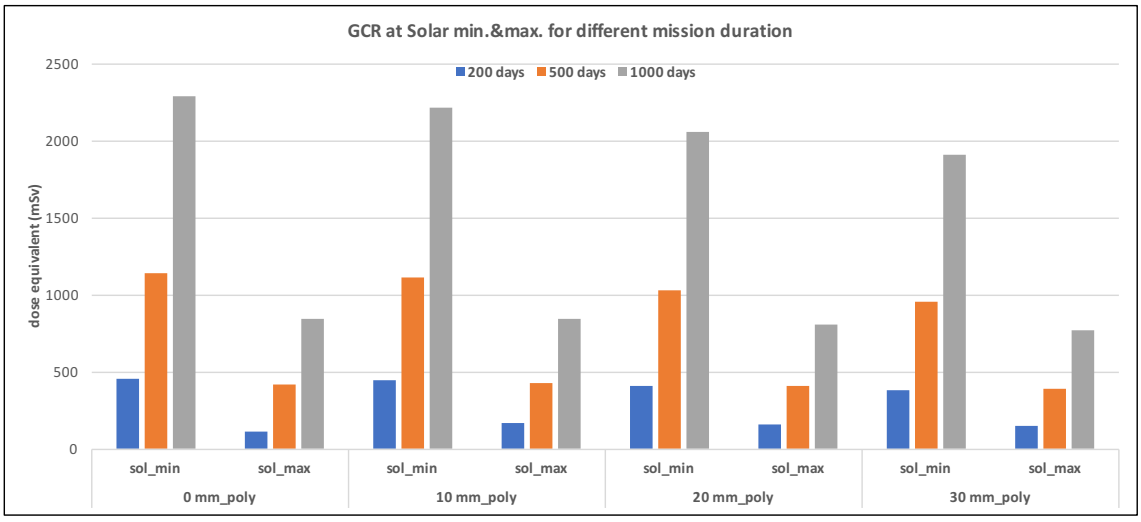

Diagram 4-16: Radiation dose equivalents caused by GCR for various mission durations for polyethylene sphere with different wall thicknesses

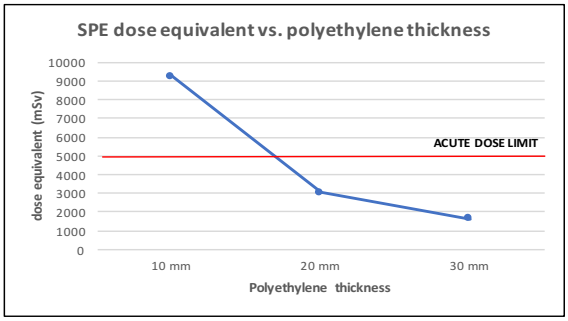

Diagram 4-17: Dose equivalent caused by SPE component for different polyethylene thicknesses

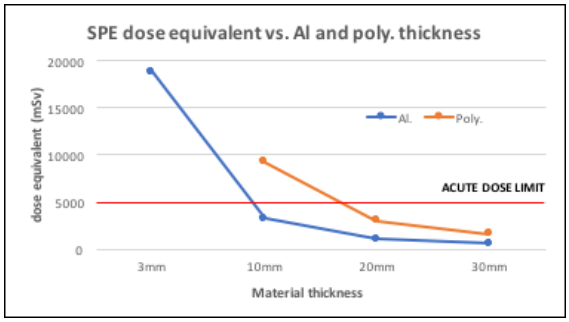

Diagram 4-18: Dose equivalent caused by SPE component for different Al and polyethylene thicknesses

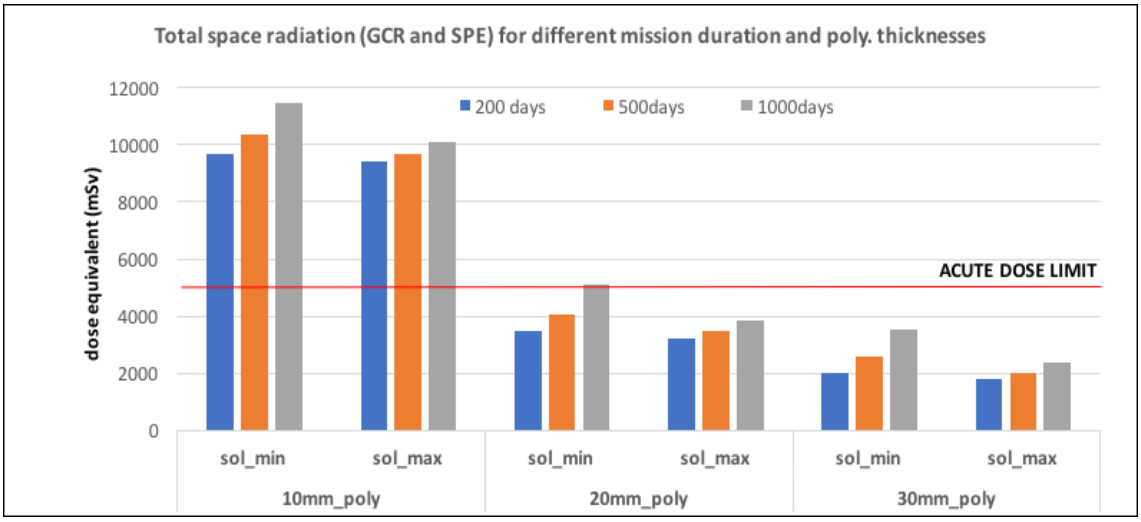

Diagram 4-19: Space radiation (GCR and SPE components) dose equivalent values for various mission duration for Al sphere with different wall thicknesses

4.3.4.2.9 Sphere Aluminium 3 mm+polyethylene 10 mm

Aluminium is considered as a basic construction material in the space industry, having good radiation protection characteristics, but when being exposed to space radiation it generates secondary particles (Subchapter 4-2-2-4). Polyethylene offers also good radiation protection, without producing secondary particles, but because of its low density, greater dimensions are required.

Next a set of simulations was performed for Aluminium - polyethylene composite material with different thicknesses, to investigate optimum thickness

for most efficient protection from space radiation. Red and violet markers present maximum values for specific component of radiation.

In first simulation set (Tables C-28 to C-30) a sphere with 3 mm Aluminium wall was modelled, facing to the open space and 10 mm of polyethylene oriented to the payload.

4.3.4.2.10 Sphere Aluminium 3 mm+polyethylene 20 mm

Next a simulation set was performed for composite of 3 mm Aluminium and 20 mm polyethylene. Simulation results are presented in Tables C-31 to C-33.

4.3.4.2.11 Sphere Aluminium 3 mm+polyethylene 30 mm

Results of simulation with composite material assembled of 3 mm Aluminium and 30 mm of polyethylene. Simulation results are presented in Tables C-34 to C-36.

4.3.4.2.12 Sphere Aluminium 6 mm+polyethylene 10 mm

In next simulations, the thickness of Aluminium as base material was increased to 6 mm with 10 mm of polyethylene as radiation protection. Simulation results are presented in Tables C-37 to C-39.

4.3.4.2.13 Sphere Aluminium 6 mm+polyethylene 20 mm

Simulation results of composite material made of 6 mm Aluminium and 20 mm of polyethylene. Simulation results are presented in Tables C-40 to C-42.

4.3.4.2.14 Sphere Aluminium 6 mm+polyethylene 30mm

Simulation results of composite material made of 6 mm Aluminium and 30 mm of polyethylene. Simulation results are presented in Tables C-43 to C-45.

Discussion:

Knowing the positive and negative effects of both materials, it was decided to model composite of both materials together in different dimensions. On the basis of structural requirements Aluminium was modelled for the outside layer and polyethylene for the inside. It was used 3 mm and 6 mm of Aluminium with different combinations of polyethylene. Dimensional limits were set regarding on structural and engineering limits which are needed to be fulfilled with CubeSat platform.

With first combination (3 mm Al+10 mm polyethylene) radiation limits were exceeded already with 500 days mission (Diagram 4-20). With almost the same GCR contribution SPE part is much higher comparing to solo 10 mm Aluminium.

Already with 3 mm Al and 20 mm polyethylene composition values stays below set limit for acute dose (Diagram 4-22). With further increase of polyethylene thickness by 10 mm - (3 mm Al and 30 mm polyethylene) (Diagram 4-24) values drop further. Also with (6 mm Al+10 mm polyethylene) (Diagram 4-21) values remain bellow set limit of 5 Sv of acute dose equivalent limit. Same is for thicker polyethylene layer in combination with 6 mm of Aluminium base (Diagrams 4-21, 4-25).

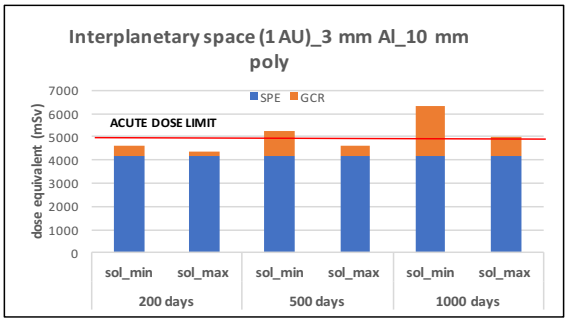

Diagram 4-20: Space radiation at 1 AU for different mission duration (3 mm Al+10 mm poly.)

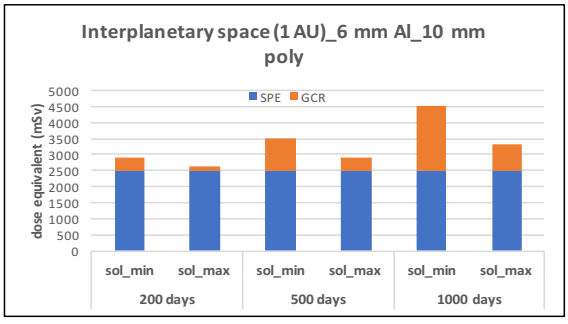

Diagram 4-21: Space radiation at 1 AU for different mission duration (6 mm Al+ 10 mm poly.)

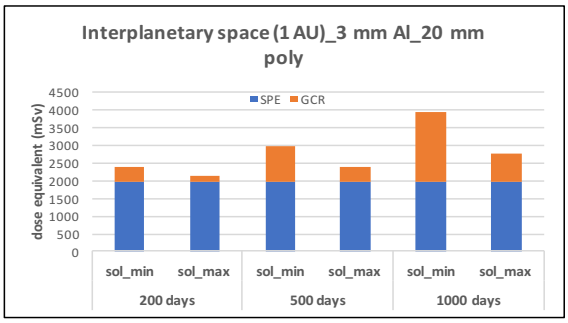

Diagram 4-22: Space radiation at 1 AU for different mission duration (3 mm Al+ 20 mm poly.)

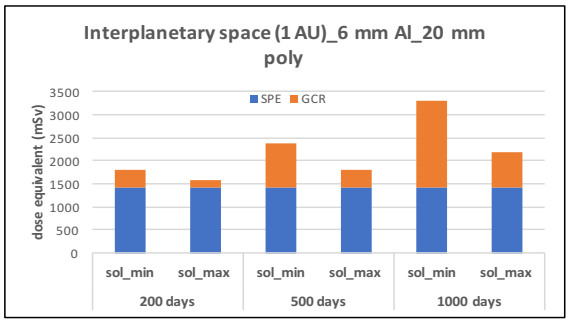

Diagram 4-23: Space radiation at 1 AU for different mission duration (6 mm Al+ 20 mm poly.)

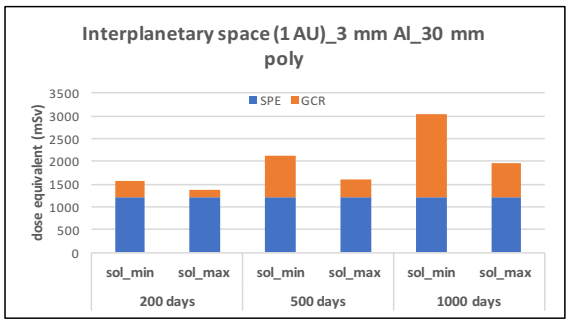

Diagram 4-24: Space radiation at 1 AU for different mission duration (3 mm Al+30 mm poly.)

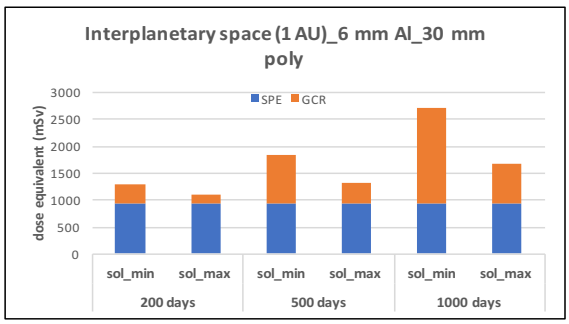

Diagram 4-25: Space radiation at 1 AU for different mission duration (6 mm Al+30 mm poly.)

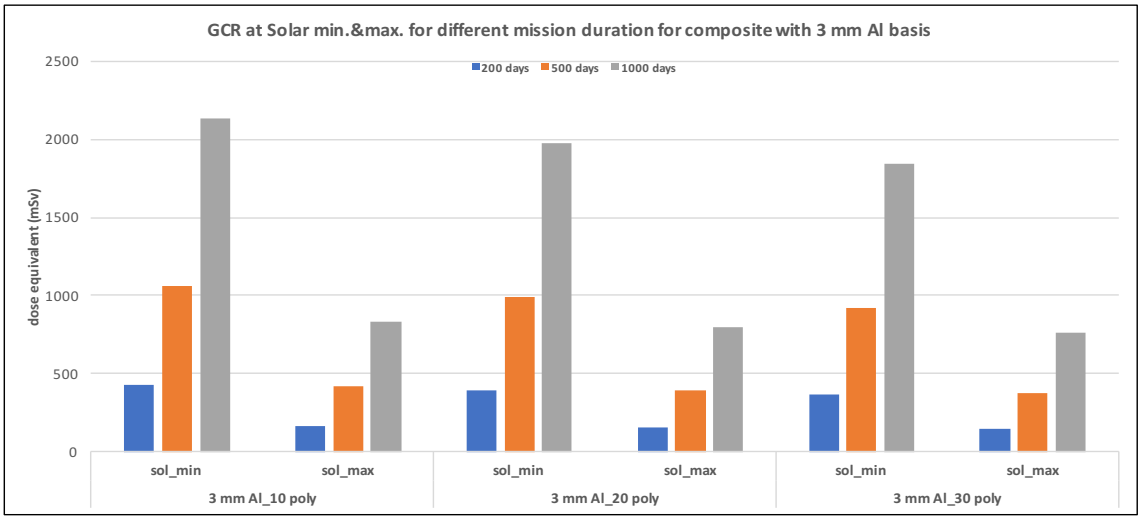

Diagram 4-26: GCR dose equivalent values for different mission durations for 3 mm Al basis composite

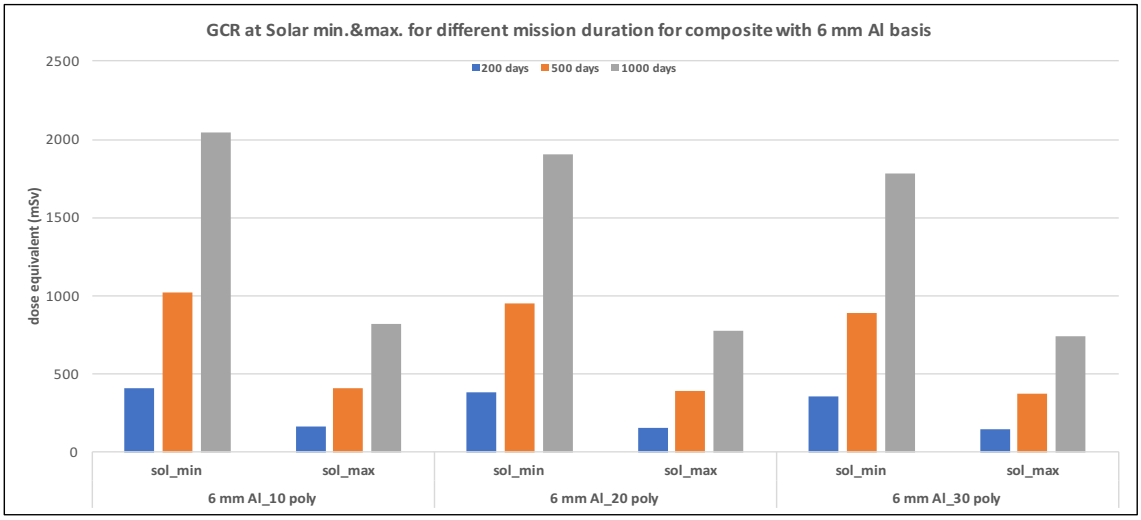

Diagram 4-27: GCR dose equivalent values for different mission durations for 6mm Al basis composite

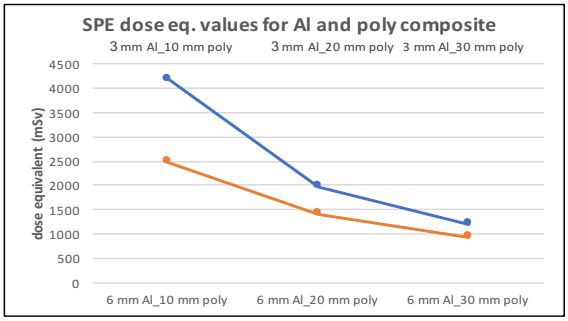

Diagram 4-28: SPE dose equivalent for 3 mm and 6 mm Al base composite

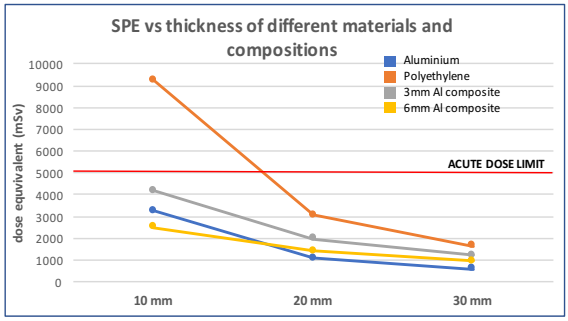

Diagram 4-29: SPE dose equivalent for different materials

The GCR component does not drop significantly between the 3 mm and 6 mm of Aluminium base in composite material (Diagrams 4-26, 4-27). More significant is the drop in SPE component (Diagram 4-28, 4-29), for composite material with 3 mm Aluminium base when the layer of polyethylene is increased from 10 to 20 mm.

A final set of simulations was performed to distinguish the difference in protection against GCR components for similar values of surface density (kg/m^2) for Aluminium and polyethylene.

It can be seen from the simulations (Diagrams 4-30, 4-31), that at same surface density (kg/m^2) polyethylene offers slightly better radiation protection, due to

weaker secondary radiation production. Expectedly, the value is more significant during long duration missions.

Modelling results for the same thickness of both materials (Diagrams 4-32, 4-33) is also presented. At 10mm thickness there is not a significant difference in the GCR radiation protection ~~also~~ even in long duration missions. At bigger thickness Aluminium offers better shielding.

It can be concluded that polyethylene of the same dimension and three times lower mass offers almost same protection against only GCR radiation, but it provides much weaker protection against SPE regarding Aluminium.

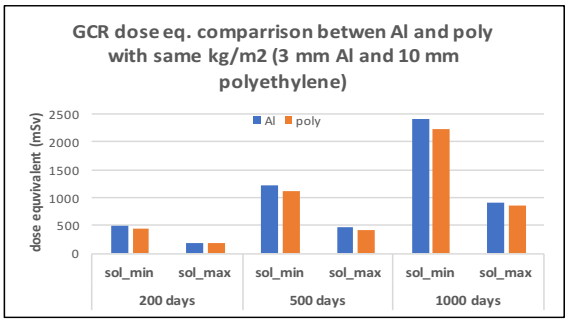

Diagram 4-30: GCR dose equivalent for same kg/m^2 for 3 mm Al and 10 mm polyethylene

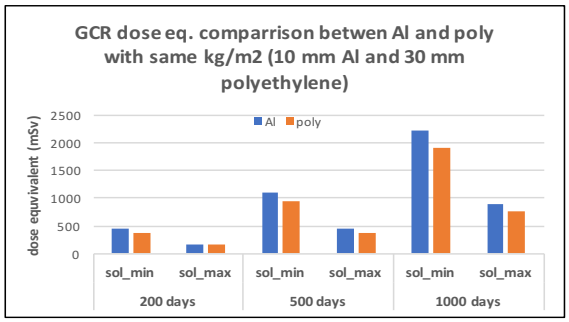

Diagram 4-31: GCR dose equivalent for same kg/m^2 for 10 mm Al and 30 mm polyethylene

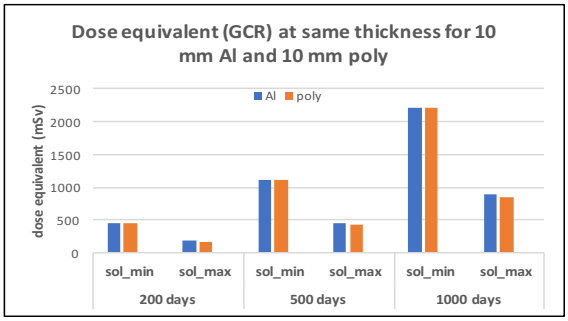

Diagram 4-32: GCR dose equivalent for same thickness of 10 mm for Al and polyethylene

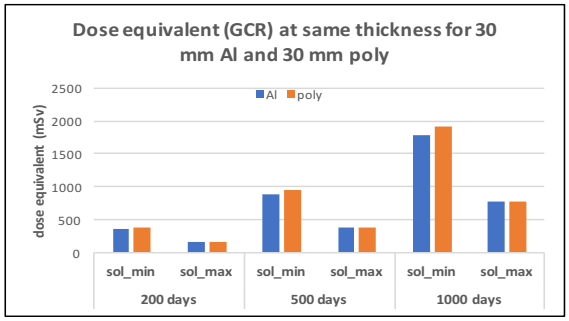

Diagram 4-33: GCR dose equivalent for same thickness of 30 mm for Al and polyethylene

4.3.4.3 Comparison of the space radiation simulation results with similar CubeSat mission

The BioSentinel CubeSat mission serves in many ways as a reference for mission designed within this thesis. Therefore, it seems also most appropriate to compare values of space radiation obtained with simulations (Chapter 4.3.4), with values which are expected during the BioSentinel mission.

The minimum expected value of space radiation (GCR and SPE), that the BioSentinel payload will be exposed to in 12 months is presented in Figure 4.17.

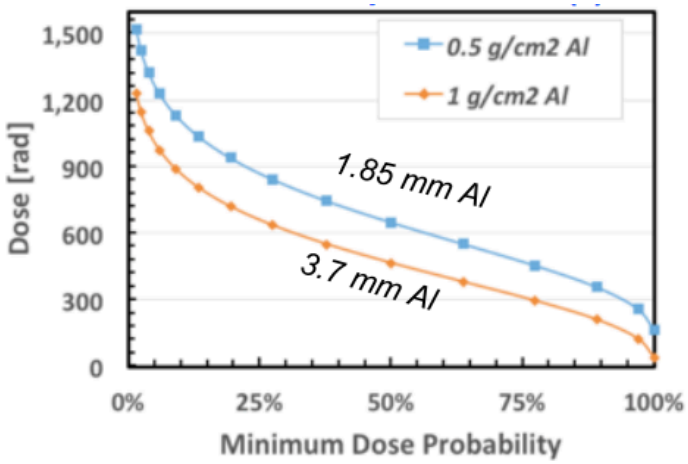

Figure 4-17: Total radiation dose expected in 12 months (GCR and possible SPE) [106]

Presented is a minimum dose probability during 12 months' mission duration with 1.85 and 3.7mm of Aluminium radiation protection. As can be seen in the diagram, there is 0% probability that the radiation dose will reach 1200 rad (12 Gy) and 100% probability the radiation dose will be around 50 rad (0.5 Gy). A large variation in value is a consequence of Solar Particle Event (SPE) contribution, which is main contributor of radiation, but its appearance is hard to predict [106].

Values can be compared and evaluated with simulations performed for a 500 days mission and 3mm of Al radiation protection (Subchapter 4.3.4.2.2 and Table 4-7). For the solar minimum, the value for GCR is 0.196 Gy and the SPE

contribution is 8.77 Gy. The total value being around 9 Gy, which presents around 10% probability for a minimum dose, if interpreted from Figure 4-17.

This mean that the model which was used with OLTARIS simulations performed in this research work would set statistical probability of receiving 9 Gy of radiation during a 500 day mission, if protected with 3mm of Aluminium to 10%. Written differently, only in 1 out of 10 missions the received radiation dose would be 9 Gy or higher. Meaning that the results obtained through the simulation work in this thesis are on the side of caution.

It must be pointed out that simulated values for space radiation are of similar order and therefore comparable. For more accurate evaluation of results more exact data about Solar Particle Event used at the radiation calculation for the BioSentinel mission would be needed as well as there are differences regarding mission duration (500 days vs. a year) and thickness of shielding material (3 mm vs. 3.7 mm).

4.3.4.4 Conclusion of space radiation modelling

The purpose of different simulation scenarios was to find out, which material in what combination and thickness would be able to fulfil the set requirements regarding radiation dose limits for biological payload, which were set before in the Chapter 4.3.4.1.3.

During the mission it is desirable for biological material inside the payload compartment to be exposed to certain amounts of space radiation, being able to study its effects on living cells. At the same time the radiation dose should not be too high - acute, to fatally damage biological material.

Specific and strict engineering design requirements standard for the CubeSat platform should also be followed at all times during the construction processes.

Based on the simulation results it can be concluded that dimension wise, Aluminium, considering it also as the basic construction material for the CubeSat platforms, the radiation requirement limits can be fulfilled with a thickness of just a little over 10 mm for longest the 1000 day mission. Aluminium is also a very efficient material for protection against solar particle events (SPE).

Polyethylene, having lower density, presents weaker protection against SPE, therefore thicker layers are needed in order to offer the same value of protection – above 20mm, if wanting not to exceed acute dose limit.

Regarding mass of the material, Aluminium being three times denser ~~as~~ than polyethylene it is also three times heavier for the same thickness and area covered.

Knowing the benefits and weaknesses of both materials, simulations with the composition of Aluminium and polyethylene in different thickness were also performed. Taking into consideration simulations and the construction requirements of the CubeSat platform, it was shown, that the optimum combination would be a composite made of 3 mm Aluminium, since it is already the basic construction material for the CubeSat platform, which would be further coated with an additional 20 mm of polyethylene. Radiation values remain below value of 4 Sv through all mission scenarios.

The combination presents a good compromise regarding mass, dimensions and engineering limits for the CubeSats.

For further work it would be very interesting to study radiation protection characteristics for more different materials. Graphite for example seems a good alternative regarding protection, mass and volume (Figure 4-7).

5. DEVELOPING A THERMAL MODEL FOR A BIO CUBESAT FOR INTERPLANETARY MISSION

5.1 Introduction

Leaving Earths protective atmospheric layer and entering outer space, every living being – astronaut, material or spacecraft component is exposed to extreme conditions which includes: micro gravity, high energy radiation, possible micrometeoroid impacts, exposure to extreme temperatures and many other effects.

The thermal environment is one of the most important factors to be considered when designing a space mission. Placed in open space above the protective shield of the Earth's atmosphere materials and components are exposed to extreme thermal environment with high and low temperature extremes and big fluctuations during the time period.

Temperatures within satellite or spacecraft depends on several factors which must be taken into consideration when designing a mission. Besides the environmental factors such as: attitude and altitude of the spacecraft (Low Earth Orbit, Moon Orbit, Deep space mission,...), absence of the surrounding atmosphere, various solar effects, also geometrical design, optical properties (presenting ratio between absorbed and emitted radiation), connecting interfaces between installed components, internal electronic heat sources and many other factors are of great importance for the thermal environment established inside the satellite or spacecraft.
In this study, designing an Interplanetary CubeSat mission with biological payload, sufficient shielding against space radiation in open space, as well as maintaining desired temperature in the payload compartment with biological samples present the greatest importance. Designing appropriate protection against space radiation was widely discussed in Chapter 4. Based on the material and dimensional selection made to fulfil adequate radiation protection for the interplanetary mission, in the following chapter thermal control analysis is performed.

Thermal control analysis contains the simulation of satellites geometry with its components placed in the space environment in order to obtain temperature values, especially for the payload compartment where the biological samples will be placed. On the basis of thermal analysis, which is performed using the modelling software ESATAN - TMS, which is widely used in the space industry as well as by space agencies for performing thermal simulations, acquired results are studied and analysed, additionally further steps and mission design are recommended.

In Appendix D and E are collected further information regarding Spacecraft Thermal modelling and creating of the TMM model in ESATAN-TMS.

5.2 Creating custom 6U CubeSat in ESATAN - TMS

5.2.1 Introduction and methodology

On the basis of Radiation environment simulations, performed in Chapter 4, and known constraints and special technological requirements for CubeSats, initially the geometry needs to be defined and orbit parameters specified for the Interplanetary Bio CubeSat mission, to allow further thermal modelling.

The main aim is to determine the Thermal environment to which the biological payload will be exposed during transfer flight to Mars. In order for the biological payload sample to survive, temperature constraints are set to 4 ºC or 37 ºC, depending on the biological material sample.

In Chapter 4 the effects of space radiation on biological material were studied, and it was defined that composite of 3 mm Al and 20 mm of polyethylene would offer adequate radiative protection for the biological material to remain below the acute radiative dose limit throughout the mission duration to Mars (Subchapter 4.3.4.1.2). This information is one of most important inputs and must be taken into consideration in the early stage during the designing process.

For the Interplanetary CubeSat mission special requirements are set for installed components. Special attention is needed at designing: power system, telecommunication module, orbit and attitude control and spacecraft autonomy. All this should be taken into account during component selection and geometry design.

Providing adequate radiation protection in the payload area and at the same time being able to accommodate components which will support a spacecraft on a long duration interplanetary flight, it was clear from the initial calculations, that at least a 6U CubeSat would be required. Consequently, the main source for the preliminary design solutions and component selection was the NASA BioSentinel BioCubeSat Interplanetary mission which is planned to fly in the near future. It will conduct the first study of biological response to space radiation outside LEO in over 40 years (with the exception of late Chang'e – 4

mission), since the last Apollo flight [83]. During the BioSentinel mission, effects of radiation will be studied on lower forms of living organisms (yeast cells). The Biological payload to be studied within this thesis presents highly advanced mammalian cells which are more comparable to human cells and therefore present better comparison and matching with human organisms. Mammalian cell samples are also much more demanding regarding environmental conditions and radiation protection than lower life form cells. This also presents the main difference between the BioSentinel mission and the mission proposed within this thesis work.

Another source of design solutions presented is the BAMMSat, interplanetary 2 Unit (2U) CubeSat platform which is under development at Cranfield University in collaboration with other research institutions and universities in UK [86].

On the basis of various input information, particularly due to the thickness of the radiation shielding material which would significantly reduce the useful volume of the payload compartment, it was decided that at least 4U are required for the biological payload experiment together with radiation protection. 2U will host the spacecraft bus. Therefore 6 unit (6U) CubeSat platform, which should be able to meet all requirements regarding the flight mission and payload limitations was selected.

In the subchapter to follow, CubeSat geometry design, material selection, design of the payload bay and proposal of suitable spacecraft components with its heat dissipation are outlined. The Spacecraft will be placed in circular equatorial orbits around the Sun, at a discrete distance from 1.1 to 1.5 AU, where thermal conditions will be monitored and studied within different spacecraft components and biological payload. Discrete distances were selected as distance from Earth to Mars – from 1 AU to 1. 52 AU.

5.2.2 Geometry and structure

Reference for design solutions and component selection was the NASA BioSentinel 6 Unit BioCubeSat Interplanetary mission (Figure 5-1) which is scheduled to fly in the near future (end of 2020). The BioSentinel was selected

as one of the secondary payload missions to fly on the first Space Launch Systems (SLS) platform. The primary objective of the BioSentinel is to detect, measure and correlate impact of space radiation to monocellular eukaryotic organism – yeast, over a long duration period beyond Low Earth Orbit (LEO). Initially spacecraft will be deployed to a lunar fly-by trajectory and further into a heliocentric orbit [83], [84], [85].

Thermal control presents a great challenge for the Interplanetary CubeSat mission. Traditional thermal insulation like MLI, blankets and surface coatings which are used for regulating incoming heat and avoiding excessive heat dissipation in order to maintain the operational temperature limits of spacecraft subsystems and payload, are needed to be combined with active control systems (heaters) for more effective and precise thermal regulation [87].

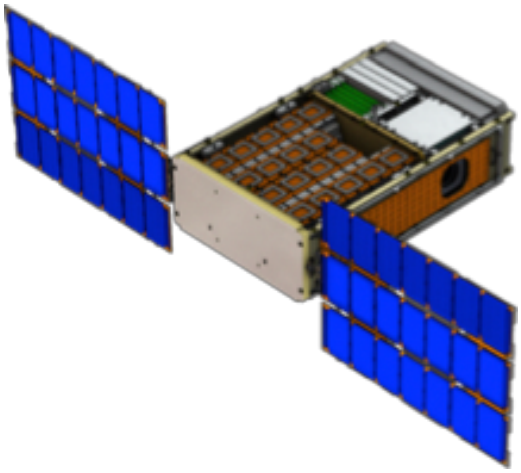

Figure 5-1: BioSentinel 6U BioCubeSat with visible components [85]

As already pointed out earlier in the text, the purpose of this research work is to check if suitable environmental conditions in the form of radiation and temperature, can be maintained within the CubeSat platform, to enable it to host biological experiments with a higher form of living organisms during the interplanetary mission. The BioSentinel will carry a lower form of living cells – yeast cells, which are not so demanding as mammalian like cells, proposed within this thesis work.

Strict temperature requirements to be maintained for the payload bay are set between **37 ºC** and **4 ºC**. These temperatures present typical limits for general bioscience experiments.

Active as well as passive thermal control will be used. Three different thermal paint coating options will be used as a passive thermal control:

- **Option 1:** Black anodised Aluminium coating for the satellite body with a graphite composite on the back side of solar cell panel – **basic design**.
- **Option 2:** Black anodised Aluminium coating for the satellite body with gold paint coating on the back side of solar cell panel.
- **Option 3:** Gold paint coating the body with gold paint coating on the back side of solar cell panel.

Option 1 presents basic geometry design without any specific optical coating laid on the outside surfaces. The CubeSat body is constructed from black anodised Aluminium, and the solar panels base material is graphite. Option 2 design is similar as Option 1, the with exception of the back side of the solar panels which are laid with gold paint coating. The solar panels are due to orientation, dimensions and construction suspected to be exposed to the biggest temperature changes. Therefore, the back side of panels was covered with thermal protective coating. With Option 3, all outside surfaces, with the exception of the solar cells upper side are cowered with gold paint coating. Gold paint coating has very similar optical properties as Kapton foil (see Appendix A, for optical properties of materials). Paint coating was used instead of Kapton foil, to prevent possible difficulties and pinching during the deployment process of the CubeSat.

Designing the 6U CubeSat mission one needs to follow the design requirements which are published in the CubeSat Design Specifications for 6U CubeSat [88]. Basically, 6U CubeSat presents a block with outer dimensions of 200 x 100 x 300 mm. Although X and Z axes can be slightly increased as stated in the standard. Therefore, the basic dimensional and weight requirement for 6U CubeSat design are:

- **Dimensions (X, Y, Z) -> 226.3 mm x 100 mm x 366 mm (± 0.1 mm)**

- **Mass < 12 kg**

These limits present main constraints for the geometry design. Additional constraints connected to this thesis project are:

- payload bay material composite: **3 mm Al and 15 mm polyethylene**

Within 6 unit (6U) design, 4 units (4U) will accommodate payload compartment and 2 units (2U) are prescribed for spacecraft bus.

The purpose of the 4U payload compartment is to accommodate biological material together with instruments needed for analysing samples and the system for controlling and maintaining environmental parameters. All is housed inside the radiative protective structure made of 3 mm Al and 15 mm polyethylene. During space radiation simulations, as optimum protection was calculated as a composite of 3 mm Aluminium and 20 mm polyethylene. After further discussion and interpolation of the simulation results between 20mm and 10 mm of polyethylene layer in composite with 3 mm Al, it was decided to reduce the thickness of protective polyethylene layer in payload bay from 20 mm to 15 mm.

Purpose for this action was not to waste too much of the space available for the experiment, but at the same time still maintaining the required level of space radiation protection. Further calculations show that the useful volume of 4U payload compartment containing 3 mm Al and 15 mm polyethylene as radiation protection would actually be reduced to around 2U of useful space for the experiment (Table 5-1). Thus, the experiment setup developed for the BAMMSat platform (Chapter 2.3.3) could be successfully implemented within this mission.

200 mm x 200 mm x 96 mm	**100%**
3 mm Al + 15 mm polyethylene	**43%**
3 mm Al + 20 mm polyethylene	**32%**

Table 5-1: Payload compartment useful volume available with different radiation protection

Within the 2U bus all the required spacecraft components are placed including: batteries, communication system, computer and data handling, integrated navigation and guidance control unit and propulsion system. Enlarged deployable solar arrays are mounted at the side of satellite body.

All installed spacecraft components need to withstand special conditions during interplanetary flight, which are much more demanding than conditions in LEO. Special consideration is needed in the designing of: power system unit, telecommunications, attitude control, data storage and others. On the basis of design requirements, a simple geometric model was created, with rough dimensional parameters of satellite body and suggested installed components. The model presented a base platform for design in ESATAN – TMS thermal modelling software (Figure 5-2).

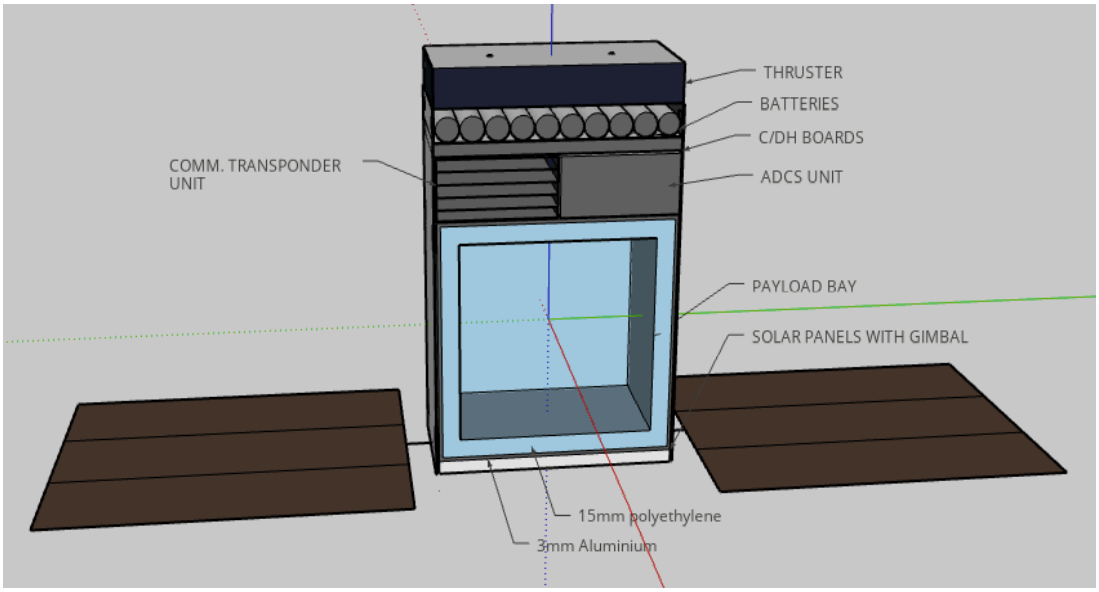

Figure 5-2: BioCubeSat basic 3D model with basic components and their Z - axis dimension

5.2.2.1 Structure

In this subchapter basic dimensions of the model and installed components are outlined. Aim is to check if designed geometry fulfils CubeSat specification requirements set for 6U [88]. The description and discussion regarding the selection of installed components follows in the next section.

The structure of the satellite has two main tasks. The first is to protect the satellite from the harsh conditions of the space environment and second to ensure rigid structure for all components and the payload during the whole mission period.

The detailed CubeSat structure with all parts like: frames, ribs and steel rods for holding components, steel screws, hexnuts, washers and spacers was not possible to model in detail.

The satellite body was modelled as four side shear panels and two end shear panels which are on the edges set together in perfect contact. Each geometric surface was divided into nods for more detailed thermal modelling (Figure 5-3, 5-4). Main body panels were divided to 5 x 10 nodes and end shear panels were divided into 5 x 5 nodes. The distribution of nodes is detailed enough to enable appropriate tracking of temperature values and gradients along the surfaces and at the same time do not require too much computer processor power for solving. Panels are made from single material – 1 mm thick black anodised Aluminium (Al 7075). Instead of panel gain antenna could be installed on the frame.

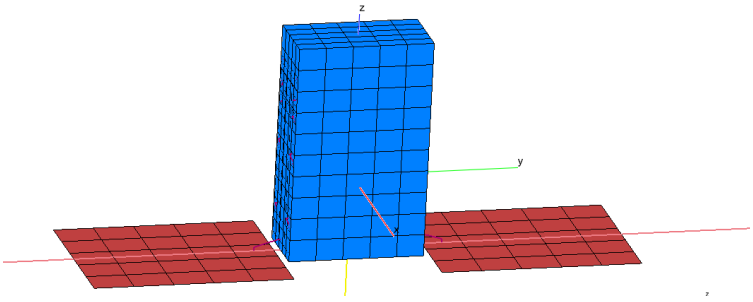

Figure 5-3: CubeSat ESATAN-TMS model structure (ESATAN - TMS)

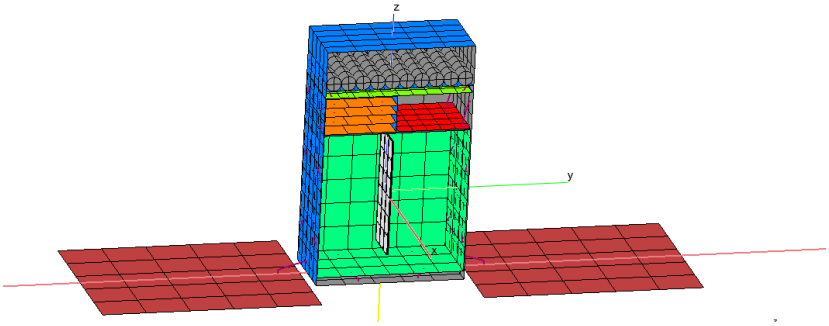

Figure 5-4: CubeSat ESATAN-TMS model structure with removed front and payload cover displaying internal components – different colours (ESATAN-TMS)

On the lower part of the satellite body folded solar panels are installed (Section 5.2.2.2.1). During the launch phase, panels are stored on the side of the body. Once the satellite is released from the launcher they are opened and spread by the guiding gimbal mechanism.

The Biological payload (Section 5.2.2.7) is placed in a 2U by 2U container, together with experiment instrumentation and radiation protection. Special environmental conditions are needed to be maintained (Figure 5-2).

Above the payload are set two components side by side. On the right is attitude determination and control system unit (ADCS) (Section 5.2.2.3) and on the left is located Deep Space Transponder used for Telecommunications (Section 5.2.2.4).

On top of these two components are set computer boards (C&DH), responsible for command protocols, on board data handling and data processing (Section 5.2.2.5).

The electrical power gained from solar panels is stored in battery pack (Section 5.2.2.2.2) – composed from 10 Li - Ion battery cells set together in a module with all required electronics.

On top of the geometry is placed thruster subsystem, enabling greater corrections on spacecraft track or orbit (Section 5.2.2.6). The components layout is presented in Figure 5-5. The component selection is discussed and described further in this section of the thesis.

Thruster	30 mm
Battery module	25 mm
Command Board	10 mm
Comm. and ADCS components	50 mm
Payload	200 mm
Solar panel gimbal	10 mm
Spacing	5 mm
TOTAL Z – axis	**330 mm**

Table 5-2: Dimensional calculation of components for Z - axis

Figure 5-5: ESATAN – TMS Geometry Model with selected components

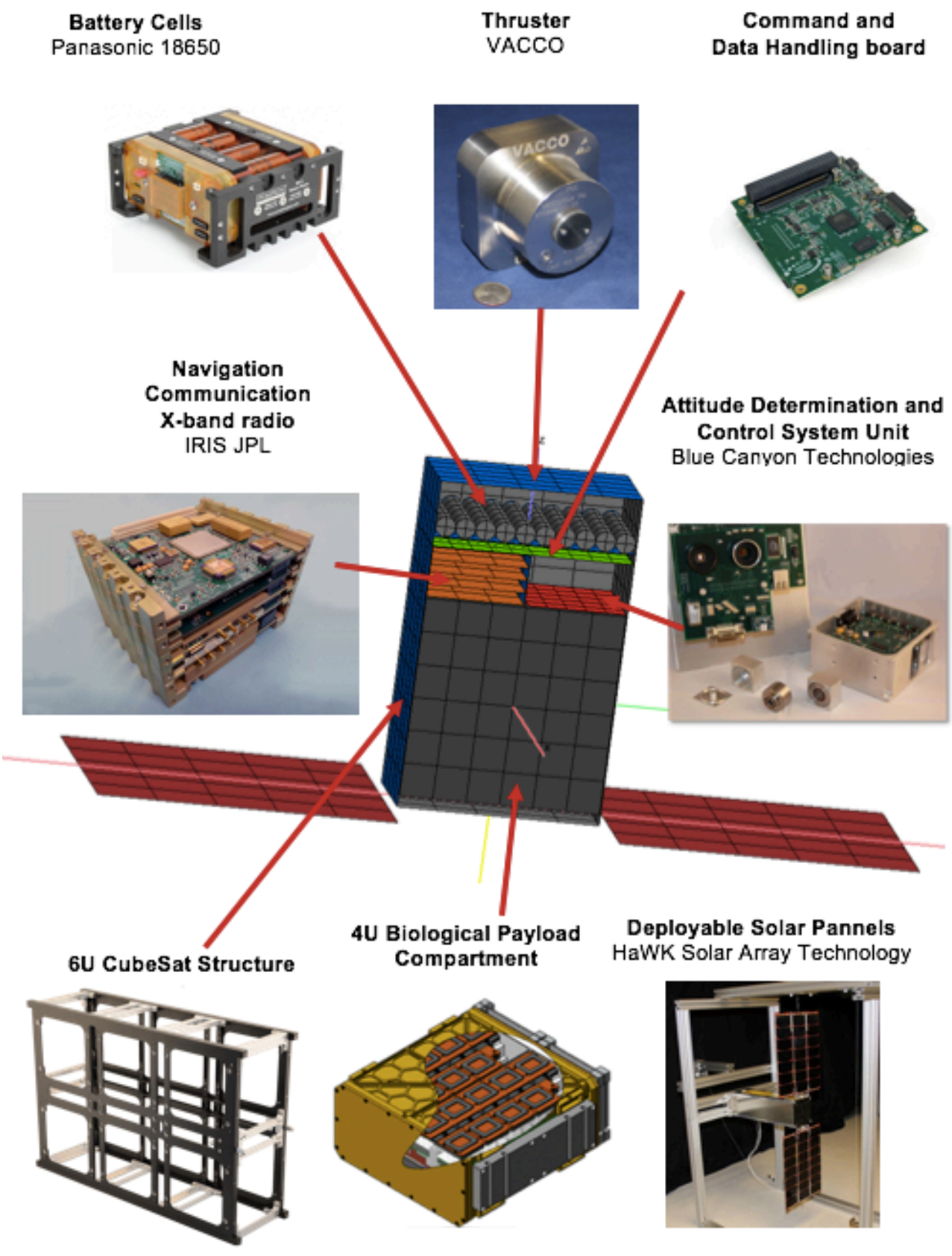

For the ESATAN – TMS Geometry model a spacing of at least 1mm between each installed component was anticipated. as well as between the satellite panels and components.

Providing spacing between body panels and installed components, there is not direct conductive heat transfer, except for user defined conductors which will be specified in calculations.

With all components installed, the geometry model is with 330 mm (Table 5-2) below the Z - axis design limit of 366 mm for 6U CubeSat [88].

For the X - axis, limited dimension regarding CubeSat design specification [88] is set to 226.3 mm. With the payload bay compartment outer X - axis dimension of 200 mm, spacing between the payload compartment bay and satellite body with panel thickness of 1 mm, there is still enough space for stowing solar panels during the launch phase. The required dimensional limit will not be exceeded. For Y - axis outside dimension of the model is exactly 100 mm.

The final outer dimensions of the geometric model are: 204 mm x 100 mm x 330 mm. For each material the physical and thermo optical characteristics were specified, and these can be found in Appendix A.

5.2.2.2 Electrical power system

The Electrical power system contains all elements which are relevant for the generation, storage and distribution of electrical energy. In the geometry model, the solar panels and battery pack unit were modelled separately.

For an interplanetary flight, the distance from the Sun and extended mission duration both significantly decrease the power generation capabilities of solar cells. The main cause of this are lower solar irradiance and cells degradation from prolonged radiation exposure on the order of many months. The current state of the art commercially available solar cells are 29.5% efficient. Prospects for the future are favourable, with efficiency greater than 50% and being less susceptible to radiation degradation [89].

Solar cell generated electrical energy is stored in Li-Ion batteries. Battery technology is advanced enough already, that battery cells can survive and support an interplanetary mission. But they have quite strict operational temperature limitations. Development of an ultra low-power avionics systems capable of providing basic computing, spacecraft monitoring, attitude determination and control and optical communication is clearly defined and solvable. Reasonable power requirement for such a system is around 7 W of average power, where 5 W of power is feeding the optical communication terminal, and remaining 2 W being used for C&DH, ADCS and other sub systems [89].

5.2.2.2.1 Solar panels

Solar panels are stowed at the side of the CubeSat body (Figure 5-6). The CubeSat dimensional limit in Y and Z axes for stored solar panels is 366 mm x 100 mm. After deployment of the satellite they expand to the full area.

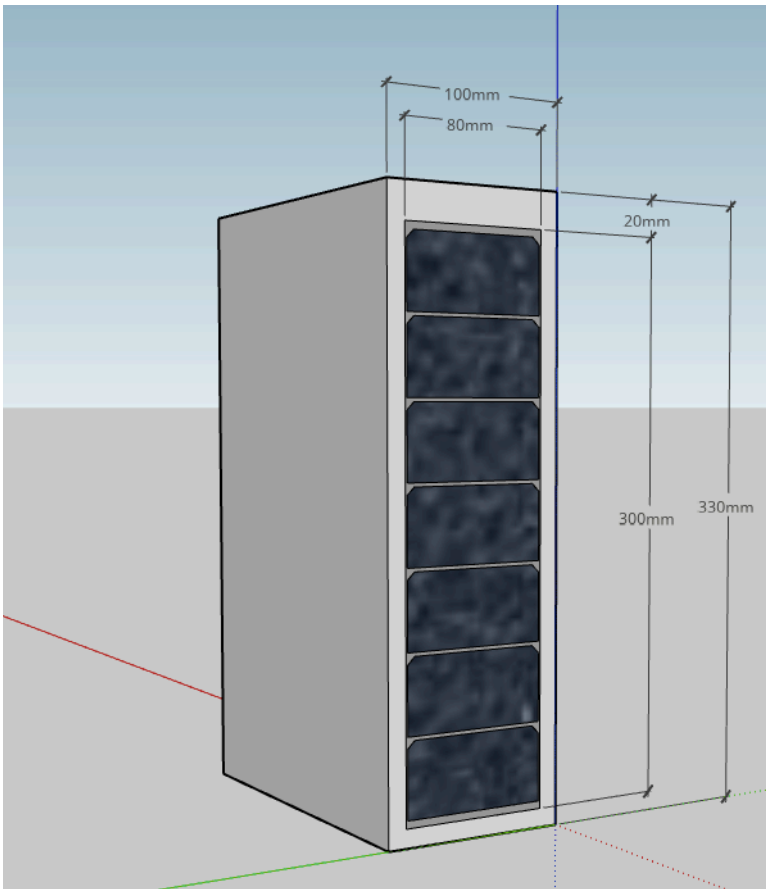

Figure 5-6: Stored solar panels for designed model [33]

The dimension of the single stored panel is 300 mm x 80 mm (Figure 5-6), the dimensions of deployed one are 300 mm x 240 mm, containing 42 solar cells. Panels are designed in ESATAN - TMS as a dual material, with 1 mm Germanium on the top and 1 mm graphite panel at the bottom as a base. Additional simulation was performed with gold thermal coating placed over graphite on the rear side of panels. Thermal properties of the materials are specified in Appendix A. Panels are with a 10 mm x 10 mm steel rod connected to the model with a gimbal mechanism which enables ±180 ° of tracking capabilities and provides Sun pointing at all times during the flight. A tracking mechanism with electronics is placed at the bottom of the CubeSat body, below the payload area. Calculated power required for gimbal is 0.4 W.

The reference solar panel for geometry design was HaWK Solar Array Technology (Figure 5-35), produced by MMA Design. They are highly mass and volume efficient with enabling modular architecture. Specified peak power output for the installed unit at 1 AU is approximately 36 W [90]. If needed the higher power E-HaWK model with 72 W of peak power is also compatible with the 6U CubeSat configuration.

Solar Cells have an operational temperature range of between -150 and 110 °C, while survival limits are between -200 and 130 °C [91].

Figure 5-7: HaWK Solar Panel placed on 3U CubeSat with gimbal mechanism [90]

5.2.2.2.2 Battery pack with board

Electrical energy produced in solar cells is stored in high energy density Li - Ion batteries cells. Cells are arranged in a battery pack which is controlled by electronics on a printed circuit board (PCB) placed below the battery pack (Figure 5-8).

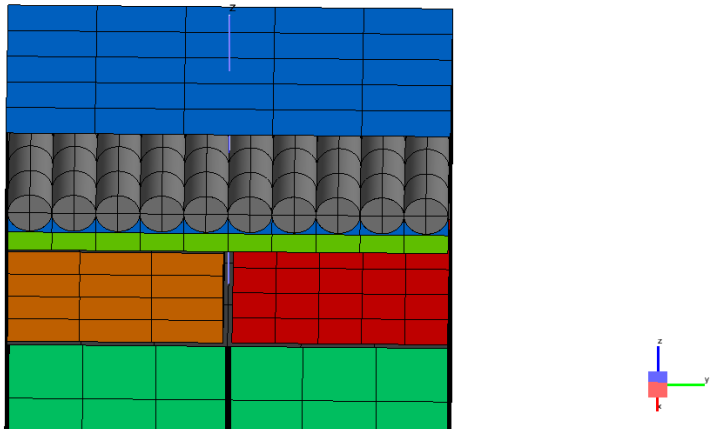

Figure 5-8: Top part of 6U CubeSat model with visible Li-Ion batteries and power board (ESATAN-TMS)

Flying interplanetary mission on a greater distance from the Sun, with reduced irradiation, needs better battery capacity to store enough electrical energy and supply electrical consumers, when provisions supplied by the photovoltaic system would be insufficient. For the model Lithium – Ion 18650 battery cells were chosen, mainly due to flight heritage and are therefore already proved to be suitable for CubeSat missions [92].

A single battery cell with a diameter of 18 mm, can provide 3.7 V at rated capacity of 2600mAh. By combining cells in series or parallels, the required voltage and current can be achieved. Cell cycles (charge, discharge and storage) are very temperature sensitive. Operational limits for 18650 Li - Ion cells are: for charge 0 °C to 45 °C, for discharge -20 °C to 60 °C and for storage -20 °C to 50 °C [92]. For the purpose of the thesis geometry model 10 cells were installed in the battery pack (permitted by dimension) on top of the electronic board which is responsible for the operation and distribution of electrical energy. (Figure 5-8).

Battery cells were modelled as a dual material cylinder with a radius of 9 mm. The outer 1 mm presents Aluminium housing while the inner 8 mm are filled with electrodes and electrolyte [93].

The electronic board works as a battery charge regulator and is also responsible for dispatching electrical energy to the components. It was modelled as a 3 mm thick dual material plate, combined from 2 mm glass reinforced epoxy laminate – FR4 at the bottom and a 1 mm copper layer, representing electrical wirings and connectors on the top (Appendix F). Power consumption during normal operation is estimated at 0.1 W and 0.2 W during the high mode.

The battery module is on each side, with two steel connecting elements in an area dimension of 1 cm x 1 cm fixed to the structure (Figure 5-9). Heat transfer conducted between connecting elements and structure is discussed in section 5.2.2.8.

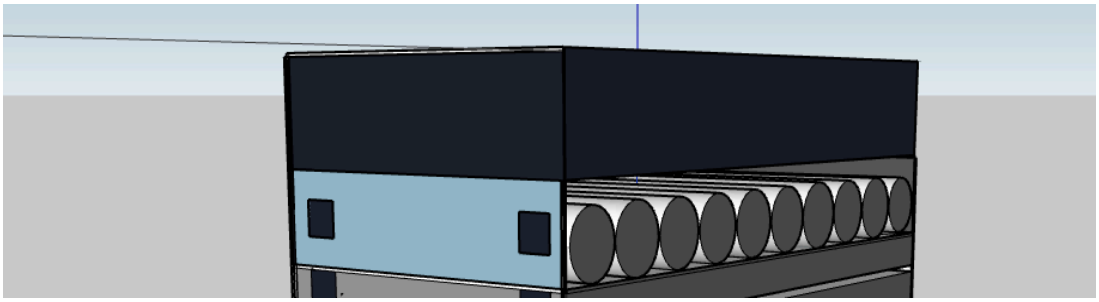

Figure 5-9: Side connectors of battery module to the structure [103]

5.2.2.3 Attitude Determination and Control System (ADCS) Unit

The precise attitude determination and control system unit is one of the most important components needed for a successful Interplanetary CubeSat mission. The main need for precise pointing capabilities comes from optical communication system which requires ±4 mrad (~ ±0.23 °) at 2σ of pointing accuracy [89].

Attitude Determination and Control System Unit has two major functions:

- to determine current attitude of the satellite using different sensors as star trackers, Sun trackers and gyroscopes.

- to change the attitude of the CubeSat by reaction wheels.

CubeSat ADCS has dramatically improved over the last decade facilitated by the development of state-of-the-art miniaturized star trackers capable of achieving precise 3 - axis attitude determination with an arc second accuracy. Additionally, several companies are offering integrated units for precise 3 - axis control, which combine different Guidance, Navigation and Control (GNC) components into a single package, to provide cutting edge solutions. Blue Canyon Technologies offers integrated CubeSat XACT attitude control system (Figure 5-10) with a stated pointing accuracy of better than 0.007 ° for all three axes what is crucial for successful interplanetary spacecraft communication[87]. The unit which was also selected for thermal control simulation geometry model occupies only 10 cm x 10 cm x 5 cm (0.5U) of space and has a mass of 0.7 kg. The slew rate of the satellite is more than 10 °/second with a nominal power consumption of less than 0.5 W and peak power requirements of 2 W [94].

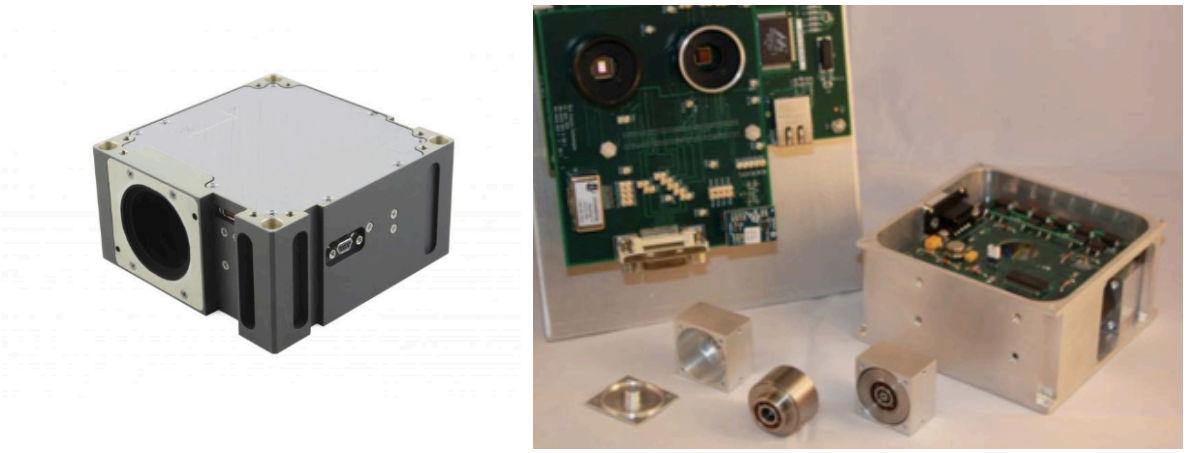

Figure 5-10: Blue Canyon Technologies, XACT attitude determination control system [94]

For designing a model of ADCS component in ESATAN – TMS, simplified geometry and material approximations were needed. The unit was initially separated into three basic components:

- ADCS electronic board,
- reaction wheels,
- housing.

With known published mass of the complete unit of 0.7 kg, it was initially divided into double mass fractions of 0.1 kg for the electronic board and remaining 0.6 kg for the steel reaction wheels and Aluminium housing. Since ESATAN – TMS software enables modelling of dual material shells, ADCS unit was modelled as the electronic board layer and second layer being combined reaction wheels and housing. On the basis of known total mass of the unit and estimated mass fractions and thicknesses, volume fractions and finally thermo-physical properties of composite materials were specified. Detailed calculations are explained in Appendix F.

The operational temperature range for the reaction wheels is from -10 to 40 °C (survival from -20 to 50 °C) and for electronic printed board (PCB) from -20 to 60 °C (survival from -40 to 75 °C) [91].

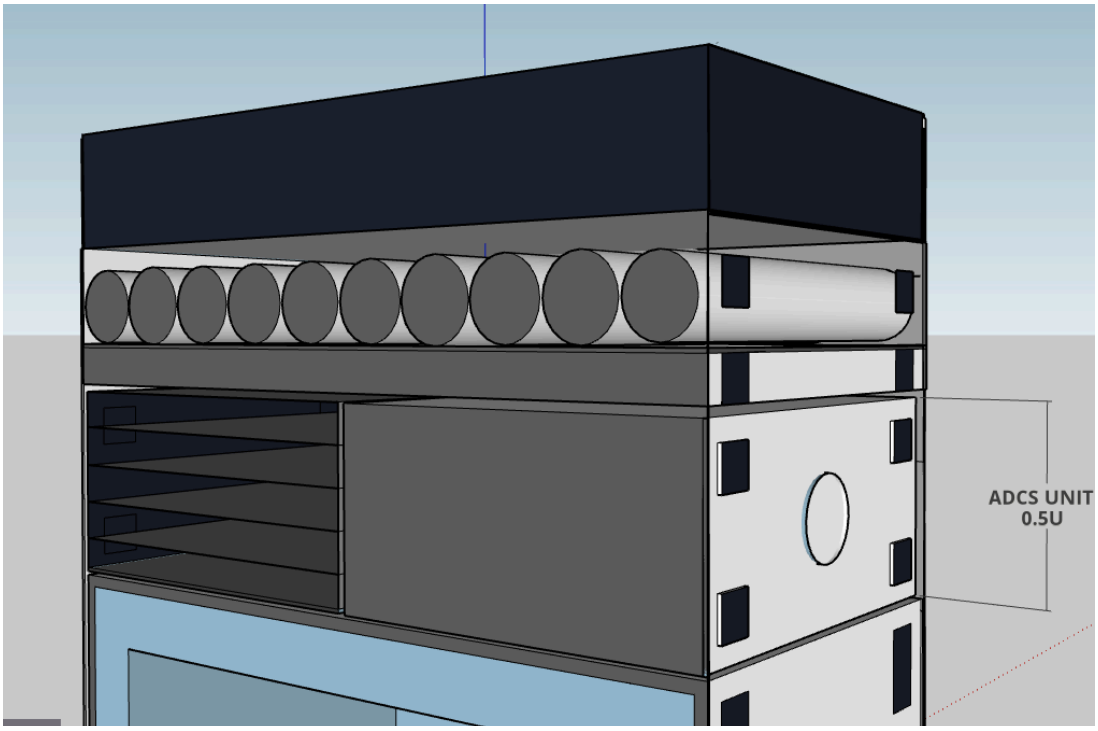

Figure 5-11: Placement of ADCS Unit in 6U CubeSat [103]

Attitude Determination and Control (ADCS) is in the 6U CubeSat geometry model placed above the payload bay. The unit is fixed to the structure with four steel connectors to the side frame (Figure 5-11).

5.2.2.4 Transponder Communication unit

The Transponder Communication unit presents the interface between the satellite and the ground station, enabling spacecraft to downlink its payload and housekeeping data to the operational centre and in reverse transmitting operational commands back to spacecraft and in addition, to maintain inter-satellite communications if needed. Most of the early CubeSat LEO missions used VHF and UHF radio frequency communications, with typical data rates of 1.2 and 9.6 Kbps[87].

A key component enabling lunar and deep space CubeSat missions is a deep-space Transponder Communication unit capable of providing traditional telecommunications features, as well as radiometric tracking support for orbit determination outside of the effective range of Global Positioning System (GPS) satellites. The NASA Jet Propulsion Laboratory (JPL) developed the Iris Transponder unit with the purpose of supporting such specific CubeSat interplanetary missions [95]. The IRIS Transponder Communication unit was included in the geometry model.

The IRIS Transponder Communication unit (Figure 5-12) is a reconfigurable software – defined radio, designed for missions requiring interoperability with NASAs Deep Space Network (DSN) on X – band frequencies (7.2 GHz uplink, 8.4 GHz downlink) for command, telemetry and navigation. The Transponder provides radiometric tracking support with DSN to provide navigational products for precise orbit determination while performing standard uplink and downlink communications. It uses radiation tolerant hardware packed in ~ 0.5U volume with 1.2 kg of mass. Power consumption when fully transponding is high at 35 W (at 3.8 W radio frequency output), 12.6 W of power consumption when in the receive mode only and 0.5 W when in the standby mode. Detailed calculation of data budget for the present model is beyond of scope for this thesis work and was not investigated. According to main references BioSentinel [84] and MarCO [107] interplanetary CubeSat missions, which use the same Transponder, achievable downlink rates from spacecraft to Deep Space Network (DSN) during the mission are specified as between 62.5 – 6000 bps for BioSentinel

with medium gain antenna and up to 8000 bps from a distance of 1.05 AU, using high gain reflector antenna for MarCO mission.

Hardware sliced architecture and reconfigurable software and firmware enable extension and adaptation to new capabilities. Among those planned are: Radio Science support (atmospheric and media measurements and occultation, gravity fields, radars and radiometers); additional frequency bands (Ka -, S -, UHF); Disrupt/ Delay Tolerant Networking; proximity operations (at other planets such as Mars); and Space Network capability [96].

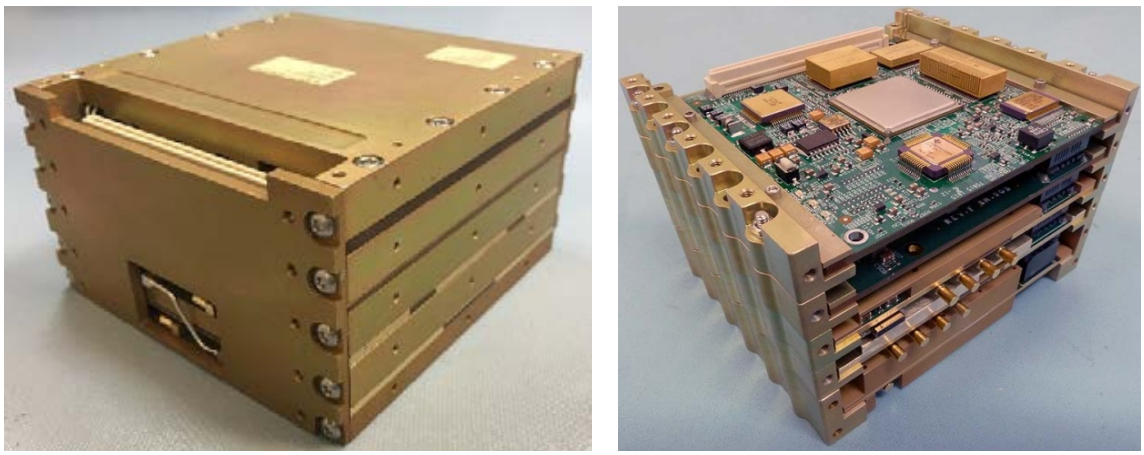

Figure 5-12: IRIS Deep Space Transponder Communication unit – closed (left) and with visible sliced architecture (right) [96]

The unit operational temperature range is between -20 and 50 °C. When building the ESATAN – TMS model it was known that the Transponder unit accommodates 0.5U of space and weights 1.2 kg [96]. As already mentioned the module is split into components (sliced architecture) and because of that presented greater challenge building an adequate model. It incorporates 5 basic components:

- Power supply board,
- X – band receiver,
- X – band exciter,
- X – band low noise amplifier
- X – band solid state power amplifier

Boards are connected with coaxial interconnect cables and board to board stacking connectors. Each individual slice is also designed for optimized thermal transfer from the device junction to the chassis walls. Slices have adequate spacing to allow the dissipated heat to be extracted to the Aluminium chassis, which is with four steel connectors (same as ADCS Unit) connected to the CubeSat frame structure. Calculating of Thermo – physical properties for IRIS Transponder unit is performed in Appendix 2.
The operational temperature range for the Transponder unit is from -20 to 60 °C, and survival from -40 to 75 °C [91].

5.2.2.5 Command and Data Handling (C&DH) board

The satellite has to be able, for a certain amount of time, to operate independently without any support and communication from the Earth. For this purpose, an on-board computer is integrated into the satellite. It performs multiple tasks such as:

- controlling the on-board components and instruments,
- telecommand distribution to the satellite,
- telemetry data collection from subsystems,
- overall supervision of spacecraft and payload functions,
- collecting scientific data from the instruments,
- temporarily storage of the scientific data,
- packing and preparing data,
- …

With Interplanetary flights, even bigger challenges arise with massive data processing and storing requirements. Additional difficulties might be presented by possible data corruption, caused by increased space radiation.

For the geometry model a 10 mm thick Command and Data Handling board (Figure 5-13) was predicted. Usually an on-board computer system consists of two boards; a primary and secondary one. They are placed below battery cells, over the whole distance, placed side by side. As a material, FR4 epoxy plate was used for the base (0.75 volume fraction) with a silicon layer as electronics

(0.25 volume fraction) on top. Plates are connected to the side frame, each with two steel connectors. Power consumption is estimated at 0.4 W for normal and 0.55 W for high operation mode. Operational temperature range is the same as for other PBC units, from -20 to 60 °C, and survival from -40 to 75 °C [91].

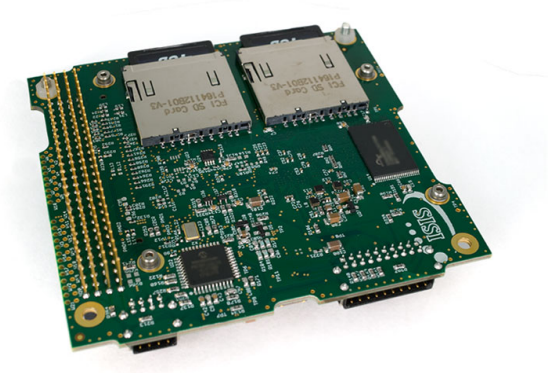

Figure 5-13: Standard 1U Command and Data Handling Board [97]

5.2.2.6 Thrusters

Sending missions to the deep space environment, both spacecraft detumble and reaction wheel momentum management must be accomplished using a thruster system, as a substitute for magnetic torque rods which can be used in Earth magnetic field environment.

In-space spacecraft propulsion systems can be divided into three categories:

- chemical propulsion system,
- electric propulsion system,
- propellant less propulsion system (Solar Sail).

Generally, chemical propulsion systems can achieve higher thrust levels although with limited specific impulse compared to electric propulsion systems. Whereas propellant less systems such as solar sails do not utilize any propellant to produce thrust, thus reducing the system complexity and mass, and potentially enabling long term interplanetary missions [87]. For building geometry model, chemical cold gas micro propulsion thrusters were selected, mainly because of their simplicity, reliability and flight heritage. Cold gas thrusters are proved to be very reliable in delivering thrust of millinewton range

using expansion of saturated gases like refrigerants (R134a, R236fa…), sulphur dioxide or isobutane. This system has many advantages such as: simplicity of design, pulse or continuous operation, it is safe to handle and has lower power consumption. The desired thrust is produced by allowing compressed gas through the nozzle [98]. For the thesis geometry model purpose VACCO cold gas Micro Propulsion System (MiPS) was used (Figures 5-14, 5-15). It is a self-pressuring system with a mass of around 0.5 kg, using isobutene propellant, which is being stored as a liquid and expelled as a gas. The single unit (at simulation geometry are proposed two units side by side on the top of satellite) can deliver 34 N-sec of Total Impulse, with up to 62,000 firings [99].

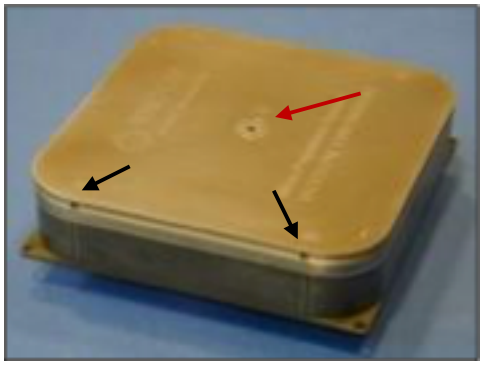

Figure 5-14: VACCO MiPS with visible 4 tangential (black arrows) and 1 axial valve (red arrow) [99]

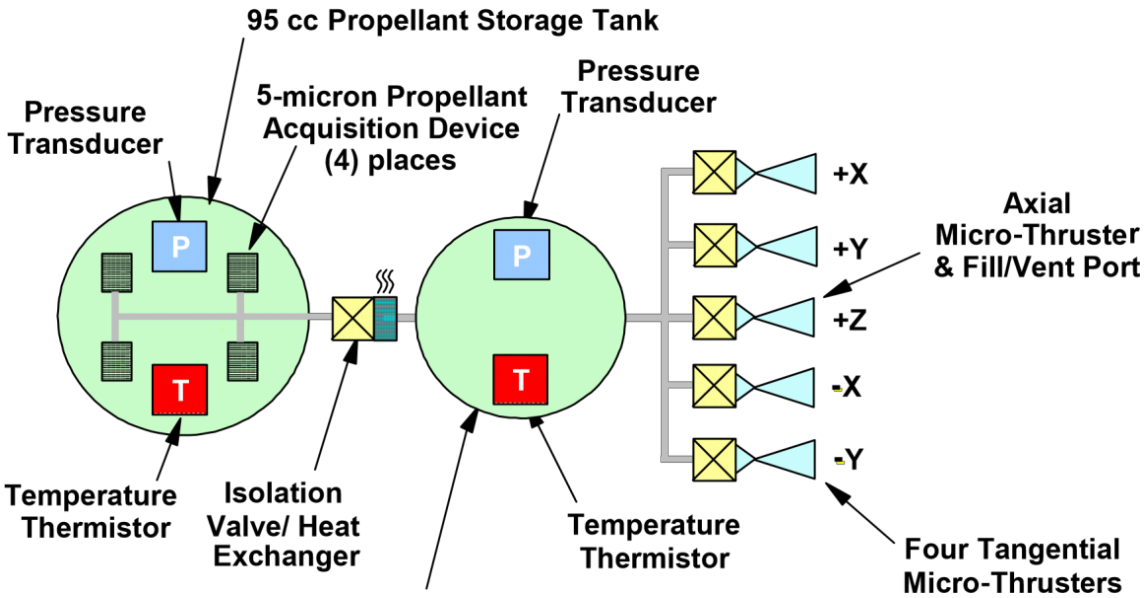

Figure 5--15: Micro-Propulsion System Schematic [99]

Side by side mounted micro-propulsion units occupy 0.3U of upper space in the satellite body. The unit is mainly composed from housing material (Aluminium) and propellant. On the basis of known mass fractions thermo – physical properties used for ESATAN – TMS simulation were calculated. The calculations can be found in Appendix F. The thruster unit is placed on the top of the CubeSat and is considered as being in perfect contact with structure and panels (Figure 5-16).

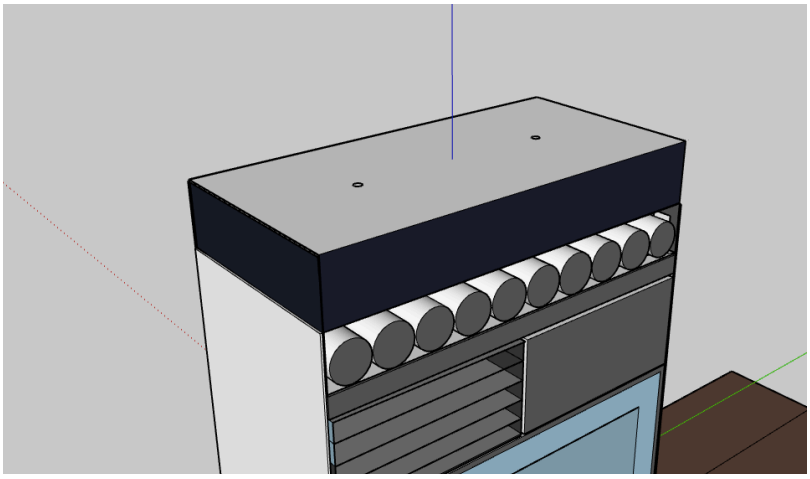

Figure 5-16: Top of the CubeSat model structure with visible thruster unit [103]

5.2.2.7 Payload Compartment

The main objective of the research work was to improve the knowledge of the negative impact that space radiation might have on humans during future long-term space exploration missions beyond LEO. This is to be investigated by studying the effects of the deep space radiative environment on a biological sample with mammalian – human like cells. There are no specific pointing requirements needed from spacecraft by the science payload. The experiment simply requires access to the deep space environment, as opposed to being pointed in a specific direction to take measurements.

Similar deep space BioCubeSat missions [84] have set experiments to study the radiation effect on genetically modified yeast cells which are much lower living forms. For the thesis designed mission C. elegans worms were proposed (Figure 5-17).

C. elegans are small soil worms (~1 mm) or nematode which shares a common ancestor with humans that lived in the pre-Cambrian era 500 - 600 million years ago. This ancestor is referred to as the urbilaterian ancestor, as it is the relative of all bilaterally symmetric multicellular organisms on the planet including invertebrates and vertebrates. As a result, C. elegans have neurons, skin, gut, muscles and other tissues that are very similar in form, function and genetics to those of humans. Because of evolutionary conservation of gene function and experimental tractability, C. elegans represent an ideal model organism to study basic genetic and molecular mechanism of human development and diseases. Therefore, they are also very suitable to be used in the study of deep space radiation effects on the human body.

Another feature that makes them very suitable for space-based experiments is their ability to enter dormant phase They are able to enter this quiescent state when exposed to harsh conditions such as lack of food, high - population density or temperature increase. This state allows C. elegans to commonly survive for up to 120 days instead of 20 normal days [100]

Figure 5-17: C. elegans worm [43]

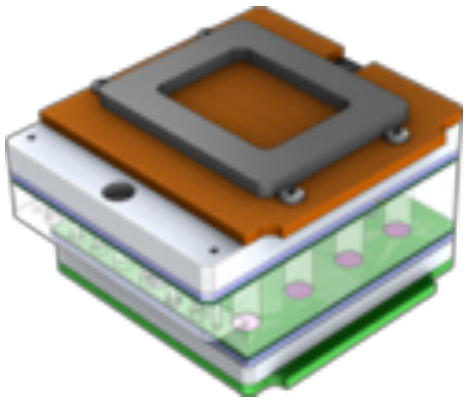

Figure 5-18: Sample of Microfluidic cards [84]

The Biological payload would be placed together with all environmental control, the house-keeping system and dual radiation protection layer in approximately 2U x 2U payload compartment below the avionic bus part of the CubeSat. The biological payload system needs to integrate micro well fluid cards with biology

samples (Figure 5-18), an optical measurement device for controlling viability and growth, an environmental control unit with sensors for relative humidity, temperature and pressure and active fluid management unit for supplying the micro wells. Similar approach was used with Cranfield's BAMMSat experiment containing sample discs with 40 individual samples together with fluorescence microscope and spectrometer packed in 2U pressure vessel (Subchapter 2.3.3) [23].

The payload compartment has an incorporated radiation protection layer which consists of a 3 mm of Aluminium wall on the outside (the main structure of payload bay) and a 15 mm of polyethylene which is placed inside the container towards the experiment, as was calculated in the Radiative chapter (Figures 5-2, 5-19).

The space inside the payload container where the experiment - payload is placed, was modelled as 33% mass fraction of Aluminium, 33% mass fraction of polyethylene and 33% mass fraction of water, with a total mass being 1.8 kg – 0.6 kg for each component.

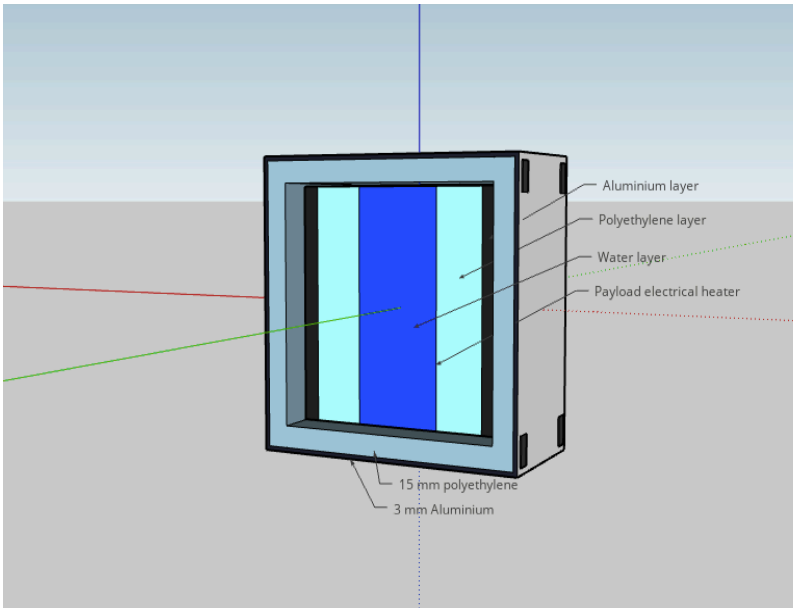

Figure 5-19: Model of Payload container [103]

Aluminium represents all instrument hardware, microfluidic cards are made mainly from polyethylene, and biological material is represented as the water

part. Placing these three evenly distributed material components in the payload bay, more adequate and realistic mass and heat capacity inputs for simulations are anticipated (Figure 5-19, 5-20). There is also ambient air component present in the payload compartment but, due to simplification, was excluded from the numerical model. It is expected that it would not present a significant contribution to the results.

On each side of the biological payload (water) twin layers of polyethylene and twin layers of Aluminium are placed. On one side of the biological payload layer electrical heater is installed, which is meant to additionally heat the samples if the temperature drops below the required limit of 4 or 37 °C (Figure 5-19). The calculating thickness of the payload layer is performed in Appendix F.

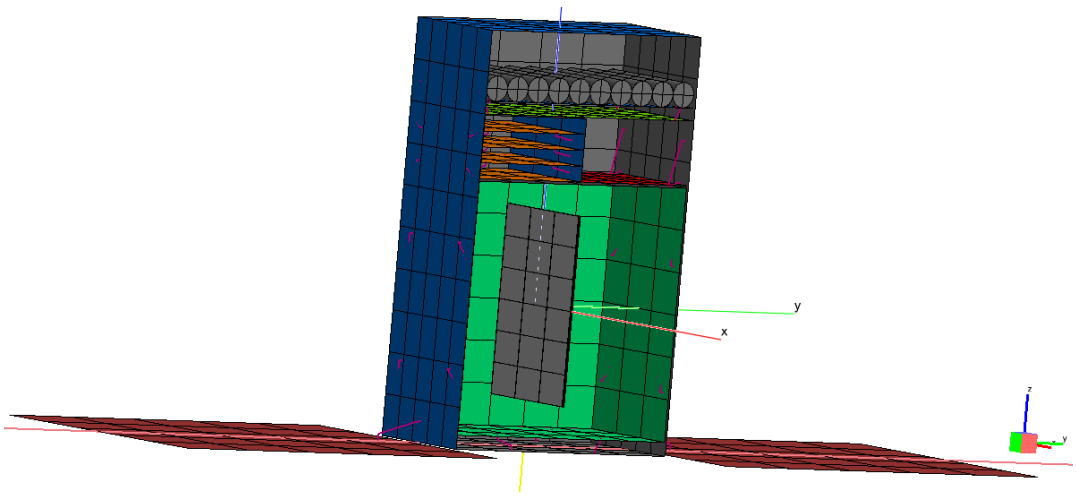

Figure 5-20: Geometry model of CubeSat with open front panel and visible payload compartment (ESATAN - TMS)

Outer dimensions of the payload container are 200 mm x 200 mm x 96 mm. Taking into account the 3 mm layer of Aluminium and 15 mm layer of polyethylene inside as radiation protection layers, the useful volume available for the biological payload is greatly reduced. As a result of this huge reduction in volume, it was decided to decrease the polyethylene layer from 20 mm to 15 mm, as discussed in subchapter 5.2.2.

The main purpose for running the ESATAN – TMS simulations was to define the temperature environment inside the CubeSat geometry model and components,

especially in the payload area, where temperature sensible biological material is placed. The temperature requirement for the payload samples are set to either 37 °C or 4 °C, depending on the sample material. To maintain the desired temperature, samples will be additionally heated with electric heater, or cooled (not very likely) by means of radiation.

5.2.2.8 User defined conductive interfaces

Besides Radiative heat transfer between components, which are in physical contact in the vacuum of space, conductive heat transfer also arises.

As explained in Appendix D, conduction is the process by which heat flows within a medium or between different mediums which are in direct physical contact. The heat flows from a region of higher temperature to a region of lower temperature.

It is assumed that the main parts of the satellite structure, such as panel, component plates, and other parts, are in perfect contact with each other – fused together. This means that two geometries form a single continuous surface, where thermal resistance across the interface is considered to be zero [82].

For other contacts it is assumed that two surfaces are linked by a physical interface with which a non-zero contact resistance is associated. For these contacts conduction which appears between surfaces via connecting element is calculated. For the geometry model simplified calculations and predictions that connecting element is just with a single face connected to the node of each two surfaces were used. Conductors for rectangular nodes are computed using the following equation:

Equation 1: Thermal conductance

$$\mathbf{G} = \frac{\mathbf{k} \cdot \mathbf{A}}{\mathbf{x}} \quad \textbf{[W/K]}$$

where G is thermal conductance (W/K), k is thermal conductivity (W/mK), A is cross section area through which heat flows (m^2), and x is the distance between adjoining nodes (m). For all our conductive heat transfers connector elements

(screws, rods, spacers) were used which connect two nodes of different geometry. User defined conductance was calculated between:

- solar panels and satellite body,
- spacers between frame and payload compartment,
- connectors of the components in the unit,
- connectors of the components to the structure.

Solar panel connection to satellite body

Solar panels are connected to the satellite body via the steel rod (arrow) connecting them with a gimbal mechanism (Figure 5-22).

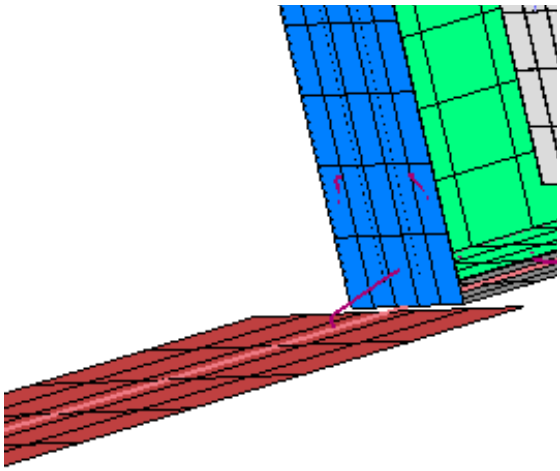

Figure 5-21: User defined conductive interface between Solar panel and satellite body (magenta line) presented in ESATAN – TMS software (ESATAN-TMS)

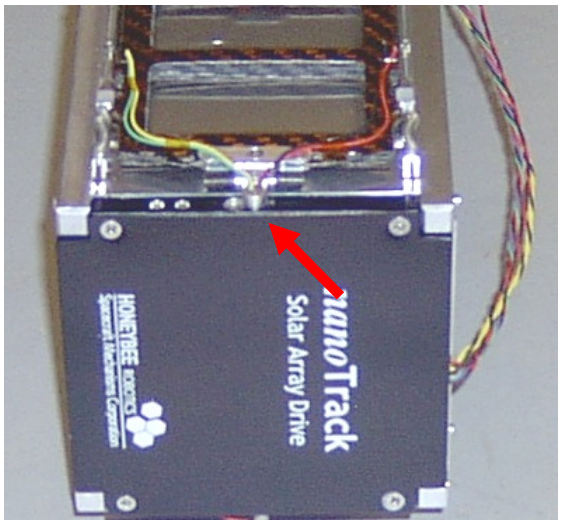

Figure 5-22: Photo of solar panel with visible (arrow) connection rod to gimbal mechanism [90]

The steel rod with 10mm x 10mm square and 25 mm length was selected. Thermal conductance was calculated from the Equation 1:

$$G = \frac{k_{steel} \cdot A}{x} = \frac{16.3 \frac{W}{mK} \cdot (0{,}01 \cdot 0.01)m^2}{0.025m} = 0.065 \frac{W}{K}$$

The calculated value for thermal conductance were set in the ESATAN-TMS menu User defined conductors (see Appendix E). As a Connection Source

reference and destination reference faces – shell nodes at the edge of solar panel and satellite body were selected (see Figure 5-21).

Spacers between frame and payload compartment

To support the payload bay and to maintain the structure and spacing between the satellite panels and payload Aluminium spacers were designed. Spacers are to be placed at the bottom (4 pieces) and at the side (4 pieces each side) of the bay (Figure 5-23). The dimensions of Aluminium spacers are 20 mm x 10 mm x 1 mm. Conductance was calculated:

$$G = \frac{k_{Al} \cdot A}{x} = \frac{121 \frac{W}{mK} \cdot (0.01 \cdot 0.02) m^2}{0.001 m} = 24.2 \frac{W}{K}$$

The calculated conductance value is much higher than in the first example, because of short distance of 1 mm for heat transfer and because of almost 90% lower heat conductivity of steel ($k_{steel} = 16.3 \frac{W}{mK}$ to $k_{Al} = 121 \frac{W}{mK}$) compared to Aluminium.

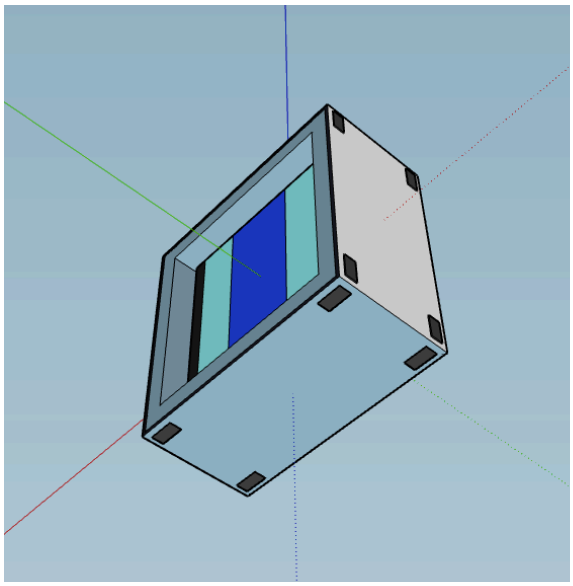

Figure 5-23: Payload bay with visible Aluminium spacers [103]

Connectors of the components to the structure

The satellite bus components, such as Attitude Determination and Control System (ADCS) unit, Communication unit, Battery pack and Command and

Data Handling (C/DH) board, are connected to the satellite frame with steel connectors – screws. The ADCS and Communication unit are connected one at each side of the satellite body with four connectors – being 1U wide. While the battery pack and Command and Data Handling boards are spread through the whole 2U width and are connected on each side of the satellite frame with two connectors (Figure 5-24).

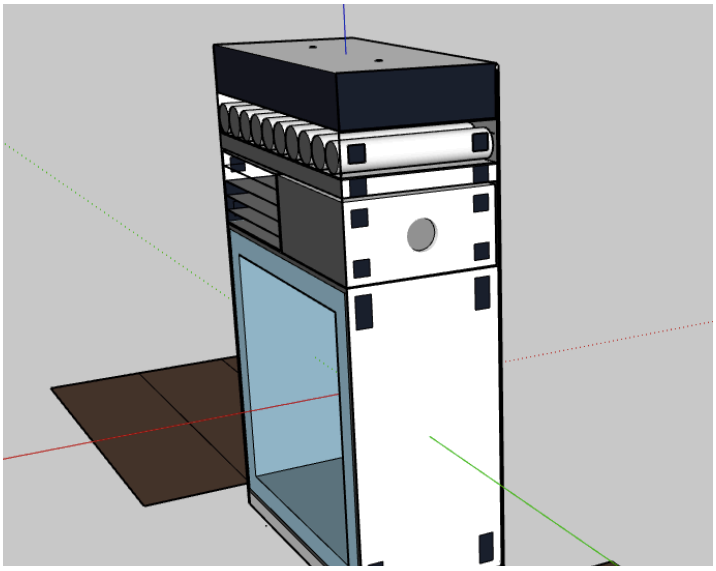

Figure 5-24: Side view of satellite frame with open side and front panels, exposing empty payload bay [103]

For calculation 10 mm x 10 mm steel connecting elements were modelled. Conductance was calculated as:

$$G = \frac{k_{steel} \cdot A}{x} = \frac{16.3 \frac{W}{mK} \cdot (0.01 \cdot 0.01) m^2}{0.001 m} = 1.63 \frac{W}{K}$$

The value is higher compared to the solar panel example, due to the shorter distance for heat transfer, but still much lower in comparison to Aluminium material.

Connectors of Transponder boards

The Transponder unit is modelled from five plates – four PCB boards and a top cover plate. The top cover Aluminium plate and bottom PCB plate are modelled as being in perfect contact with side plates. Three PCB boards inside the unit

are connected with side plates with two Aluminium connectors of 10 mm x 10 mm x 1 mm on each side of the plate (Figure 5-25).

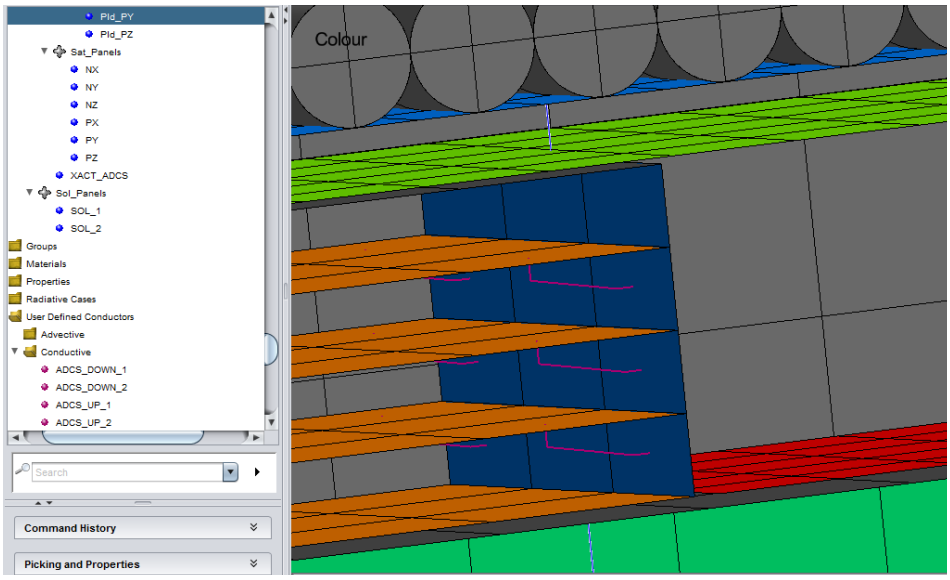

Figure 5-25: ESATAN – TMS model with visible defined conductors (magenta lines) for PCB plates inside Transponder unit (ESATAN - TMS)

Conductance for connecting elements was calculated:

$$G = \frac{k_{Al} \cdot A}{x} = \frac{121 \frac{W}{mK} \cdot (0.01 \cdot 0.01) m^2}{0.001 m} = 12.1 \frac{W}{K}$$

5.2.2.9 Boundary conditions - Heat dissipation of electronic components

Prior to performing the Radiative and Thermal Analysis case, boundary conditions of the geometry model were needed to be set. With boundary conditions are specified additional heat sources such as electronic components heat dissipation during the mission. As explained in Appendix D for the Earth orbit case, various sources of thermal energy are presented. With interplanetary mission, heat dissipation of electronic components, together with reduced Solar radiation presents the only source of thermal energy.

For the project three operational modes were predicted:

- **zero (0) heat dissipation (i.e. lower worst case),**
- **normal (NORM) - operational heat dissipation (i.e. typical operation)**
- **high (HIGH) - maximum heat dissipation (i.e. upper worst case).**

With zero heat dissipation, operation of all electronic components is excluded from the model. Meaning all electronic devices in the CubeSat are turned off and batteries are not operational. There is no additional heat source in the satellite. This scenario is not very common, since at all times during the mission at least one computer unit of the satellite and batteries are working and therefore some heat is dissipated.

The second example presents heat dissipation for all components during normal operational mode. Additional dissipation within batteries occurs due to conversion of chemical energy into electricity.

With the high heat dissipation example, maximum operation and heat load from individual electrical unit was modelled. In this scenario all ADCS modules are operating, the Transponder is in receiving and transmitting mode, the computer boards and all power boards are operational, the gimbal mechanism is slewing the solar array and thrusters are operating. The high dissipation example with all electronic components on board performing at maximum power is almost as unusual and uncommon as the example with zero dissipation.

Zero and maximum heat dissipation scenarios are performed to obtain values for comparing normal operation with extreme cold and hot scenarios.

For different installed components different fractions of electrical power to be dissipated into heat were predicted.

- **Thrusters**

Thrusters are used for reaction wheels momentum management and detumble. The system operates in different regimes from least power demanding Operation and command protocol monitoring mode, to Standby mode and Thruster operating mode. According to the available literature, for this type of propulsion system, average power consumption during operation is 2 W per unit and an additional 0.35 W for electronics. For two installed units (sided by side) it gives 4.7 W [101]. During basic health and status monitoring mode power consumption is expected to be less than 1 W. On the basis of available data

and estimations it was selected normal operational heat dissipation to be 0.5 W and 4.7 W during thruster fully operating mode.

As explained in Subchapter 5.5.2.6, cold gas thrusters were used for modelling purpose because of their simple operational characteristics. During the simulation process possible cooling effect due to expansion of the firing gas was not taken into calculation, since it is expected to be negligible. Future study is recommended to confirm this assumption.

- **Attitude Determination and Control System Unit (ADCS)**

The ADCS Unit has a number of components that use power. The XACT Module was selected for simulation, nominal power consumption is specified to be 0.5W and peak power consumption being 2 W [94].

During peak power consumption PCB electronic uses 0.35 W of power, 1 W is used by reaction wheels and the remaining 0.65 W is used by the star tracker and additional electronics. The total for all components is 2 W. Most of the time, just electronic PCB is operational. Dissipation of the PCB board is expected to be 100%. The power dissipation of the reaction wheels and star trackers is assumed to be 30% of the consumed power. Therefore, for minimum heat dissipation from the ADCS unit 0.35 W was specified and during the maximum operation 0.9 W (0.33 W for the reaction wheels and 0.22 W for the star tracker) [76].

- **Transponder Communication unit**

The Deep Space Transponder Communication unit (Subchapter 5.2.2.4) is the most power consuming component installed in the CubeSat. As seen in Table 5-5 the input power requirement varies from 0.5 W when only the battery is connected and up to 35 W for full transmit/ receive mode. As specified in other research work, 75% of input power is transformed into heat while the remaining 25% is sent to Earth as a signal [76].

Transpond. Comm. operational mode	Power input required (W)
Battery Connected	0.5
X – Receive Only	12.6
X – Transmit Only	30.8
X – Transmit/ Receive	35.0

Table 5-3: El. power required for different operational modes of Transponder Communication unit [96]

For the geometry model, values of 0.5 W for normal operational mode and 20 W of dissipated heat for high operational mode were selected. The lower value is just above the battery connect only power requirement, while the higher value of 20 W is approximately 75% of the power input during X - Transmit mode. In the model, dissipated heat is evenly distributed through four main PCB plates of IRIS Communication/ Transponder unit.

- **Batteries (Battery cells + Battery PCB)**

The batteries do not use any power, but there is efficiency loss when charging and discharging. Meaning battery cells thermal dissipation is dependent on the operational status of other electrical components installed.

Efficiency loss is the heat dissipation over the battery internal resistance, which is equal to 70 mΩ for installed battery model [92]. Using the current over the battery, the power dissipation can be calculated according to basic Equation 27:

Equation 2: Electrical power

$$\mathbf{P = I^2 \cdot R}$$

Where P is the power dissipated in the resistor as heat, I the current flowing through the resistor and R the resistors resistance. Regarding to available data for our Panasonic 18650 battery cells maximum current during charge is 2.5 A and during discharge 3.75 A. Typical values for both cases are 1 A [92].

Meaning during discharge the maximum possible heat dissipation for single battery cell unit regarding the Equation 26 would be almost 1 W.

For the thesis model more conservative estimation of maximum heat dissipation for batteries was proposed. Being 0.4W during maximum operation - discharging and 0.3 W during normal operation.
Additional heat dissipation of 0.1 W during normal and 0.2 W during high performance was specified for the Battery PCB board, where 100% of input electric energy is dissipated into heat.

- **Command and Data Handling Board (C&DH PCB)**

For the Command and Data Handling Unit as with any PCB board; all electrical power consumed dissipates into heat. For the model a high performance processing unit available on the market was selected [97]. Specified power consumption for the unit is 0.4 W for normal with 0.55 W during high performance.

- **Solar tracker**

Into consideration are taken just mechanism and supporting electronics responsible for the operation of the Solar panel slewing mechanism. The system is operational just when the Sun tracking mode is engaged. The estimated power consumption during operation is calculated as 0.4 W with 0.2 W of heat dissipated.

- **Payload compartment**

The payload area, in particular the part where the biological payload is placed is the most temperature sensible environment in the CubeSat. As previously mentioned, the environment temperature should be set at 37 °C or 4 °C, depends of the biological sample. An additional electronic heater was installed on the surface of the biological payload sample, with the intention of maintaining the desired temperature values.

- **Summary of heat dissipation for electronic components**

All specified values are just rough calculations and estimations on the basis of available information and data for the installed components (Table 5-4). For more exact numbers, experimental set up would be needed to obtain more realistic figures during different operational regimes of the single electronic component.

Normal operation heat dissipation (W)	Components	High operational heat dissipation (W)
0.3	Battery cell (single)	**0.4**
0.1	Battery PCB	**0.2**
0.4	C&DH Board	**0.55**
0.5	Trans. Comm. Unit	**20**
0.35	ADCS Unit	**1**
0.5	Thrusters	**4.7**
0	Solar tracker	**0.2**

Table 5-4: Heat dissipation for different electrical components

In the ESATAN – TMS software dissipated heat is modelled as a boundary condition of the system. Calculated values of dissipated heat were set to the desired face of specific component geometry as Total Area Heat Load in unit (W).

If Total Area Heat Load is applied to a region including more than one thermal node, the specified heat load is divided between the nodes in proportion to the area of the faces that make up each node [82]. Therefore, in the model, heat load was applied to the Reference face and evenly distributed between the nodes.

During the Thermal Analysis set up boundary conditions can be included or excluded from the simulation, by marking or unmarking from the Boundary

Conditions menu (Figure 5-26). A list of boundary conditions inputs is specified in Appendix K:

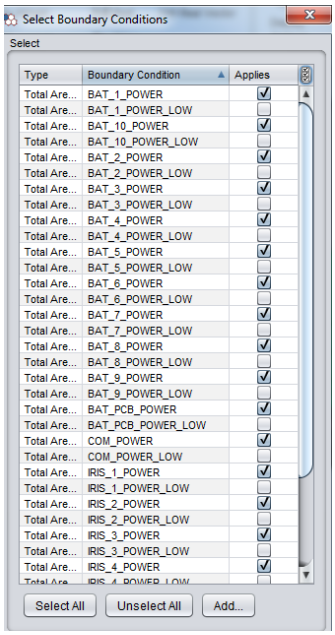

Figure 5-26: Boundary Conditions Select menu for our simulation (ESATAN-TMS)

5.2.3 Creating Radiative case

Inside the Radiative module are defined orbital parameters and running radiative calculations for designed geometry. Two sets of radiative simulations were performed; initial pre-check of the model parameters and temperatures in Low Earth Orbit and full deep space mission simulation on flight from Earth to Mars. New Radiative case simulation must be run for any kind of geometry correction performed on the model or changes of environment parameters.

5.2.3.1 Low Earth Orbit Simulation

After completing designing geometry and setting boundary conditions for the CubeSat model in ESATAN - TMS, it was placed into Low Earth Orbit (LEO). The purpose of it was to obtain some basic temperature results for initial impression regarding the correctness and adequacy of the model. Most important input values in Radiative Case Dialog Window for LEO example were:

Radiative Case Dialog → Environment

- *Celestial body: Earth*
- *Inertial Coordinate System: Sun*

Radiative Case Dialog → Orbit

- *Eccentricity: 0 °*
- *Semi – Major Axis: 900 km*
- *Radius of Apogee: 900 km*
- *Radius of Perigee: 900 km*
- *Inclination: 0 °*

Radiative Case Dialog → Pointing

Primary pointing

- Pointing vector: [1.0,0.0,0.0]
- Pointing direction: velocity

Secondary pointing

- Pointing vector: [0.0,0.0, -1.0]
- Pointing direction: zenith

In general it means that the CubeSat was placed in orbit around Earth (Figure 5-27, 5-28), with circular orbit 900 km above the planate surface and with an inclination of 0 ° - equatorial plane. While in orbit, the satellite is traveling inbound its +X axis – are set with Primary pointing parameters. With the Secondary pointing it was defined that the lower part of the CubeSat body (-Z), where the solar panels are is oriented towards zenith. The Solar panels with gimbal mechanism track the Sun at all times.

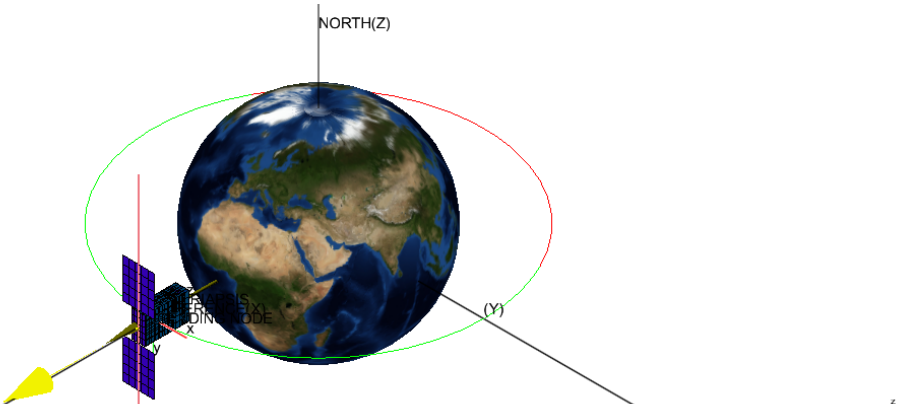

Figure 5-27: Single position of Satellite in LEO presented in Radiative Case (ESATAN - TMS)

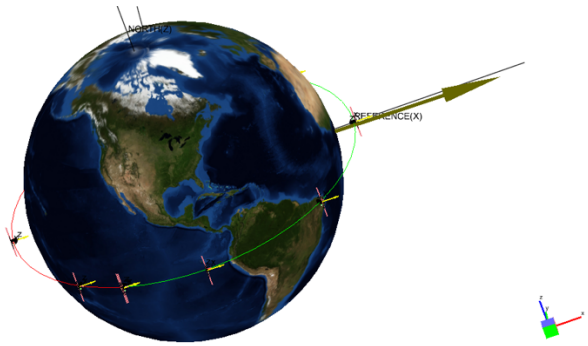

Figure 5-28: Multi position of Satellite during LEO orbit presented in Radiative Case (ESATAN - TMS)

By performing the Radiative Case simulations, values for all heat fluxes to and from the satellite during traveling the Earth orbit were obtained.

5.2.3.2 Deep space simulation

The main purpose of thermal simulation work was to investigate temperature conditions inside the CubeSat for the payload sample and different electronic components during a flight from Earth to Mars.

Distance from the Sun to Earth is roughly 149,598,000 km and it is commonly known as 1 Astronomical Unit (1 AU). Mars is placed in orbit at approximate distance of 1.52 AU.

The intention of the research was to check temperature conditions at different discrete distances during a transfer flight from Earth to Mars from1.0 AU to 1.5 AU:

1.1 AU or 164,557,800 km

1.2 AU or 179,517,600 km

1.3 AU or 194,477,400 km

1.4 AU or 209,437,200 km

1.5 AU or 224,397,000 km.

Deep space flight has big differences from the Earth Orbit case. There is no sudden change in temperature as a consequence of the eclipse phase during

~~the~~ orbit, no sunlight reflected from the planet (planet heat flux) or moon and no infrared radiation (IR) emitted from the surface or atmosphere of the celestial body.

Deep space flight can therefore be considered to be influenced just from direct sunlight – Solar heat flux which decrease with distance travelled from the Sun. Therefore, deep space transfer flight with the certain distance from nearest celestial body can be thermally threated as steady. Biggest thermal fluctuations are caused by the operational phases of installed electronic components.

For simulation purposes the satellite was placed in an circular orbit around the Sun with above specified discrete distances from 1.0 AU to 1.5 AU (Figure 5-29).

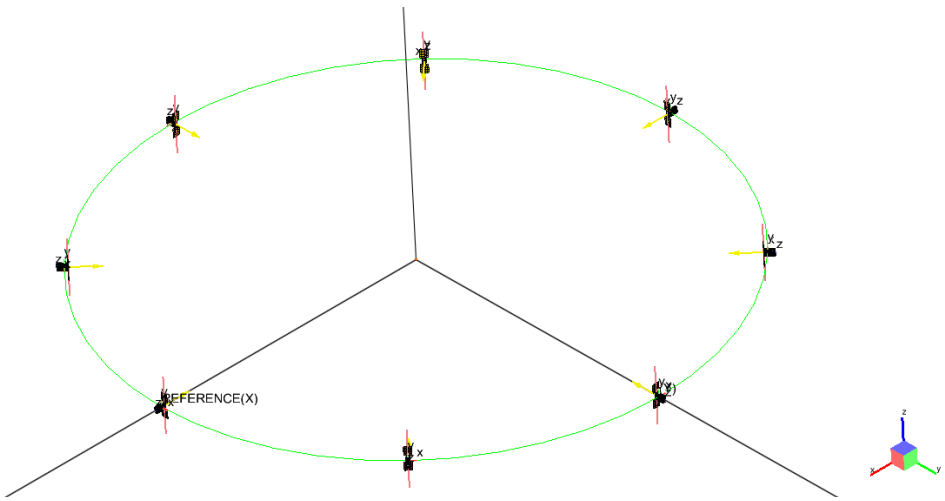

Figure 5-29: Deep space Radiative case simulation with spacecraft placed in orbit around the Sun in ESATAN - TMS

For each different optical coating of the satellite the outside structure, individual Radiative case was run. Therefore three Radiative calculations for each distance (List of Radiative cases can be found in Appendix 8.4). Input values for simulating deep space Radiative Case at distance 1.1 AU are:

Radiative Case Dialog → Environment

- *Celestial body: Sun*
- *Inertial Coordinate System: Sun*

Radiative Case Dialog → Orbit

- *Eccentricity: 0 °*
- *Semi – Major Axis: 164,557,800 km*
- *Radius at Aphelion: 164,557,800 km*
- *Radius at Perihelion: 164,557,800 km*
- *Inclination: 0 °*
- *Angle gap (deg): 45*
- *Number of Positions: 8*

Radiative Case Dialog → Pointing

Primary pointing

- Pointing vector: [1.0,0.0,0.0]
- Pointing direction: velocity

Secondary pointing

- Pointing vector: [0.0,0.0, 1.0]
- Pointing direction: zenith

In the above described example the CubeSat was placed in circular orbit around the Sun at a distance of 1.1 AU in equatorial plane (0 ° inclination). The satellite which is traveling inbound +X axis with the solar panels part of the body (-Z) oriented towards the Sun at all times is seen throughout 8 positions around the orbit (Figure 5-30).

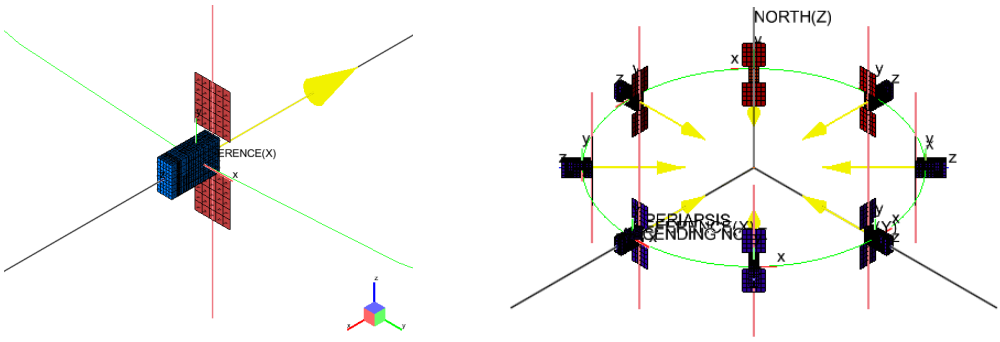

Figure 5-30: Position of CubeSat in simulated orbit around the Sun with Heat Flux results (right) and detailed view of single position (left) (ESATAN - TMS)

The described approach is the only possible approximation for simulating spacecraft flight from Earth to Mars. Scenarios when close to the celestial body were not taken into calculations. Orientation and attitude of the Satellite body was unchanged throughout the simulation procedure, to obtain comparable results. During the real transfer mission from Earth to Mars, the satellite would hold the same position with panels oriented towards the Sun. If needed for communication, track correction or other purposes attitude could be adjusted with the installed ADCS unit and thrusters. In future studies it would be interesting to investigate changes in the CubeSat thermal environment with different orientation of the body and solar panels.

Similar simulations as for a distance of 1.1 AU, were performed for all discrete distances from the Sun toward Mars.

Finishing Radiative case simulations results were exported to the Thermal analysis module to obtain temperatures values.

5.2.4 Thermal Analysis Control

The final stage of the ESATAN – TMS Workbench processing of a model is to output results in the form of an analysis file. The analysis file is used by the thermal analyser to solve the thermal model. Output results are temperature values for different components of different Radiative environments.
For the research work, geometry model simulations were performed for:

- ***three different geometries – optical coating configurations*** (Chapter 5.2.2),
- ***five different Radiative environments*** (from 1.1 AU to 1.5 AU) and for
- ***three sets of Boundary conditions*** (zero, normal - operational and high - maximum heat dissipation of electronic components).

On top of basic thermal simulations were also investigated additional heat load requirements (in W) needed to maintain temperature conditions of 4 °C and 37 °C in the biological payload compartment.
All together were performed 27 thermal analysis simulations for each discrete distance, making all together 135 simulation sets (Appendices H, I).

Finally an additional investigation was performed to find out what extra thermal input would be needed to sustain vital electronic components within temperature operational, or at least survival, level.

The most important settings to be set in the Analysis Case Menu are the following:

- ***Radiative Data***

Initially sources of Radiative case simulation must be specified. As the Analysis Case Type the Single Radiative Case option is selected, and in the next input line under Radiative Case, the Radiative Case simulation which to be used in calculation is specified.

- **Conductors**

Within this menu it is defined how conduction within surfaces will be included in the simulation. The generated and user defined option to be included in calculation are marked in the menu. Values of user defined conductors were calculated manually, as seen in Section 5.2.2.8.

- **Boundary Conditions**

Within the boundary condition the amount of heat dissipation to be taken into calculation is set. Here are ticked values either for zero, minimum or maximum heat dissipation options (Figure 5-59). For investigating additional heat load required to maintain temperature conditions for the payload or electronic component, extra heat load was included in simulation (Heat loads are listed in Appendix K).

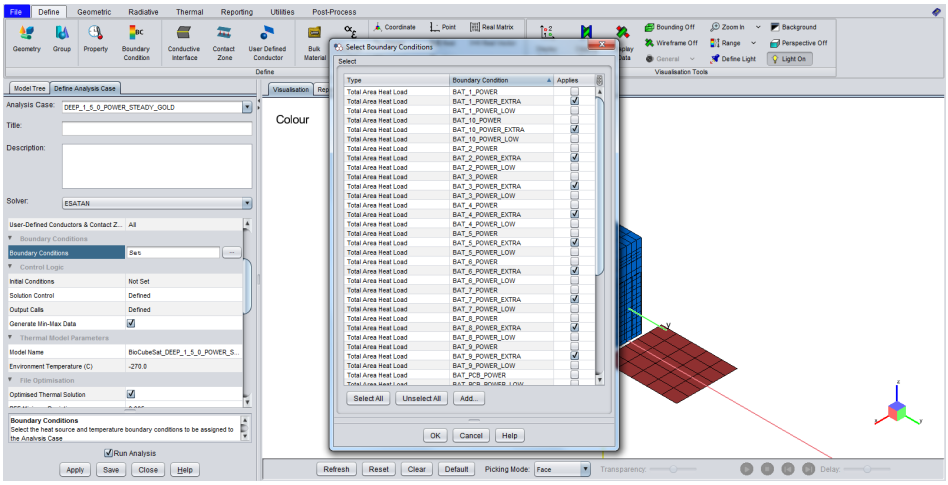

Figure 5-31: Selecting Boundary Conditions in Analysis Case Window (ESATAN - TMS)

- **Control Logic**

Default values were set for initial conditions and Steady State solutions were selected for Solution Control, not expecting to have any rapid temperature changes. Parameters such as Maximum Number of Iterations and Convergence criterion were left at default setting (Figure 5-32). Furthermore, within **Thermal Model Parameters, File Optimisation and Model files menus** default settings are left.

- **Advanced Options**

Performing deep space environment simulation, the settings at Heat Flow (HF) Output Format window are needed to be modified. For Orbital and Planet Surface Analysis, HF Output format controls the way in which data for three types of HF (Solar - S, Albedo - A and Planet - P) are included in the analysis file, either separately or combined in various different ways [82].

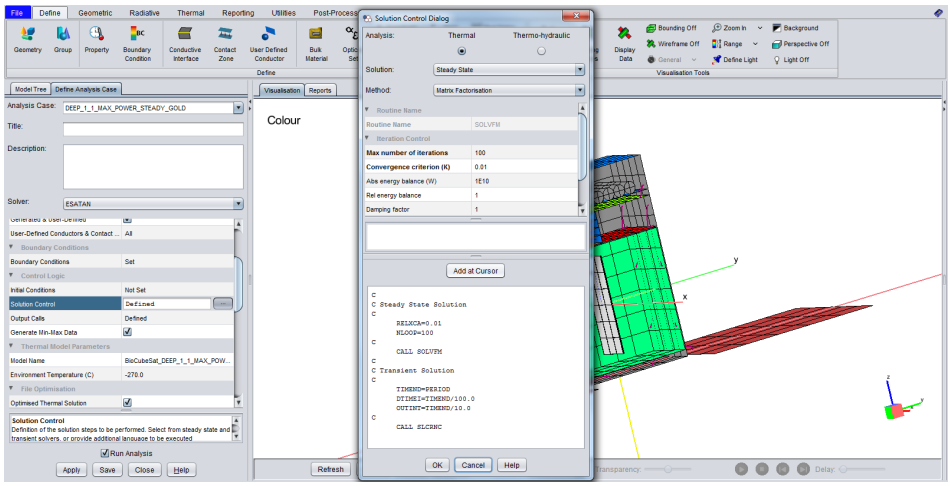

Figure 5-32: Solution Control dialog for Steady State (ESATAN - TMS)

For deep space environment simulation, it is important to select only values for Solar (S) heat flux to be included in analysis, since there is no albedo and planet heat flux present.

Setting all input parameters, the Analysis case is created and Analysis file generated.

5.2.5 Post processing and displaying results

Once thermal analysis results are obtained, they are Post- Processed by using attribute charts. Charts can be plotted for all thermal model parameters of an Analysis Case. The data for an Analysis Case is stored within Thermal Model Data sets (TMD files) which can be found in the Results Files folder in the Model Tree. Inside the TMD file Steady state data are saved and inside TMD2 for Transient simulations.

Average Temperature output returns the average temperature of active nodes in the geometry at the single time step [82]. As seen in the Results chapter, temperature conditions for different installed components, the biological payload compartment and CubeSat as a whole are displayed (Figure 5-33).

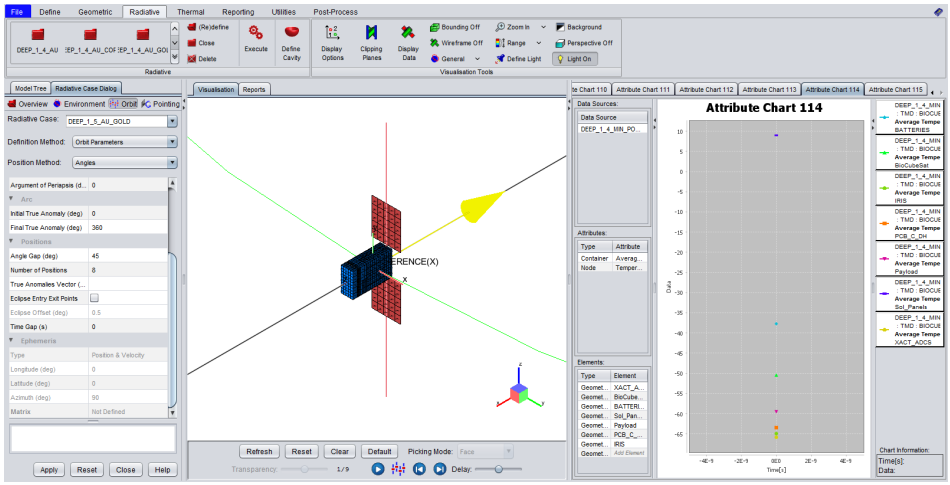

Figure 5-33: Attribute Chart sample presentation (right side of display) with plotted Steady state, Average Temperature conditions for different installed components

Temperature values were recorded, saved and further processed in suitable editor software – MS Excel.

5.2.6 Conclusion

In Chapter 5 the modelling software ESATAN – TMS was introduced. In Appendix E an overview of the software with a basic introduction of modules and commands was performed. It can be used as a tutorial. In section, a custom 6U CubeSat model suitable for deep space mission with a biological

payload on board was built. Suitable geometry was designed and appropriate components installed for supporting deep space mission. It is important to point out that just provisional components selection was performed. On the basis of the known mission information and literature available it was impossible to make more accurate selection and design.

CubeSat geometry model was virtually placed in the deep space environment, the same as expected to appear during transfer flight from Earth to Mars. Thermal values inside the payload compartment and for the satellite body and installed components were further calculated and evaluated by running a thermal analysis case (Chapter 5.3).

5.3 Thermal simulations

5.3.1 Introduction and methodology

The following chapter presents the results for the ESATAN – TMS thermal simulations at different discrete distances during interplanetary flight from Earth to Mars for the CubeSat model with a high form of biological payload. Three different geometry surface thermal coatings were investigated:

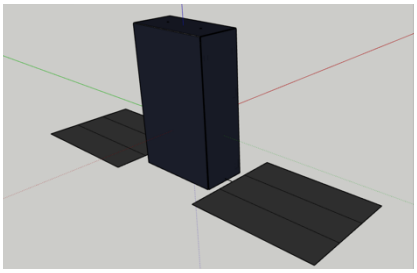

Option 1:

Black anodised Aluminium body structure with graphite composite the back side of the solar cell panel – **basic design**.

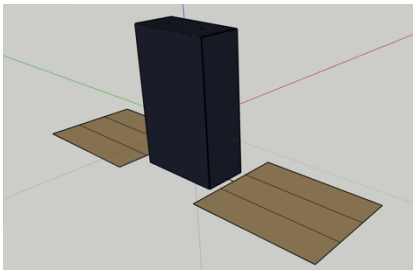

Option 2:

Black anodised Aluminium body structure with gold surface coating on the back side of the solar cell panel.

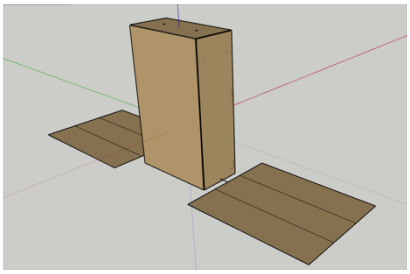

Option 3:

Gold anodised Aluminium body with gold surface coating on the back side of the solar cell panel.

Thermo – optical properties for the gold surface coating and Kapton foil are very similar, therefore results obtained for the gold coating are also taken into consideration for the Kapton foil [80], [81]. By comparing results from thermal analysis, it will be further investigated, which thermo – optical coating finish would be most efficient and suitable for the designed model. Temperature values were simulated as average temperature for different components and structure:

- **Batteries** – average temperature of installed batteries and belonging PCB board,
- **Bio CubeSat** - average temperature of whole satellite model,
- **Transponder** – average temperature of Transponder Communication unit,
- **C&DH PCB** – average temperature of Computer and Data Handling PCB unit,
- **Payload Box** – average temperature of complete payload container,
- **Payload Sample** – average temperature of biological payload sample,
- **ADCS** – average temperature of Attitude Determination and Control System Unit,
- **Solar Panel** – average temperature of Solar panels.

Simulations were performed for **zero (0)**, **normal (NORM)** and **high (HIGH)** heat dissipation caused by installed electronic components operating at different working regimes at discrete distances from **1.1** to **1.5 AU**. Calculation of heat dissipation for electronic components is discussed in Subchapter 5.2.2.9.

After obtaining temperature conditions, it was further investigated what additional heat load would be required to be added, to maintain the temperature of the biological payload sample at **4 °C** or **37 °C.** Additional heat load required

was modelled as being in contact with the biology payload sample (Subchapter 5.2.2.7, Figure 5-19). For a better interpretation temperature values at the biological payload sample were marked with blue (zero heat dissipation), green (normal heat dissipation) and red (high heat dissipation) markers in the result presentation tables.

Temperature environment is also of great importance for normal operation of different installed electronic components. Operational and Survival Temperature values as specified in the literature (Table 5-5).

Equipment	*Operational temp. (°C)*	*Survival temp. (°C)*
Avionics Baseplates	- 20 → 60	- 40 → 75
Batteries	10 → 30	0 → 40
Solar Arrays	- 150 → 110	- 200 → 130
Antennas	- 100 → 100	- 120 → 120
Reaction Wheels	- 10 → 40	- 20 → 50

Table 5-5: Working temperatures for specific electrical components [91]

Temperature conditions for most sensible electronic components were also investigated and required additional heat loads calculated.

5.3.2 Presentation of the results

5.3.2.1 Temperature conditions and additional heating required for biological payload sample and installed components.

Remark: decimal values in Tables 5-6 to 5-14 are marked with ",".

Values for temperature conditions in the payload compartment with a biological payload are marked **blue** for **zero (0)** electronic heat dissipation scenario, **orange** for heat dissipation of electronic components during **normal (NORM)** operation and **grey (HIGH)**, as heat dissipated during maximum performance of installed electronic components (Table 5-4).

The same colour presentation is also valid ~~also~~ for Diagram presentations throughout the Thermal chapter.

Distance	1.1 AU			1.2 AU			1.3 AU			1.4 AU			1.5 AU		
Heat dissipation	0	NORM	HIGH	0	NORM	HIGH	0	NORM	HIGH	0	NORM	HIGH	0	NORM	HIGH
Batteries	-53,42	-19,15	19,09	-59,51	-23,24	16,34	-64,96	-26,80	14,02	-69,89	-29,91	12,02	-74,38	-32,67	10,29
BioCubeSat	-34,38	-17,87	16,17	-42,10	-24,58	11,23	-48,95	-30,39	7,00	-55,09	-35,52	3,35	-60,65	-40,10	0,16
Transponder	-48,07	-37,09	28,99	-54,72	-43,03	25,29	-60,63	-48,25	22,13	-65,94	-52,90	19,40	-70,77	-57,07	17,03
C&DH PCB	-51,40	-37,31	8,89	-57,76	-42,88	5,27	-63,42	-47,79	2,19	-68,52	-52,16	-0,47	-73,16	-56,09	-2,79
Payload Box	-28,93	-22,69	3,33	-37,42	-30,55	-2,62	-44,89	-37,40	-7,66	-51,52	-43,42	-11,99	-57,49	-48,78	-15,75
Payload Sample	-28,94	-22,69	3,32	-37,44	-30,56	-2,64	-44,90	-37,40	-7,69	-51,54	-43,43	-12,01	-57,49	-48,80	-15,77
ADCS	-47,95	-37,88	-3,63	-54,61	-43,85	-7,65	-60,54	-49,10	-11,08	-65,87	-53,77	-14,03	-70,70	-57,95	-16,60
Solar Panel	126,47	127,23	130,38	107,37	108,31	112,12	90,44	91,59	96,10	75,29	76,66	81,93	61,62	63,25	69,30

Table 5-6: Option 1 Simulation results - Black anodized Aluminium body structure with graphite solar panel base (Temp. in °C)

4°	0	NORM	HIGH
1.1 AU	0,93	0,78	0,02
1.2 AU	1,12	0,97	0,21
1.3 AU	1,27	1,12	0,37
1.4 AU	1,39	1,24	0,49
1.5 AU	1,50	1,34	0,60

Table 5-7: Additional heat power (W) required at payload sample to maintain 4 °C

37°	0	NORM	HIGH
1.1 AU	2,20	2,05	1,30
1.2 AU	2,39	2,24	1,49
1.3 AU	2,54	2,39	1,65
1.4 AU	2,67	2,52	1,77
1.5 AU	2,77	2,62	1,87

Table 5-8: Additional heat power (W) required at payload sample to maintain 37 °C

Distance	1.1 AU			1.2 AU			1.3 AU			1.4 AU			1.5 AU		
Heat dissipation	0	NORM	HIGH	0	NORM	HIGH	0	NORM	HIGH	0	NORM	HIGH	0	NORM	HIGH
Batteries	-60,48	-23,86	16,00	-67,11	-28,16	13,19	-73,02	-31,84	10,83	-78,34	-35,04	8,82	-83,17	-37,85	7,10
BioCubeSat	-46,66	-28,94	7,20	-54,61	-35,62	2,42	-61,64	-41,41	-1,61	-67,91	-46,50	-5,07	-73,56	-51,00	8,06
Transponder	-55,87	-44,04	24,72	-63,03	-50,36	20,91	-69,39	-55,89	17,70	-75,07	-60,77	14,95	-80,21	-65,13	12,58
C&DH PCB	-58,78	-43,76	4,79	-65,66	-49,71	1,06	-71,77	-54,92	-2,09	-77,25	-59,53	-4,78	-82,21	-63,65	-7,10
Payload Box	-39,78	-32,77	-4,38	-48,69	-40,92	-10,36	-56,48	-47,97	-15,38	-63,40	-54,13	-19,65	-69,55	-59,58	-23,32
Payload Sample	-39,79	-32,77	-4,40	-48,70	-40,93	-10,39	-56,49	-47,99	-15,40	-63,44	-54,14	-19,67	-69,56	-59,57	-23,33
ADCS	-55,77	-44,87	-8,26	-62,95	-51,22	-12,39	-69,32	-56,77	-15,88	-75,02	-61,67	-18,85	-80,16	-66,04	-21,41
Solar Panel	47,27	48,04	51,26	32,76	33,71	37,70	19,93	21,07	25,55	8,48	9,83	14,98	-1,83	-0,25	5,61

Table 5-9: Option 2 Simulation results - Black anodized Aluminium body structure with gold coated solar panel base (temp. in °C)

4°	0	NORM	HIGH
1.1 AU	1,17	1,02	0,27
1.2 AU	1,34	1,19	0,45
1.3 AU	1,48	1,33	0,59
1.4 AU	1,59	1,44	0,70
1.5 AU	1,68	1,53	0,79

Table 5-10: Additional heat power (W) required at payload sample to maintain 4 °C

37°	0	NORM	HIGH
1.1 AU	2,44	2,29	1,55
1.2 AU	2,62	2,47	1,73
1.3 AU	2,76	2,61	1,87
1.4 AU	2,87	2,72	1,98
1.5 AU	2,95	2,81	2,09

Table 5-11: Additional heat power (W) required at payload sample to maintain 37 °C

Distance	1.1 AU			1.2 AU			1.3 AU			1.4 AU			1.5 AU		
Heat dissipation	0	NORM	HIGH	0	NORM	HIGH	0	NORM	HIGH	0	NORM	HIGH	0	NORM	HIGH
Batteries	-65,95	-27,41	13,69	-72,24	-31,36	11,14	-77,85	-34,76	9,00	-82,90	-37,70	7,18	-87,49	-40,29	5,61
BioCubeSat	-52,81	-34,04	3,65	-60,31	-40,26	-0,71	-66,95	-45,66	-4,40	-72,87	-50,40	-7,57	-78,22	-54,60	-10,31
Transponder	-61,81	-49,29	21,55	-68,57	-55,19	18,09	-74,57	-60,35	15,17	-79,93	-64,91	12,68	-84,79	-68,97	10,52
C&DH PCB	-64,46	-48,67	1,71	-70,97	-54,24	-1,68	-76,74	-59,12	-4,55	-81,93	-63,43	-6,99	-86,62	-67,28	-9,10
Payload Box	-47,55	-39,91	-9,71	-55,80	-47,38	-15,06	-63,04	-53,86	-19,55	-69,44	-59,52	-23,37	-75,18	-64,53	-26,66
Payload Sample	-47,57	-39,92	-9,74	-55,80	-47,40	-15,08	-63,09	-53,86	-19,57	-69,45	-59,51	-23,38	-75,19	64,52	-26,68
ADCS	-61,73	-50,14	-11,70	-68,50	-56,07	-15,45	-74,51	-61,25	-18,61	-79,89	-65,82	-21,31	-84,75	-69,90	-23,63
Solar Panel	46,35	47,18	50,58	31,84	32,85	36,88	19,00	20,22	24,91	7,54	8,98	14,36	-2,78	-1,10	5,01

Table 5-12: Option 3 Simulation results - Gold anodized Aluminium body structure with gold coating sol. panel base (Temp. in °C)

4°	0	NORM	HIGH
1.1 AU	1,32	1,17	0,43
1.2 AU	1,47	1,32	0,58
1.3 AU	1,59	1,44	0,70
1.4 AU	1,68	1,53	0,80
1.5 AU	1,76	1,61	0,88

Table 5-13: Additional heat power (W) required at payload sample to maintain 4 °C

37°	0	NORM	HIGH
1.1 AU	2,60	2,45	1,71
1.2 AU	2,74	2,60	1,86
1.3 AU	2,86	2,71	1,97
1.4 AU	2,96	2,81	2,07
1.5 AU	3,03	2,89	2,15

Table 5-14: Additional heat power (W) required at payload sample to maintain 37 °C

5.3.2.2 Option 1: Black anodized Aluminium body structure with graphite solar panel base

A black anodized Aluminium body structure with graphite epoxy solar panel structure base was selected as the basic option. In this example no additional optical coating on the satellite body or on solar panels was used, so no passive thermal control was introduced. Temperature results for different distances are presented in Tables: 5-6, 5-7, 5-8 and Diagram 5-1.

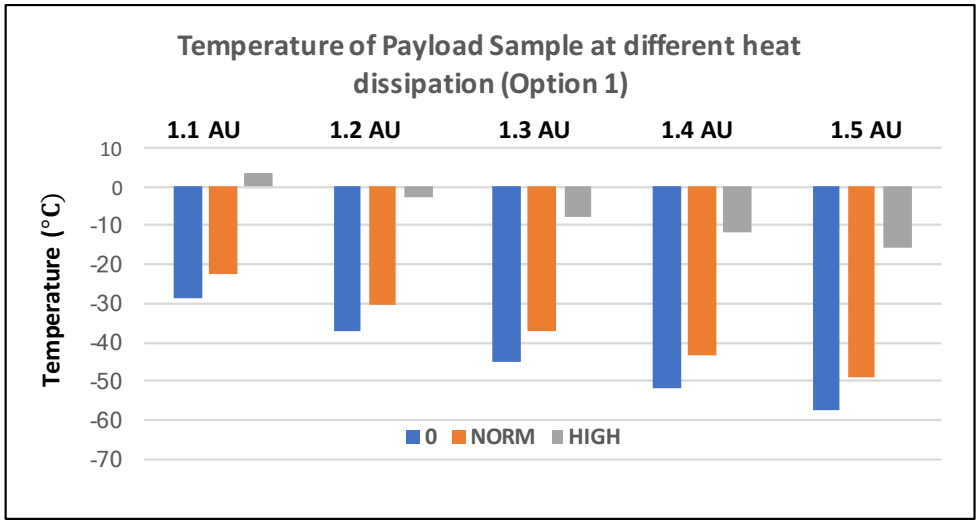

Diagram 5-1: Temperature of payload sample for different heat dissipation, at different distances for optical coating Option 1

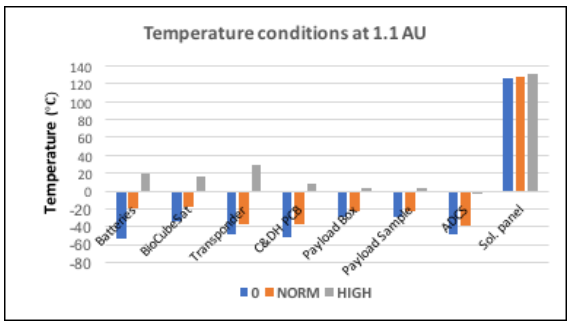

Diagram 5-2: Temperature conditions for components at 1.1 AU for Option 1

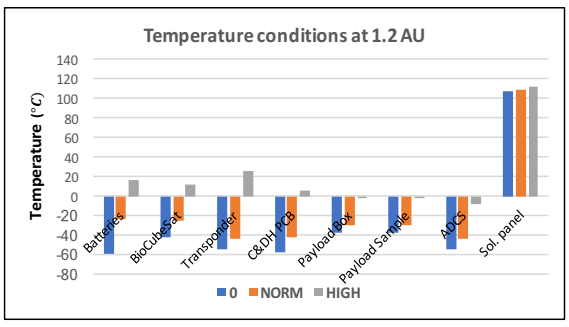

Diagram 5-3: Temperature conditions for components at 1.2 AU for Option 1

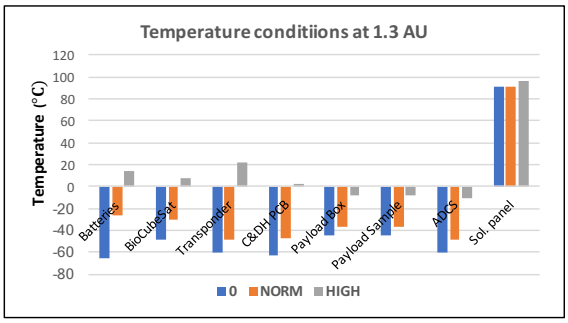

Diagram 5-4: Temperature conditions for components at 1.3 AU for Option 1

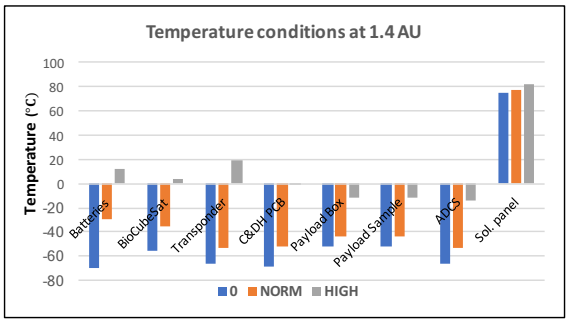

Diagram 5-5: Temperature conditions for components at 1.4 AU for Option 1

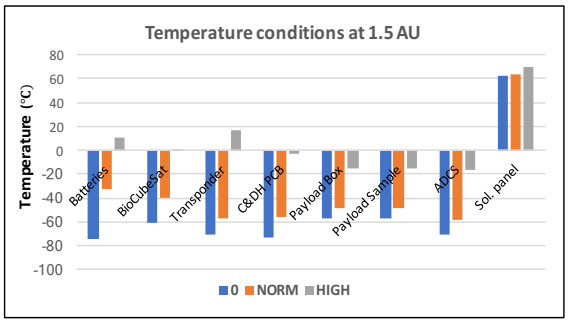

Diagram 5-6: Temperature conditions for components at 1.5 AU for Option 1

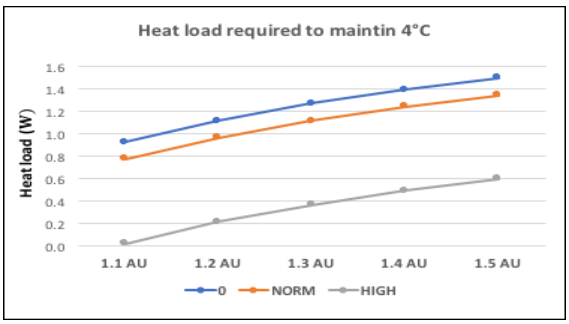

Diagram 5-7: Additional heat load required to maintain 4 °C at biological payload at different distances from Sun for Option 1

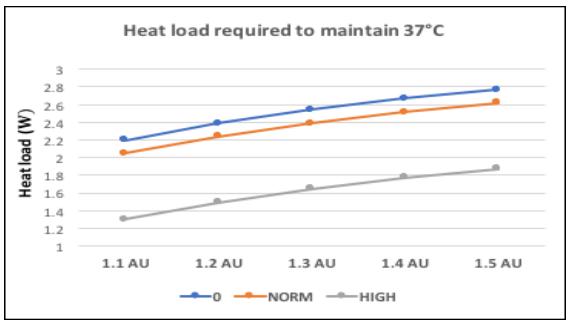

Diagram 5-8: Additional heat load required to maintain 37 °C at biological payload at different distances from Sun for Option 1

It can be noticed that temperature at the biological payload drops to nearly -58 °C at a distance of 1.5 AU and constant external heat load of nearly 2.8 W is

required to maintain a temperature of 37 °C or 1.5 W for maintaining 4 °C (Diagrams 5-8, 5-7) .

Regarding electronic components, batteries and C&DH PCB board cool down to approximately -75 °C at a distance of 1.5 AU when there is no internal heat dissipation from electronic equipment (Diagrams 5-2 to 5-6).

High temperature of solar panels from around 130 °C at 1.1 AU to 60 °C at 1.5 AU can also be noticed. This happens because no optical coating is applied to the back of satellite panels.

As seen in the results at specific distances from the Sun and with none or low internal heat dissipation from electrical components, additional heat load is required to maintain most temperature sensitive components within survival or operational limits.

5.3.2.2.1 Additional heating requirements for electronic components

The main task of ESATAN-TMS thermal simulation work was to provide an appropriate temperature environment for the biological payload compartment.

But not just the biological payload, also electronic components and other subsystems of the satellite have specific operational and survival temperature requirements which need to be meet for normal operation. Temperature requirements are outlined in Table 5-5.
For the basic satellite configuration (black anodized body and graphite epoxy solar panel base) set of simulations for most temperature sensitive components have been performed, to investigate what amount of additional heat load would be required to sustain desired temperature. Simulations were performed just for the worst case scenario – at distance of 1.5 AU.

- **Batteries**

Batteries supplying energy are one of the most important components for normal operation of the space craft and also one of the most temperature sensitive components. As seen in Table 5-5, the survival temperature range is

between 0 °C and 40 °C, while operational constraint is even narrower between 10 °C and 30 °C.

The additional heat needed to be supplied to the single battery unit, to maintain survival (0 °C) or operational (10 °C) limit at distance of 1.5 AU was investigated through simulations (Table 5-15). Simulations were performed with no, low or maximum heat dissipation from other electronic equipment installed on board without optical coating (Option 1). As a result, the average temperature of all batteries in the battery unit was checked.

	Survival (0 °C)	**Operational (10 °C)**
0 heat diss.	**0.86 W**	**1.02 W**
NORM heat diss.	**0.44 W**	**0.65 W**
HIGH heat diss.	**/**	**/**

Table 5-15: Additional heat power (W) required for single battery at 1.5 AU with zero, normal and high heat dissipation from installed electronic components

- **Command and data handling board**

The Command and Data Handling electronic board is also a temperature sensitive component, with less strict limits than for batteries, operational being between -20 °C to 60 °C and survival between -40 °C to 75 °C. Simulation was performed in the same way as for batteries and at a distance of 1.5 AU, for satellite without an optical coating (Option 1). Additional heating required to survive or for normal operation is specified in Table 5-16.

	Survival (-40 °C)	Operational (-20 °C)
0 heat diss.	**4.9 W**	**7.4 W**
NORM heat diss.	**2.7 W**	**5.1 W**
HIGH heat diss.	**/**	**/**

Table 5-16: Additional heat power (W) required for Command and Data Handling board at 1.5 AU with zero, normal and high heat dissipation from installed electronic components

- **Reaction wheels**

Reaction wheels are part of the Attitude Determination and Control System (ADCS) unit and are also temperature sensitive with operational range between -10 °C to 40 °C and survival from -20 °C to 50 °C.

Simulation was performed for a ADCS unit where reaction wheels and body of the unit are incorporated. This surface is made mainly from Aluminium and steel, therefore there are also higher heat requirements for obtaining specific temperature. Additional heat required is specified in Table 5-17.

	Survival (-20 °C)	Operational (-10 °C)
0 heat diss.	**16.2 W**	**19.2 W**
NORM heat diss.	**12.6 W**	**16 W**
HIGH heat diss.	**1.2 W**	**4.4 W**

Table 5-17: Additional heat power (W) required for ADCS with reaction wheels at 1.5 AU with zero, normal and high heat dissipation from installed electronic components

- **Transponder Communication unit**

The Transponder Communication unit is assembled from electronic boards combined as slots in a box. Additional heat required for each of the four electronic boards was calculated. Temperature was calculated as average

temperature of a whole unit. Operational and survival temperature limits are the same as for the Command and Data Handling board. Additional heat required for the single board is specified in Table 5-18.

	Survival (-40 °C)	Operational (-20 °C)
0 heat diss.	**2.8 W**	**4.1 W**
NORM heat diss.	**1.7 W**	**3.1 W**
HIGH heat diss.	**/**	**/**

Table 5-18: Additional heat power (W) required for single 1of 4 electronic board plates installed in Transponder Communication unit at 1.5 AU with zero, normal and high heat dissipation from installed electronic components

5.3.2.3 Option 2: Black anodized Aluminium body structure with gold coated solar panel base

For the second example same optical properties of the satellite body were selected – black anodized Aluminium, but optical properties of the back side of the solar panels was changed. High temperature values were noticed when no passive thermal control was applied. In this example, the base of the solar panels was covered with an anodized gold layer, which has the same optical properties as Kapton thermal protection foil. Simulation results are visible in Tables and in Diagrams bellow.

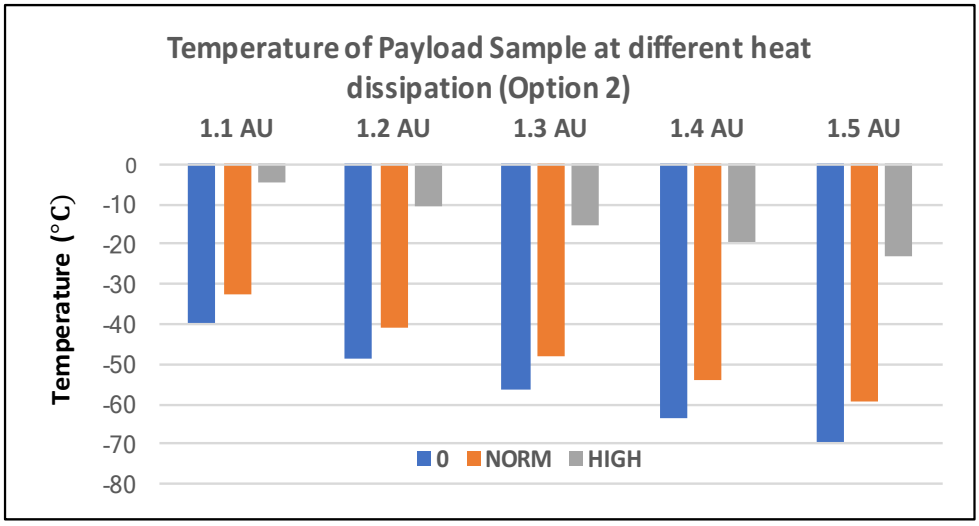

Diagram 5-9: Temperature of payload sample for different heat dissipation at different distances for optical coating Option 2

Comparing with Option 1 can be seen lower temperatures at biological payload sample, which might be because of the lower temperatures of the solar panels (Diagram 5-9).

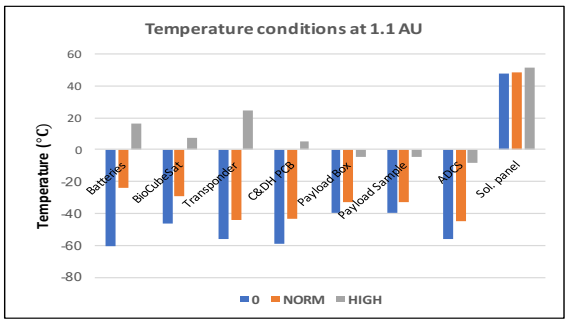

Diagram 5-10: Temperature conditions for components at 1.1 AU for Option 2

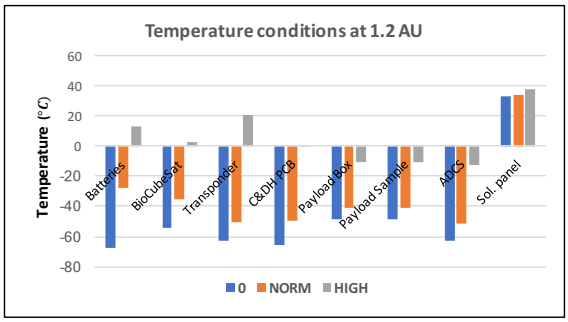

Diagram 5-11: Temperature conditions for components at 1.2 AU for Option

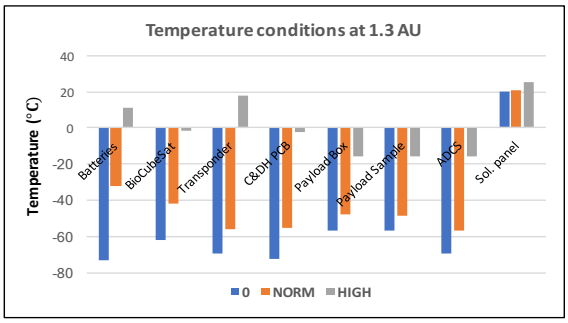

Diagram 5-12: Temperature conditions for components at 1.3 AU for Option 2

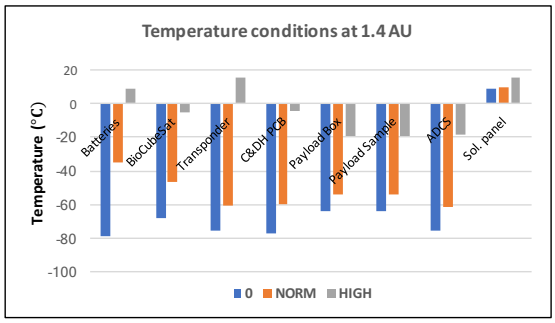

Diagram 5-13: Temperature conditions for components at 1.4 AU for Option 2

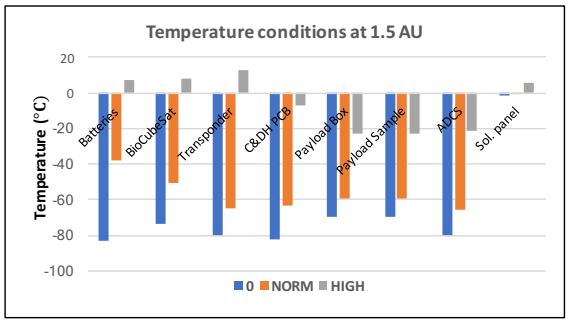

Diagram 5-14: Temperature conditions for components at 1.5 AU for Option 2

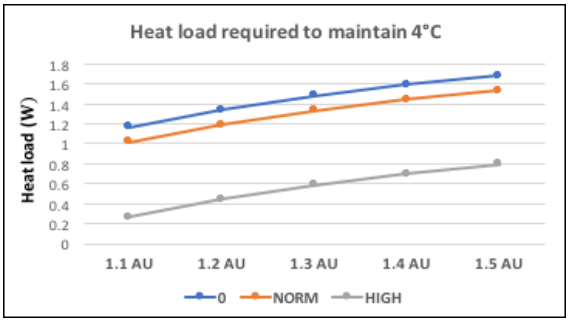

Diagram 5-15: Additional heat load required to maintain 4 °C at biological payload at different distances from Sun for Option 2

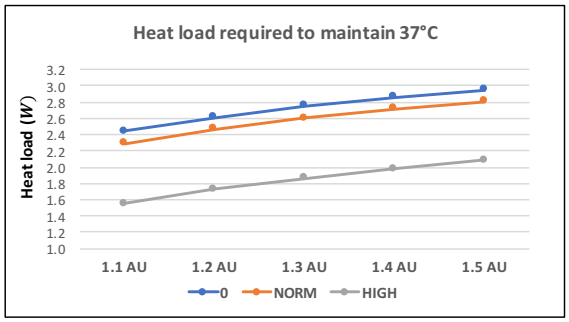

Diagram 5-16: Additional heat load required to maintain 37 °C at biological payload at different distances from Sun for Option 2

Comparing results, much lower temperature of solar panels can be noticed. Therefore, also lower temperature of the components installed in the satellite. (Diagrams 5-10 to 5-14). The temperature of the solar panels with the optical

coating Option 2 at 1.1 AU is around 50 °C while with the optical coating Option 1 temperature of the panels reached around 130 °C. At 1.5 AU with Option 1 solar panels still have around 60 °C while with optical coating Option 2 just 0 °C.

To maintain the desired temperature environment at the biological payload sample higher thermal power input is needed. At 1.5 AU with zero heat dissipation around 3 W is needed to maintain 37 °C (Diagram 5-16) while with optical coating Option 1 around 2.8 W is needed for the same task.

5.3.2.4 Option 3: Gold anodized Aluminium body with gold coating solar panel base

For the final set of simulations, the solar panel base as well as the satellite body was coated with an anodized gold coating. Results of the simulation set are presented in Table and Diagrams below. The temperature conditions in the biological payload for optical coating Option 3 are presented in Diagram 5-17.

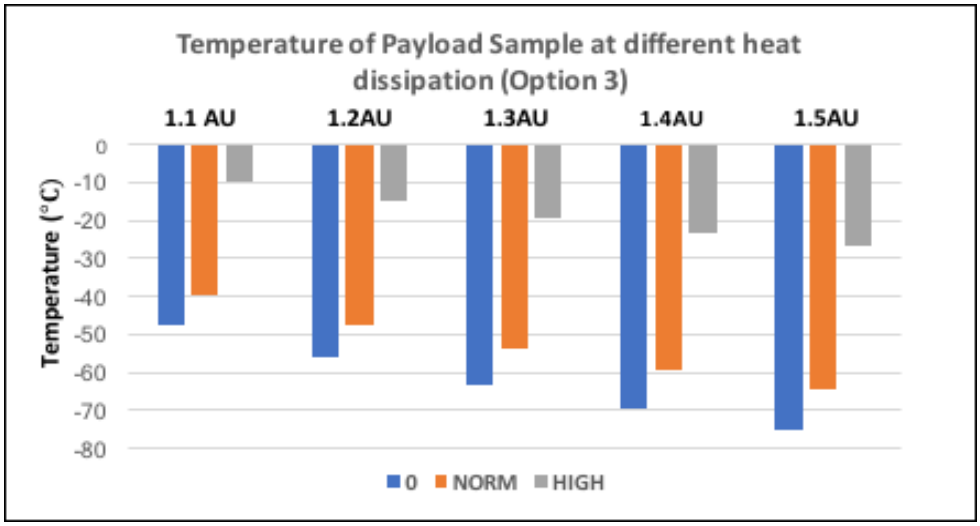

Diagram 5-17: Temperature of payload sample for different heat dissipation at different distances for optical coating Option 3.

Compared with the first two sets of simulations (Option 1, 2), it can be noticed that the temperature of the biological payload with the applied gold coating to the satellite structure and solar panels base, is the lowest (Diagram 5-17).

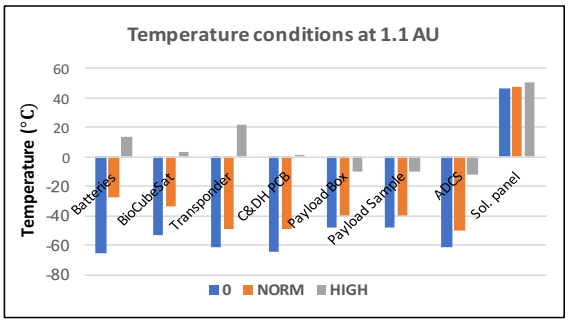

Diagram 5-18: Temperature conditions for components at 1.1 AU for Option 3

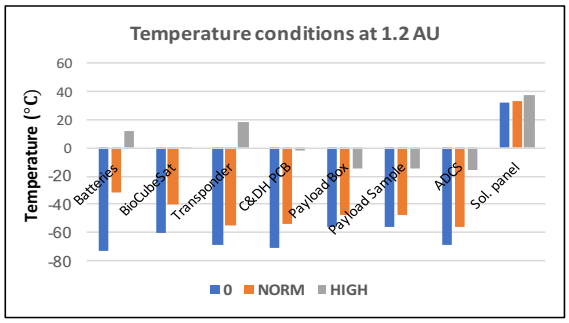

Diagram 5-19: Temperature conditions for components at 1.2 AU for Option 3

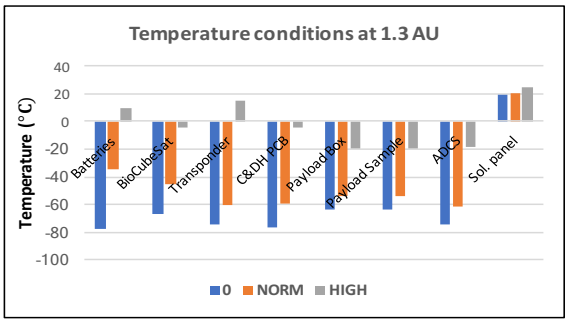

Diagram 5-20: Temperature conditions for components at 1.3 AU for Option 3

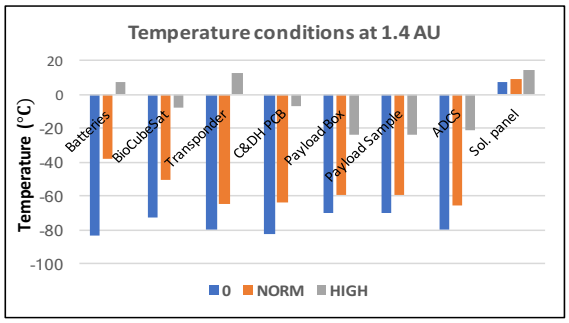

Diagram 5-21: Temperature conditions for components at 1.4 AU for Option 3

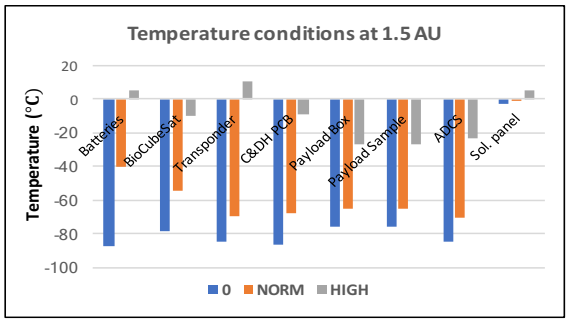

Diagram 5-22:Temperature conditions for components at 1.5 AU for Option 3

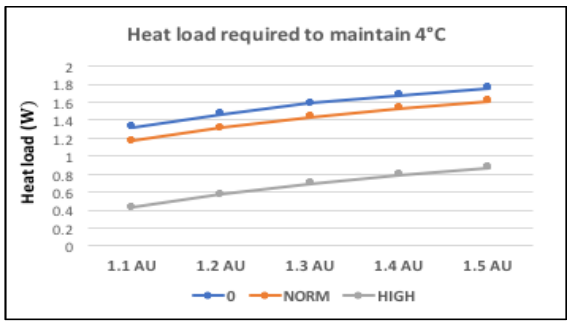

Diagram 5-23: Additional heat load required to maintain 4 °C at biological payload at different distances from Sun for Option 3

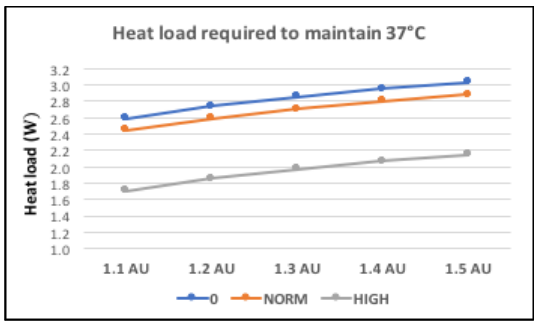

Diagram 5-24: Additional heat load required to maintain 37 °C at biological payload at different distances from Sun for Option 3

Diagrams 5-18 to 5-22 show temperature conditions of electronic components inside the satellite.

As already discussed, for the optical coating presented in Option 3, the biggest amount of heat load is required to maintain the desired temperature condition for the biological payload and would not be the optimum solution for longer interplanetary space flight (Diagrams 5-23 and 5-24).

5.3.3 Comparison of the thermal simulation results with similar CubeSat mission

As previously discussed throughout the work, the main reference regarding the CubeSat spacecraft design with the biological payload is presented by the future NASA BioSentinel mission [17], [18], [19], [110].

Performed thermal simulations were therefore compared with the BioSentinel thermal control data available for the similar orbital parameters [17]. The BioSentinel is planned to be placed ~~to~~ in an Earth like heliocentric orbit at an approximate distance of less than 1 AU from the Sun (Figure 5-34). Therefore, only temperature values obtained within the thesis simulation work for a distance of 1.1 AU (Tables 5-6, 5-9, 5-12) could be comparable, although BioSentinel will be placed at an even closer distance to the Sun, therefore higher temperatures are expected.

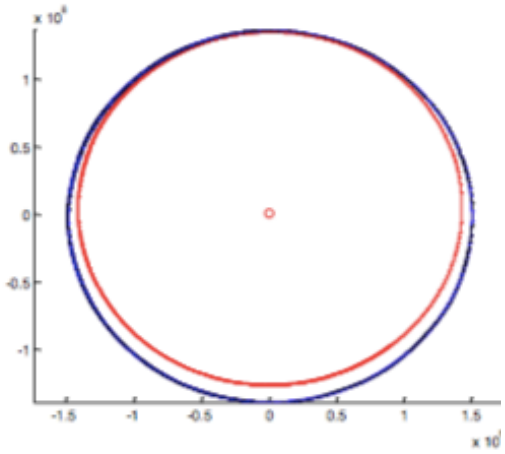

Figure 5-34: BioSentinel heliocentric orbit (red) and Earth orbit (blue) with Sun in the centre [17]

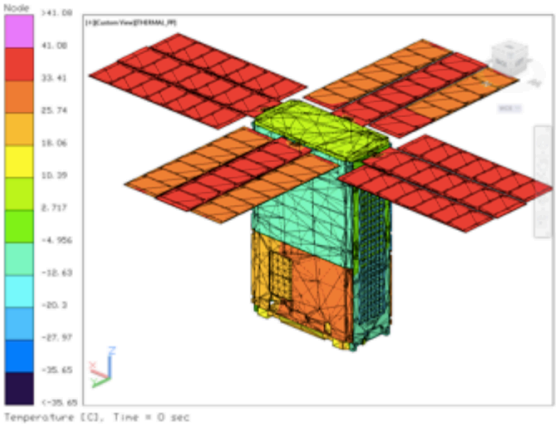

Figure 5-35: Thermal analyse results for the BioSentinel CubeSat [110]

As observed in the temperature range in Figure 5-35, temperatures for the BioSentinel simulation lies between **-35 °C** (blue) **and 41 °C** (magenta) which is comparable with values obtained within thesis work. The temperature range for Option 1, without any heat dissipation effect of the installed electronics lies in the range from -53 °C and 126 °C (Table 5-6) for Option 2 without any heat dissipation between -60 °C and 47 °C (Table 5-9) and for Option 3 without any heat dissipation between -65 °C and 46 °C (Table 5-12).

Deviations in the results are expected, as already pointed out due to Biosentinel being in closer orbit to the Sun and possible different values considered during simulations such as: different calculations and values for heat dissipation of electronic components, alternate approaches to passive heating and cooling phenomena, calculation of user defined conductors, materials with different thermo - optical characteristics and others.

For more exact analysis, more data would be needed to correlate the results.

5.3.4 Conclusion and discussion of thermal modelling work

During the thermal modelling simulations, additional thermal power required for maintaining desired environmental temperature at the biological payload sample was calculated for discrete distances from 1.1 AU to 1.5 AU for different optical coatings (Option 1, 2 and 3). Also, additional thermal power needed to maintain most sensitive electronic components at survival or operational temperature level for the worst case scenario at distance of 1.5 AU was investigated. Additional heat power requirements for electronic components were calculated just for the basic optical coating design (Option 1).

It can be seen from the calculations, that for a successful deep space CubeSat mission, regardless of optical coating design, passive heat control will not suffice, active heat control (electrical heating) will be required to maintain the desired temperature condition of the biological payload and to sustain at least survival temperature limits of installed electronic components.

In the first scenario, basic design with black anodised Aluminium satellite body and graphite solar panels base (Option 1) was investigated. As expected, minimum temperature conditions would appear at a distance of 1.5 AU without any heat dissipation (0) of internal electronics. In order to maintain the required environmental temperature for sensitive electronic components, additional heat power of: 45.8 W for survival and 60.6 W for operational regime would be required for electronic components: batteries with battery board, C&DH board, ADCS unit and Transponder (Subchapter 5.3.2.2.1) and additional 1.5 W for maintaining 4 °C (Table 5-7) or 2.77 W when 37 °C (Table 5-8) would be needed at the biological payload. This is the worst case, just a theoretically possible scenario. In reality, some heat dissipation would be present at all time during the charging and discharging process of batteries and some electronic components would be at least in stand-by mode.

In the designed model the installed solar panels (Subchapter 5.2.2.2.1) have a power peak output at a distance of 1 AU where solar irradiation is around 1371 W/m^2, of approximately 36 W. With an increased distance from the Sun, irradiation decreases with the square of the distance. Meaning that at Mars (distance of approximately 1.5 AU), solar irradiation would decrease to a value

of 586 W/m^2, roughly just 42% of the irradiation value at Earth. Electrical production of solar cells will also decrease proportionally to 15.1 W. Solar panel power production would not suffice for the thermal power needs for thermal control of the biological payload and sensitive electronic components.

The only suitable reference regarding a similar mission scenario and installed components, apart from the planned BioSentinel, are presented in the case of the MarCO CubeSat mission which was launched to Mars in mid - 2018. For the MarCO mission the same solar panels developed by the MMA Company - model HaWKS, with a peak power output of 36 W at 1AU, were installed, as was done in model designed for this thesis work [107]. Furthermore, similar main electronic components were used in the MarCO mission for: Transponder Communication unit, attitude control, cold gas thrusters and Command and Data Handling boards (Subchapter 5.2.2) [108].

Calculating power output at a Mars distance of approximately 1.5 AU, it is clear that less than a little more than 15 W of electrical energy will be available through the Solar panel production due to the greater distance. Therefore, the installed solar panels would not provide the sufficient electrical power requirements of nearly 50 W (45.8 W of thermal power required for maintaining at least survival temperature conditions for the electronic components +1.5 W or 2.77 W of the additional thermal power input for the biological payload additional heating), as calculated through the simulation. For maintaining operational thermal conditions of the electronics, power requirements are as discussed even higher, being around 64 W.

There is limited information published about thermal control technology used for the MarCO mission, to which thesis results could be directly compared.

Studying the results for optical coating Option 1 (Table 5-6) of the simulation it can be seen that at a distance of 1.5 AU, temperature of solar panels will still reach around 61 °C. It would be possible to use heat straps, to transport excessive heat from solar panels to sensitive electronic components and the biological payload compartment. With this solution, electrical heating requirements would be greatly reduced.

Another possible option is to install bigger solar panels, like E-HaWK and even more advanced models, available for 6U CubeSat platforms, with 72 W of peak electrical production at 1 AU [90]. Bigger solar panels combined with excessive heat transfer technology should more than satisfy thermal requirements for the mission.

Using thermal straps, the temperature of the solar panels would decrease, which would further increase their efficiency. With increasing temperature, performance of the solar cell degrades rapidly. Under standard test conditions the conversion effectivity of the Silicon solar cell decreases at a rate of about 0.4 – 0.5% for each degree rise above optimum operational temperature [35]. Peak power production for HaWK and E-HaWK are measured at a temperature of 70 °C [90].

Another issue which should be addressed is the uncertainty of material composition, dimensions, power requirements, heat conductance and heat dissipation of satellite geometry and installed components. Having better input information would produce more accurate results regarding the thermal behaviour of the satellite model and individual components. For the purpose of designing thesis geometry model and installed components, composite material characteristics were calculated (Appendix F) on the basis of previous experiences and information available from the published literature of similar space missions (BioSentinel, MarCO). Data regarding dimensions and component selection were obtained solely from rare published data which provided just basic information without immense detail, therefore a lot of simplification was needed. It must be pointed out that acquired calculated values for temperature response of individual electronic components as well as the biological payload are more of an advisory nature. For most detailed values further tests of installed components and their thermal response within the CubeSat geometry should be performed in a Thermal Vacuum Chamber (TVC).

For Option 2 and Option 3 geometry design was same, just different surface optical coatings were proposed (Subchapter 5.3.1). Instead of the basic surface layer, golden coating - with a similar optical characteristic to Kapton foil was placed on the satellite body or solar panel base (Appendix A). Using the golden

coating instead of Kapton foil presents less chances for the satellite getting trapped during deployment from the CubeSat launcher.

Coating the satellite surface and solar panel base with the golden optical coating, temperature conditions in general in the CubeSat as well as of the solar panel drop and also more electrical power is required for maintaining the temperature environment at the biological payload compartment (Table 5-6 to 5-14). It can be also observed that without the golden optical coating (Option 1, Table 5-6), during closer distances to the Sun, the solar panels overheat (around 126 °C) and therefore their efficiency would also drop [35]. But as already pointed out, for the same optical coating surface at a distance of 1.5 AU the temperature of the solar panels still reaches 61 °C and excessive heat could be used for heating other parts of the spacecraft. At a distance of 1.5 AU for optical coating Option 3, where a gold anodized coating is applied to the satellite body as well as to the solar panel base structure, a steady power of 1.76 W to maintain a temperature of 4 °C and 3.03 W to maintain 37 °C would be required (Table 5-13 and 5-14). For optical coating Option 2, where just the solar panel base is coated with an anodized gold coating, 1.68 W would be required to maintain 4 °C and 2.95 W to maintain 37 °C at all times (Table 5-10 and 5-11). Temperature of the solar panels when gold coated drops at 1.5 AU to -1.83 °C and when the satellite body is also coated to -2.78 °C. This is because the gold coating has lower absorptivity and higher emissivity than graphite epoxy being the basic material of the solar panel base.

Optical coating applied to the base of solar panels seems more beneficial at closer distances to the Sun (at 1 AU), to reduce high temperatures, which would further decrease efficiency of solar cells (Option 2, Option 3). At greater distances, closer to Mars, redundant temperature from the solar panels could be used for heating other electronic components, as aforementioned. At greater distances from the Sun, applying a gold optical coating is not a good solution. The best option would be a basic option without any optical coating (Option 1).

Discussed examples were calculated for the worst-case scenario, without considering any heat dissipation from electronic components at the distance of 1.5 AU. This is just a theoretical scenario. In a real situation, components would

operate at normal mode (marked NORM), for example batteries being charged and therefore also battery control board would be operational. Most energy demanding units such as the Transponder Communication unit, attitude control unit (ADCS) and thrusters, are controlled by Command and Data Handling (C&DH) subsystem and would be fully operational (marked HIGH) just occasionally in the need of communication procedures and attitude corrections. During normal operation (marked as NORM), minimum input beyond basic connection power should be necessary for these components. In the case of estimated high operational modes, especially of the Transponder Communication unit, thrusters and ADCS, requirements for additional heating drops, but nevertheless some additional heating is still required (Table 5-4, Subchapter 5.3.2.9). This trend can be observed in Graphs (Subchapters 5.3.2.2, 5.3.2.3, 5.3.2.4) and is discussed in the final Chapter 6.
At the end of the thermal chapter it must be once again pointed out that since the described technology of the interplanetary CubeSat is new, with only one successful launched mission up to date in mid - 2018 (MarCO) and another planed for near future (BioSentinel) there is limited published and available reference data with which results in the present thesis work could be compared and properly evaluated.

5.3.5 Further work in the area of thermal modelling

The objective of this thesis section was to build a model and conduct a thermal analysis of the 6U CubeSat with a biological payload which would fly an interplanetary mission.

The basis for the geometry design presented in NASA's MarCO and BioSentinel missions. While MarCO has already been launched to Mars as a support for the InSight mission, BioSentinel will be put into heliocentric orbit around the Sun at 1 AU in the near future. Thermal analysis simulations were conducted on the basis of already performed space radiation simulations (Chapter 4) which set requirements for material and dimensional selection of the biological payload area in order to protect biology from fatal space radiation.

Geometry as well as component selection was performed on the basis of a few published documents and papers on similar missions and selection and needs to be considered only representative but still sufficient to allow a meaningful thermal analysis to be performed to give context for considering the likely viability of meeting the biological payload thermal requirements, and knowing special requirements for interplanetary flights in CubeSat platform.

The author is aware that every numerical simulation is full of uncertainties and “grey zones” which must be minimised to an acceptable level during the work process. This is so for various reasons such as: lack of information or data, need for simplifying of complex systems, units and components and a realistic view of available computer power for the modelling and many others. Therefore, it is advisable to compare simulation results with similar work performed and published from other groups or authors (Subchapter 5.3.3).

In the thermal analysis chapter, further ideas arise, which could be of help for future simulation work performed in a similar research area:

- Designing of more exact geometry model, with detailed dimensions, material selection, properties and optical characteristics of installed components would be beneficial.
- For complex materials - composites, thermo-physical properties were manually calculated (Appendix A). Approximation brings a lot of uncertainties, not knowing exact fractions and dimensions of material in the composite.
- More exact values for heat dissipation during different regimes of operation (normal operation, high operation) would be needed for installed electrical components.
- Values for user defined conductance between the installed components and between components and the satellite body structure, should be more exact, preferably gained through experimental work with a Thermal Vacuum Chamber (TVC).
- Further numerical and experimental tests should be performed on how to optimise heat transfer inside the satellite, using heat straps from places

where heat is in excess (solar panels) to more low temperature sensitive units such as battery packs, reaction wheels, payload bay…).

- To model in ESATAN - TMS how heat transfer from solar panels to the satellite body and components effects the temperature drop of solar panels and what would be steady state condition at different distances from the Sun.
- Determination of the efficiency factor for heat straps used in the spacecraft.
- Air trapped in the payload compartment was neglected during the simulation process.
- It would be beneficial to test various surface covers, paints and insulations with different absorption and emittance coefficients for the satellite body and especially for the solar panel bodies where highest temperature gradients are expected.
- Performed simulations were performed for single orientation of the satellite body. Temperature values for different geometry pointing vectors should be investigated. How the temperature environment in spacecraft would be changed with different orientation of it.

The most suitable approach would be if being able to test in spacecraft satellite model with components and conductive interfaces in in spacecraft Thermal Vacuum chamber (TVC). Results from the Thermal Vacuum Chamber would be correlated with data acquired from in spacecraft Thermal model simulation and possible deviations could be corrected. If unable to build and test a complete satellite model, just the smaller most sensitive components – details where the biggest temperature gradients or extremes are expected, could be investigated in TVC.

6. FINAL DISCUSSION AND FUTURE WORK

6.1 Introduction

In the final chapter of the research work a final discussion of the results and outlined future work which could be derived from the work performed is given.

6.2 Main findings and discussion

CubeSat technology has been present in the space sector for almost twenty years and is already very well established and accepted. Up to the recent period, all CubeSat missions were placed in Earth's orbit. With rapid space technology and development also into deep space, interplanetary CubeSat missions are becoming a reality.

The main purpose of the research work was to investigate whether the present CubeSat technology is advanced enough to support complex biological experimental set up, with mammalian cells samples, to be sent on missions beyond Low Earth Orbit. Research objectives were to investigate two main technology challenges:

- can CubeSat platform with its known limitations provided sufficient space radiation protection for the biological payload experiment during a long duration interplanetary mission,
- are present CubeSat technology and installed special components advanced enough that energy (electrical, thermal) production and consumption will suffice to support temperature sensitive higher forms of biological payload during long duration and distance interplanetary flight.
- A further intention was also to advance the development status of the BAMMSat platform.

Results of the Radiation protection and Thermal simulation analysis were detailed discussed at the end of each Chapter Section (Subchapter 4.3.4.2 for Radiation protection and Subchapter 5.3.2 for Thermal control).

The main findings of the thesis research work can be put in three areas:

- **Radiation environment study output**

This radiation study investigated what protection is required for higher life form cell samples to survive (received radiation dose remains below the set acute limit – Subchapter 4.3.4.1.3) for as long as up to 1000 days on a space mission into interplanetary space. As shielding materials, Aluminium, as being a basic construction material in satellite and spacecraft technology and polyethylene - hydrogen rich and light material with good shielding characteristics, were selected.

A drawback of selecting denser (2,700 kg/m^3) Aluminium is the high secondary particle production when being exposed to space radiation, while for polyethylene being a lightweight material (975 kg/m^3), bigger volume is required. Running multiple sets for different material thicknesses and mission duration simulations, it was concluded that with a 20 mm thick Aluminium (Diagram 4-8) and 30 mm polyethylene sphere (Diagram 4-15), radiation values inside each sphere would remain below the set acute limit of 5 Sv. Obtained dimensions were weight and volume wise unacceptable for the CubeSat project.

With the next set of simulations, radiation protection characteristics of the composite material were investigated. Results showed that with a composite material of 3 mm Aluminium on outer layer and 20 mm of polyethylene oriented inside where the biological sample is placed, the received radiation level throughout the 1000 day deep space mission would remain less than 4 Sv (Diagram 4-22), so well below the acute limit of 5 Sv which was initially set. With further considerations and discussion, the final geometry dimension was set as a 3 mm Aluminium and 15 mm polyethylene concentric sphere.

Simulations for different durations and material combinations were performed with the NASA developed Space radiation modelling software OLTARIS. Results were compared with similar published calculations performed for the BioSentinel CubeSat mission (Subchapter 4.3.4.3). Radiation dose values obtained through the thesis simulation work for a 500 day mission and 3 mm of Aluminium protection are around 9 Gy, with SPE contribution of 8.77 Gy and

GCR of 0.196 Gy (Table 4-7). In comparing with the BioSentinel modelled values for a 365 day mission and 3.7 mm of Aluminium protection (Figure 4-17), it can be seen that the thesis simulation results correlate with published results (Subchapter 4.3.4.3).

- **Spacecraft system design and sub systems unit selection**

After determined materials and dimensions for suitable radiation protection, the spacecraft system design and component selection were performed. Of prime interest was the payload compartment. It should be spacious enough to accommodate the biological payload sample together with instrumentation. From initial calculations for thickness of radiation protection material it was clear that a 4U payload compartment would be needed. At 4U the payload compartment with embedded radiation protection walls of 3 mm Aluminium and 20 mm of polyethylene, usable volume would shrink to 32% of original unobstructed volume. With reducing the thickness of the protecting material to 3 mm of Aluminium and 15 mm of polyethylene the useful volume would increase to 43% of the original space (Subchapter 5.2.2) and radiation protection would still be sufficient. This volume is comparable with the 2U payload bay volume developed for the BAMMSat platform, without special radiation protection. Therefore, the development of the biological sample set up and instrumentation could be compared and exchanged. The decision was made, that the final radiation protection design would be composed from 3 mm of Aluminium and 15 mm of polyethylene composite.

The 4U payload compartment would be supported with electronic components placed in the 2U spacecraft bus during the interplanetary space flight. Total CubeSat configuration would be 6U. For interplanetary flight, traveling away from the Sun, special consideration must be placed on sufficient electrical energy production and storage, long distance communication difficulties and a suitable Attitude Determination and Control System (ADCS). The references for geometry design and similar components were selected as for the BioSentinel and MarCO CubeSat missions. MarCO was sent to Mars in mid - 2018, while

the BioSentinel is scheduled to be put into heliocentric orbit with distance from Earth of 0.43 AU to 0.73 AU in near the future [84].

The geometry model proposed solar panels (Subchapter 5.2.2.2.1) are able to produce 36 W of electrical power at a distance of 1 AU. At Mars' distance of approximately 1.5 AU, solar cells electrical production will decrease to 42% of the initial value, to around 15.1 W. The MarCO mission faced the same power reduction, while the BioSentinel mission being placed in heliocentric orbit, the distance will be approximately 1 AU through all time, giving the same or higher solar cell peak output at all time. It is expected the bigger model (E-HaWK of solar panels should be installed.

Electrical consumption of installed components highly depends on the operational mode. Biggest consumer of electrical energy is the Transponder Communication unit with 35 W of electrical power consumption when fully operational, 12.6 W with receiver mode only and 0.5 W when in standby mode (Subchapter 5.2.2.4). The ADCS unit has a maximum power consumption of 2 W and nominal of 0.5 W (Subchapter 5.2.2.3). Thrusters have a maximum power consumption of 4.7 W when fully operational and during normal stand by mode less than 1 W (Subchapters 5.2.2.6 and 5.2.2.9). For Command and Data Handling boards (C&DH) power consumption is expected to be 0.4 W on average with 0.55 W during the higher demands and for battery PCB 0.1 W for normal and 0.2 W for peak performance. In determining electrical power budget, it should be specified how often some components will be fully operational. Considering the biggest electrical energy consumer, Transponder Communication unit, as specified for the BioSentinel mission it will be required to be operational with Deep Space Network (DSN) assets for 4 hours per pass, twice per week to retrieve mission science data [84]. The same schedule was applicable for the thesis designed mission, in total. Thrusters are planned to be used just to detumble and momentum management of ADCS unit a few hours per week and will be the same as the Transponder Communication unit, very rarely operational.

During general operation, the Command and Data Handling boards (C&DH) and the battery control board would be in high operational regime (HIGH) most of the time. Other components are expected to be in stand by (NORM) mode.

The electrical consumption power budget for the installed components during standard operation is: 0.5 W (ADCS unit – normal standby operation) + 0.5 W (Transponder Communication unit – normal standby operation) + 0.55 W (C&DH – high operation) + 0.2 W (battery control board – high operation) + 1 W (thrusters – normal standby operation) + 0.4 W (Solar panel gimbal electronic board – high operation). Total electrical power consumption for operating electronic components is estimated to be approximately 3.05 W for normal - standby phase. In this situation the majority of electrical demanding components would operate at high performance at the same time, electrical consumption would surpass 40 W.

The electrical power required when in normal standby operation, could be supplied with installed solar panels proposed in the thesis work with 36 W of peak power production. During high electrical requirements (Transponder Communication unit fully operational, thruster firings, ADCS operational) (Table 5-21), solar cell production especially at a greater distance from the Sun would not suffice to satisfy all demands, therefore electrical energy from the battery would also be used during high demand.

As published in the literature, the reasonable power requirement for such an interplanetary CubeSat system is 7 W of average power required where 5 W powers the Transponder Communication terminal, leaving 2 W for the remaining C&DH, ADCS and electrical power systems [89]. In this thesis calculated values do not differ greatly from figures published in the literature for the same referenced projects.

- **Thermal modelling**

Passive heat control is expected, not to be sufficient to maintain environmental temperature requirements for the payload compartment and sensitive electronic components during a long period deep space flight. Active thermal control

would also be required. As calculated 45.8 W of additional heat would be needed to maintain electronics at survival temperature level and 60.6 W of additional heating for operational mode. Biological payload would be additional heated with 1.5 W for maintaining 4 °C or 2.77 W for 37 °C. Additionally to this at least 3.05 W would be needed for basic operation of electronic components. Calculations were performed for a zero - heat dissipation model without any special optical coating (Option 1).

The installed solar panels with peak power supply of 36 W at 1 AU, would not provide enough electrical energy for all demands. Even bigger E-HaWK solar panels with 72 W of peak power production would probably not suffice.

A possible solution is in the transportation of “redundant” heat loads from warmer parts of the spacecraft - solar panels, to cooler electronic components and the payload area. At the distance of 1.5 AU for Option 1, the temperature of the solar panel is still 61.62 °C and average temperature of satellite body and all components is calculated as -60.65 °C (Table 5.6). Let it be called high temperature gradient scenario. With Equations 15 and 16 heat load transferred with copper heat strap (material properties Appendix A) of dimension 15 mm x 4 mm and on distance for example 15 cm can be calculated simply. Calculated ideal heat load (no heat losses during transfer) per solar panel would be 18.9 W. For space applications high performance graphite fibre thermal straps should be used with high thermal conductivity (up to 1000 W/mK) and long space heritage [109]. For this case heat load would be increased to 48.9 W per solar panel. With decreased temperature gradient, transferred heat load would also decrease, and would be if heat were transferred to the payload compartment where temperature would be set to 37 °C, reduced to 3.8 W/ panel for copper and 9.8 W per panel for graphite fibre thermal straps. Let us call this the low temperature gradient scenario. These are two extreme examples. In real situations, temperature of the solar panel would drop, and temperature of the satellite components connected with heat straps would increase until steady state appears. This situation, giving the exact amount of available redundant heat from the solar panels should be investigated in future

thermal simulation research work. Further consideration should be given to the thermal efficiency factor of heat straps, where there are incorporated loses during thermal transfer. Efficiency of different heat straps would be investigated best experimentally in TVC.

- **Total energy power budget**

The total energy power budget can be presented as power gained - red shading and power spent – blue shading.

Calculations were performed for basic design (Option 1) of the black anodised Aluminium body structure with graphite composite back side of solar panel (Subchapter 5.3.1), at a distance of 1.5 AU.

Power is gained as electrical power from installed solar cells and as a waste - redundant heat from solar panels. I

For the simulation work HaWK solar panels with peak power production of 36 W at distance of 1 AU were selected. As a possible bigger alternative the bigger E-HaWK model with peak production of 72 W (1 AU) was proposed, which would be a more convenient solution for deep space, interplanetary missions. At the distance of Mars (approximately 1.5 AU) electricity production of solar cells drops to 42% of the nominal value at Earth distance; 15.1 W for HaWK and 30.2 W for E-HaWK model.

An Additional source of thermal power is redundant heat from solar panels, which could be transferred to the cooler parts of the CubeSat, mainly to the biological payload compartment and to the sensible electronic components. As a possible method of heat transfer heat straps made from basic copper or graphite material were discussed, which has much higher heat conductance and good space heritage. Values in Table 5-19 are calculated for high temperature gradient at a distance of 1.5 AU, with a temperature difference between average temperature of the solar panel and average temperature of the CubeSat model (Table 5-6). As a low temperature gradient was calculated, the temperature difference between the average temperature of the solar panel

and 37 °C as one of the selected ambient temperatures at the biological sample.

Solar panels electrical output		**1.5 AU**	
	HaWK	15.1 W	
	E-HaWK	30.2 W	
Solar panels redundant heat		**copper**	**graphite**
	high temp. grad.	2 x 18.9 W	2 x 48.9 W
	low temp. grad.	2 x 3.8 W	2 x 9.8 W
Operation required - el. components		**NORM**	**HIGH**
		3.05 W	≈ 40 W
Thermal required - el. components		**survival**	**operational**
	0	45.8 W	60.6 W
	NORM	29.2 W	45.1 W
	HIGH	1.2 W	4.4 W
Thermal required - biological payload		**4 °C**	**37 °C**
	0	1.4 W	2.77 W
	NORM	1.34 W	2.62 W
	HIGH	0.60 W	1.87 W

Table 5-19: Power budget for Interplanetary CubeSat mission

Energy would be spent in means of electrical power needed for operation of the components and additional required heating.

At a distance of 1.5 AU at normal - standby operation mode – explained in Subchapter 6.2, power consumption is estimated to be 3.05 W. With additional

activities of the Transponder Communication unit, the ADCS system and thrusters, consumption could be increased to over 40 W of electricity.

Additional heating at a distance of 1.5 AU would be required for a biological payload to maintain an experiment set environmental temperature of 4 or 37 °C, as well as for sensitive electronic components to be kept at survival or operational temperature level. Additional heat required is dependant on the operational status of the installed electronic components. Level of dissipated heat is different if they are not operative (0), in normal regime (NORM) or in high operational mode (HIGH) (Table 5-4). More heat is dissipated from installed electronic components, less additional heating is required.

Considering results from the energy budget (Table 5-19) different operational scenarios can be studied. An initial suggestion would be for an interplanetary mission to install more capable solar panels E-HaWK, with 30.2 W of peak electrical power production at a distance of 1.5 AU.

Usage of heat straps would drastically reduce electrical requirement for heating. Especially when advanced graphite fibred thermal straps are used. Calculated are ideal values without efficiency factor and transfer losses, for high and low temperature gradient. Real values should be somewhere in between of the two temperature gradient values. But it can be noticed that the amount of thermal energy waste from solar panels would be able to provide major part of thermal heating for electronic components in the satellite, during electronic components normal operation (45.1 W).

When the Transponder Communication unit and other big electricity consumers are not in high performance, electrical energy requirements for satellite operation are low, at 3.05 W as well as additional heat requirements for the biological payload sample 2.77 W for 37 °C. With Transponder Communication unit and other electronic components at high operational mode, operational electricity demands highly increase, but at the same time less additional heating is needed due to higher dissipation (Table 5-19; Thermal required – el. components; HIGH operational mode).

Having in mind the mission energy budget, of special concern during the designing process should be the selection of advanced and efficient solar panels and implementation of state-of-the-art passive thermal control technology (highly efficient heat straps, effective optical coatings and others).

After conducting intensive research work including reviewing the available literature, performed space radiation protection simulations, designing of the CubeSat geometry and the final thermal analysis of the spacecraft it can be concluded that present space technology and available components are advanced enough to provide adequate radiation protection for a high living form biological payload and enough thermal power for maintaining environmental conditions and sufficient electricity for normal operation of the 6U CubeSat spacecraft and its components during the interplanetary mission. However special concern should be addressed to solar panel electrical production and effective passive thermal control technology.

6.3 Future work

The performed work also triggered a lot of engineering and technological questions which are beyond the scope of this thesis research and need to be addressed in further research efforts. As a short term plan:

- List proposed and planned interplanetary space missions and analyse them as possible secondary payload carriers. Performed classifications would provide answers for many initial questions about possible CubeSat mission design and scenarios (Where? How long? Payload options…)
- An investigation of adequate survival strategy for mammalian cells, during pre - flight phase.
- Perform similar simulation work with possible radiation protection on a different selection of materials. As an interesting option regarding weight and level of protection, graphite has already been mentioned. A wide spectre of different materials and composites would enable optimum selection of radiation protection for different missions.
- Extend the selection of available electronic components which could be used for interplanetary CubeSat missions.

- For different materials and optical coatings to perform thermal control analysis. Numerically obtained results should be additionally tested in a Thermal-vacuum chamber (TVC). Results could be correlated, to improve the numerical model.
- Investigate the performance characteristics and efficiency of different material heat straps and other possible means of waste heat transfer management.

In the long term, it would be useful to investigate:

- Permanent research in the development of energy efficient components, processes and effective solar cells technology.
- Further investigation into different heat transfer options between components installed in the satellite with purpose to reduce need for active heat control.
- Acquire and Investigate results from future flown interplanetary CubeSat missions and compare real time measurements with simulations.

7. REFERENCES

[1] CubeSat Design Specifications, REV. 13; The CubeSat Program, Cal Poly.

[2] Space Mission Engineering: The New SMAD; J.R. Wertz at al; Space Technology Library, 2015.

[3] CubeSats: Cost-effective science and technology platforms for emerging and developing nations; Kirk Woellert et al; Elsevier 2010.

[4] The CubeSat Approach to Space Access; A. Toorian, K. Diaz, S. Lee; NASA, Jet Propulsion Laboratory, IEEE, 2008.

[5] 6 U CubeSat Design Specifications, REV. PROVISIONAL; The CubeSat Program, Cal Poly.

[6] CubeSat evolution: Analysing CubeSat capabilities for conducting science missions; A. Poghosyan, A. Golkar; Progress in Aerospace Sciences, 2017.

[7] The GeneSat -1 Test Demonstration Project: A Unique use of Smallsats; Yost et al; 19th Annual AIAA/ USU Conference on Small Satellites.

[8] PharmaSat: Drug dose response in microgravity from a free-flying integrated biofluidic/optical culture-and-analysis satellite; Ricco A.J. et al, SPIE 2011.

[9] The O/OREOS Mission: First Science Data from the Space Environment Survivability of Living Organisms (SESLO) Payload; Nicholson et al; Astrobiology Volume 11, November 2011.

[10] Space as a Tool for Astrobiology: Review and Recommendations for Experimentations in Earth Orbit and Beyond; J.M. Kotler et al; Science Review, June 2017.

[11] The SEVO Experiment Onboard NASAs O/OREOS Small Satellite; Cook A. et al; IAU Symposium 280, Poster 20, Session 1; Toledo, Spain 2011.

[12] SporeSat Investigating the Gravitational Threshold for Calcium Ion Channel Activation using a Nanosatellite Platform-Based Lab-on-a-Chip; NASA Facts, 2014.

[13] SporeSat; Andres Martinez, Presentation, NASA Ames Research Centre, 2014.

[14] SpacePharma web page (www.space4p.com).

[15] Mars Cube One Demo; NASA JPL; (https://www.jpl.nasa.gov/news/press_kits/insight/appendix/mars-cube-one/).

[16] On the Development of Spacecraft Operating Modes for a Deep Space CubeSat; Matt Nehrenz, Matt Sorgenfrei; American Institute of Aeronautics and Astronautics, 2015.

[17] BioSentinel: Monitoring DNA Damage Repair Beyond Low Earth Orbit on a 6U Nanosatellite; B. Lewis et al; 28th Annual AIAA/USU Conference on Small Satellites.

[18] BioSentinel; NASA Fact Sheet page: (https://www.nasa.gov/centers/ames/engineering/projects/biosentinel.html).

[19] BioSentinel: Mission Development of a Radiation Biosensor to Gauge DNA Damage and Repair Beyond Low Earth Orbit on a 6U Nanosatellite; H. Sanchez; 12th Annual CubeSat Developers Workshop, San Luis Obispo, 2016.

[20] Interplanetary CubeSats: Opening the Solar System to a Broad Community at Lower Cost; Staehle R., et al. (2013): JoSS, Vol. 2, No. 1, pp. 161-186.

[21] JPL's Advanced CubeSat Concepts for Interplanetary Science and Exploration Missions; Sara Spangelo, Julie Castillo-Rogez, Andy Frick, Andy Klesh, Brent Sherwood, NASA JPL/ Caltech CubeSat Workshop, Logan, Utah, August 2015.

[22] BAMMSat: Development status of a platform for bioscience, astrobiology, medical and materials science on CubeSats and CubeSat-like payloads; Cullen D.C. et al; The 4S Symposium 2016.

[23] BAMMSat: Development status of a platform for bioscience, astrobiology, medical and materials science on CubeSats and CubeSat-like payloads; Cullen

D.C. et al; 5th Interplanetary CubeSat workshop (iCubeSat) University of Oxford, UK 24th to 25th May 2016.

[24] BIOSTACK a study of the biological effects of HZE galactic cosmic radiation; Bucker H.,SP-368 Biomedical Results of Apollo; https://history.nasa.gov/SP-368/s4ch1.htm.

[25] The biological effectiveness of HZE-particles of cosmic radiation studied in the Apollo 16 and 17 Biostack experiments; H. Bucker, G. Horneck, Acta Astronautica Vol 2. 247-264,1974.

[26] Apollo light flash investigations; Osborne W.,Z.; Pinsky L.,S.;Bailey J.,V.; SP-368 Biomedical Results of Apollo; https://history.nasa.gov/SP-368/s4ch2.htm.

[27] The Apollo 16 microbial response to space environment experiment; Taylor G.,T.; SP-368 Biomedical Results of Apollo; https://history.nasa.gov/SP-368/s4ch3.htm.

[28] The Apollo 17 pocket mouse experiment (BIOCORE); Hymaker W., Benton E.,V., Simmonds R.,C., ; NASA Ames Research Center; SP-368 Biomedical Results of Apollo; https://history.nasa.gov/SP-368/s4ch4.htm.

[29] Nanosatellite data base; https://www.nanosats.eu/.

[30] E.R. Benton, E.V. Benton; Space radiation dosimetry in low-Earth orbit and beyond; 2001.

[31] M.Maalouf, M.Durante, N.Foray; Biological Effects of Space Radiation on Human Cells: History, Advances and Outcome; J. Radiat. Res., 52, 126–146 (2011).

[32] J.L. Barth; Space and Atmospheric Environments: from Low Earth Orbits to Deep Space, NASA/ Goddard Space Flight Centre.

[33] G.Reitz, R.Facius, H.Sandler; Radiation Protection in Space; Acta Astronautica, 1995.

[34] NOAA Space Weather Scales; www.swpc.noaa.gov.

[35] H.Miyahari, Y.Yokoyama, Y.T.Yamaguchi; Influence of the Schwabe/ Hale cycles on climate change during the Maunder Minimum; Solar and Stellar Variability: Impact on Earth and Planets Proceedings IAU Symposium No. 264, 2009.

[36] Guide to Modeling Earth's Trapped Radiation Environment; American Institute of Aeronautics and Astronautics, AIAA G-083-1999; 1999.

[37] Managing Space Radiation Risk in the New Era of Space Exploration; Committee on the Evaluation of Radiation Shielding for Space Exploration Aeronautics and Space Engineering Board Division on Engineering and Physical Sciences, The National Academies Press, Washington D.C., 2001.

[38] Humans in Space and Space Biology, K. Legner, Seminars of the United Nations Programme on Space Applications, United Nations, New York, 2004, SAO/ NASA ADS.

[39] Basics of Radiation Therapy; Elaine M.Zeman, Eric C. Schreiber and Joel E. Tepper; https://clinicalgate.com; 2015.

[40] Toxicological profile for ionizing radiation; U.S. Department of health and and human services; Public Health Service Agency for Toxic Substances and Disease Registry; 1999.

[41] Radiation Damage in Living Organisms; Radiation Challenge, J.Rask, W.Vercoutere, A.Krauser, B.Navarro, NASA.

[42] Space Faring; The Radiation Challenge; J.Rask, W.Vercoutere, B.Navarro, A.Krause; Marshall Space Flight Center; NASA.

[43] Wikipedia, https://en.wikipedia.org.

[44] S. Mattsson and C. Hoeschen (eds.), Radiation Protection in Nuclear Medicine, Chapter 2 : Dose Quantities and Units for Radiation Protection; Springer – Verlag Berlin Heidelberg 2013.

[45] Sources and effects of ionizing radiation; United Nations Scientific Committee on the Effects Of Atomic Radiation; UNSCEAR 2008, Volume ; New York 2010.

[46] Space Radiation Risk Limits and Earth-Moon_Mars Environmental Models; F.A.Cucinotta, S.Hu, N.A.Schwadron, K.Kozarev, L.W.Townsend, M.H.Kim; NASA Lyndon B.Johnson Space Centre.

[47] HUMEX A Study on the Survivability and Adaptation of Humans to Long – Duration Exploratory Missions; European Space Agency 2003.

[48] Radiation Risk Acceptability and Limitations; Cucinotta F.; 2010.

[49] Medical consequences of radiological and nuclear weapons; Acute Radiation Syndrome in Humans – Chapter 2; Goans R.E., Flynn D.F.; 2012.

[50] Radiobiology of the acute radiation syndrome, Garau M.M., Calduch A.L., Lopez E.C., Reports of practical oncology and radiotherapy; 2011; ELSEVIER.

[51] Nicogossian A, Huntoon C, Pool S; Space Physiology and Medicine. 3rd ed. Philadelphia: Lea and Feinger; 1994.

[52] Chronic Radiation Syndrome (CRS) in residents of the Techa riverside village; A.V. Akleyev, Federal Medical – Biological Agency (Russia), Urals Centre for Radiation Medicine; ConRad, Munich 2013.

[53] Orbital Space Settlement Radiation Shielding; Globus A., Strout J.; 2017.

[54] Space Radiation; Risk of Radiation Carcinogenesis; Cucinotta F.A, NASA Johnson Space Center.,M. Durante, GSI Germany; 2009.

[55] Managing Lunar, Radiation Risks, Part I: Cancer, Shielding Effectiveness; Cucinotta, F. A., M.H. Y. Kim, L. Ren; 2005.

[56] Overview of active methods for shielding spacecraft from energetic space radiation; L.W.Townsend; Department of Nuclear Engineering, The University of Tennessee; 11th Annual NASA Space Radiation Health Investigators Workshop; Arona, Italy, 2000.

[57] Radiation Shielding Techniques for Human Spaceflight; A. Clark, Coursework; Stanford University, 2015.

[58] Analysis of a Lunar Base Electrostatic Radiation Shield Concept, Final Report; R.Buhler; ASRC Aerospace Corporation, Kennedy Space Centre, Florida; 2005.

[59] Shielding Space Travellers; Eugene N. Parker; Scientific American 2006.

[60] New radiation environment and effects models in the European Space Agency's Space Environment Information System (SPENVIS); D.Heyndrickx, J.Wera, E.J.Daly, H.D.R.Evans; Space weather Vol.2, 2004.

[61] SPENVIS webpage: https://www.spenvis.oma.be.

[62] On-Line Tool for the Assessment of Radiation in Space – Deep Space Mission Enhancments; Sandridge C.A., Blattnig S.R., Norman B., Slaba T.C.; NASA Langley Research Canter; IEEE 2011.

[63] OLTARIS: On-Line Tool for the Assessment of Radiation in Space; Singleterry R.C., Blattnig S.R., Clowdsley M.S., Qualls G.D., Sandridge C.A.,Simonsen L.C., Norbury J.W.; NASA Langley Research Center, Hampton, Virginia, 2010.

[64] Great Solar Energetic Particle Events of 1989 Observed from Geosynchronus Orbit; G.D. Reeves, T.E. Cayton, S.P. Gary, R.D. Belian; Journal of Geophysical Research; 1992.

[65] OLTARIS – Overview and recent updates; C.A.Sandridge; NASA Langley Research Center; NASA Human Research Program Investigators Workshop (2014); 3056.pdf.

[66] HUMEX, a study on the survivability and adaptation of humans to long – duration exploratory missions, part II: Missions to Mars; G.Horneck et al; Advances in Space Research 2006.

[67] Large solar event of September 29, 1989: ten years after; L.I. Miroshnichenko, C.A. De Koning, R. Perez-Enriquez; Space Science Review; 2000.

[68] What is solar cycle minimum?; K.L. Harvey, O.R. White; Jurnal of Geophysical Research, 1999.

[69] International Comission on Radiological Protection; www.icrp.org.

[70] OLTARIS Home Page; https://oltaris.larc.nasa.gov/.

[71] Radiative Heat Transfer; M.F. Modest; Academic Press, Elsevier 2013.

[72] Fundamentals of Heat and Mass Transfer; DeWitt, Bergman, Lavine; John Wiley & Sons; 2007.

[73] P. Fortescue, G. Swinerd, and J. Stark. *Spacecraft Systems Engineering*. John Wiley & Sons Ltd London, 4th edition, 2011.

[74] Essential Heat Transfer; Cristopher A. Long; Longman 1999.

[75] Messerschmidt, E. & Fasoulas, S. (2005), Raumfahrtsysteme, 2 edn, Springer.

[76] Thermal modelling of the PICSAT nanosatellite platform and synergetic prestudies of the CIRCUS nanosatellite; Tobias Flecht; Luleå University of Technology, MSc Thesis, 2016.

[77] European Cooperation for Space Standardization (2008), Space engineering - Thermal control general requirements, number ECSS-E-ST-31C, ESA Requirements and Standards Division.

[78] ESATAN – TMS Thermal Modelling Suite webpage : https://www.esatan-tms.com/.

[79] ESATAN-TMS Workbench Getting Started Guide; ITP Engines UK Ltd; December 2017.

[80] Solar Absorbance and Thermal Emmitance of some common spacecraft thermal control coatings; John H. Henninger; NASA Reference Publication; April 1984.

[81] Spacecraft Thermal Control Handbook; Volume 1 Fundamental Technologies; David G. Gilmore; The Aerospace Corporation; 2002.

[82] ESATAN-TMS Workbench User Manuel; ITP Engines UK Ltd; December 2017.

[83] BioSentinel NASA web Page: https://www.nasa.gov/centers/ames/engineering/projects/biosentinel.html.

[84] BioSentinel: Monitoring DNA Damage Repair Beyond Low Earth Orbit on a 6U Nanosatellite; B. Lewis et al., NASA Ames Research Center, 28th Annual AIAA/ USU Conference on Small Satellites.

[85] BioSentinel: Mission Development of a Radiation Biosensor to gauge DNA Damage and Repair Beyond Low Earth Orbit on a 6U Nanosatellite, H. Sanchez, 12th Annual CubeSat Developers Workshop, San Luis Obispo, California, April 2016.

[86] BAMMsat - A platform for beyond LEO space environments studies on biological systems in CubeSats and CubeSat-like payloads; D. Cullen et al.; 5th Interplanetary CubeSat workshop (iCubeSat) University of Oxford, UK 24th to 25th May 2016.

[87] CubeSat evolution: Analysing CubeSat capabilities for conducting science missions; A. Poghosyan, A. Golkar; Progress in Aerospace Sciences 88 (2017) 59-83.

[88] 6U CubeSat Design Specification Rev. PROVISIONAL; www.cubesat.org.

[89] Interplanetary CubeSats: Opening the Solar System to a Broad Community at Lower Cost; Staehle R., et.al., JoSS, Vol. 2, No. 1, pp. 161-186, 2013.

[90] HaWK Solar Array Technology Advanced Deployable Satellite Power Solution; 12th Annual CubeSat Developers Workshop; April 2015.

[91] Space Mission Engineering: The New SMAD; J.R. Wertz, D.F.Everett, J.J. Puschell; Space Technology Library; 2015.

[92] Lithium Ion 18650 cells for space flight products; Datasheet, www.gomspace.com.

[93] Thermal Properties of Lithium-Ion Battery and Components; H. Maleki et al.; Journal of The Electrochemical Society, 146 (3) 947-954 (1999).

[94] Attitude Determination Control Systems XACT; Blue Canyon Technologies; Data Sheet.

[95] Iris Deep-Space Transponder for SLS EM-1 CubeSat Mission; M. Kobayashi; Jet Propulsion Laboratory, California Institute of Technology; 31st Annual AIAA/USU Conference on Small Satellites.

[96] Iris V2.1 CubeSat Deep Space Transponder; X - , Ka - , S – Band and UHF Deep Space Telecommunications and Navigation, Data Sheet; NASA.

[97] CubeSat shop; www.cubesatshop.com.

[98] Cold gas micro propulsion development for satellite application; R. Ranjan et al.; Energy Procedia 143 (2017).

[99] VACCO ChEMS Micro Propulsion System; Micro – Propulsion System overview; VACCO space products; http://www.vacco.com/images/uploads/pdfs/mips2112.pdf.

[100] Understanding the Mechanism of the Dormant Dauer Formation of C. elegans: From Genetics to Biochemistry; Y. Wang et al; School of Life Sciences, Centre for Protein Science, Peking University, Beijing, China; Life, June 2009.

[101] Nanosatellite orbit control using MEMS cold gas thrusters; U. Kwell et al.; Proceedings of the Estonian Academy of Sciences, 2014, 63, 2S, 279–285.

[102] Propulsion Unit for CubeSat; VACCO; 11044000-01; Technical Data sheet.

[103] Sketchup 3D modelling; www.sketchup.com.

[104] Eco Innovation; Germanium Solar Cells Fuel greener future; https://ec.europa.eu/environment/ecoap/about-eco-innovation/experts-interviews/32_en.

[105] Investigation of the Effect Temperature on Photovoltaic (PV) Panel Output Performance; A.R. Amelia et al; International Journal on Advanced Science Engineering Information Technology; 2016.

[106] Studying the effect of radiation in the context of deep space travel; Sharmila Bhattacharya; NASA Ames Research Center; International Conference of Radiation Research. Hyderabad, CA.

[107] MarCO: CubeSats to Mars in 2016; A. Klesh, J. Krajewski; 29th Annual AIAA/ USU Conference on Small Satellites.

[108] MarCO: Interplanetary Mission Development on a CubeSat scale; J. Schoolcraft et al; Jet Propulsion Laboratory; SpaceOps Conference 2016.

[109] Technology Application Inc; web page: https://www.techapps.com/.

[110] BioSentine – A Deep Space Radiation Biosensor Mission; B. Hanel, J. Chartres, H. Sanches; CubeSat Developers workshop 2017; CalPoly, San Luis Obispo, CA 2017.

[111] Properties and Characteristics of graphite; For industrial applications; POCO Graphite; January 2015.

8. APPENDICES

Appendix A: Physical and thermal properties of the materials

Component	Material	k $\left[\frac{W}{mK}\right]$	ρ $\left[\frac{kg}{m^2}\right]$	C_p $\left[\frac{J}{kgK}\right]$	α_S [ ]	ε_{IR} [ ]
Structure	Aluminium (Al7072)	121	2770	960	0,65	0,82
Structure	Steel	16,3	8030	504	0,42	0,11
PCBs	Copper	387	8860	390	0,32	0,02
Structure	Kepton	/	/	/	0,45	0,82
Solar Panels	Germanium	60	5260	324	0,52	0,09
PCBs	Silicon	148	2330	700	0,11	0,05
Solar Panels	Graphite epoxy**	96	2260	710	0.66	0.25
Batteries	Lithium – Ion***	1,84	2368	610	0,8	0,6
PCBs	FR4	0,32	1850	950	0,72	0,89
Thruster	Fuel (isobutane)	0,017	604	1675	/	/
Payload	Water	0,591	1000	4200	0,28	0,96
Structure	Gold surfacecoating	/	/	/	0,48	0,82
Component	**Composite**					
ADCS	PCB board	236	3602	810	0,72	0,89
ADCS	react.wheels/housing	52	4874	778	0,65	0,82
Transpon./Comm.	copper/silicon	294	4289	607	0,11	0,05
Thruster	isobutane/housing	109	2040	1200	/	/

Reference: Spacecraft Thermal Control Handbook; Volume 1 Fundamental Technologies; David G. Gilmore; The Aerospace Corporation; 2002.

**: Reference [111]

***: Reference [93]

Appendix B: Effects of space radiation on biological material

B.1 Effects of space radiation on biological material

Human beings are composed of approximately 10^{14} living cells engaged in parallel processes and generation of information. Cells aggregate in correlated groups; tissues and organs. Two minimum conditions must be met for organisms to function: all critical parts must be present and they must function properly together. The number of cells required for proper tissue and organ function is determined by the ability of divide and maintain their structure. The function of tissue and organs is determined by the ability of constituent cells to keep communicating in the form of sending and receiving molecules. All of these aspects of the living system can be perturbed, in many cases permanently, by exposure to radiation [37].

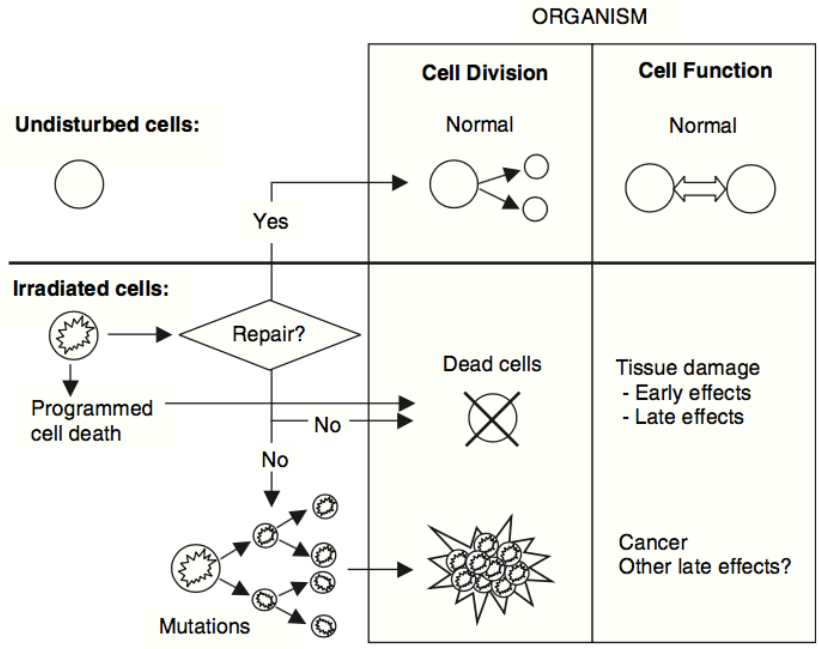

Figure B-1 : Pathways of biological damage produced by exposure to radiation [37]

The primary biologic effect of low and moderate radiation doses, such as those found in the space environment, is damage to genetic material – deoxyribonucleic acid (DNA) in living cells (Figure B-1).

When an organism is exposed to radiation, the energy from the radiation is deposited at the cellular level by interactions between the radiation and the electrons of molecules building the cells. As a consequence, carbon, oxygen, nitrogen and other atoms that make up complex molecules may lose the electron bonds that tie them to the rest of the molecule.

The mechanisms causing mutation in cells are complex, involving physical energy transfer, free radical formation and alteration of the molecular structure of DNA. There are two major ways space radiation can damage can damage living cells (Figure B-2):

- Radiation collides with DNA molecules directly **(direct effect).**
- The water in the organism (e.g. human body) absorbs a large portion of radiation and becomes ionized to form highly reactive, water derived radicals. Free radicals then react with DNA molecules causing breaking of chemical bonds or oxidation **(secondary effect).**

Both mechanisms cause decay of the DNA molecular structure [38].

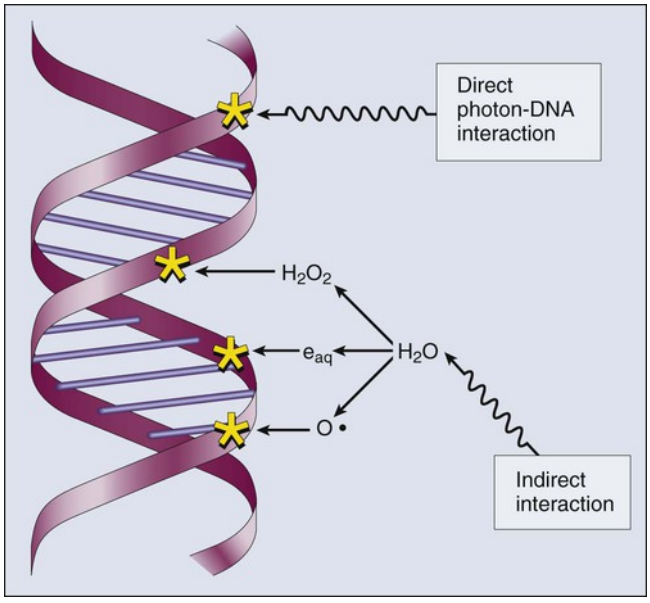

Figure B-2: Direct and indirect effect [39]

A DNA molecule consists of two long polynucleotide chains composed of four types of nucleotide subunits. Each of these chains is known as a DNA chain, or

a DNA strand. Hydrogen bonds between the base portions hold the two chains together. DNA molecules are responsible for carrying genetic information in the cells. Breaks as a result of radiation can occur at single or both of the DNA chains (Figure B-3). Interactions that result in breaks of both chains are believed to be of more biological significance. When a single DNA chain breaks, the cell can usually repair the damage and resume normal function. This repair process can happen because the double – helix nature of the DNA molecule allows the undamaged strand to serve as a template for the repair of the damaged one. With double – chain breaks the repair is more difficult and cells may be changed permanently or die. If too many tissue cells die, organ function will be compromised.

The damage – repair process depends also on exposure time to the radiation. If the radiation dose is delivered over a period of time that is long compared with the repair time constant of the cells, the damaged cells can repair and maintain, or delete and replace a sufficient number of cells for function to be undisturbed. Cellular repair mechanisms are not always full successful. In some cases, repair can leave the cell in sufficiently good shape although damaged and modified to undergo through another few cell divisions. The daughter cells will inherit some of the original incompletely or poorly repaired damage and die off or lead to dying or aberrant cells in subsequent division. This unstable state of the cell is called genomic instability.

If full repair of cells fails, but not to the point of leading to the death of subsequent generation of cells, damaged cells may survive and transform into cancer cells and further develop into tumours [37].

As discussed, effects of the damage from ionising radiation can be short-term (destroying cells) or long-term (effecting next generations of reproducing cells), depending on the timing and severity of the exposure.

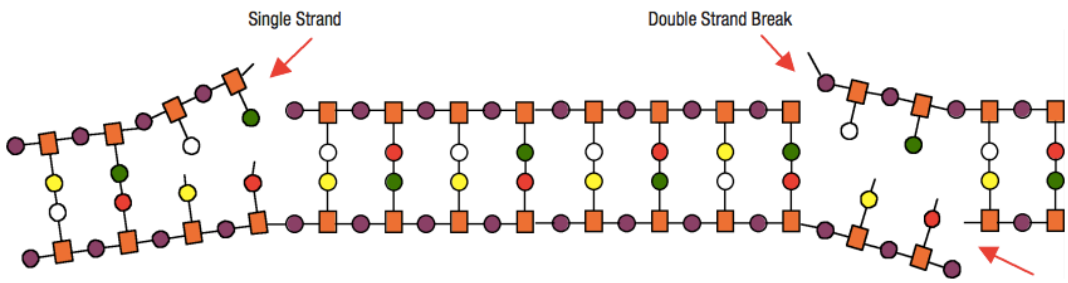

Figure B-3: DNA molecule model with single and multiple strand break [41]

B.1.1 Direct effect

A direct interaction occurs when an particle (α particle, β particle, proton, neutron) or γ ray hits and ionizes atom or molecule.

Both high LET (neutrons, protons, α - particles) and low LET (X - rays, γ - rays, β - particles) can directly ionize a molecule at the point of impact, producing two adjacent pieces, which are chemically reactive. If the two pieces immediately recombine to produce the same original molecule, no damage results.

Alternately, the pieces may drift apart, engaging neighbouring atoms and molecules in any stabilizing chemical reactions that are thermodynamically possible. Each such chemical reaction produces a different molecule.

In case of high LET radiation or high intensity of low LET radiation, the distance between ionizing events is short enough that the radiation can ionize adjacent molecules or even multiple bonds on the same molecule. For a large macromolecule such as DNA with its multi-strand structure in chromosomes, these actions can damage the molecular structure in a number of ways. Radiation can remove large or small pieces of the molecules, and can open purine rings (leading to depurination) and break phosphodiesterase bonds. This action may result in the genetic damage.

Genetic damages such as: deletions, mutations, chromosomal aberrations, breaks are main harmful effects of exposure to ionizing radiation.

If the repair mechanisms fail to perfectly repair the damage to the chromosomes, restoring it to original pre - ionized structure, or do not repair

damage at all, the chromosomes may not replicate properly. This results in deleting portions of the chromosome during replication cycle, leading to cell death or genetic mutations [40].

B.1.2 Secondary effects

Secondary effects are molecular damages which occur at distance from the radiations direct interaction site.

Indirect interactions are caused by radiation produced chemical substances (free radicals and oxidizers) with sufficient life time and reactivity to diffuse away from the primary site and damage molecules they collide.

Some of the radiation degradation (radiolysis) products of water, including the hydrogen and hydroxyl radicals are cytotoxins.

Water makes up approximately 60% of the total body mass of humans, and 75-80% of the chemical compositions of the living cell. When radiation interacts with water molecules surrounding DNA, the end products are drifted away and react with and DNA that is in their path. Hence the reason biological material that has low water content, exhibits a greater resistance to radiation effects.

Radiolysis of water:

Equation B-1: Radiolysis of water

$$\mathbf{H_2O + radiation \rightarrow e^- + H_2O^+}$$

In the first reaction (Equation B-1), radiation interacts with free cellular water to produce one free electron (e^-) and one ionized water molecule H_2O^+, a reaction commonly known as radiolysis.

Equation B-2: Production of free radicals

$$\mathbf{e^- + H_2O \rightarrow H_2O^- \rightarrow OH^- + H^*}$$

This free electron is highly reactive and interacts with another un-ionized water molecule to produce a negatively charged and highly unstable water molecule. This molecule quickly decomposes to form the OH^- ion and the H^* free radical (Equation B-2). The H^* radical is reactive, OH^- is more stable and can then diffuse out into the cellular fluid and can interact with macromolecules it encounters on its path, such as molecules of DNA [40].

Equation B-3: Production of hydrogen ion and hydroxyl radical

$$H_2O^+ \rightarrow H^+ + OH^*$$

Remaining H_2O^+ molecules can also transform into a free and ionized hydrogen ion H^+ (affecting intracellular or extracellular pH) and the hydroxyl OH^* radical (Equation B-3).

Of the radiolysis products, 55% are either H^* or OH^- which have greatest effect on biology. They have a lifetime of approximately 10^{-11} seconds, which is lone enough to damage DNA and other macromolecules. Damage occurs in the form of loss of atoms or pieces of the molecules, resulting in structural degradation, cross-linking, breakage of chemical bonds and other effects.

B.1.3 Dose limits

The accurate measurement of astronaut exposure to ionizing radiation during space flight, may well represent the single most difficult challenge in radiation dosimetry.

There are several properties of radiation that must be considered when measuring or quantifying radiation. These include the nature and energy of radiation, the amount of radiation in the environment and the amount of radiation energy that is absorbed in biological material – human body. These properties determine the nature of the radiation itself. It is very important to understand that equal doses of different kinds of radiation are not equally damaging. To account for the difference, we need to distinguish between effective absorbed dose, dose equivalent and effective dose values (Figure B-4).

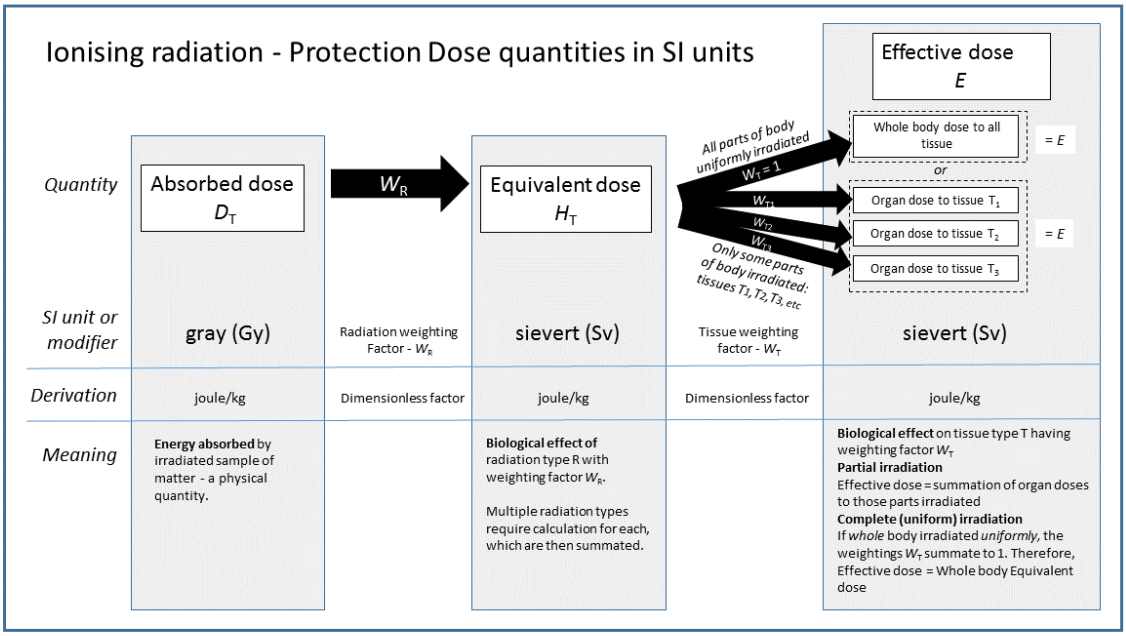

Figure B-4: Effective dose and dose equivalent differences [43]

B.1.3.1 Absorbed dose, Dose equivalent and Effective dose

As already mentioned, there are two distinguished categories of measuring radiation dose:

- **Absorbed dose (D_T)**, also known as physical dose, defines the amount of energy deposited from an ionizing radiation in a unit mass in human tissue or other media. Formally it is defined as:

Equation B-4: Absorbed dose

$$D_T = \frac{\Delta E}{\Delta m} \quad [J/kg = 1\ Gy\ (Gray)]$$

Where ΔE is the mean energy transferred by the radiation to a mass Δm. In the past unit *rad* was also used where: 1 Gy = 100 rad.

- **Equivalent dose (H_T)**

Equivalent dose reflects the fact that the biological damage caused by a particle depends not only on the total energy deposited, but also on the rate of energy loss per unit distance travelled by the particle.

For example, α particles do much more damage per unit energy deposited than do electrons. Equivalent dose is defined as:

Equation B-5: Equivalent dose

$$H_T = D_T \cdot W_R \quad [J/kg = 1\ Sv\ (Sievert)]$$

Where D_T is the absorbed dose and W_R is the dimensionless quality factor, which is dependent on both particle type and energy.

Quality factor (W_R) is defined to be a function of linear energy transfer (LET). LET is the energy lost per unit length of path through a material. Different types of radiation have different LET values. Photons, electrons, X – rays and γ – rays are known as low LET radiation, with a quality factor value of 1.0.

Higher LET is more destructive to biological material then low LET radiation at the same dose. Therefore is quality factor for neutrons between 2 – 10 and for α - particles even 20.

For the common situation where a spectrum of energies and a mixture of particle types are present (as in the case of space radiation), the value of quality factor (W_R) for the complete radiation field is an average over the spectrum of LET present weighted by the absorbed dose as a function of LET [44].

The unit for the equivalent dose is Sievert (Sv) if absorbed dose is measured in Grays.

If absorbed dose is measured in rad, equivalent dose is presented in rem. 1 Sv equals 100 rem.

Radiation	W_R
Photons, electrons and muons of all energies	1
Neutrons	See Fig.
Protons >2 MeV (except recoil protons)	2
Alpha particles and heavy ions	20

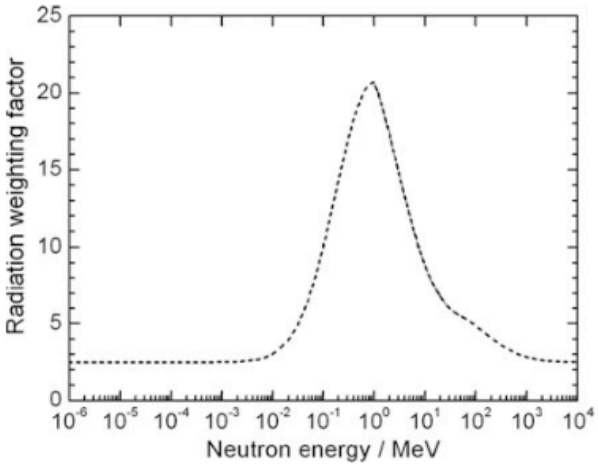

Figure B-5: Radiation weighting factors [44]

- **Effective dose (E)**

Equivalent dose multiplied by tissue weighting factor is called Effective dose (E). It takes into account the type of radiation and the nature of each organ or tissue being irradiated.

To obtain an effective dose (E), the calculated absorbed dose (D_T) is first corrected for the radiation type using factor W_R to give a weighted average of the equivalent dose quantity H_T received in irradiated body tissue, and the result is further corrected for the tissues or organs being irradiated using tissue weighting factor W_T (Figure B-6) to produce the effective dose quantity E.

Equation B-6: Effective dose

$$E = H_T \cdot W_T \quad [J/kg = 1\ Sv\ (Sievert)]$$

The tissue weighting factors summate to 1.0. If the entire body is radiated with uniformly penetrating external radiation, the Effective dose for the entire body is equal to the Equivalent dose for entire body.

Organ	Tissue weighting factors, w_T		
	ICRP 30 [I36] 1979	ICRP 60 [I3] 1991	ICRP 103 [I6] 2008
Gonads	0.25	0.20	0.08
Red bone marrow	0.12	0.12	0.12
Colon		0.12	0.12
Lungs	0.12	0.12	0.12
Stomach		0.12	0.12
Bladder		0.05	0.04
Breasts	0.15	0.05	0.12
Liver		0.05	0.04
Oesophagus		0.05	0.04
Thyroid	0.03	0.05	0.04
Skin		0.01	0.01
Bone surfaces	0.03	0.01	0.01
Salivary glands			0.01
Brain			0.01
Remainder	0.30	0.05	0.12

Figure B-6: Summary of tissue weighting factors for different International Commission for Radiation Protection (ICRP) revised standards from 1979, 1991 and 2008 [69]

B.1.3.2 Astronaut dose limit

Nowadays, bold plans are proposed for extended - long duration space missions beyond Low earth orbit (LEO), towards the Moon habitat and further flights and colonisation of planet Mars.

As missions progress away from protection of Earth's magnetic shielding (1000 km – 60000 km above the surface), the radiation exposures that astronauts face include more intense deep space radiation environment including full galactic cosmic rays (GCR) spectrum and solar particle events (SPE).

Since the beginning of space exploration, just Apollo astronauts experienced journey outside the Earth magnetic protective shield into the interplanetary space, on their way to the Moon. There are still large uncertainties in projecting the risk from long term exposure to space radiation for human being.

Cancer risk that is caused by exposure to space radiation is generally considered as the main obstacle for long duration human interplanetary travel. Debates continues on what level of cancer risk is acceptable for astronauts.

For terrestrial workers exposed to radiation in environments such as: nuclear reactors, accelerators, hospitals annual total exposure is around 1 - 2 mSv/y

with a dose limit set at 50 mSv/y. Similarly, transcontinental pilots receive annual exposure of about 1 - 5 mSv/y [46].

For spaceflight the limit is higher. The specific organ and career exposure limits are determined by age and gender.

NASA permissible exposure limits says:

"Career exposure to radiation is limited to not exceed 3% risk of exposure – induced death (REID) from fatal cancers. An ancillary requirement assures that this risk limit is not exceeded at a 95% confidence level using a statistical assessment of the uncertainties in the risk projection calculations to limit the cumulative effective dose (in units of Sievert) received by an astronaut throughout his or her career." [46].

NASA limit for exposure in Low - Earth orbit is 0.50 Sv/y. Values are lower for younger astronauts. It is presumed that exposure to larger amounts of radiation early in the career could present greater health risk during old age [42].

Career limits for NASA astronauts dependent of age and gender are specified in the Figure B-7.

Career Exposure Limits for NASA Astronauts by Age and Gender*				
Age (years)	25	35	45	55
Male	1.50 Sv	2.50 Sv	3.25 Sv	4.00 Sv
Female	1.00 Sv	1.75 Sv	2.50 Sv	3.00 Sv

Figure B-7: Age and gender dependent whole body equivalent dose for 10 years/ career NASA astronaut limit for a lifetime excess risk of fatal cancer of 3%, for LEO (NCRP 1989) [42]

Further dose limits are introduced to prevent clinically significant non-cancer health effects for blood forming organs (BFO) to prevent nausea, vomiting and fatigue. Dose limits for cataracts, skin, heart disease and damage to the central nervous system (CNS) are implemented to prevent risk of degenerative tissue diseases (stroke, coronary heart disease or dementia) that could occur post mission. Limiting values are specified in Figure B-8.

Depth of Radiation Penetration and Exposure Limits for Astronauts and the General Public (in Sv)				
	Exposure Interval	Blood Forming Organs (5 cm depth)	Eyes (0.3 cm depth)	Skin (0.01 cm depth)
Astronauts	30 Days	0.25	1.0	1.5
	Annual	0.50	2.0	3.0
	Career	1-4	4.0	6.0
General Public	Annual	0.001	0.015	0.05

Figure B-8: Organ specific dose limits during different exposure intervals for NASA astronauts and general public. (NCRP1989) [42]

The European Space Agency (ESA) (Figure B-9), Russian Space Agency (RSA)(Figure B-10) and Japanese Space Agency (JAXA) use dose limits for astronauts and cosmonauts largely based on the recommendations of the International Commission on Radiological Protection (ICRP) for ground-based works with some modifications for 30 - day and annual limits for non-cancer effects [48].

Limit	Value	Comment
Career	1 Sv (1000 mSv)	ICRP- no age or gender dependence
Blood Forming Organs (BFO)	0.25 Sv for 30 d; 0.5 Sv for Annually	ISS Consensus limits
Eye	0.5 Sv for 30 d; 1.0 Sv Annually	
Skin	1.5 Sv for 30 d 3.0 Sv for Annually	

Figure B-9: European Space Agency ESA Dose Limits for astronauts [48]

Limit	Value	Comment
Career	1 Sv (1000 mSv)	ICRP- no age or gender dependence
Blood Forming Organs (BFO)	0.15 Sv for Acute (1-time) 0.25 Sv for 30 d; 0.5 Sv for Annually	
Eye	0.5 Sv for 30 d; 1.0 Sv Annually 2.0 Sv for Career	
Skin	1.5 Sv for 30 d 3.0 Sv for Annually 6.0 Sv for Career	

Figure B-10: Russian Space Agency (RSA) Dose Limits for astronauts [48]

Values presented in Figures B-8, B-9 and B-10 are specified for LEO scenarios. For missions beyond LEO further considerations and health risk projection models will be needed to be introduced and developed on the basis of further experimental data and theoretical/ numerical information. Future planned deep space missions, investigating effects of deep space radiation on human like mammalian cells, will greatly increase the level of knowledge and further help to improve numerical model for simulation work. Therefore, such missions are of great importance in preparation and planning of manned long duration space travel beyond Low Earth Orbit

It is important to understand that all of the above mentioned forms of long term radiation exposure contribute to cumulative radiation dose and delayed effects on human body and specific organs. Astronauts are exposed to radiation for longer period of time.

B.1.3.3 Acute dose limits

When a significant amount of ionizing radiation is delivered in a short period of time – a few days or even a few hours - as in the case of, for example in the terrestrial environment, atomic bomb explosions or other nuclear disasters, in the space environment such catastrophic events present as Solar eruptions or Solar flares resulting in Solar Particle Events (SPE) destructive outbursts, we are talking about acute radiation.

Acute radiation syndrome (ARS) results from high level external exposure to ionizing radiation, either of the whole body or a significant portion (> 60%) of it.

High level means a dose greater than 1 Gy delivered at a relatively high dose rate. From a physiological standpoint Acute radiation syndrome is a combination of syndrome. These syndromes appear in stages and are directly related to the level of radiation received. They begin to occur within hours after exposure and may last for several weeks. Acute radiation syndrome (ARS) includes a:

- Subclinical phase (< 1 Gy)

And three syndromes resulting from either whole body irradiation or irradiation to a significant fraction of the body [20]:

- Hematopoietic syndrome (1 – 8 Gy)
- Gastrointestinal syndrome (6 – 20 Gy)
- Neurovascular syndrome (20 – > 50 Gy)

As seen hematopoietic stem cells (blood forming cells in red bone marrow) are highly sensitive to ionizing radiation. Animal studies indicate that a dose of 0.95 Gy reduces the population of stem cells to 37%. For this reason, hematopoietic syndrome – rapid degradation of hematopoietic stem cells, is seen with radiation exposures exceeding 1 Gy. As the absorb dose increases, more and more hematopoietic stem cells will be destroyed. The probability to recover will depend on absorbed dose, the dose rate and the overall bone marrow volume irradiated. If no regeneration, death usually occurs at doses of 4.5 – 6 Gy [50].

More short-term effects on human bodies exposed to different dose of ionizing radiation are presented in the Figure B-11.

Dose (rem)*	Probable Physiologic Effects
10-50	No obvious effects, except minor blood changes
50-100	5% to 10% experience nausea and vomiting for about 1 day; fatigue, but no serious disability; transient reduction in lymphocytes and neutrophils; no deaths anticipated
100-200	25% to 50% experience nausea and vomiting for about 1 day, followed by other symptoms of radiation sickness; 50% reduction in lymphocytes and neutrophils; no deaths anticipated
200-350	Most experience nausea and vomiting on the first day, followed by other symptoms of radiation sickness, eg, loss of appetite, diarrhea, minor hemorrhage; up to 75% reduction in all circulating blood elements; mortality rates 5% to 50% of those exposed
350-550	Nearly all experience nausea and vomiting on the first day, followed by other symptoms of radiation sickness, eg, fever, hemorrhage, diarrhea, emaciation; mortality rates of 50% to 90% within 6 weeks; survivors convalesce for about 6 months
550-750	All experience nausea and vomiting within 4 hours, followed by severe symptoms of radiation sickness; death up to 100%
750-1000	Severe nausea and vomiting may continue into the third day; survival time reduced to less than 2.5 weeks
1000-2000	Nausea and vomiting within 1-2 hours; always fatal within 2 weeks
4500	Incapacitation within hours, always fatal within 1 week

**100 rem = 1 Sv*

Figure B-11: Expected short – term effects in human from acute whole body radiation [51]

As seen in Figure B-11, severe symptoms occur at dose range from 3.5 – 5 Sv, where bone marrow suppression is nearly total. There is 50 – 90% chance of mortality from damage to hematopoietic system if remain untreated.

B.1.3.4 Chronic radiation effects

As already presented in the chapter regarding Astronaut dose limits, ionizing radiation has effects on the human body and biological material in longer periods of time - after months or years of chronic exposure to ionizing radiation. This radiation exposure would be presented in long term interplanetary space missions, traveling far beyond Earth orbit.

Chronic radiation syndrome (CRS) develops with a speed and severity proportional to the radiation dose received. It is distinct from acute radiation syndrome in that it occurs at dose rates low enough to permit natural repair mechanisms to compete with the radiation damage during the exposure period. The lower threshold for chronic radiation syndrome is between 0.7 – 1.5 Gy, at a dose rates above 0.1 Gy/y.

Latent period (time interval between exposure and development of disease) is from 1-5 years, and it coincides with the period of maximum radiation dose. The recovery period is 3 – 12 months after exposure is terminated, or following a considerable decrease in the dose rate.

At the initial stage CRS shows as a deregulatory pathology formed on the basis of radiation induced disorders in: regulatory systems of man (nervous, endocrine and immune system) and as changes in cardio – vascular, digestive, reproductive and other systems, and this disorders are reversible.

Higher doses to regulatory and visceral organs induce irreversible changes to the organism (cardiovascular diseases, oncological diseases, respiratory diseases…) [52].

Appendix C: Radiation modelling data

C.1 Introduction

Presented are radiation simulation data discussed in Chapter 4. Results for specific mission location (LEO, deep space) and duration (7, 200, 500, 1000 days) are split into different components of radiation (GCR, trapped particles, SPE) and presented in Tables C-1 to C-45 bellow. Different colour markers were used to easily distinguish higher values for specific components of space radiation. A **yellow marker** was used for maximum radiation values caused by trapped particles in Earth magnetic field, a **red marker** for maximum values of galactic centre radiation (GCR) and a **violet marker** for higher values of radiation caused by solar particle events (SPE).

C.2 Massless sphere

LOW EARTH ORBIT (LEO), 7 DAYS, 600 km

		0 DEG.	30 DEG.
SOLAR MAX (26.9 - 3.10 1989)	GCR	5.56E-02 mGy	8.56E-02 mGy
		4.01E-01 mSv	6.03E-01 mSv
	TRAPPED p AND n	1.14E+01 mGy	3.90E+02 mGy
		1.802E+02 mSv	4.37E+03 mSv
	TOTALS	1.14E+01 mGy	3.90E+02 mGy
		1.80E+02 mSv	4.37E+03 mSv
SOLAR MIN (15.9 - 22.9.1996)	GCR	6.65E-02 mGy	1.08E-01 mGy
		4.75E-01 mSv	7.60E-01 mSv
	TRAPPED p AND n	5.34E+01 mGy	6.37E+02 mGy
		8.13E+02 mSv	8.73E+03 mSv
	TOTALS	5.35E+01 mGy	6.37E+02 mGy
		8.14E+02 mSv	8.74E+03 mSv

Table C-1: Radiation results for Low Earth Orbit (7 days, 600 km) with inclination 0 ° and 30 ° for massless sphere

DEEP SPACE (1 AU)

200 DAYS

GCR	SOLAR MAX (1991)	2.58E+01 mGy
		1.68E+02 mSv
	SOLAR MIN (1997)	7.20E+01 mGy
		4.58E+02 mSv
SPE	sept.1989	5.78E+05 mGy
		1.04E+07 mSv

Table C-2: Massless sphere deep space 200 days mission

500 DAYS

GCR	SOLAR MAX (1991)	6.45E+01 mGy
		4.20E+02 mSv
	SOLAR MIN (1997)	1.80E+02 mGy
		1.14E+03 mSv
SPE	sept.1989	5.78E+05 mGy
		1.04E+07 mSv

Table C-3: Massless sphere deep space 500 days mission

1000 DAYS

GCR	SOLAR MAX (1991)	1.29E+02 mGy
		8.40E+02 mSv
	SOLAR MIN (1997)	3.60E+02 mGy
		2.29E+03 mSv
SPE	sept.1989	5.78E+08 mGy
		1.04E+07 mSv

Table C-4: Massless sphere deep space 1000 days mission

C.3 Sphere Aluminium 3 mm (8.1 kg/m^2)

LOW EARTH ORBIT (LEO), 7 DAYS, 600 km

		0 DEG.	30 DEG.
SOLAR MAX (26.9 - 3.10 1989)	GCR	6.31E-02 mGy	9.73E-02 mGy
		4.34E-01 mSv	6.56E-01 mSv
	TRAPPED p AND n	1.61E+00 mGy	4.81E+01 mGy
		2.64E+00 mSv	8.02E+01 mSv
	TOTALS	1.68E+00 mGy	4.82E+01 mGy
		3.08E+00 mSv	8.09E+01 mSv
SOLAR MIN (15.9 - 22.9.1996)	GCR	7.55E-02 mGy	1.28E-01 mGy
		5.16E-01 mSv	8.28E-01 mSv
	TRAPPED p AND n	5.49E+00 mGy	7.07E+01 mGy
		1.04E+01 mSv	1.15E+02 mSv
	TOTALS	5.57E+00 mGy	7.71E+01 mGy
		1.10E+01 mSv	1.16E+02 mSv

Table C-5: Radiation results for Low Earth Orbit (7 days, 600 km) with inclination 0 ° and 30 ° for Aluminium sphere with 3 mm wall thickness

DEEP SPACE (1 AU)

200 DAYS

GCR	SOLAR MAX (1991)	2.86E+01 mGy
		1.83E+02 mSv
	SOLAR MIN (1997)	7.78E+01 mGy
		4.82E+02 mSv
SPE	sept.1989	8.769E+03 mGy
		1.88E+04 mSv

Table C-6: 3 mm Aluminium sphere deep space 200 days mission

500DAYS

GCR	SOLAR MAX (1991)	7.16E+01 mGy
		4.57E+02 mSv
	SOLAR MIN (1997)	1.96E+02 mGy
		1.20E+03 mSv
SPE	sept.1989	8.77E+03 mGy
		1.88E+04 mSv

Table C-7: 3 mm Aluminium sphere deep space 500 days mission

1000 DAYS

GCR	SOLAR MAX (1991)	1.43E+02 mGy
		9.14E+02 mSv
	SOLAR MIN (1997)	3.89E+02 mGy
		2.41E+03 mSv
SPE	sept.1989	8.77E+03 mGy
		1.88E+04 mSv

Table C-8: 3 mm Aluminium sphere deep space 1000 days mission

C.4 Sphere Aluminium 10 mm (27 kg/m^2)

LOW EARTH ORBIT (LEO), 7 DAYS, 600 km

		0 DEG.	30 DEG.
SOLAR MAX (26.9 - 3.10 1989)	GCR	6.90E-02 mGy	1.06E-01 mGy
		4.29E-01 mSv	6.48E-01 mSv
	TRAPPED p AND n	1.06E00 mGy	3.22E+01 mGy
		1.67E+00 mSv	4.93E+01 mSv
	TOTALS	1.134E00 mGy	3.23E+01 mGy
		2.10E00 mSv	4.99E+01 mSv
SOLAR MIN (15.9 - 22.9.1996)	GCR	8.26E-02 mGy	1.35E-01 mGy
		5.11E-01 mSv	8.19E-01 mSv
	TRAPPED p AND n	2.39E+00 mGy	4.92E+01 mGy
		3.96E+00 mSv	7.54E+01 mSv
	TOTALS	2.47E+00 mGy	4.93E+01 mGy
		4.47E+00 mSv	7.63E+01 mSv

Table C-9: Radiation results for Low Earth Orbit (7 days, 600 km) with inclination 0 ° and 30 ° for Aluminium sphere with 10 mm wall thickness

DEEP SPACE (1 AU)

200 DAYS

GCR	SOLAR MAX (1991)	3.02E+01 mGy
		1.77E+02 mSv
	SOLAR MIN (1997)	7.92E+01 mGy
		4.42E+02 mSv
SPE	sept.1989	1.81E+03 mGy
		3.26E+03 mSv

Table C-10: 10 mm Aluminium sphere deep space 200 days mission

500 DAYS

GCR	SOLAR MAX (1991)	7.55E+01 mGy
		4.43E+02 mSv
	SOLAR MIN (1997)	1.98E+02 mGy
		1.10E+03 mSv
SPE	sept.1989	1.81E+03 mGy
		3.26E+03 mSv

Table C-11: 10 mm Aluminium sphere deep space 500 days mission

1000 DAYS

GCR	SOLAR MAX (1991)	1.51E+02 mGy
		8.85E+02 mSv
	SOLAR MIN (1997)	3.96E+02 mGy
		2.21E+03 mSv
SPE	sept.1989	1.81E+03 mGy
		3.26E+03 mSv

Table C-12: 10 mm Aluminium sphere deep space 1000 days mission

C.5 Sphere Aluminium 20 mm (54 kg/m^2)

DEEP SPACE (1 AU)

200 DAYS

GCR	SOLAR MAX (1991)	3.11E+01 mGy
		1.66E+02 mSv
	SOLAR MIN (1997)	7.92E+01 mGy
		3.94E+02 mSv
SPE	sept.1989	6.59E+02 mGy
		1.09E+03 mSv

Table C-13: 20 mm Aluminium sphere deep space 200 days mission

500 DAYS

GCR	SOLAR MAX (1991)	7.78E+01 mGy
		4.15E+02 mSv
	SOLAR MIN (1997)	1.98E+02 mGy
		9.85E+02 mSv
SPE	sept.1989	6.59E+02 mGy
		1.09E+03 mSv

Table C-14: 20 mm Aluminium sphere deep space 500 days mission

1000 DAYS

GCR	SOLAR MAX (1991)	1.56E+02 mGy
		8.30E+02 mSv
	SOLAR MIN (1997)	3.96E+02 mGy
		1.97E+03 mSv
SPE	sept.1989	6.59E+02 mGy
		1.09E+03 mSv

Table C-15: 20 mm Aluminium sphere deep space 1000 days mission

C.6 Sphere Aluminium 30 mm (81 kg/m^2)

DEEP SPACE (1 AU)

200 DAYS

GCR	SOLAR MAX (1991)	3.15E+01 mGy
		1.55E+02 mSv
	SOLAR MIN (1997)	7.87E+01 mGy
		3.56E+02 mSv
SPE	sept.1989	3.65E+02 mGy
		5.86E+02 mSv

Table C-16: 30 mm Aluminium sphere deep space 200 days mission

500 DAYS

GCR	SOLAR MAX (1991)	7.89E+01 mGy
		3.89E+02 mSv
	SOLAR MIN (1997)	1.97E+02 mGy
		8.91E+02 mSv
SPE	sept.1989	3.65E+02 mGy
		5.86E+02 mSv

Table C-17: 30 mm Aluminium sphere deep space 500 days mission

1000 DAYS

GCR	SOLAR MAX (1991)	1.58E+02 mGy
		7.77E+02 mSv
	SOLAR MIN (1997)	3.94E+02 mGy
		1.78E+03 mSv
SPE	sept.1989	3.65E+02 mGy
		5.86E+02 mSv

Table C-18: 30 mm Aluminium sphere deep space 1000 days mission

C.7 Sphere polyethylene 10 mm, (9 kg/m^2)

DEEP SPACE (1 AU)

200 DAYS

GCR	SOLAR MAX (1991)	2.75E+01 mGy
		1.70E+02 mSv
	SOLAR MIN (1997)	7.49E+01 mGy
		4.44E+02 mSv
SPE	sept.1989	5.11E+03 mGy
		9.24E+03 mSv

Table C-19: 10 mm polyethylene sphere deep space 200 days mission

500 DAYS

GCR	SOLAR MAX (1991)	6.88E+01 mGy
		4.24E+02 mSv
	SOLAR MIN (1997)	1.87E+02 mGy
		1.11E+03 mSv
SPE	sept.1989	5.11E+03 mGy
		9.24E+03 mSv

Table C-20: 10 mm polyethylene sphere deep space 500 days mission

1000 DAYS

GCR	SOLAR MAX (1991)	1.37E+02 mGy
		8.48E+02 mSv
	SOLAR MIN (1997)	3.74E+02 mGy
		2.22E+03 mSv
SPE	sept.1989	5.11E+03 mGy
		9.24E+03 mSv

Table C-21: 10 mm polyethylene sphere deep space 1000 days mission

C.8 Sphere polyethylene 20 mm (18 kg/m^2)

DEEP SPACE (1 AU)

200 DAYS

GCR	SOLAR MAX (1991)	2.80E+01 mGy
		1.63E+02 mSv
	SOLAR MIN (1997)	7.49E+01 mGy
		4.11E+02 mSv
SPE	sept.1989	1.91E+03 mGy
		3.05E+03 mSv

Table C-22: 20 mm polyethylene sphere deep space 200 days mission

500 DAYS

GCR	SOLAR MAX (1991)	7.00E+01 mGy
		4.06E+02 mSv
	SOLAR MIN (1997)	1.87E+02 mGy
		1.03E+03 mSv
SPE	sept.1989	1.91E+03 mGy
		3.05E+03 mSv

Table C-23: : 20 mm polyethylene sphere deep space 500 days mission

1000 DAYS

GCR	SOLAR MAX (1991)	1.40E+02 mGy
		8.13E+02 mSv
	SOLAR MIN (1997)	3.75E+02 mGy
		2.06E+03 mSv
SPE	sept.1989	1.91E+03 mGy
		3.05E+03 mSv

Table C-24: 20 mm polyethylene sphere deep space 1000 days mission

C.9 Sphere polyethylene 30 mm (27 kg/m^2)

DEEP SPACE (1 AU)

200 DAYS

GCR	SOLAR MAX (1991)	2.83E+01 mGy
		1.55E+02 mSv
	SOLAR MIN (1997)	7.46E+01 mGy
		3.82E+02 mSv
SPE	sept.1989	1.07E+03 mGy
		1.62E+03 mSv

Table C-25: 30 mm polyethylene sphere deep space 200 days mission

500 DAYS

GCR	SOLAR MAX (1991)	7.06E+01 mGy
		3.88E+02 mSv
	SOLAR MIN (1997)	1.86E+02 mGy
		9.57E+02 mSv
SPE	sept.1989	1.07E+03 mGy
		1.62E+03 mSv

Table C-26: 30 mm polyethylene sphere deep space 500 days mission

1000 DAYS

GCR	SOLAR MAX (1991)	1.41E+02 mGy
		7.76E+02 mSv
	SOLAR MIN (1997)	3.73E+02 mGy
		1.91E+03 mSv
SPE	sept.1989	1.07E+03 mGy
		1.62E+3 mSv

Table C-27: 30 mm polyethylene sphere deep space 1000 days mission

C.10 Sphere Aluminium 3 mm+polyethylene 10 mm

DEEP SPACE (1 AU)

200 DAYS

GCR	SOLAR MAX (1991)	2.81E+01 mGy
		1.67E+02 mSv
	SOLAR MIN (1997)	7.54E+01 mGy
		4.28E+02 mSv
SPE	sept.1989	2.53E+03 mGy
		4.18E+03 mSv

Table C-28: 3 mm Al+10 mm poly. sphere composite deep space 200 days mission

500 DAYS

GCR	SOLAR MAX (1991)	7.03E+01 mGy
		4.17E+02 mSv
	SOLAR MIN (1997)	1.88E+02 mGy
		1.06E+03 mSv
SPE	sept.1989	2.53E+03 mGy
		4.18E+03 mSv

Table C-29: 3 mm Al+10 mm poly. sphere composite deep space 500 days mission

1000 DAYS

GCR	SOLAR MAX (1991)	1.41E+02 mGy
		8.34E+02 mSv
	SOLAR MIN (1997)	3.77E+02 mGy
		2.13E+03 mSv
SPE	sept.1989	2.53E+03 mGy
		4.18E+03 mSv

Table C-30: 3 mm Al+10 mm poly. sphere composite deep space 1000 days mission

C.11 Sphere Aluminium 3 mm+polyethylene 20 mm

DEEP SPACE (1 AU)
200 DAYS

GCR	SOLAR MAX (1991)	2.84E+01 mGy
		1.59E+02 mSv
	SOLAR MIN (1997)	7.50E+01 mGy
		3.95E+02 mSv
SPE	sept.1989	1.28E+03 mGy
		1.97E+03 mGy

Table C-31:3 mm Al+20 mm poly. sphere composite deep space 200 days mission

500 DAYS

GCR	SOLAR MAX (1991)	7.09E+01 mGy
		3.98E+02 mSv
	SOLAR MIN (1997)	1.88E+02 mGy
		9.88E+02 mSv
SPE	sept.1989	1.28E+03 mGy
		1.97E+03 mSv

Table C-32: 3 mm Al+20mm poly. sphere composite deep space 500 days mission

1000 DAYS

GCR	SOLAR MAX (1991)	1.42E+02 mGy
		7.96E+02 mSv
	SOLAR MIN (1997)	3.75E+02 mGy
		1.98E+03 mSv
SPE	sept.1989	1.28E+03 mGy
		1.97E+03 mSv

Table C-33: 3 mm Al+20 mm poly. sphere composite deep space 1000 days mission

C.12 Sphere Aluminium 3 mm+polyethylene 30 mm

DEEP SPACE (1 AU)
200 DAYS

GCR	SOLAR MAX (1991)	2.85E+01 mGy
		1.52E+02 mSv
	SOLAR MIN (1997)	7.46E+01 mGy
		3.69E+02 mSv
SPE	sept.1989	8.11E+02 mGy
		1.20E+03 mSv

Table C-34: 3 mm Al+30mm poly. sphere composite deep space 200 days mission

500 DAYS

GCR	SOLAR MAX (1991)	7.13E+01 mGy
		3.79E+02 mSv
	SOLAR MIN (1997)	1.86E+02 mGy
		9.22E+02 mSv
SPE	sept.1989	8.11E+02 mGy
		1.20E+03 mSv

Table C-35: 3mm Al+30mm poly. sphere composite deep space 500 days mission

1000 DAYS

GCR	SOLAR MAX (1991)	1.42E+02 mGy
		7.59E+02 mSv
	SOLAR MIN (1997)	3.73E+02 mGy
		1.84E+03 mSv
SPE	sept.1989	8.11E+02 mGy
		1.20E+03 mSv

Table C-36: 3 mm Al+30 mm poly. sphere composite deep space 1000 days mission

C.13 Sphere Aluminium 6 mm+polyethylene 10 mm

DEEP SPACE (1 AU)
200 DAYS

GCR	SOLAR MAX (1991)	2.85E+01 mGy
		1.63E+02 mSv
	SOLAR MIN (1997)	7.56E+01 mGy
		4.09E+02 mSv
SPE	sept.1989	1.58E+03 mGy
		2.48E+03 mSv

Table C-37:6 mm Al+10 mm poly. sphere composite deep space 200 days mission

500 DAYS

GCR	SOLAR MAX (1991)	7.13E+01 mGy
		4.09E+02 mSv
	SOLAR MIN (1997)	1.89E+02 mGy
		1.02E+03 mSv
SPE	sept.1989	1.58E+03 mGy
		2.48E+03 mSv

Table C-38:6 mm Al+10 mm poly. sphere composite deep space 500 days mission

1000 DAYS

GCR	SOLAR MAX (1991)	1.43E+02 mGy
		8.18E+02 mSv
	SOLAR MIN (1997)	3.78E+02 mGy
		2.04E+03 mSv
SPE	sept.1989	1.58E+03 mGy
		2.48E+03 mSv

Table C-39: 6 mm Al+10 mm poly. sphere composite deep space 1000 days mission

C.14 Sphere Aluminium 6 mm+polyethylene 20 mm

DEEP SPACE (1AU)
200 DAYS

GCR	SOLAR MAX (1991)	2.86E+01 mGy
		1.56E+02 mSv
	SOLAR MIN (1997)	7.50E+01 mGy
		3.80E+02 mSv
SPE	sept.1989	9.37E+02 mGy
		1.41E+03 mSv

Table C-40:6 mm Al+20 mm poly. sphere composite deep space 200 days mission

500 DAYS

GCR	SOLAR MAX (1991)	7.16E+01 mGy
		3.89E+02 mSv
	SOLAR MIN (1997)	1.87E+02 mGy
		9.51E+02 mSv
SPE	sept.1989	9.37E+02 mGy
		1.41E+03 mSv

Table C-41:6 mm Al+20 mm poly. sphere composite deep space 500 days mission

1000 DAYS

GCR	SOLAR MAX (1991)	1.43E+02 mGy
		7.79E+02 mSv
	SOLAR MIN (1997)	3.75E+02 mGy
		1.90E+03 mSv
SPE	sept.1989	9.37E+02 mGy
		1.41E+02 mSv

Table C-42: 6 mm Al+20 mm poly. sphere composite deep space 1000 days mission

C.15 Sphere Aluminium 6 mm+polyethylene 30mm

DEEP SPACE (1 AU)
200 DAYS

GCR	SOLAR MAX (1991)	2.87E+01 mGy
		1.48E+02 mSv
	SOLAR MIN (1997)	7.45E+01 mGy
		3.56E+02 mSv
SPE	sept.1989	6.42E+02 mGy
		9.41E+02 mSv

Table C-43: 6 mm Al+30 mm poly. sphere composite deep space 200 days mission

500 DAYS

GCR	SOLAR MAX (1991)	7.18E+01 mGy
		3.71E+02 mSv
	SOLAR MIN (1997)	1.86E+02 mGy
		8.89E+02 mSv
SPE	sept.1989	6.42E+02 mGy
		9.41E+02 mSv

Table C-44: 6 mm Al+30 mm poly. sphere composite deep space 500 days mission

1000 DAYS

GCR	SOLAR MAX (1991)	1.43E+02 mGy
		7.42E+02 mSv
	SOLAR MIN (1997)	3.72E+02 mGy
		1.78E+03 mSv
SPE	sept.1989	6.42E+02 mGy
		9.41E+02 mSv

Table C-45: 6 mm Al+30 mm poly. sphere composite deep space 1000 days mission

Appendix D: Spacecraft Thermal modelling

D.1 Basics of Thermal space environment

D.1.1 Introduction and methodology

Absence of atmosphere and strong solar radiation are main factors behind characteristics of the thermal environment in space which are discussed in the following appendix.

D.1.2 Methods of heat transfer

The simplified explanation of the Second law of Thermodynamics states, that heat transfers from an object of a higher temperature to that of a lower temperature, in order to maintain thermal equilibrium. Heat transfer occurs in order to maintain this principle when an object is at a different temperature from another object or its surrounding.

Thermal energy is transported by three concepts: Radiative heat transfer, Conductive heat transfer and Convective heat transfer.

D.1.2.1 Radiative heat transfer

With the radiative heat transfer we describe physical phenomena where heat is transferred with electromagnetic waves. All materials continuously emit and absorb electromagnetic waves, or photons, by lowering or raising their atomic and molecular energy levels. The strength and wavelengths of emission depend on the temperature of the emitted material. For heat transfer applications wavelengths between 10^{-7} and 10^{-3} m (ultraviolet, visible and infrared) are of greatest importance.

An important distinguished feature between other mechanisms of transferring energy - convection and conductance (which are discussed later), is the difference in their temperature dependencies. Conductive and convective heat transfer are generally proportional to temperature difference, while radiative heat transfer rates (Equation D-1) are proportional to differences in temperature to the fourth power, where q is heat flux in (W/m^2) and T temperature.

Equation D-1: Radiative heat transfer

$$\mathbf{q} \propto \mathbf{T^4} - \mathbf{T_\infty^4}$$

- **Black body**

The opaque surface that does not reflect any radiation is called the perfect absorber or a black body. Thus black bodies absorb the maximum possible amount of radiative energy and are therefore standard for classification of all other surfaces. At the same time black surfaces also emits a maximum amount of radiative energy over all wavelengths [71].

The monochromatic emissive power of a blackbody is given by Planck distribution (Equation D-2).

Equation D-2: Emissive power of black body

$$\mathbf{E_{\lambda,b}(\lambda, T)} = \frac{\mathbf{2\pi \cdot h \cdot c_0^2}}{\boldsymbol{\lambda}^{\mathbf{5}}} \cdot \frac{\mathbf{1}}{\mathbf{e^{\left(\frac{h \cdot c_0}{\lambda \cdot k \cdot T}\right)} - 1}}$$

where is $E_{b,\lambda}$ emissive power of a blackbody at specific λ wavelength, T temperature of black body, h Planck constant, c_0 speed of light and k Boltzmann constant. Plotting spectral emissive power of a blackbody over the wavelength for different temperatures gives Planck distribution (Figure D-1).

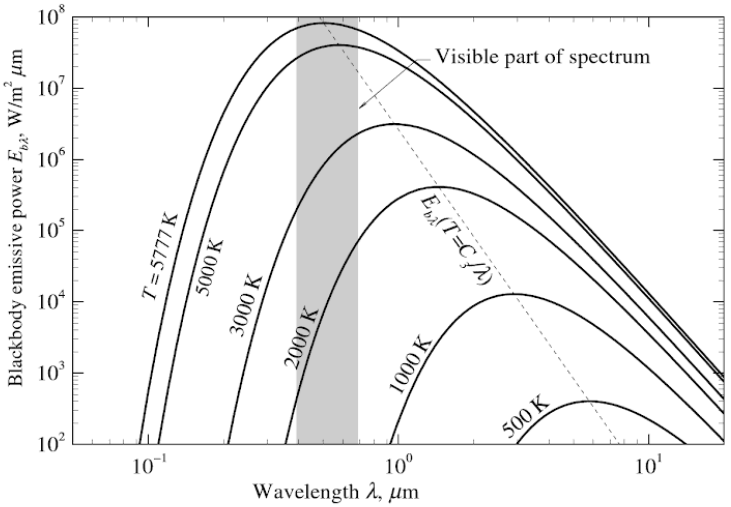

Figure D-1: **Blackbody emissive power spectrum – Planck distribution [71]**

The striped area marks the visible frequency range, and the dotted line represents Wien's displacement law, which states at which wavelengths the body emits most energy depending on its temperature. Integrating Equation D-2 over the whole wavelength spectrum derives the Stefan – Boltzmann law (Equation D-3).

Equation D-3: Energy fluence emitted by the black body

$$\mathbf{E_b} = \int_0^{\infty} \left(\frac{\mathbf{2\pi \cdot h \cdot c_0^2}}{\boldsymbol{\lambda}^5} \cdot \frac{\mathbf{1}}{\mathbf{e}^{\left(\frac{\mathbf{h \cdot c_0}}{\boldsymbol{\lambda} \cdot \mathbf{k} \cdot \mathbf{T}}\right)} - \mathbf{1}} \right) \mathbf{d\lambda}$$

$$\mathbf{E_b} = \boldsymbol{\sigma} \cdot \mathbf{T}^4$$

Where σ is the Stefan-Boltzmann constant and E_b the energy fluence emitted by the black body, the equation is only valid for bodies, which can be assumed as black bodies. For black body absorptivity (α) and emittance (ε) values are 1. For real bodies more properties of the emitting and absorbing surface materials have to be taken into consideration to properly describe the radiative heat transfer mechanism [72]. The heat $\dot{Q}_{rad,ij}$ in (W) is transferred by radiation from a surface i to surface j is described by Equation D-4.

Equation D-4: Radiative heat transfer

$$\dot{\mathbf{Q}}_{\mathbf{rad,ij}} = \mathbf{A_i} \cdot \mathbf{F_{ij}} \cdot \boldsymbol{\varepsilon}_{\mathbf{ij}} \cdot \boldsymbol{\sigma} \cdot (\mathbf{T_i^4} - \mathbf{T_j^4})$$

Where A_i is the area of surface i, F_{ij} the view factor of surface j as seen from surface i, ε_{ij} the effective emittance, σ the Bolzmann constant and T temperature of both surfaces, the assumption is made that the view factor remains constant for the whole surface [73].

The quantity of transferred heat is significantly influenced by the geometry of the surfaces and their alignment. The aspect is considered by introducing the radiative view factor F_{ij}, which is defined as the fraction of radiation leaving surface A_i that reaches surface A_j. For two different surfaces the view factor is

determined by Equation D-5.

Equation D-5: Radiative view factor

$$F_{ij} = \frac{1}{A_i} \cdot \iint \frac{\cos \phi_i \cdot \cos \phi_j}{\pi \cdot s^2} dA_i dA_j$$

Where s is the distance between two elements on the surfaces. The angle ϕ_i is the angle between the surface normal and the direction of the radiated point on the second surface and ϕ_j is the angle between the surface normal of the second surface and the line between the observed point. An important point of Equation D-5 is symmetry, which allows to deduce a reciprocity relationship for the two surfaces Equation D-6 and Figure D-2 [73]:

Equation D-6: Reciprocity relationship of surfaces

$$\mathbf{A_i \cdot F_{ij} = A_j \cdot F_{ji}}$$

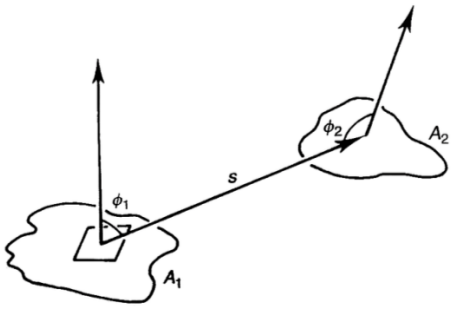

Figure D-2: Dependencies of the view factor [73]:

- **Radiative properties – absorption and emittance**

Some fraction of irradiation that hit the surface (Figure D-3) may be reflected, the rest is either absorbed by the material or transmitted through it. These fractions are described by the properties known as reflectivity, absorptivity, and transmissivity, which are given the respective symbols ρ, α and τ. The sum of the reflected, absorbed and transmitted component must equal the irradiation, thus:

Equation D-6: Irradiation equation

$$\rho + \alpha + \tau = 1$$

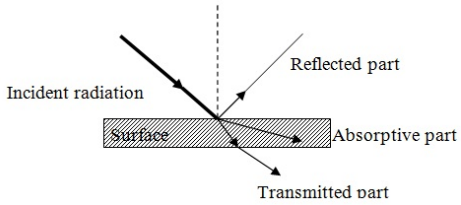

Figure D-3: Surface irradiation and its components

Every body with specific temperature emits some radiation. The black body behaviour, given by the Planck distribution (Equation D-2) is a theoretical upper limit for the thermal radiation emitted by a body. The ratio of radiation emitted by the surface to that of a black body at the same temperature is known as emittance (ε).

Equation D-7: Emittance equation

$$\boldsymbol{\varepsilon = \frac{E}{E_b}}$$

where E is radiation emitted by real surface compared by E_b, radiation emitted by black body surface. It can be concluded, that absorptivity (α) and emittance (ε) are always <1 for real surfaces and are dependable of incident angle and wave length of radiation [74].

- **Optical properties of the surfaces – Kirchhoff's Law**

The relationship between absorptivity and emittance properties of material surface (Figure D-4) are of great importance for passive thermal control.

$$\frac{\alpha}{\varepsilon} < 1 \rightarrow cooling$$

$$\frac{\alpha}{\varepsilon} > 1 \rightarrow heating$$

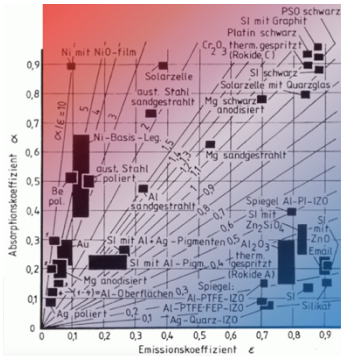

Figure D-4: α and ε coefficients for different materials [75]

Kirchhoff's law of thermal radiation (Equation D-8) states that the absorptivity and the emittance of a surface at a given wavelength and angle of incidence are equal:

Equation D-8: Kirchhoff's Law

$$\alpha = \varepsilon$$

For different wavelength, values are not equal. Absorptivity refers mainly to visible - UV wavelength of the spectrum, while emittance mainly to IR part of it. Therefore, usually optical characteristics of the surfaces are expressed with the absorptivity factor in Solar - UV part of spectrum as α_S and emittance in IR part or as ε_{IR}. Knowing both optical values for surface materials, passive cooling or heating can be designed (Figure D-4).

D.1.2.2 Conductive heat transfer

Conduction is the mode of heat transfer that is a result of the motion of atoms, molecules, electrons and the vibrations in the atomic lattice. This mechanism occurs within and between the solid parts of the spacecraft which are in contact. This physical phenomenon is the major mechanism in transporting thermal energy inside and between the components as well as from inside of the spacecraft to the outer panels and vice versa.

The equation for simplified one dimensional conductive heat transfer $\dot{Q}_{c,ij}$ in (W) is based on Fourier's law of conductance (Equation D-9). In real situations usually 2D or 3D heat transfer occurs.

Equation D-9: Heat transfer

$$\dot{\mathbf{Q}}_{\mathbf{c,ij}} = \mathbf{h}_{\mathbf{ij}} \cdot (\mathbf{T}_{\mathbf{i}} - \mathbf{T}_{\mathbf{j}})$$

The coefficient of thermal conductance - h_{ij} (W/ °C) describes the capability of the material to transfer heat. It depends on the cross-section area A, the conductive path length l and the thermal conductivity λ (Equation D-10):

Equation D-10: Coefficient of thermal conductance

$$\mathbf{h}_{\mathbf{ij}} = \frac{\boldsymbol{\lambda} \cdot \mathbf{A}}{\mathbf{l}}$$

The inverse of the conductance is thermal resistance R (Equation D-11).

Equation D-11: Coefficient of thermal resistance

$$\mathbf{R}_{\mathbf{ij}} = \frac{\mathbf{1}}{\mathbf{h}_{\mathbf{ij}}}$$

Thermal resistance is calculated in the manner of analogue to electrical resistance for both series and parallel configuration (Figure D-5). The total resistance R_{tot} for a series of k resistances is calculated as (Equation D-12):

Equation D-12: Total resistance for a series

$$R_{tot} = \sum_{n=0}^{k} R_n$$

and for parallel as (Equation D-13):

Equation D-13: Total resistance for parallel

$$\mathbf{R}_{\mathbf{tot}} = \sum_{\mathbf{n=0}}^{\mathbf{k}} \frac{\mathbf{1}}{\mathbf{R}_{\mathbf{n}}}$$

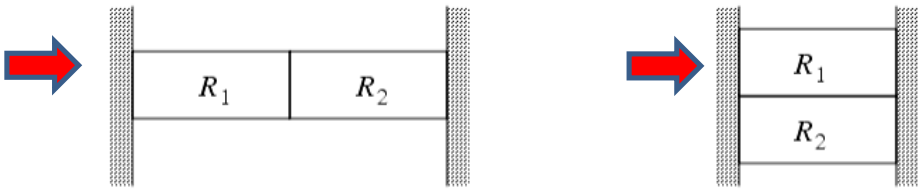

$$\frac{1}{R_{tot}} = \frac{1}{R_1} + \frac{1}{R_2}$$

$$R_{tot} = R_1 + R_2$$

Figure D-5: Thermal resistance for series and parallel configuration [73]

D.1.2.3 Convective heat transfer

Convective heat transfer or simply convection is the transfer of heat from one place to another by the movement of fluids. It is usually the dominant form of heat transfer in liquids and gases. Since space can be assumed to be a vacuum, this mechanism is irrelevant for most space missions and is also not taken into consideration for our example.

D.1.3 Thermal space environment

Spacecraft operating in an orbit or in interplanetary space is exposed to different external heat sources (Figure D-6). Possible heat sources are:

- Direct Solar radiation,
- Albedo radiation,
- Planetary IR radiation,
- Radiation emitted from the spacecraft,

A spacecraft placed in sufficiently high orbit around Earth is only influenced by the Solar radiation, the albedo and planetary IR radiation (Figure D-6).

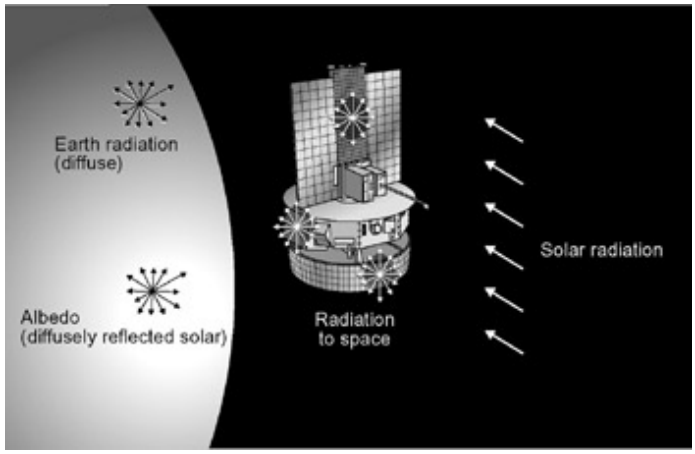

Figure D-6: Satellite thermal environment [81]

For interplanetary spaceflights, away from vicinity of any celestial bodies only the Solar radiation plays a significant role. Other effects that affect temperature conditions in interplanetary space are radiation emitted from the spacecraft itself and heat generated within spacecraft. Below three main external heat sources are described.

D.1.3.1 Direct Solar radiation

Solar radiation is the greatest source of environmental heating incident on most spacecraft in Earth's orbit and beyond. It is directly emitted from the Sun, star in centre of our Solar system. The Sun can be modelled as a black body with a temperature of 5800 K. The energy is mostly emitted in the wavelength range

between 150 nm and 10 μm with a spectral intensity maximum in the visible range at 450 nm.

The intensity of Sun radiation F_{Sun}, decreases with the square of the radial distance – d_{Sun} from the Sun (Equation D-14):

Equation D-14: Intensity of Sun radiation

$$\mathbf{F_{Sun}} = \frac{\mathbf{P_{Sun}}}{\mathbf{4 \cdot \pi \cdot d_{Sun}^2}}$$

From the average output power of the Sun, P_{Sun}= 3.857 10^{26} W, intensity at Earth distance of d_{Earth}=1 AU is around 1371,5 W/m^2 ± 5 W. This value is known as Solar constant [73].

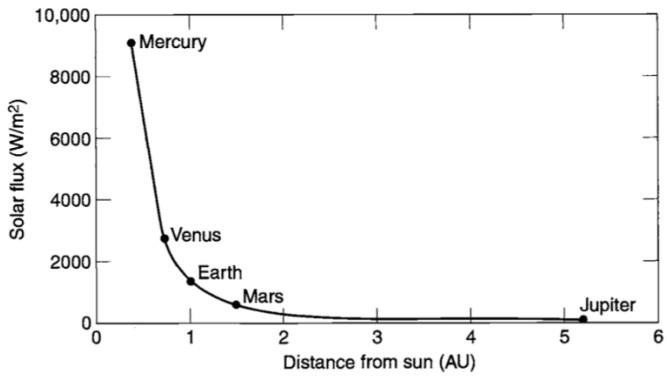

Figure D-7: Solar flux as a function of distance from the Sun [81]

Heat input from direct Solar radiation into spacecraft is calculated as (Equation D-15):

Equation D-15: Heat input from direct solar flux

$$\dot{\mathbf{Q}}_{\mathbf{Sun}} = \boldsymbol{\alpha} \cdot \mathbf{F_{Sun}} \cdot \mathbf{A_{\perp Sun}}$$

where $\dot{Q}_{Sun}$ (W) is the heat input from direct solar flux, α is the absorptivity of the optical coating, F_{Sun} (W/m^2) solar flux at specific distance and $A_{\perp Sun}$ (m^2) area of the surface or spacecraft perpendicular to the Sun. With increased distance from the Sun, the flux value decreases drastically (Figure D-7).

D.1.3.2 Albedo

Sunlight reflected off a planet or moon is known as albedo. A planets albedo is usually expressed as the fraction of incident sunlight that is reflected back to space and is highly variable. Usually, reflectivity is greater over continental regions than oceanic regions and generally increases with decreasing local solar - elevation angles and increasing cloud coverage. Albedo also tends to increase with latitude [81]. In the case of planet Earth, values vary between 0.05 over the surface and 0.8 over the cloud layer. In practice, a constant average albedo value is used for the thermal design of spacecraft. The average albedo of the Earth is settled at 0.35 [83]. Values for albedo of other Solar System bodies are presented in Table D-1.

Planet	Mercury	Venus	Earth	Mars
Albedo [ ]	$0.06 - 0.10$	$0.60 - 0.76$	$0.31 - 0.39$	0.15

Table D-1: Planetary albedo values of the planets in the inner solar system [81]

Heat input $\dot{Q}_{Albedo}$ (W) is the heat input into reference surface – spacecraft (Equation D-16).

Equation D-16: Heat input by albedo

$$\dot{Q}_{Albedo} = \alpha \cdot F_{Sun} \cdot a \cdot A_{\perp Earth} \cdot \frac{R_{Earth}^2}{(R_{Earth} + h)^2}$$

where a is a dimensionless albedo factor, $A_{\perp Earth}$ (m^2) is surface area perpendicular to the Earth, R_{Earth} Earth's radius in (m) and h (m) spacecraft altitude.

D.1.3.3 Planetary IR radiation

In addition to the reflected solar radiation, the spacecraft also receives radiation from the planet or planetary body itself. As already explained, every body with a non-zero temperature emits heat in the form of electromagnetic radiation. Earth radiates heat in IR range between 2 μm and 50 μm, with a maximum at 10 μm. The intensity of Earth's thermal radiation has a temporal and spatial

dependency. Similar to solar radiation, the planetary IR radiation - $\dot{Q}_{IR}$ (W) spreads radially as stated in Equation D-17:

Equation D-17: Heat input by IR

$$\dot{\mathbf{Q}}_{\mathbf{IR}} = \boldsymbol{\epsilon} \cdot \mathbf{F}_{\mathbf{Earth-IR}} \cdot \mathbf{A}_{\perp \mathbf{Earth}} \cdot \frac{\mathbf{R}_{\mathbf{Earth}}^{\mathbf{2}}}{(\mathbf{R}_{\mathbf{Earth}} + \mathbf{h})^{\mathbf{2}}}$$

where ϵ is the emissivity of the satellite optical coating, $F_{Earth-IR}$ (W/m^2) is planetary IR flux (W/m^2) [73].

Unlike short – wavelength solar energy, Earth IR loads incident on a spacecraft cannot be reflected away from radiator surfaces with special thermo – control coating, since the same coating would prevent the radiation of waste heat away from the spacecraft. Because of this, Earth-emitted IR energy can present a particularly heavy backload on spacecraft radiators in low Earth orbits [81].

D.1.3.4 Radiation emitted from the spacecraft

In atmospheric environmental conditions, objects are cooled via convection. This heat transfer mechanism is not possible in space conditions. Instead energy has to be radiated into space. Operating spacecraft in a temperature range similar to Earth's conditions ≈ 20 °C, the radiation will be in the infrared spectrum. The IR radiation will be emitted into space from the outer surfaces of the spacecraft and possible additionally attached radiators. This is the only possibility to remove thermal energy from the system [76].

D.1.3.5 Thermal characteristics of interplanetary spaceflight

Our CubeSat model will be placed in interplanetary thermal environment, which can be much more severe than those encountered in Earth orbit. During most of the interplanetary cruise, the only environmental heating comes from the direct Sun component. Therefore, during an interplanetary cruise, a spacecraft's distance from the Sun determines the thermal environment at all times except during possible planetary flybys. If the mean solar intensity near Earth is defined as 1, then a spacecraft would be exposed to factor of 6.5 value at the mean orbit of Mercury, and only 0.0006 of Earths value at the mean orbit of Pluto

(Figure D-7). Thermal environment encounter during interplanetary mission can be expressed by concept of reference sphere. Reference sphere is an isothermal sphere with absorbance (α) and emittance (ε) of 1. Equilibrium temperature of the sphere indicates local thermal environmental at different distances from the Sun (Figure D-8).

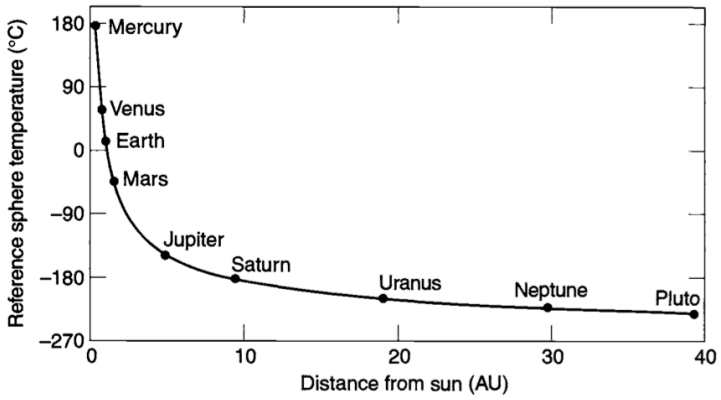

Figure D-8: Reference temperature as a function of distance from the Sun [81]

At Earth's distance, the spheres temperature is relatively comfortable at 6 °C. At the average orbital distance of Mercury, it reaches 174 °C and at Mars it falls to -47 °C. For the outer planets, temperature drops sharply: -150 °C for Jupiter, -183 °C for Saturn -209 °C for Uranus, -222 °C for Neptune and -229 °C for Pluton. During planetary flybys, planet IR and albedo loads are added to the Solar load for short periods of time. On most spacecraft, the thermal mass of the vehicle largely damps out the temperature rise of most components during flyby. Exposed lightweight components may be significantly affected. For our scenario we did not consider any flyby situation therefore solely Solar radiation was included as heat source in calculations for interplanetary environment [81].

D.1.4 Methods of Thermal control in the space environment

The main objective of thermal control is to maintain temperatures of on-board equipment and the payload samples within specific operational and survival ranges. It must also ensure that temperature gradients are not too large and maintain good temperature stability. Passive and active thermal control

techniques are used for regulating spacecraft thermal budget based on mission requirements. The thermal budget of spacecraft is influenced by external heat inputs from direct sunlight, which is the most important external heat source, Earth or planetary albedo and IR energy emitted from the surface or atmosphere of the central body (see Section D.2.3) in addition to heat generated by internal components of the spacecraft. The thermal control of spacecraft is attained by balancing the heat inputs against energy emitted by satellite or spacecraft. With interplanetary missions we expose satellite to a wide range of thermal environments usually determined by the distance between the Sun and spacecraft.

D.1.4.1 Passive and active thermal control

Passive thermal control of spacecraft is performed by balancing the heat inputs against the energy emitted by the satellite. It is a function of the optical properties of the surface materials. It can be accomplished by a variety of techniques such as: Multi – Layer Insulation (MLI), thermal coatings, Sun shields, thermal straps, louvers, radiators and heat pipes. Passive approach has significant advantages such as reliability, low mass, volume and costs, which makes it particularly suitable for CubeSat applications. Active thermal control relies on power input for operation. This sort of thermal control might be required for more efficient thermal control of missions requiring precise temperature ranges such as temperature sensitive biological payload in our simulation model. Examples of active thermal control systems include thermal straps, heaters and cryocoolers. Traditional (passive) thermal insulation could be combined with active control systems for more effective and precise thermal regulation. This is called hybrid active-passive thermal control approach and is essential for successfully enduring cold temperatures during deep space interplanetary CubeSat missions. Means of passive and active thermal control are shown in Table D-2.

PASSIVE	ACTIVE
Radiation • coating • MLI blanket • radiator **Conduction** • structural materials • doubler, filler, adhesive • washer, strap, bolt, stand-off **Latent heat & Ablation** • thermal protection system • phase change material	**Heaters** • thermostat control • electronic control • ground control **Heat pipes & fluid loops** • fixed/ variable conductance • loop heat pipe • mono/ diphasic fluid **Peltier element** **Louvres**

Table D-2: Thermal control means

D.1.5 Conclusion

The section on thermal space environment introduces different mechanisms of heat transfer which might occur in the space environment. After the initial part, different heat sources that appear in the space environment and can affect space mission whether being placed in Low Earth's orbit or beyond – in the interplanetary environment, are discussed. In the final part, methods of active and passive heat management methods are outlined.

D.2 Basics of Space Environment Thermal Modelling

D.2.1 Introduction and methodology

The concept of space environment thermal modelling is to virtually place realistic spacecraft geometry with all heat transfers in the specific space environment. Basic statements of the thermal modelling are:

- thermal models can never fully describe real conditions,
- every model building requires a certain portion of simplification and modification,
- for meaningful abstraction of reality, experience is needed,
- every simulation requires a unique approach.

D.2.2 Creating Thermal Mathematical Model (TMM)

The temperature condition of the satellite is not homogenous but varies depending on the time and location. To solve this complex task, a simplified model of the satellite is created. This model is called the Thermal Mathematical Model (TMM). The creation of the TMM is divided into two steps:

- Creation of the **Geometrical Mathematical Model (GMM)**
- Creation of the **Thermal Mathematical Model (TMM)**

The Geometrical Mathematical Model (GMM) represents a model in which an item and its surrounding are represented by radiation exchange surfaces characterised by their thermo-optical properties. The GMM generates the absorbed environmental heat fluxes and the radiative couplings between the surfaces [77].

For GMM the nodes have no properties, except their geometry, attitude and their orientation in space at given time. In order to reduce calculation time, the geometry of the nodes is simplified to basic shapes (cylinders, rectangular plates, circles…). For the simulation the nodes are assumed to be spatially isothermal. Therefore, where higher temperature gradient is expected, more precise nodding is required to obtain more realistic results.

The thermal Mathematical Model (TMM) is an extension of the GMM. In the TMM thermal aspects are added to the model. The TMM is a numerical representation of an item and its surrounding represented by concentrated thermal capacitance nodes or elements, coupled by a network made of thermal conductors (radiative, conductive and convective). Numerical representation can be performed by lumped parameter, finite difference or finite element methods [77].

Added thermal aspects of the TMM are:

- properties of the nodes,
- radiative and conductive links of the nodes,
- external received heat.

Three properties are allocated to the nodes which are relevant for the thermal analysis:

- heat capacity,
- surface opto – physical properties,
- internal heat dissipation.

The heat capacity C_p describes how much energy has to be transferred to the node to achieve certain temperature changes. It depends on the material the node is made of. For the TMM it is assumed that the whole surface of the node has a homogenous material and surface properties. The nodes are linked with each other via conductive and radiative links. Also, external heat flux coming from an external source and internally dissipated heat from electronic components has to be estimated in the calculation.

Equation D-18: Energy equilibrium equation for single node (i)

$$\underbrace{C_{p,i}\frac{dT_i}{dt}}_{\text{inner energy}} = \underbrace{\dot{Q}_{external,i}}_{\substack{\text{external}\\ \text{heat load}}} + \underbrace{\dot{Q}_i}_{\substack{\text{heat}\\ \text{dissipation}}} - \underbrace{\sigma\epsilon_i A_{space,i} T_i^4}_{\substack{\text{heat}\\ \text{radiated to}\\ \text{space}}} - \underbrace{\sum_{j=1}^{N} h_{ij}(T_i - T_j)}_{\substack{\text{conductive}\\ \text{transfer btw.nodes}}} - \underbrace{\sigma \sum_{j=1}^{N} A_i F_{ij} \epsilon_{ij}(T_i^4 - T_j^4)}_{\substack{\text{radiative transfer}\\ \text{btw.nodes}}}$$

where inner energy of a single node (i) with capacity $C_{p,i}$ and temperature T_i is combined from heat load from external sources (mainly Sun), heat dissipated

inside the node, heat radiated to outer space, and heat conducted or radiated to other node in vicinity [73].

For steady state stands: $\frac{dT_i}{dt} = 0$ and for transient state: $\frac{dT_i}{dt} \neq 0$

During the calculation process the energy equilibrium equation (Equation D-18) must be solved for every single node in a mesh of the geometry model.

There are various commercially available thermal modelling software packages on the market today. For the space sector, some of most used are: SYSTEMA/ THERMICA developed by the Airbus company, Thermal Desktop from the US company C&R Technologies and ESATAN - TMS by ITP Aero. Selection of a modelling software for the present research work was made on the basis of past work experiences with the software, heritage as being main thermal modelling software for ESA missions and financial availability, in terms of a free licence grant for a limited period of time. The thermal simulation work was performed using the ESATAN – TMS software.

Apendix E: Creation of a TMM in ESATAN-TMS

E.1 Thermal modelling with the ESATAN – TMS platform

E.1.1 Introduction and methodology

In following section the Thermal Analysis Network Software – the Thermal Modelling Suite (ESATAN - TMS), which was used for thermal simulation work performed in this research is presented. The software selection process was briefly described at the end of the previous section.

The ESATAN - TMS is a powerful and flexible software product supporting the complete thermal analysis process. The heritage of the software is from the Space Industry, where ESATAN - TMS is used over 25 years including designing European Space Agency (ESA) missions [78].

E.1.2 Creating model in ESATAN - TMS

It presents a complete environment for thermal analysis. The Graphical User Interface (GUI) provides an intuitive and simple to use environment, providing extensive 3D model building and pre- and post- processing capabilities (Figure E-1).

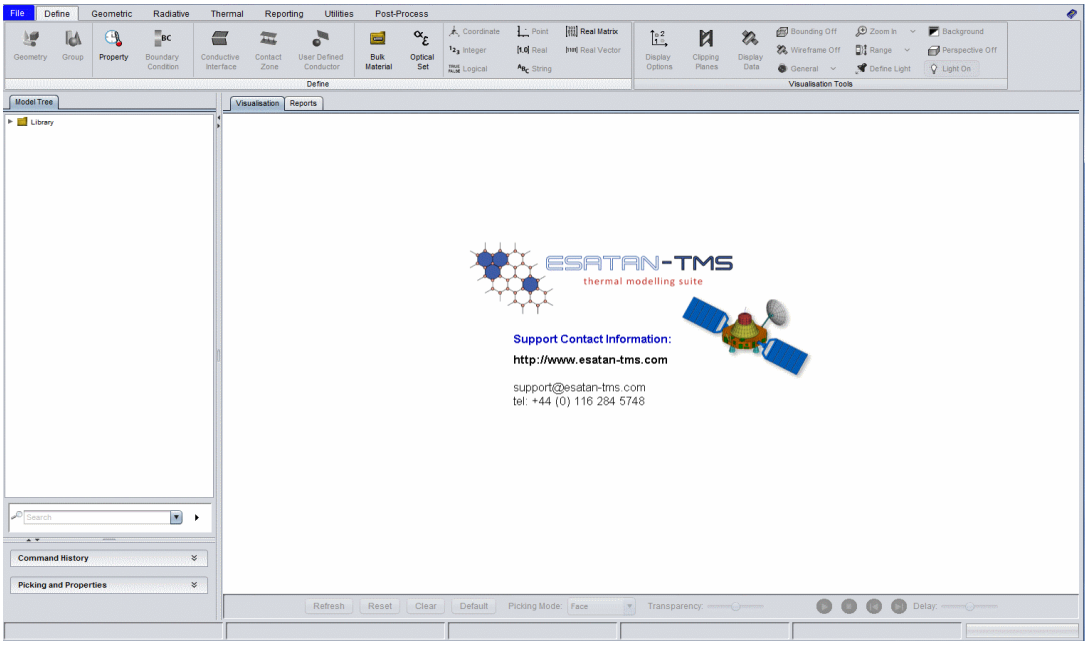

Figure E-1: The ESATAN - TMS Workbench window [79]

There are three main modules which are used for complete analysis:

- Building the **geometric** model of object,
- Calculating models' **radiative** characteristics,
- Defining and creating the **thermal** model.

Two further models enable us to produce reports and run data analysis.

The interaction is via menus, dialogs and buttons. Detailed knowledge of program language on which the platform is based on is not required. The main steps in the modelling process are:

- Generating geometry model,
- Define and run the radiative case (orbit and radiative analysis),
- Validate the results using visualisation and reporting,
- Define and run the analysis case (thermal model and thermal solution),
- Validate the thermal results using visualization [79].

Every model is built with special ribbon bars and drop down menus.

E.1.2.1 Defining Geometry

The initial step of modelling work was to define the geometry of the model in Workbench. Main stages in creating a model are in following sequence (Figure E-2):

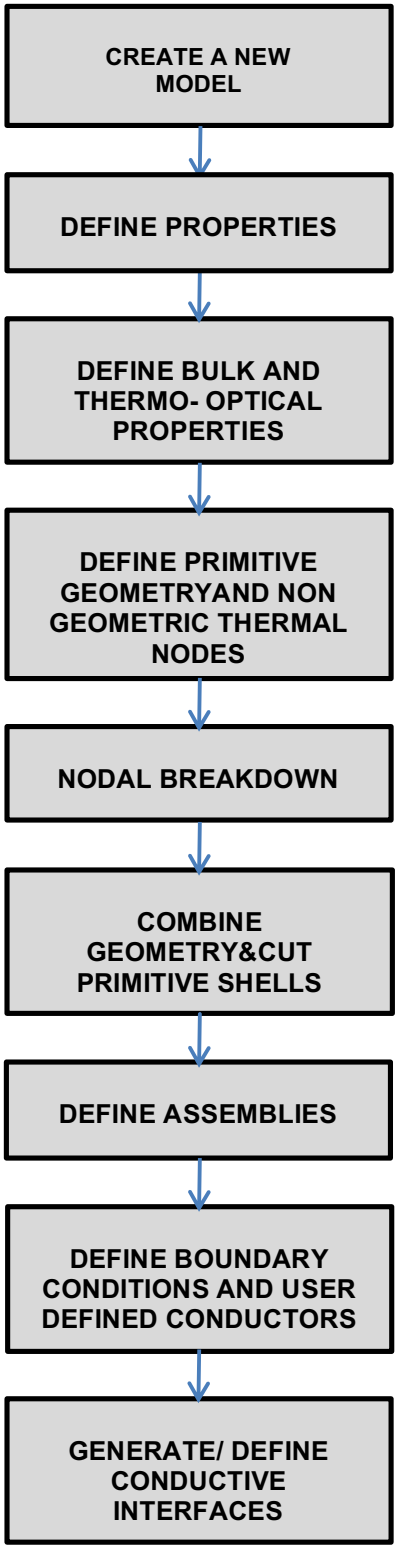

Figure E-2: Geometric modelling process in ESATAN - TMS [75]

More important actions of geometric modelling processes are described more in detail.

- **Defining the bulk and thermo - optical properties of materials**

For every material used in the simulation it is necessary to define and sign material characteristics (density - ρ, thermal conductivity – k and specific heat – c_p) and also thermo – optical properties which are of great importance in space thermal control (Infrared emissivity - ε_{IR} and Solar absorptivity – α_S) (Figure E-3,). Values are to be found in specific tables [80], [81] and are for materials used in thesis research work summoned in Appendix A.

On the basis of inputs, values for infrared and solar reflectivity are calculated automatically in a way that the sum of four coefficients for both the Infrared and Solar wave band equals to 1 (Infrared Emissivity + Infrared Specular Reflectivity = 1 and Solar Absorptivity + Solar Specular Reflectivity = 1).

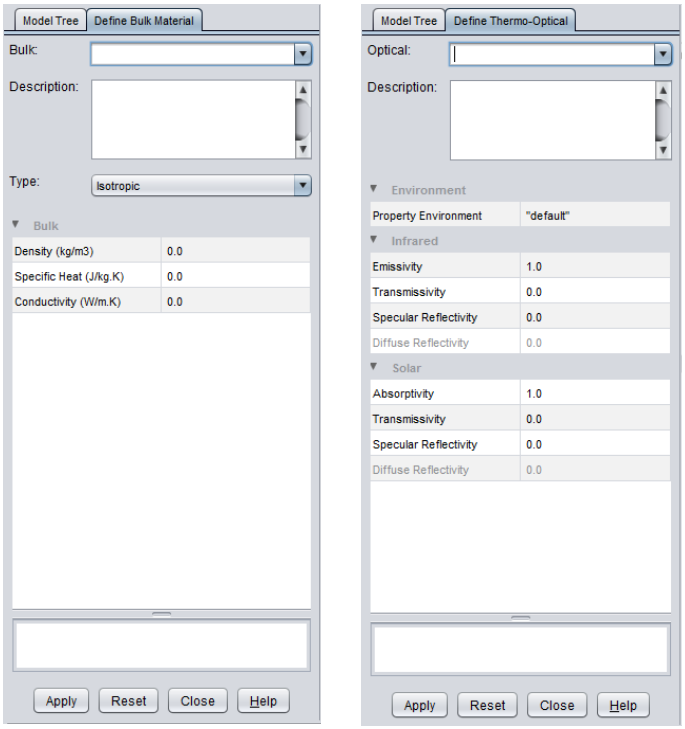

Figure E-3: Windows for defining bulk and thermo – optical properties of the material (ESATAN - TMS)

- **Defining a geometry and non-geometric thermal nods**

Geometry models are constructed from shells or solids. The simplest form of a shell or a solid is a primitive shell or primitive solid. They can be of different types and are defined with respect to a right-handed Cartesian coordinate system.

There are various methods of defining geometry, by: parameters, points, directions and can vary for shells and solids. Primitive geometry can be assembled, combined or cut, to produce more complex geometric model, as well as removed or changed later.

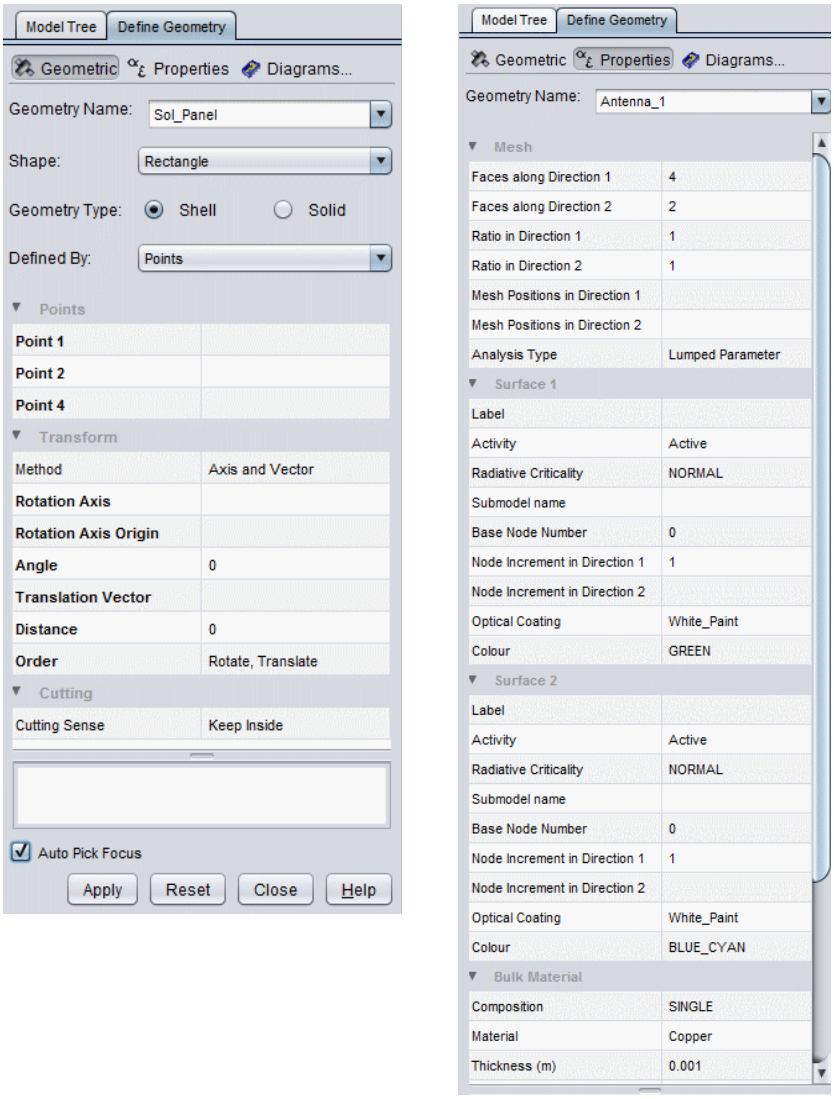

Figure E-4: Geometry and properties defining (ESATAN - TMS)

Designing geometry, properties (Figure E-4) for each surface of the geometry needs to be specified. Within properties activity of the surfaces are defined, node separation and numbering, material composition, thickness and optical coating. With defining activity of the shell (active, radiative, conductive or inactive) its indicates whether it plays a role in radiative and/ or conductive analysis of a model. An active surface is used for radiative and conductive calculations, whilst radiative surface is used only for radiative and conductive surface only for conductive calculations. Inactive surfaces do not take part in any calculations. Activity of surface is also set up in Property Tab (Figure E-4)

In completing these steps geometry and characteristics of the materials and surfaces which are used for creating the model are defined (Figure E-5).

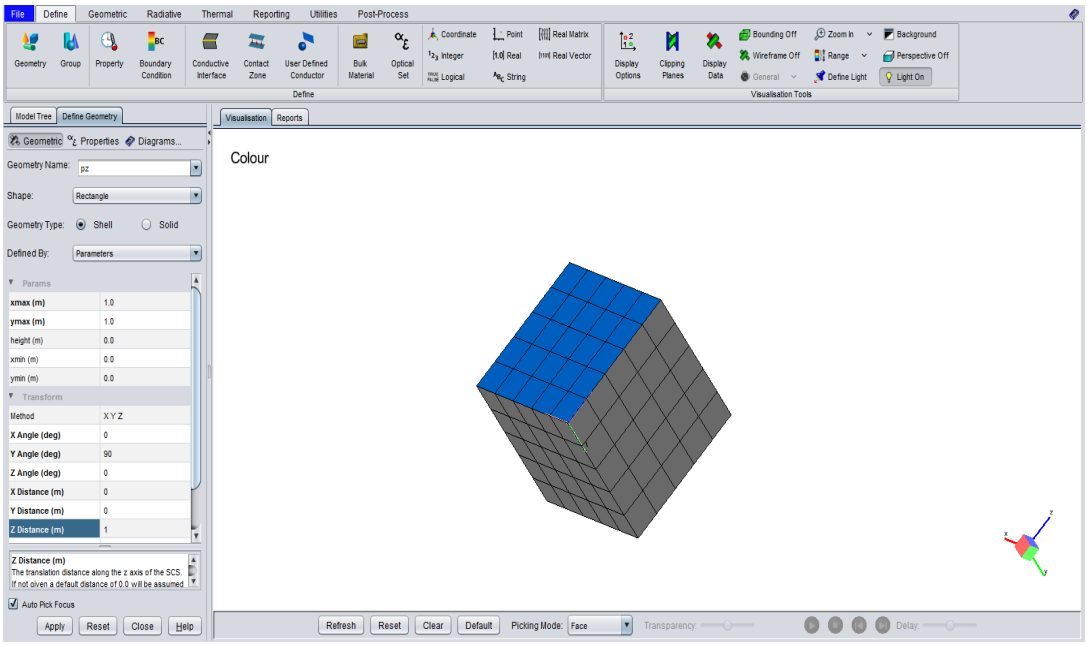

Figure E-5: Building a model by designing shells with parameters (ESATAN - TMS)

There may be occasion, where parts of the model do not need to be defined geometrically, but still need to be accounted for in the thermal model. It is a modelling technique which simplifies the behaviour of the component and represents it as a single thermal node in the thermal model. In this way a non – geometric thermal node is defined. With this feature electrical units inside the main body of the model, for example, can be modelled. Non – geometric

thermal nodes can be represented as a sphere in the visual model of the geometry, for easier visualisation.

- **Geometry nodal breakdown and creating a mesh**

Different parts of geometry or surfaces can be exposed to different environmental or physical effects. For example, one part of the surface may be in the shade, while the rest of it is in direct sunlight. The process of division geometry or surface is known as meshing. Each surface of a geometry can be divided into faces along each of its parametric directions, distributed uniformly or non-uniformly it mainly depends on conditional changes expected in dimension.

If bigger variation in output values is expected, due to uneven geometry or different environmental effects meshing should be more precise (Figure E-6).

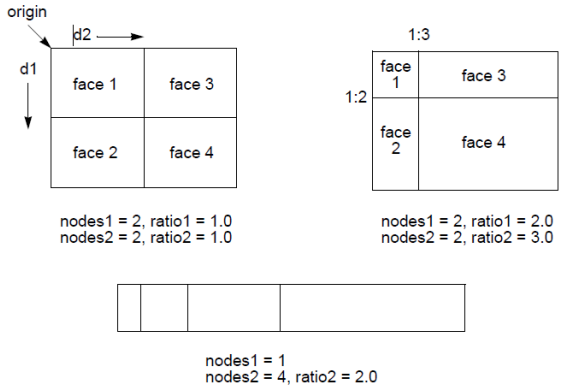

Figure E-6: Uniform and non-uniform face distribution [82]

Each node and face is assigned a unique name, derived from node and face numbers. Node numbering must be done carefully not to repeat the numbers already assigned. An example of node numbering can be seen in our geometry model (Figure E-7).

Details of Thermal modelling were explained previously, in Appendix D.

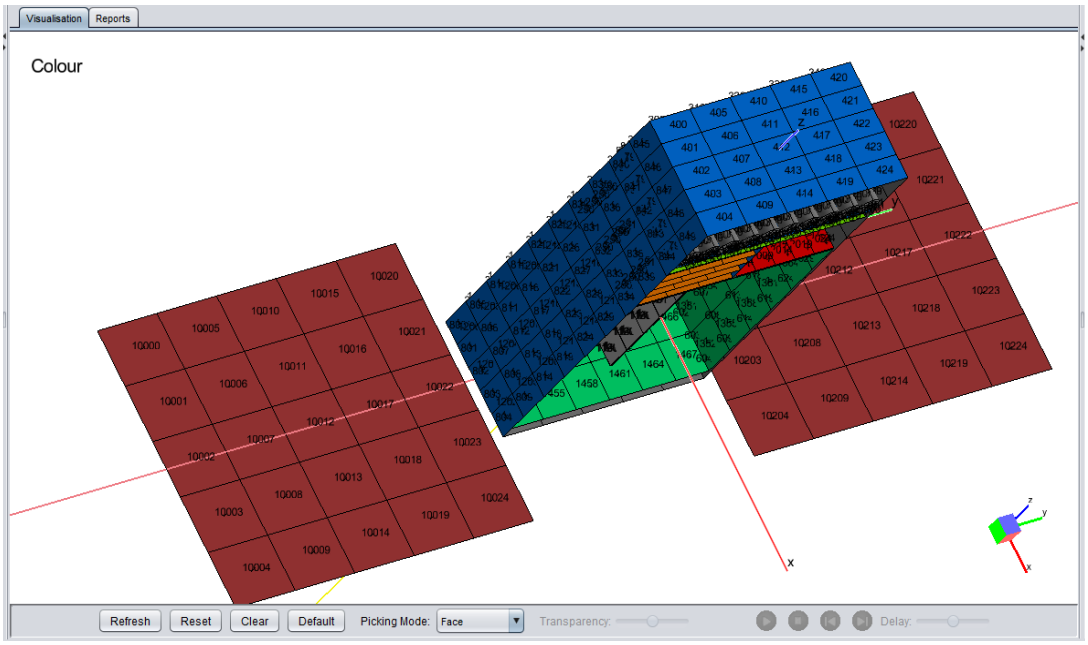

Figure E-7: Geometric model with visible node distribution and numbering (ESATAN - TMS)

- **Combining geometry**

A number of unconnected geometry which were created, must be put together, to create a model. A model should be designed hierarchally, so that it breaks down into meaningful components – a model tree. This is especially useful for pre and post processing. In Figure E-8 an example of the model hierarchy for CubeSat model, developed during thesis research, can be seen.

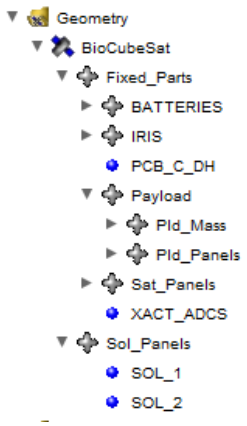

Figure E-8: CubeSat model tree which can be broken down further into components and subcomponents (ESATAN - TMS)

Combining geometry should be done with meaning – firstly to separate moving and fix parts, and fix parts later further fragment down to satellite body, payload section, avionics section, battery section...

Good combining of geometry components gives more overview transparency of the model and helps with navigating and understanding of the included components and subcomponents.

- **Model assemblies**

In assembling a model, fix – reference components and moving components are defined. With this procedure, the relationship is set which includes relative motion between model components. The two components are known as the reference body and the moving body.

In the thesis research model, the reference body is a 6U CubeSat and moving bodies are two solar panels. With the rotation axis of the moving component is specified around which axis geometry is moving – rotating (Y - axis in designed model) and with a pointing vector is defined where the moving parts should be oriented (- Z in model) Figures E-9, E-10.

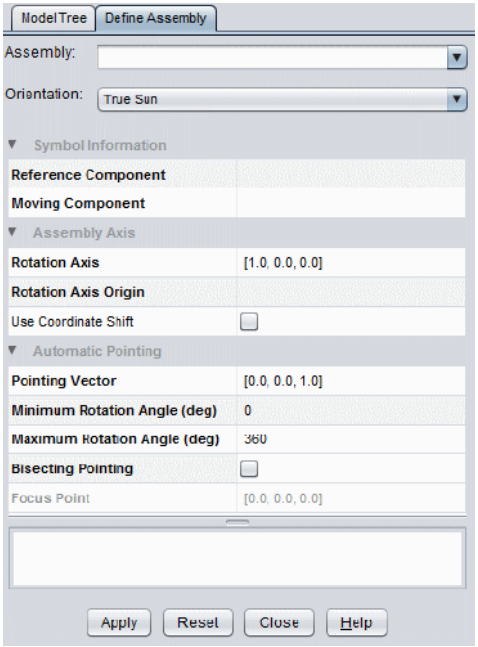

Figure E-9: Define Assembly dialog box (ESATAN - TMS)

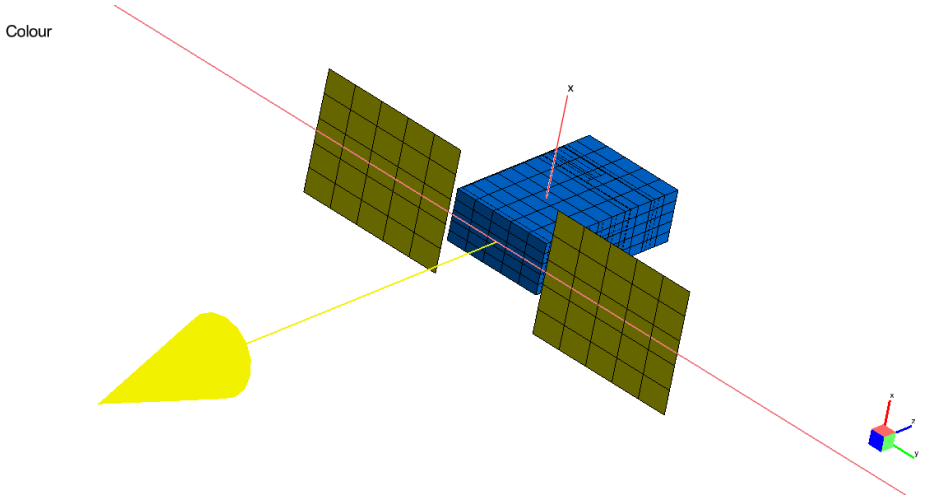

Figure E-10: Assembled model (ESATAN - TMS)

- **Define boundary conditions and user defined conductors**

In a Workbench specified boundary conditions (Figure E-11), are assigned to the Radiative case (directed UV emissions) or more often to the Analysis case (temperature and heat load boundary conditions). Heat load boundary conditions can be thermostatically controlled.

With boundary conditions any additional power can be simulated- heat loads which appear inside the model.

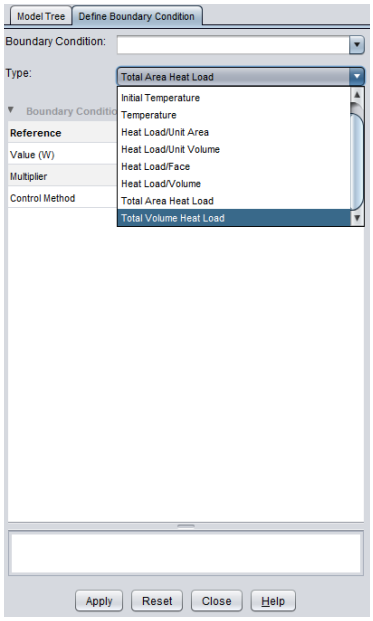

Figure E-11: Boundary condition dialog box (ESATAN - TMS)

The Control method of the Boundary condition can be set to always on, for the heat load to be applied throughout the analysis, or thermostat mode, for the heat load to be thermostatically controlled.

When thermal conductance exists between geometry parts and components or between components, it can be specified as user defined conductance. The type of user defined conductor can be either: conductive, convective or radiative. Source reference and destination reference can be node, surface, face or group of them (Figure E-12).

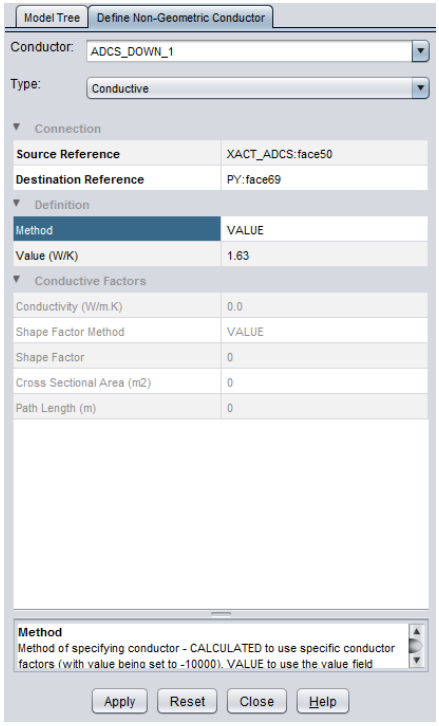

Figure E-12: User defined conductor dialogue box (ESATAN - TMS)

For user defined conductors conductance is manually calculated and set in the dialog box as a Value. Conductive type of conductance are usually used (Figure E-12).

- **Conductive Interfaces**

The last stage of defining the geometric elements of the model is to define connections where shells or solids make contact with each other. These connections are known as conductive interfaces and are used by the thermal analysis process to generate conductive couplings between shells.

Conductive interfaces can be defined individually or software can search them out and define automatically [79].

Each Conductive interface has a connection type – which specifies the kind of connection that exists between the two geometry. There are five possible values for the connection type: Fused, Contact, Not Connected, Not Required and Not Processed.

A satellite body and payload container model was used in creating a Fused type of contact, which indicates, that two geometry form a single continuous surface, for which the thermal resistance across the interface is taken to be zero. Fused contacts are presented with yellow colour (Figure E-13).

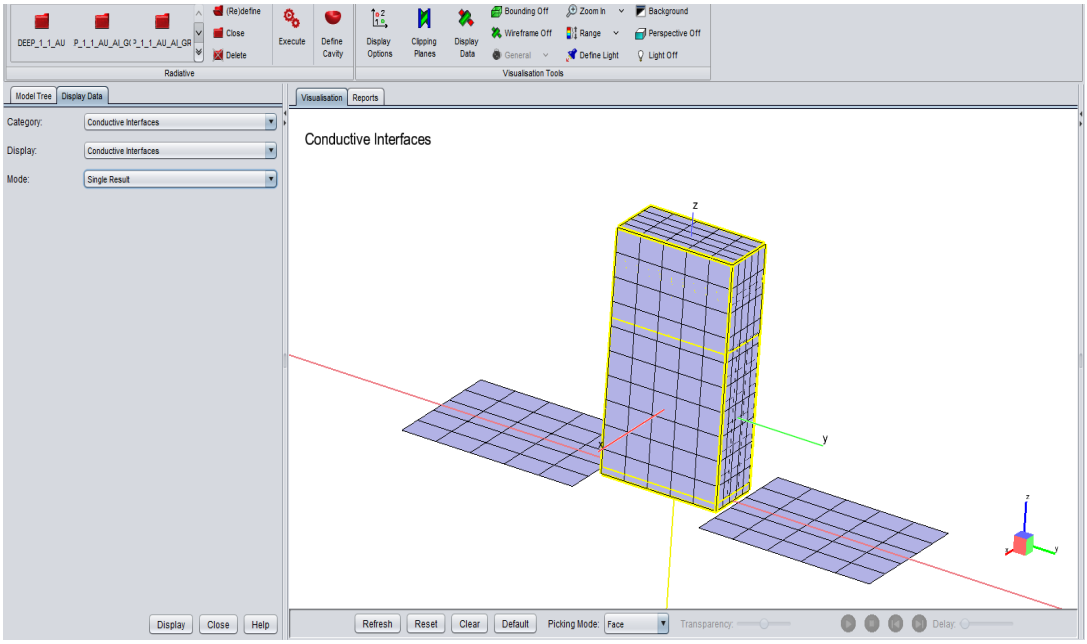

Figure E-13: Fused geometry shells (ESATAN - TMS)

After creating the model, the Visualisation module can be used, with its tools to inspect and verify attributes of the created module. This enables one to visually verify, that geometry is as specified, and calculations performed are as expected [82].

D.1.2.2 Running the radiative case

When the geometry of the model is being defined, the Radiative module of ESATAN - TMS software can be used to define orbit parameters and to run radiative calculations.

The Radiative module provides the facilities for the calculation of the radiative couplings between the faces of the model and external heat fluxes onto the faces of the model. Calculated are:

- **view factors (VFs)**: the fraction of the energy diffusely emitted by face i that is directly incident on face j. View factor are determined by the model geometry and are independent of thermo-optical properties.
- **radiative exchange factors (REFs):** is a radiative exchange factor between faces i and j and is defined as a fraction of the energy diffusely emitted by i that is absorbed by face j. The calculation takes into account not only the geometry but also the thermo-optical properties associated with models faces.
- **direct heat fluxes:** it accounts only for the radiation which is directly incident on the faces of the model, no reflections are considered. Calculations depend only on the model geometry and its relative position and orientation with respect to the heat flux source. Four different types of direct heat fluxes are calculated: solar, albedo, planet heat fluxes which are related to the Sun or planet and emission of heat flux.
- **absorbed heat flux:** account for the radiation which is eventually absorbed on the faces of the model, directly or via reflections or transmission. The calculation of absorbed heat flux depends on the model geometry, relative position and orientation with respect to the heat flux source and thermo-optical properties associated with the models faces.

Each radiative case relates to a single radiative analysis for a single spacecraft with a single behaviour defined in a single orbit. Any changes to the geometry, its behaviour, the orbit or the analysis run require an additional Radiative case to be executed [9], [82].

The calculation of view factors, direct heat fluxes and Radiative exchange factors is performed by the Monte Carlo ray tracing method. In principle, this method calculates radiative couplings and heat fluxes by means of a ray-tracing procedure which considers the individual history of the thermal radiation energy pockets, from the point of emission to the point of absorption. In reality, these energy packets may follow an infinite number of paths. They can be emitted from any point on every radiative face in any direction and may reach and be reflected by any other radiative face in model. Since it is not possible to follow the path of an infinite number of rays, an estimate of the radiative couplings of heat fluxes can be made by averaging the results obtained from a firing finite random sample of rays [82].

In the Radiative Case Dialog box general information is initially defined - under the Overview menu. Within three additional drop down menus Environmental conditions are defined, Orbit conditions and Pointing of the geometry model (Figure E-14).

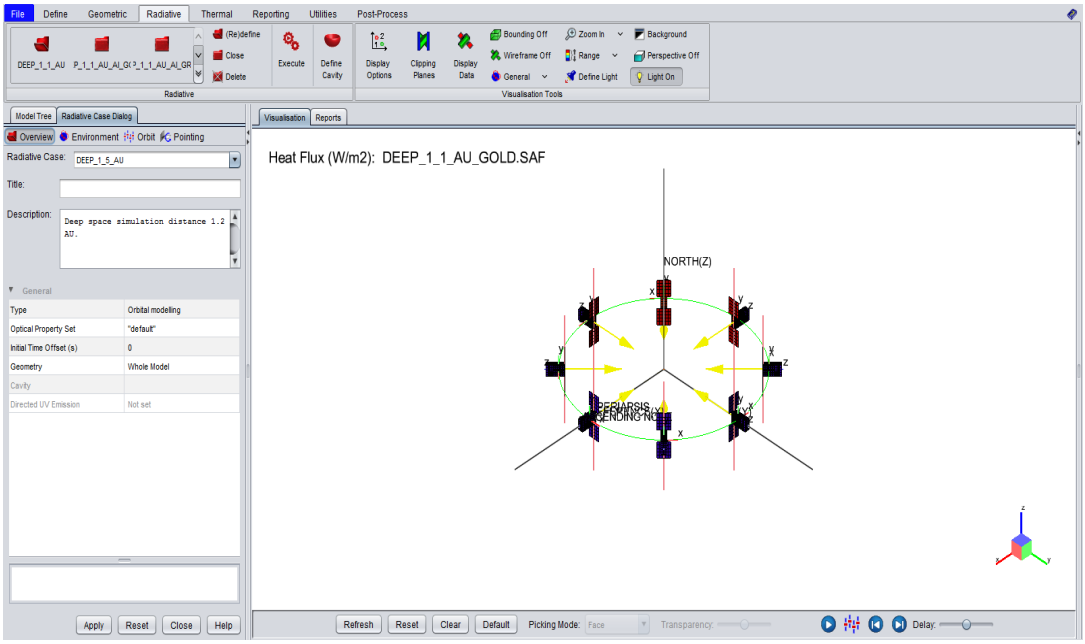

Figure E-14: Radiative Case Dialog box (ESATAN - TMS)

Inside the Environment Menu the celestial body is defined around which the simulated geometry will be placed into orbit. For satellites around Earth, the

Earth is chosen in this place. For interplanetary missions, the Celestial body: Sun must be selected. As an ICS system is also selected Sun (Figure E-15).

In the windows below basic information regarding the selected celestial body are presented (orbital parameters, Sun specifications, planet albedo and others).

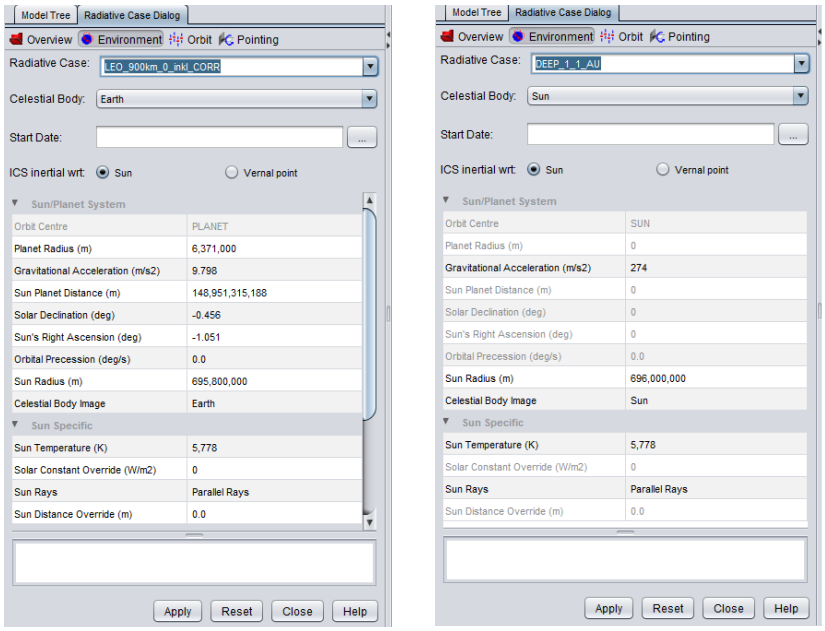

Figure E-15: Environmental window for LEO and Interplanetary Radiative case ESATAN - TMS)

In the case of Interplanetary mission simulations performed within this research work, the celestial body the Sun was selected. In the Orbit menu (Figure E-16), the geometry model is placed and oriented at specific orbit around the chosen celestial body. Earth's orbital parameters are defined as: Altitude of apogee, altitude of perigee, Inclination of the orbit, Right Ascension and others.

For interplanetary mission simulations the following need to be defined, among others: radius of aphelion, perihelion and inclination, which is zero is object is placed in planetary plane.

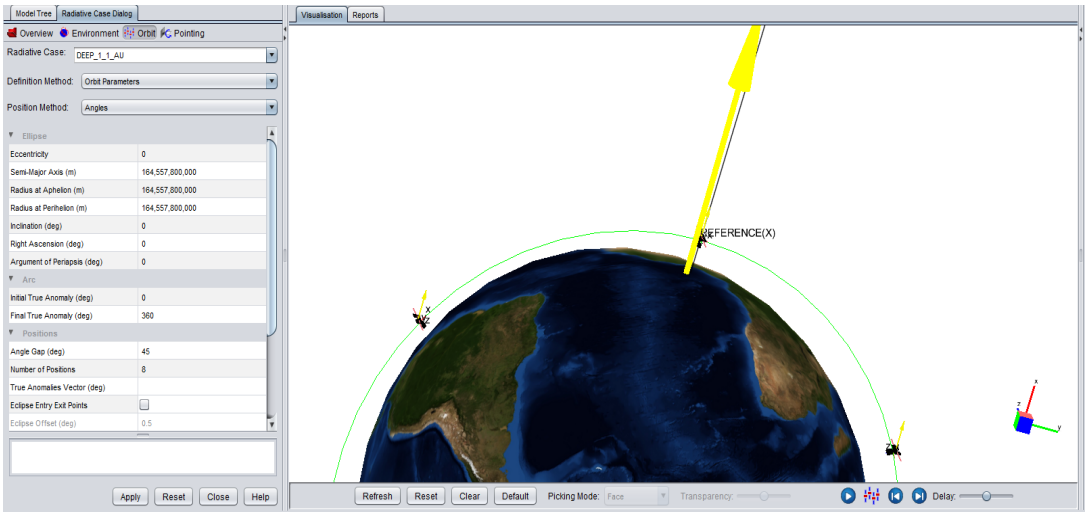

Figure E-16: Determining Orbital parameters for Earth Orbit model (ESATAN-TMS)

In the final dialog window, Pointing directions (Figure E-17) of the model are defined with Pointing Method. A spacecraft position is defined with respect to the Model Coordinate System (MCS) and must then be oriented with respect to the Inertial Coordinate System (ICS). The Primary pointing option is used to define the orientation of Solar panels, which should face the Sun at all times. The Secondary pointing is used to define the orientation of the spacecraft.

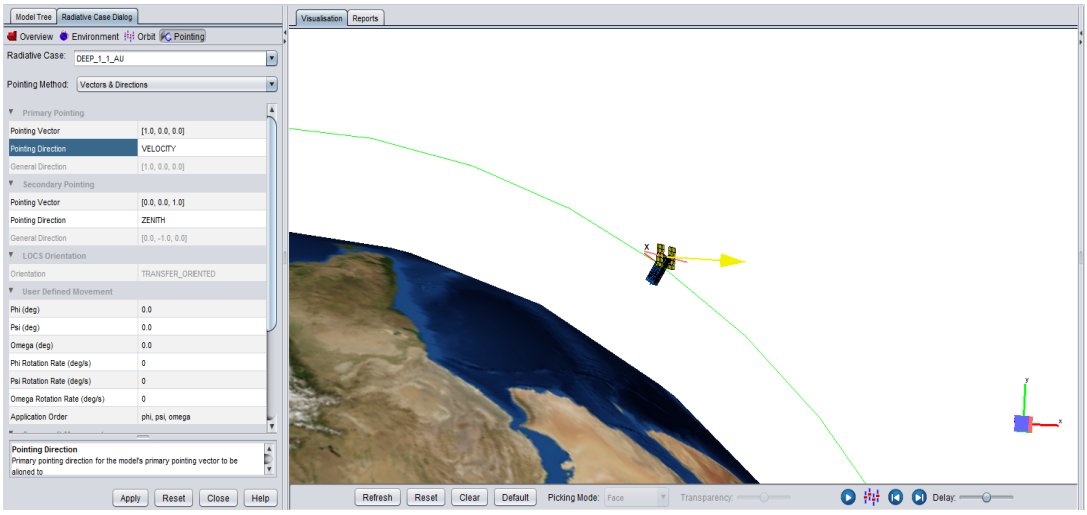

Figure E-17: Defining Pointing of the spacecraft (ESATAN - TMS)

Up to now the celestial body environment was selected, the model was placed in orbit around that body with specific orientation towards it.

Further on, Radiative results in the form of view factors, exchange factors and different heat fluxes can be calculated. For calculations standard default settings can be used for a fixed number of rays per face, for accuracy control and for ray density.

Checking Radiative results is done by visualisation and by reporting (Figure E-18).

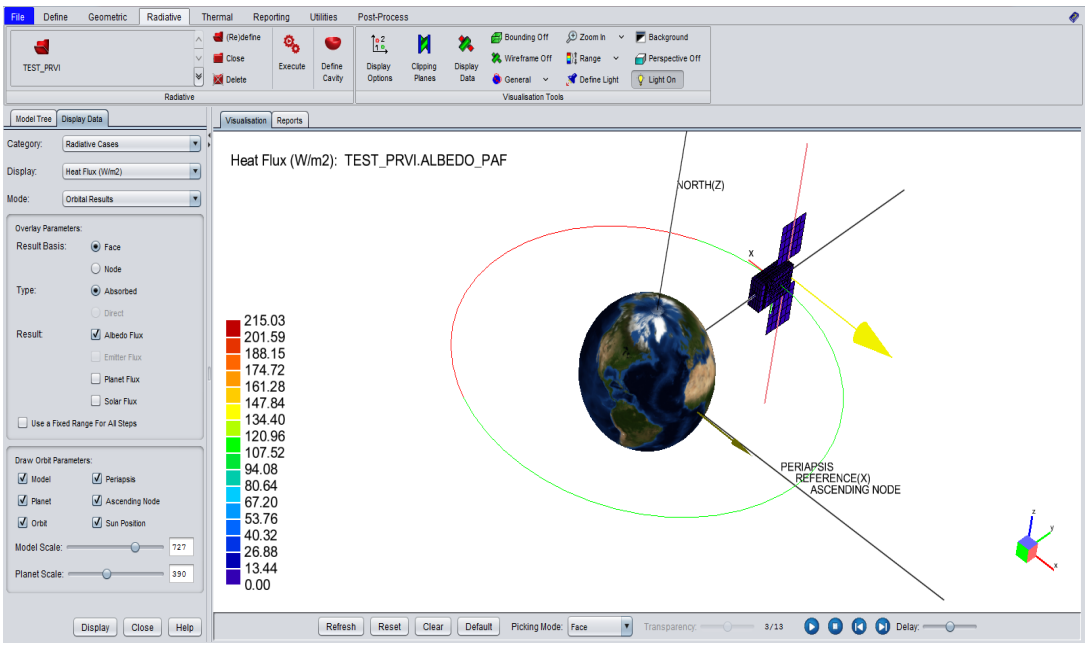

Figure E-18: Radiative results in heat flux (W/m^2) values for CubeSat in LEO (ESATAN - TMS)

The geometry model can be displayed using the Visualisation window, with faces being coloured according to the value of the resulted variable, which can be selected as a single, orbital or averaged result. Different variables such as: Heat flux, heat power, Radiative exchange factor (REF) and others can also be displayed.

Having obtained Radiative results, finally Thermal Analysis can be executed.

D.1.2.3 Thermal Analysis

When radiative results are calculated and verified, the thermal model can be run. Using the Thermal Module, ESATAN - TMS Workbench to calculate conductive couplings, and output, a thermal model in terms of a thermal

network of nodes, conductance and materials, ready to input to a thermal analyser [79].

The Define Analysis Case dialog enables us to specify all the data required to build and run thermal analysis.

Initially there is a need to select already processed Radiative case which will be used for performing Thermal analysis. A further step is to define conductors/ user defined conductors to be included in calculation, as well as selecting a set of initial and boundary conditions (Figure E-19).

An important step is also selecting a solution routine, which is to be performed. One can select between steady-state solution which is based on the averaged orbital conditions and transient analysis, which is performed over a number of orbits to achieve a cyclically repeating results – the temperature repeats within a given margin between one orbit and the next.

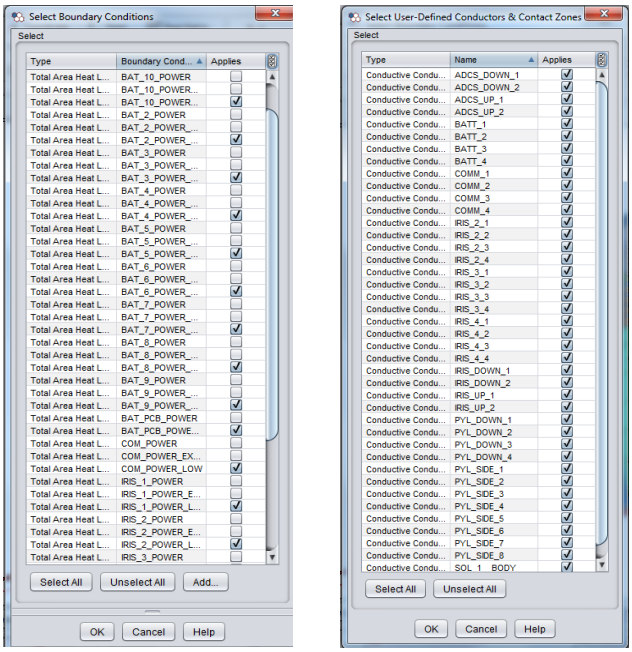

Figure E-19: Selecting Boundary Conditions and User defined conductors in Analysis Case definition (ESATAN - TMS)

Using the Advanced option settings, Heat Flux is selected, which is included in calculations. For Earth Orbit simulations, where as a Celestial body the Earth is selected (defined in Radiative case) Heat Flux is generated from: Solar flux, Planet, and Albedo (abbreviations S, P, A). The setting for HF Output Format must therefore be: S+P+A.

For performing simulations in interplanetary space, just the Solar flux (S) value should be included in the calculation.

After finishing the Analysis Case, obtained results can be presented in the Graphical interface where the Attribute Charts are plotted (Figure E-20), or temperature data is further exported to another software platform for additional analysis.

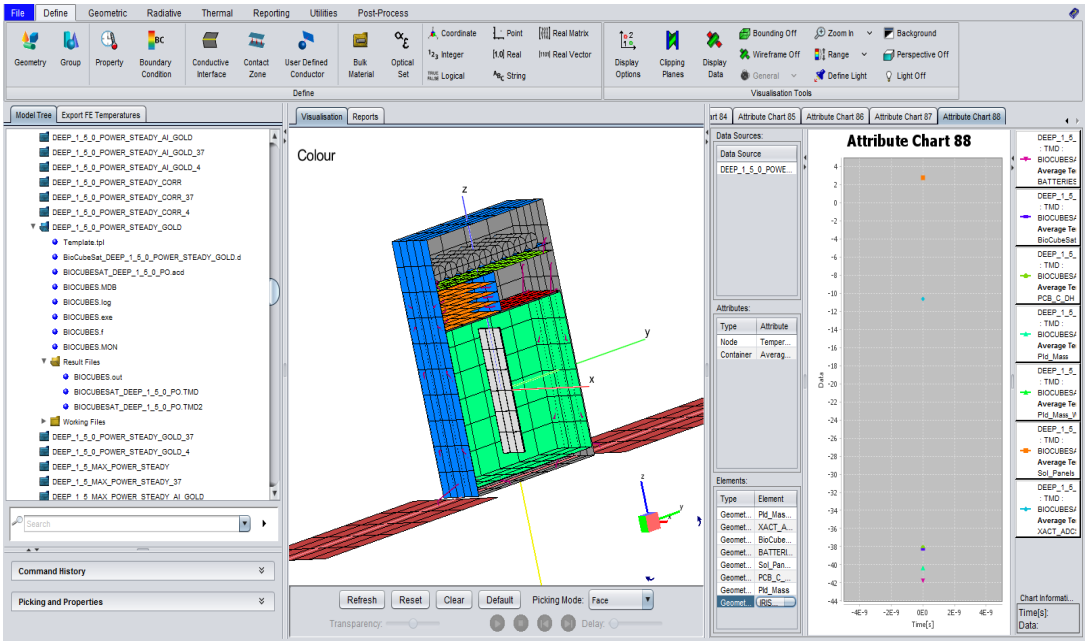

Figure E-20: Finished Analysis case with Steady state result presentation (ESATAN - TMS)

E.1.2.4 Conclusion

Presented are basic steps of designing a model in the ESATAN - TMS package. Starting with designing a model geometry, setting proper boundary conditions and conductance between components. Basic geometry designing is followed using Radiative Case Analysis, where the model is placed in orbit with parameters and orientation, around the selected celestial body. The final Thermal results are calculated and presented in the Thermal Analysis Case.

For further detailed information, is recommended to study tutorial material supplied with ESATAN - TMS software [78], [79], [82].

Appendix F: Calculation of Thermal properties of dual composite material

Basic equations:

- mass fraction from volume fraction;

Equation F-1: Mass fraction

$$\mathbf{x_{m,1}} = \frac{\mathbf{x_{V,1}} \cdot \boldsymbol{\rho_1}}{(\mathbf{x_{V,1}} \cdot \boldsymbol{\rho_1}) + (\mathbf{x_{V,2}} \cdot \boldsymbol{\rho_2})}$$

- volume fraction from mass fraction;

Equation F-2: Volume fraction

$$\boldsymbol{x_{V,1}} = \frac{\boldsymbol{\rho_2}}{\boldsymbol{\rho_{1 \cdot \left(\frac{1}{x_{m,1}} - 1\right) + \rho_2}}}$$

Equation F-3: Density of composite material

$$\boldsymbol{\rho_{dual}} = \boldsymbol{x_{V,1}} \cdot \boldsymbol{\rho_1} + \boldsymbol{x_{V,2}} \cdot \boldsymbol{\rho_2}$$

Equation F-4: Specific heat composite material

$$\boldsymbol{c_{p,dual}} = \boldsymbol{x_{V,1}} \cdot \boldsymbol{c_{p,1}} + \boldsymbol{x_{V,2}} \cdot \boldsymbol{c_{p,2}}$$

Equation F-5: Thermal conductivity of composite material

$$\boldsymbol{k_{dual}} = \boldsymbol{x_{m,1}} \cdot \boldsymbol{k_1} + \boldsymbol{x_{m,2}} \cdot \boldsymbol{k_2}$$

- **ADCS unit**

ESATAN – TMS uses simplified geometry model capabilities, therefore dual materials with different thermal properties need to be combined into single composite material.

Thermal properties calculations were performed on the example of Attitude Determination Control System (ADCS) unit.

The ADCS unit (total 0.7 kg) was modelled as a dual layer shell, the first layer was an electronic board composed of FR4 board and copper (0.1 kg) and the second layer of the reaction wheels and module housing (0.6 kg).

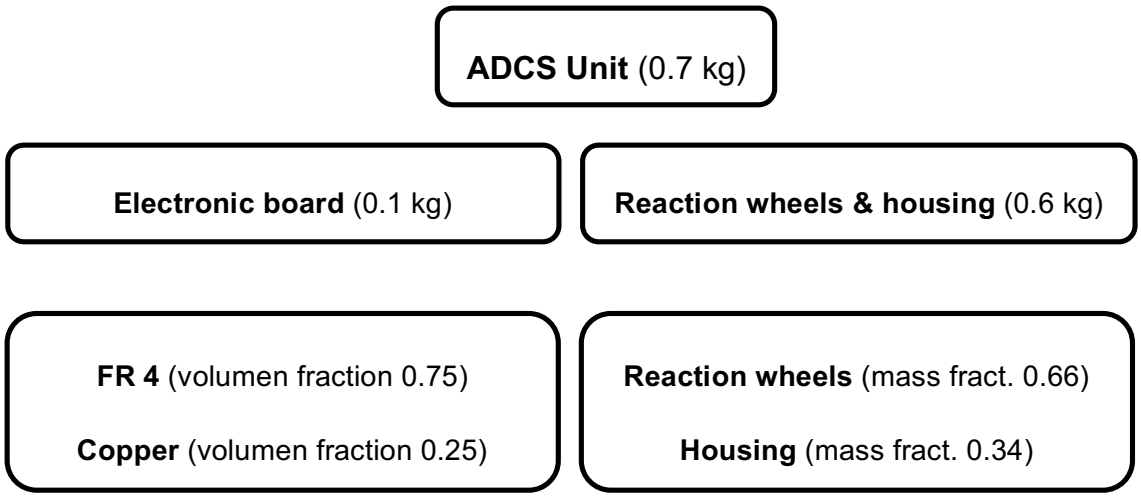

1. **Calculating Thermal properties of Electronic board (PCB)**

Base of the electronic board is made from FR4 and electrical wiring – copper.

Calculating mass fraction (x_m) of copper (Cu) from volume fraction (X_V):

$$x_{m,Cu} = \frac{x_{V,Cu} \cdot \rho_{Cu}}{(x_{V,Cu} \cdot \rho_{Cu}) + (x_{V,FR4} \cdot \rho_{FR4})} = 0.61$$

$$x_{m,FR4} = 0.39$$

Mass fraction of copper is $X_{m,Cu}$ = 0.61 and FR4 board $X_{m,FR4}$ = 0.39.

Knowing the values for volume and mass fractions of components, the thermal properties of the electronic board (PCB) can be calculated as:

Density: $\rho_{PCB} = x_{V,Cu} \cdot \rho_{Cu} + x_{V,FR4} \cdot \rho_{FR4}$

Specific heat: $c_{p,PCB} = x_{V,Cu} \cdot c_{p,Cu} + x_{V,FR4} \cdot c_{p,FR4}$

Thermal conductivity: $k_{PCB} = x_{m,Cu} \cdot k_{Cu} + x_{m,FR4} \cdot k_{FR4}$

As seen in the equations above, density and specific heat are functions of volume fraction while thermal conductivity is a function of mass fraction.

2. Calculating of Thermal properties for reaction wheels and housing

Steel reaction wheels - 0.4 kg and Aluminium housing - 0.2 kg, combined weight 0,6 kg. Therefore mass fractions are: $X_{m,wheels}$ = 0.66 and $X_{m,housing}$ = 0.34. Volume fractions for both components are calculated as:

$$x_{V,wheels} = \frac{\rho_{housing}}{\rho_{wheels}\cdot\left(\frac{1}{x_{m,wheels}}-1\right)+\rho_{housing}} = 0.40$$

$$x_{V,housing} = 0.60$$

The same as in the first example of the electronic board, also the properties for the composite of the reaction wheels and component housing was calculated.

Density: $\rho_{wheels+housing} = x_{V,wheels} \cdot \rho_{wheels} + x_{V,housing} \cdot \rho_{housing}$

Specific heat: $c_{p,wheels+housing} = x_{V,wheels} \cdot c_{p,wheels} + x_{V,housing} \cdot c_{p,housing}$

Thermal conductivity: $k_{wheels+housing} = x_{m,wheels} \cdot k_{wheels} + x_{m,housing} \cdot k_{housing}$

Results of the calculations are presented in Appendix A Table.

Having calculated the thermo-physical properties of composites and knowing the mass, the thickness of both shells for the ESATAN – TMS geometry model can be calculated.

Optical properties for the layer with reaction wheels and Aluminium housing is selected black anodised Aluminium, while for bottom PCB plate, FR4 (Appendix A).

- **Transponder Communication unit**

Basic input data, available for modelling, specifies that the IRIS Transponder Communication unit has a volume of 0.5U and total mass of 1.2 kg. The unit has sliced architecture with 4 PCB boards, two side plates and the top plate. 4 PCB slices have a weight of 0.8 kg and the rest of the 0.4kg is evenly spread between side panels (2 x 0.133 kg) and the top plate (0.133 kg).

Each PCB slice weighed 0.2 kg and was modelled as a dual material of 0.2 mass fraction of epoxy FR4 board and 0.8 mass fraction of a combination of copper and silicon. Furthermore, the copper and silicon layer consists of 0.7 silicon and 0.3 of copper volume fraction.

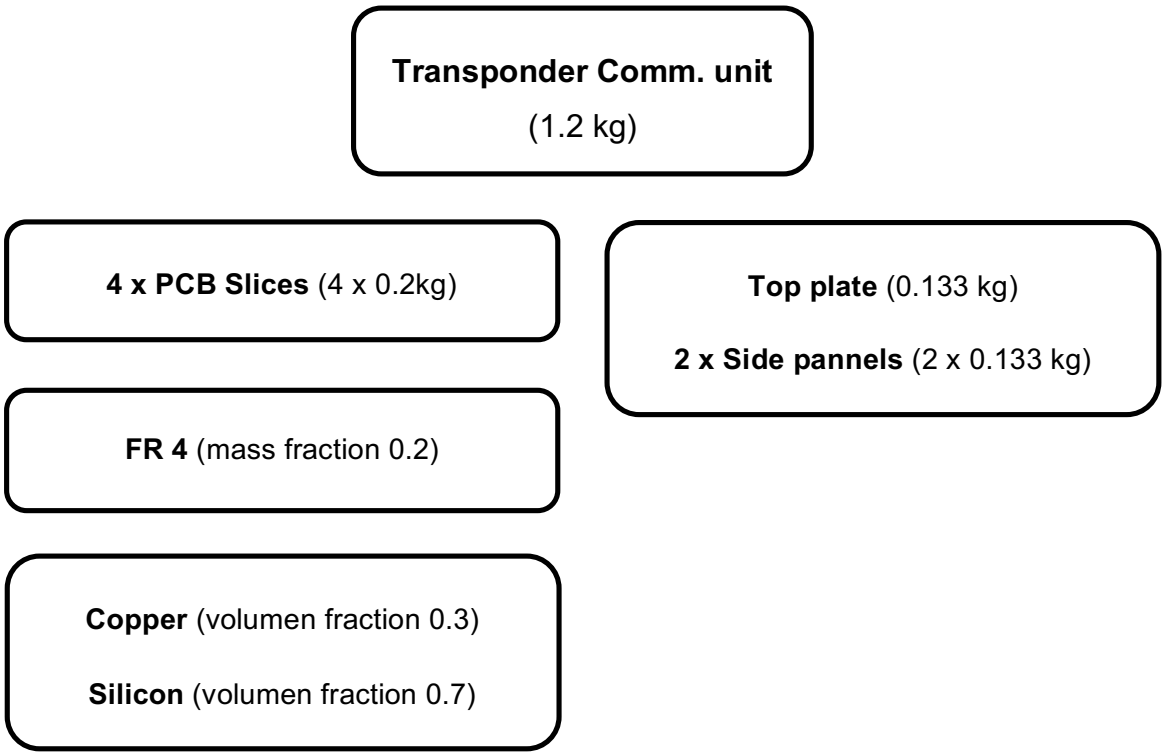

Calculating mass fraction for copper ($Xm_{,Cu}$):

$$x_{m,Cu} = \frac{x_{V,Cu} \cdot \rho_{Cu}}{(x_{V,Cu} \cdot \rho_{Cu}) + (x_{V,Si} \cdot \rho_{Si})} = 0.61$$

$$x_{m,Cu} = 0.61$$

$$x_{m,Si} = 0.39$$

Calculated thermo-physical properties for copper/ silicon composite material:

Density: $\rho_{Cu/Si} = x_{V,Cu} \cdot \rho_{Cu} + x_{V,Si} \cdot \rho_{Si}$

Specific heat: $c_{p,Cu/Si} = x_{V,Cu} \cdot c_{p,Cu} + x_{V,Si} \cdot c_{p,Si}$

Thermal conductivity: $k_{Cu/Si} = x_{m,Cu} \cdot k_{Cu} + x_{m,Si} \cdot k_{Si}$

Calculated values are specified in Appendix 1.

From calculating thermo-physical properties and knowing mass and dimensions, thickness of each layer to be put in ESATAN – TMS software can be determined. For PCB plate were calculate thicknesses of 2.1 mm for FR4 base and 3.7 mm for upper layer made from copper and silicon.

- **Thruster**

Regarding the specifications, MiPS VACCO the propulsion system has a total mass of 509 g, where fuel weight 53 g and housing remaining 456 g. On the basis that this specified mass fraction of fuel is $x_{m,fuel} = 0.1$ and housing $x_{m,housing} = 0.9$, volume fractions are calculated as:

$$x_{V,isobutane} = \frac{\rho_{housing}}{\rho_{isobutane} \cdot \left(\frac{1}{x_{m,isobutane}} - 1\right) + \rho_{housing}} = 0.33$$

$$x_{V,housing} = 0.67$$

Calculated values thermo-physical values for combination of Aluminium housing and isobutene fuel:

Density : $\rho_{isobutane/housing} = x_{V,isobutane} \cdot \rho_{isobutane} + x_{V,housing} \cdot \rho_{housing}$

Specific heat: $c_{p,isobutane/housing} = x_{V,isobutane} \cdot c_{p,isobutane} + x_{V,housing} \cdot c_{p,housing}$

Therm. conduct.:$k_{isobutane/housing} = x_{m,isobutane} \cdot k_{isobutane} + x_{m,housing} \cdot k_{housing}$

Calculated values are specified in Appendix A.

- **Calculating components in payload compartment**

As already described in subchapter 5.2.2.7 in the explanation of the Payload compartment, the total mass of the payload is predicted to be 1.8 kg, and it is evenly distributed between the Aluminium part, the polyethylene part and the water part, each of the three component weighing of 0.6 kg. Water (biology sample) was placed in the middle, surrounded by twin polyethylene layers and twin Aluminium layers on each side (see Figure 5-19).

With 3 mm of Aluminium and 15 mm of polyethylene as radiation protection, dimensions of inside box are reduced from 200 mm x 200 mm x 98 mm to 164 mm x 164 mm x 62 mm. Calculations were performed with 160 mm x 60 mm layers.

Knowing density of material, thickness for each layer can be calculated:

- each of two 0.3 kg Aluminium layer = 11.2 mm
- each of two 0.3 kg polyethylene layer = 34.7 mm
- 0.6 kg water layer = 62.5 mm.

Appendix G: Geometry model tree (ESATAN-TMS)

+ BATTERIES

- **+ BAT_1_ALL**
  - **BAT_1**
  - **BAT_1_1**
  - **BAT_1_2**
- **+ BAT_2_ALL**
  - **BAT_2**
  - **BAT_2_1**
  - **BAT_2_2**
- **+ BAT_3_ALL**
  - **BAT_3**
  - **BAT_3_1**
  - **BAT_3_2**
- **+ BAT_4_ALL**
  - **BAT_4**
  - **BAT_4_1**
  - **BAT_4_2**
- **+ BAT_5_ALL**
  - **BAT_4**
  - **BAT_4_1**
  - **BAT_4_2**
- **+ BAT_6_ALL**
  - **BAT_6**
  - **BAT_6_1**
  - **BAT_6_2**
- **+ BAT_7_ALL**
  - **BAT_7**
  - **BAT_7_1**
  - **BAT_2_2**
- **+ BAT_8_ALL**
  - **BAT_8**
  - **BAT_8_1**
  - **BAT_8_2**
- **+ BAT_9_ALL**
  - **BAT_9**
  - **BAT_9_1**
  - **BAT_9_2**
- **+ BAT_10_ALL**
  - **BAT_10**
  - **BAT_10_1**
  - **BAT_10_2**

Materials/ Optical properties
BATTERIES
BAT_1_ALL (complete single battery unit 1 of 10)
BAT_1 (body of battery unit 1 of 10)
NODES:5x4;
SURFACE OUT: Al black anodized;
THICKNESS MATERIAL OUT;
SURFACE IN: Li-Ion composite;
THICKNESS MATERIAL IN;
RADIUS;
DIMENSION of unit;
BAT_1_1 (battery cover 1 of 2 on each single battery unt)
NODES:1x4
SURFACE OUT:Al black anodized;
SURFACE IN: Al black anodized;
THICKNESS single material;
RADIUS;
BAT_PLATE (plate for battery pack)
NODES:5x10
SURFACE OUT OPT: Al black anodized;
SURFACE IN OPT: Al black anodized;
THICKNESS single material: Al;
IRIS (Transponder unit)
IRIS_v2_1 (Transponder PCB plate 1 of 4)
NODES: 3x3
SURFACE OUT OPT: Si; MATERIAL:IRIS_PCB_Cu_Si;
THICKNESS MATERIAL OUT;
SURFACE IN OPT: FR4; MATERIAL: FR4;
THICKNESS MATERIAL IN;
IRIS_v2_side1 (side wall 1 of 2)
NODES: 4x3
SURFACE OUT OPT: Al black anodized;
SURFACE IN OPT: Al black anodized;
THICKNESS single material: Al;
IRIS_v2_top (top cover of Transponder)
NODES: 3x3;
SURFACE OUT OPT: Al black anodized;
SURFACE IN OPT: Al black anodized;
THICKNESS single material: Al;
PCB_C_DH (Command & Data Handling PCB board)
NODES: 5x10
SURFACE OUT OPT: Si; MATERIAL: Si;
THICKNESS MATERIAL OUT;
SURFACE IN OPT: FR4; MATERIAL: FR4;
THICKNESS MATERIAL IN;
PAYLOAD (Payload container)
Pld_Mass (Payload experiment unit)
Pld_Mass_Al_1 (Al part of experiment 1of 2 units)
NODES: 3x6;
SURFACE OUT OPT: Al black anodized;
SURFACE IN OPT: Al black anodized;
THICKNESS single material: Al;

+ BAT_PLATE
+ IRIS
- **+ IRIS_v2_1**
- **+ IRIS_v2_2**
- **+ IRIS_v2_3**
- **+ IRIS_v2_4**
- **+ IRIS_v2_side_1**
- **+ IRIS_v2_side_2**
- **+ IRIS_v2_top**

+ PCB_C_DH
+ PAYLOAD
- **+ Pld_Mass**
  - **Pld_Mass_Al_1**
  - **Pld_Mass_Al_2**
  - **Pld_Mass_Poly_1**
  - **Pld_Mass_Poly_2**
  - **Pld_Mass_Water**
- **+ Pld_Panels**
  - **Pld_NX**
  - **Pld_NY**
  - **Pld_NZ**
  - **Pld_PX**
  - **Pld_PY**
  - **Pld_PZ**

+ SAT_PANELS
- **NX**
- **NY**
- **NZ**
- **PX**
- **PY**
- **PZ**

+ XACT_ADCS
+ SOL_PANELS
- **Sol_1**
- **Sol_2**

Pld_Mass_Poly_1 (Polyethylene part of exp., 1 of 2 units)
NODES: 3x6;
SURFACE OUT OPT: Polyethylene;
SURFACE IN OPT: Polyethylene;
THICKNESS single material: Polyethylene;
Pld_Mass_Water_1 (Biological part of exp., 1 of 2 units)
NODES: 3x6;
SURFACE OUT OPT: Water;
SURFACE IN OPT: Al Water;
THICKNESS single material: Water;
Pld_Panels (panels of payload container)
Pld_PX & Pld_NX (payload container panels in x-axis)
NODES: 6x6
SURFACE OUT OPT:Al black anodized; MATER: Al;
THICKNESS MATERIAL OUT;
SURFACE IN OPT: poly.; MATERIAL: polyethylene;
THICKNESS MATERIAL IN;
Pld_PY & Pld_NY (payload container panels in y-axis)
NODES: 3x6
SURFACE OUT OPT:Al black anodized; MATER: Al;
THICKNESS MATERIAL OUT;
SURFACE IN OPT: poly.; MATERIAL: polyethylene;
THICKNESS MATERIAL IN;
Pld_PZ & Pld_NZ (payload container panels in y-axis)
NODES: 3x6
SURFACE OUT OPT:Al black anodized; MATER: Al;
THICKNESS MATERIAL OUT;
SURFACE IN OPT: poly.; MATERIAL: polyethylene;
THICKNESS MATERIAL IN;
SAT_PANELS (body panels)
PX & NX (x-axis satellite panels)
NODES: 10x5;
SURFACE OUT OPT Al black anodized;
SURFACE IN OPT: Al black anodized;
THICKNESS single material;
PY & NY (y-axis satellite panels)
NODES: 10x5;
SURFACE OUT OPT Al black anodized;
SURFACE IN OPT: Al black anodized;
THICKNESS single material;
PZ (positive z-axis satellite panels- thruster unit)
NODES: 5x5;
SURFACE OUT OPT Al black anodized;
SURFACE IN OPT: Al black anodized;
THICKNESS single material: A;
NZ (negative z-axis satellite panels- sol.panel gimbal)
NODES: 5x5;
SURFACE OUT OPT Al black anodized;
SURFACE IN OPT: Al black anodized;
THICKNESS single material: A;
XACT_ADCS (attitude det. and control sys. unit)
NODES: 5x5
SURFACE OUT OPT:Al black anodized; MATER: XACT_react wheels body
THICKNESS MATERIAL OUT;
SURFACE IN OPT: FR4.; MATERIAL: XACT_PCB_board;
THICKNESS MATERIAL IN;

SOL_PANELS (solar panels unit)
Sol_1 & Sol_2 (solar panels)
NODES: 5x5
SURFACE OUT OPT: Germanium; MATER: Ger.;
THICKNESS MATERIAL OUT;
SURFACE IN OPT: Graphite.; MATERIAL: Graphite;
THICKNESS MATERIAL IN;

Appendix H: List of performed RADIATIVE CASES

Different Radiative cases were executed for every change in the model geometry (dimensions, materials, optical coatings…) or every change of the location.

1. Radiative cases calculated for black anodized Aluminium satellite body with graphite solar panel base at discrete distances from 1.1 AU to 1.5 AU:

DEEP 1_1_AU_Al_GRAPH
DEEP 1_2_AU_Al_GRAPH
DEEP 1_3_AU_Al_GRAPH
DEEP 1_4_AU_Al_GRAPH
DEEP 1_5_AU_Al_GRAPH

2. Radiative cases calculated for black anodized Aluminium satellite body with gold anodized solar panel base at discrete distances from 1.1 AU to 1.5 AU:

DEEP 1_1_AU_Al_GOLD
DEEP 1_2_AU_Al_GOLD
DEEP 1_3_AU_Al_GOLD
DEEP 1_4_AU_Al_GOLD
DEEP 1_5_AU_Al_GOLD

3. Radiative cases calculated for gold anodized Aluminium satellite body with gold anodized solar panel base at discrete distances from 1.1 AU to 1.5 AU:

DEEP 1_1_AU_GOLD
DEEP 1_2_AU_GOLD
DEEP 1_3_AU_GOLD
DEEP 1_4_AU_GOLD
DEEP 1_5_AU_GOLD
All together we performed 15 different Radiative cases.

Appendix I: List of performed THERMAL ANALYSIS CASES

Different Thermal analysis case were executed for every change of the boundary conditions (performance, heat dissipation…)

DEEP_1_1_0_POWER_STEADY_Al_GRAPH
DEEP_1_1_0_POWER_STEADY_Al_GRAPH_4
DEEP_1_1_0_POWER_STEADY_Al_GRAPH_37
DEEP_1_1_0_POWER_STEADY_Al_GOLD
DEEP_1_1_0_POWER_STEADY_Al_GOLD_4
DEEP_1_1_0_POWER_STEADY_Al_GOLD_37
DEEP_1_1_0_POWER_STEADY_GOLD
DEEP_1_1_0_POWER_STEADY_GOLD_4
DEEP_1_1_0_POWER_STEADY_GOLD_37

DEEP_1_1_MIN_POWER_STEADY_Al_GRAPH
DEEP_1_1_MIN_POWER_STEADY_Al_GRAPH_4
DEEP_1_1_MIN_POWER_STEADY_Al_GRAPH_37
DEEP_1_1_MIN_POWER_STEADY_Al_GOLD
DEEP_1_1_MIN_POWER_STEADY_Al_GOLD_4
DEEP_1_1_MIN_POWER_STEADY_Al_GOLD_37
DEEP_1_1_MIN_POWER_STEADY_GOLD
DEEP_1_1_MIN_POWER_STEADY_GOLD_4
DEEP_1_1_MIN_POWER_STEADY_GOLD_37

DEEP_1_1_MAX_POWER_STEADY_Al_GRAPH
DEEP_1_1_MAX_POWER_STEADY_Al_GRAPH_4
DEEP_1_1_MAX_POWER_STEADY_Al_GRAPH_37
DEEP_1_1_MAX_POWER_STEADY_Al_GOLD
DEEP_1_1_MAX_POWER_STEADY_Al_GOLD_4
DEEP_1_1_MAX_POWER_STEADY_Al_GOLD_37
DEEP_1_1_MAX_POWER_STEADY_GOLD
DEEP_1_1_MAX_POWER_STEADY_GOLD_4
DEEP_1_1_MAX_POWER_STEADY_GOLD_37

A list of Thermal analysis cases performed at a distance of 1.1 AU is presented as an example.
Simulations were performed with 0, NORM and HIGH heat dissipation of installed electronic components and also extra heat input for maintaining 4 °C or 37 °C at the biological sample bay.
The same set of simulations were performed at each discrete distance, thus a total of over 135 executions of thermal analysis cases were performed.

For 1.5 AU distance some extra thermal analysis cases were executed for calculating extra heat requirements for maintaining survival or operational temperatures of different electrical components (Chapter 5.3.2.2.1) for a basic black anodized Aluminium body with graphite solar panel base configuration. Simulations were performed for the 4 different installed electrical components which are most sensitive to low temperature conditions (batteries, C&DH board, reaction wheels, Transponder Communication unit), at different heat dissipation status (zero, min. and max. heat dissipation) of components, with intention to determine required heat input to maintain survival or operation temperature:

DEEP_1_5_0_POWER_STEADY_Al_GRAPH_BATT_SURVIVAL
DEEP_1_5_MIN_POWER_STEADY_Al_GRAPH_BATT_SURVIVAL
DEEP_1_5_MAX_POWER_STEADY_Al_GRAPH_BATT_SURVIVAL
DEEP_1_5_0_POWER_STEADY_Al_GRAPH_BATT_OPERAT
DEEP_1_5_MIN_POWER_STEADY_Al_GRAPH_BATT_OPERAT
DEEP_1_5_MAX_POWER_STEADY_Al_GRAPH_BATT_OPERAT

Same sets of simulations were performed for every 4 electronic components. **All together were performed 24 additional thermal analysis cases.**

Appendix J: List of User Defined Conductors used in ESATAN– TMS simulation

ADCS_DOWN_1 **ADCS_DOWN_2** **ADCS_UP_1** **ADCS_UP_2**	ADCS connection to structure
BATT_1 **BATT_2** **BATT_3** **BATT_4**	Connection of Battery plate to structure
COMM_1 **COMM_2** **COMM_3** **COMM_4**	Connection of Command and Data handling board to structure
IRIS_2_1 **IRIS_2_2** **IRIS_2_3** **IRIS_2_4**	Connection of IRIS slot 2 to unit body
IRIS_3_1 **IRIS_3_2** **IRIS_3_3** **IRIS_3_4**	Connection of IRIS slot 3 to unit body
IRIS_4_1 **IRIS_4_2** **IRIS_4_3** **IRIS_4_4**	Connection of IRIS slot 4 to unit body
IRIS_DOWN_1 **IRIS_DOWN_2** **IRIS_UP_1** **IRIS_UP_2**	Connection of IRIS unit to satellite structure
PYL_DOWN_1 **PYL_DOWN_2** **PYL_DOWN_3** **PYL_DOWN_4**	Connection of payload container on bottom side
PYL_SIDE_1 **PYL_SIDE_2** **PYL_SIDE_3** **PYL_SIDE_4** **PYL_SIDE_5** **PYL_SIDE_6** **PYL_SIDE_7** **PYL_SIDE_8**	Connection of payload container on side to structure
SOL_1_BODY **SOL_2_BODY**	Connections of solar panels to the body

Appendix K: List of Boundary conditions used in ESATAN – TMS simulations

BAT_1_POWER **BAT_1_POWER_LOW**	Battery 1 dissipated heat
BAT_1_POWER_EXTRA	Extra heating to maintain temperature
BAT_2_POWER **BAT_2_POWER_LOW**	Battery 2 dissipated heat
BAT_2_POWER_EXTRA	Extra heating to maintain temperature
BAT_3_POWER **BAT_3_POWER_LOW**	Battery 3 dissipated heat
BAT_3_POWER_EXTRA	Extra heating to maintain temperature
BAT_4_POWER **BAT_4_POWER_LOW**	Battery 4 dissipated heat
BAT_4_POWER_EXTRA	Extra heating to maintain temperature
BAT_5_POWER **BAT_5_POWER_LOW**	Battery 5 dissipated heat
BAT_5_POWER_EXTRA	Extra heating to maintain temperature
BAT_6_POWER **BAT_6_POWER_LOW**	Battery 6 dissipated heat
BAT_6_POWER_EXTRA	Extra heating to maintain temperature
BAT_7_POWER **BAT_7_POWER_LOW**	Battery 7 dissipated heat
BAT_7_POWER_EXTRA	Extra heating to maintain temperature
BAT_8_POWER **BAT_8_POWER_LOW**	Battery 8 dissipated heat
BAT_8_POWER_EXTRA	Extra heating to maintain temperature
BAT_9_POWER **BAT_9_POWER_LOW**	Battery 9 dissipated heat
BAT_9_POWER_EXTRA	Extra heating to maintain temperature
BAT_10_POWER **BAT_10_POWER_LOW**	Battery 10 dissipated heat

BAT_10_POWER_EXTRA	Extra heating to maintain temperature
BAT_PCB_POWER **BAT_PCB_POWER_LOW**	Battery plate dissipated heat
COMM_POWER **COMM_POWER_LOW**	Comm. and data handling board dissipated heat
COMM_POWER_EXTRA	Extra heating to maintain temperature
IRIS_1_POWER **IRIS_1_POWER_LOW**	IRIS slot 1 dissipated heat
IRIS_1_POWER_EXTRA	Extra heating to maintain temperature
IRIS_2_POWER **IRIS_2_POWER_LOW**	IRIS slot 2 dissipated heat
IRIS_2_POWER_EXTRA	Extra heating to maintain temperature
IRIS_3_POWER **IRIS_3_POWER_LOW**	IRIS slot 3 dissipated heat
IRIS_3_POWER_EXTRA	Extra heating to maintain temperature
IRIS_4_POWER **IRIS_4_POWER_LOW**	IRIS slot 4 dissipated heat
IRIS_4_POWER_EXTRA	Extra heating to maintain temperature
SOLAR_PANEL_POWER **SOLAR_PANEL_POWER_LOW**	Solar panel mechanism board dissipated heat
THRUSTER_POWER **THRUSTER_POWER_LOW**	Thruster electronic dissipated heat
ADCS_POWER **ADCS_POWER_LOW**	ADCS electronic board heat dissipation
ADCS_POWER_EXTRA	Extra heating to maintain temperature
PAYLOAD_EXTRA	Payload extra heating